

NUREG/CR-5541
BNL-NUREG-52550

**SYSTEM SCALING
FOR THE
WESTINGHOUSE AP600 PRESSURIZED WATER REACTOR
AND RELATED TEST FACILITIES**

Analysis and Results

Manuscript completed: January 1998

Prepared by
Wolfgang Wulff and Upendra S. Rohatgi
Department of Advanced Technology
Brookhaven National Laboratory
Upton, NY 11973-5000

D. Bessette, NRC Project Monitor

Prepared for
Division of Systems Technology
Office of Nuclear Regulatory Research
U.S. Nuclear Regulatory Commission
Washington, DC 20555-0001
NRC JCN W-6670

ABSTRACT

The global system scaling analysis for the Advanced Pressurized Water Reactor AP600 of Westinghouse has been performed in five main time phases for the 1-inch Cold-Leg break, to determine whether three related and already existing test facilities, namely the Advanced Plant Experiment (APEX) facility located at Oregon State University (OSU) at Corvallis, the Rig of Safety Assessment (ROSA) Large Scale Test Facility located in Tokai-mura, Japan, and the Simulatore per Esperienze di Sicurezza (Simulator for Safety Experimental Analysis, SPES-2) located in Piacenza, Italy, represent the AP600 reactor. The scaling analysis is the top-down, global system analysis. It is intended to establish thermodynamic similarity between AP600, APEX, ROSA, and SPES at the level of overall system response and dynamic interaction between the system components. It is intended also to rank global transport processes according to their importance and to identify possible deviations from thermohydraulic similarity, or scale distortion.

The causative process related and the fractional scaling methods were employed, the former for its ability to scale separately the capacitance terms of the governing conservation equations, for assessing individual process response frequencies, the latter for assessing directly the fractional impact of transport processes on the time rates of change. Both methods provide *scaling groups*, which measure the impact of processes on the system response, serve to rank phenomena and assess scale distortions.

The total of 127 phenomena has been scaled for the five main time phases with four subphases. Of the 127 phenomena, 75 were found to be of *first-order importance* and 39 to have top priority importance, respectively, because the corresponding scaling groups are greater than 1/10 and 8/10 of the respective greatest scaling group.

At least one of the three test facilities APEX, ROSA, and SPES scales every important phenomenon at least once for every phase and subphase, except two, without significant *distortion*, because the scaling groups corresponding to the first-order important phenomena fall for at least one of the test facilities between $\frac{1}{2}$ and 2 times the value of the corresponding important AP600 scaling group. Both exceptions are important for code assessment, only the second one (due to PRZ injection during ADS-4 Blowdown) is important for simulating minimum liquid inventory in the Reactor Pressure Vessel. The simulation of minimum liquid inventory due to PRZ injection is conservatively distorted in ROSA and SPES. Scaling alone cannot decide whether the distortion in APEX is conservative, since the distortion causes two competing processes.

The largest number of first-order important phenomena evaluated for any one phase is 19; this number covers primary and secondary side system depressurizations, inventories of the system, the Pressurizer, the Core Make-up Tanks, and the Passive Residual Heat Rejection system, the temperatures of the single-phase liquid in the primary system and the above components, and the mass flow rates of the seven-loop system.

The mathematical models, the scope, the scaling method and scaling principles, and the scaling results of the scaling analyses of INEL for AP600, APEX, ROSA, and SPES, and of Westinghouse for AP600, APEX, and SPES have been compared with the scaling analyses presented in this report. Serious limitations were found in these analyses, and there are conflicts between the assessment of scale distortions presented here and in the previously published analyses by INEL and Westinghouse.

This report describes generically the system and transient scenario, and presents the results of the scaling analysis but no proprietary information about the AP600 system.

TABLE OF CONTENTS

	Page
ABSTRACT	iii
TABLE OF CONTENTS	v
LIST OF FIGURES	xi
LIST OF TABLES	xiii
EXECUTIVE SUMMARY	xix
PREFACE	xxv
ACKNOWLEDGMENTS	xxvii
NOMENCLATURE	xxix
Symbols	xxix
Latin Symbols	xxix
Greek Symbols	xxx
Subscripts	xxxii
Superscripts	xxxiii
Acronyms	xxxiv
1. INTRODUCTION	1 - 1
1.1 Background	1 - 1
1.2 Objectives of Scaling Analysis	1 - 1
1.3 Organization of Report	1 - 3
2. AP600 SYSTEM DESCRIPTION	2 - 1
2.1 Primary System	2 - 1
2.2 Safety Systems	2 - 1
2.2.1 Safety Injection Systems	2 - 1
2.2.2 Heat Rejection System	2 - 2
2.2.3 Depressurization Systems	2 - 2
3. SCENARIO AND PARTITIONS OF SMALL-BREAK LOSS OF COOLANT ACCIDENT	3 - 1
3.1 Phase 1. Initial Depressurization	3 - 4
3.1.1 Subphase 1.1 Before Reactor Scram	3 - 4
3.1.2 Subphase 1.2 After Reactor Scram	3 - 4
3.2 Phase 2. Passive Heat Removal	3 - 4
3.2.1 Subphase 2.1 Before Accumulator Injection	3 - 5
3.2.1.1 Steam Generators as Heat Sink	3 - 5
3.2.1.2 Steam Generators as Heat Source	3 - 5
3.2.2 Subphase 2.2 After Accumulator Injection	3 - 5
3.3 Phase 3. ADS-123 Blow - Down	3 - 5
3.4 Phase 4. ADS-4 Depressurization	3 - 6

TABLE OF CONTENTS (Cont'd.)

	Page
3.5 Phase 5. IRWST and Sump Injections	3 - 6
3.6 Closing Remarks on Partitioning of Transient	3 - 6
4. SCALING METHODOLOGY	4 - 1
4.1 Top-down and Global System Scaling	4 - 1
4.2 Scaling Criteria	4 - 1
4.3 Principles of Scaling	4 - 2
4.4 Scaling Approach	4 - 4
4.4.1 Identification of Control Volume	4 - 5
4.4.2 Model Derivation	4 - 6
4.4.3 Selection, Calculation, and Validation of Reference Parameters	4 - 6
4.4.4 Normalization of Modeling Equations	4 - 6
4.4.5 Scaling of Conservation Equations and Scaling Criteria	4 - 7
4.4.5.1 Conservation Equations Scaled on the Basis of the Causative Process	4 - 7
4.4.5.2 Fractional Scaling of the Conservation Equations	4 - 9
4.4.6 Scaling of Loop System	4 - 10
4.4.6.1 Global System Dynamics	4 - 12
4.4.6.2 Distribution and Interaction of Flows	4 - 13
The Inertia Metric, SI,	4 - 13
The Impedance Metric, SP,	4 - 14
4.5 Criterion of Relevant Phenomenon	4 - 15
4.6 Criterion of Scale Distortion	4 - 15
5. MODELING EQUATIONS	5 - 1
5.1 Model Selection	5 - 1
5.2 Modeling Assumptions and Limitations	5 - 2
5.3 Validation of Models	5 - 2
5.4 Conservation Equations	5 - 3
5.4.1 Mass and Energy Conservation	5 - 4
5.4.1.1 Control Volumes for Mass and Energy Balance Equations	5 - 5
5.4.1.2 Time Rate of Pressure Change	5 - 7
5.4.1.3 Time Rate of Inventory Change	5 - 9
5.4.1.4 Time Rate of Temperature Change	5 - 10
5.4.2 Momentum Balance	5 - 11
5.4.2.1 System Momentum Balance	5 - 11
5.4.2.2 System Admittance Matrix	5 - 17
5.4.2.3 Inertia Matrix	5 - 18
5.4.2.4 Impedance Matrix	5 - 23
5.5 Reference Parameters	5 - 28
5.5.1 Time References	5 - 29
5.5.2 Pressure References	5 - 30
5.5.3 Volumetric Flow Rate References	5 - 31
5.5.4 Mass Flow Rate References	5 - 34
5.5.5 Comparison of Reference Parameters with Test Data	5 - 36

TABLE OF CONTENTS (Cont'd.)

	Page
6. SCALING GROUPS	6 - 1
6.1 Scaled Equations and Scaling Groups	6 - 1
6.1.1 Depressurization	6 - 1
6.1.1.1 Causative-Process Related Scaling of Depressurization	6 - 1
6.1.1.2 Fractional Scaling of Depressurization	6 - 3
6.1.2 Inventory	6 - 5
6.1.2.1 Causative-Process Related Scaling of Liquid Inventory Loss	6 - 5
6.1.2.2 Fractional Scaling of Inventory Loss	6 - 6
6.1.3 Temperatures	6 - 8
6.1.3.1 Causative-Process Related Scaling of Temperature Change	6 - 8
Primary-System Temperature Change, Break Flow Dominating	6 - 8
Primary-System Temperature Change, Dominated by Wall Heating or Cooling	6 - 10
Primary-System Temperature Change, Domination by PRHR Cooling	6 - 11
Temperature Change in Core Make-up Tank	6 - 13
Temperature Change in Passive Residual Heat Rejection System	6 - 14
Primary System Temperature Change after Start of Accumulator Injection	6 - 14
6.1.3.2 Fractional Scaling of Energy Equation	6 - 15
6.1.4 Flow Rates, Inertia and Impedance	6 - 18
6.1.4.1 Forced Circulation	6 - 18
6.1.4.2 Natural Circulation	6 - 21
6.2 Evaluation of Scaling Groups, Ranking and Scale Distortions	6 - 22
6.2.1 Phase 1, Initial Depressurization	6 - 23
6.2.1.1 Phase 1.1, Before Scram	6 - 24
6.2.1.1.1 Depressurization Before Scram	6 - 24
6.2.1.1.2 Inventory Before Scram	6 - 25
6.2.1.1.3 System Temperature Before Scram	6 - 27
6.2.1.1.4 Flow Rates, Inertia, and Impedance for Phase 1	6 - 29
6.2.1.2 Phase 1.2, After Scram	6 - 34
6.2.1.2.1 Depressurization After Scram	6 - 34
6.2.1.2.2 Inventory After Scram	6 - 36
6.2.1.2.3 System Temperature After Scram	6 - 38
6.2.2 Phase 2, Natural Circulation and Passive Decay Heat Removal	6 - 40
6.2.2.1 Depressurization	6 - 41
Primary System Before Accumulator Trip	6 - 41
Secondary System, Phase 2	6 - 43
Primary System After Accumulator Trip	6 - 44
6.2.2.2 Inventory Change During Phase 2	6 - 45
Primary System Inventory, Before Accumulator Trip	6 - 45
Core Make-up Tank Inventory, Before Accumulator Trip, Phase 2.1	6 - 47
Primary System Inventory, After Accumulator Trip	6 - 51

TABLE OF CONTENTS (Cont'd.)

	Page
6.2.2.3 Temperature Changes During Phase 2, Passive Heat Removal	6 - 54
Primary System, Before Accumulator Trip	6 - 54
Core Make-up Tank, Before Accumulator Trip	6 - 55
Passive Residual Heat Rejection System, Before Accumulator Trip	6 - 56
Fractional Scaling of Temperature Response During Subphase 2.1, Before Accumulator Trip	6 - 57
Primary System, After Accumulator Trip	6 - 59
6.2.2.4 Flow Rates, Inertia and Impedance for Phase 2	6 - 60
6.2.3 Phase 3, ADS-123 Depressurization	6 - 69
6.2.3.1 Depressurization	6 - 70
6.2.3.2 Inventory Change	6 - 72
Pressurizer Inventory Change During Phase 3	6 - 72
Inventory Change in Core Make-up Tanks During Phase 3	6 - 75
6.2.3.3 Temperatures	6 - 77
6.2.3.4 Flow Rates, Inertia and Impedance	6 - 77
6.2.4 Phase 4, ADS-4 Depressurization	6 - 77
6.2.4.1 ADS-4 Depressurization	6 - 78
6.2.4.2 Inventory Changes During Phase 4	6 - 79
System Inventory Change During Phase 4	6 - 80
Inventory Change in Reactor Pressure Vessel	6 - 81
Inventory Change in Core Make-up Tank During Phase 4	6 - 85
Inventory Change in Pressurizer During Phase 4	6 - 87
6.2.4.3 Temperature Changes During Phase 4	6 - 90
6.2.4.4 Flow Rates, Inertia and Impedance for Phase 4	6 - 91
6.2.5 Phase 5, IRWST and SUMP Injections	6 - 91
6.2.5.1 Depressurization	6 - 92
6.2.5.2 Inventory Changes During Phase 5	6 - 92
Inventory Change of Reactor Pressure Vessel During Phase 5	6 - 92
Inventory Change of Pressurizer During Phase 5	6 - 96
Inventory Change of In-containment Refueling Water Storage Tank During Phase 5	6 - 97
6.2.5.3 Temperatures During Phase 5	6 - 98
RPV Internal Energy	6 - 98
Liquid Subcooling Temperature	6 - 101
Nonboiling Length in Core	6 - 103
6.2.5.4 Flow Rates, Inertia and Impedance	6 - 103
6.3 Summary of Scale Distortions and their Interpretation	6 - 107
Scope of Scaling Analysis	6 - 107
Important Phenomena	6 - 108
Scale Distortions	6 - 109
6.3.1 Global Scale Distortions in APEX	6 - 109
6.3.2 Global Scale Distortions in ROSA	6 - 110
6.3.3 Global Scale Distortions in SPES	6 - 112
6.3.4 Scale Distortions of Local Inertia, Gravity, and Impedance Distributions	6 - 113

TABLE OF CONTENTS (Cont'd.)

	Page
7. PRESENT VERSUS PREVIOUS SCALING ANALYSIS RESULTS	7 - 1
7.1 The INEL Scaling Analysis	7 - 1
7.1.1 Modeling in the INEL Scaling Analysis	7 - 2
7.1.2 Scope of the INEL Scaling Analysis	7 - 2
7.1.3 INEL Scaling Method and Scaling Principles	7 - 3
7.1.4 INEL Scaling Results	7 - 3
7.2 The Westinghouse Scaling Analysis	7 - 4
7.2.1 Modeling in the Westinghouse Scaling Analysis	7 - 4
7.2.2 Scope of the Westinghouse Scaling Analysis	7 - 5
7.2.3 Westinghouse Scaling Method and Scaling Principles	7 - 5
7.2.4 Westinghouse Scaling Results	7 - 5
8. CONCLUSIONS	8 - 1
9. REFERENCES	9 - 1

TABLE OF CONTENTS (Cont'd.)

LIST OF FIGURES

	Page
Figure 1.1	Schematic of AP00 Thermal Hydraulic System 1 - 3
Figure 3.1	Schematic of Depressurization and Phase Sequence 3 - 1
Figure 4.1	Initial Rate of Change in Scaled Time of Specific State Variable 4 - 8
Figure 4.2	Initial Rate of Change in Scaled Time of Overall System 4 - 8
Figure 4.3	Fractions of Total Change Rate 4 - 9
Figure 4.4	Schematic of Two-Loop System 4 - 10
Figure 4.5	Inertia Metric for Two-Loop System 4 - 13
Figure 4.6	Impedance Metric for Two-Loop System 4 - 14
Figure 4.7	Phenomenon Importance in Column of Π -Group Matrix 4 - 15
Figure 4.8	Phenomenon Distortion in Row of Π -Group Matrix 4 - 16
Figure 5.1	General Subvolume Assembly 5 - 1
Figure 5.2	Primary System Control Volume for Phase 1 5 - 5
Figure 5.3	Primary System Control Volume for Phase 2 5 - 6
Figure 5.4	Primary System Control Volume for Phase 4 5 - 6
Figure 5.6	Four-Loop Control Volume for Normal Operation and for Phase 1 5 - 13
Figure 5.7	Seven-Loop Control Volume for Phase 2, Passive Heat Removal 5 - 13
Figure 5.8	Seven-Loop Control Volume for Phase 3, ADS-123 Blowdown 5 - 14
Figure 5.9	Seven-Loop Control Volume for Phase 4, ADS-4 Depressurization 5 - 14
Figure 5.10	Six-Loop Control Volume for Phase 5, IRWST Injection 5 - 15

LIST OF TABLES

		Page
Table 5.1	Inertia Matrix for Four-Loop Operation of AP600, APEX, and SPES	5 - 19
Table 5.2	Numerical Values of Inertia Matrix for Four-Loop Operation: AP600	5 - 20
Table 5.3	Numerical Values of Inertia Matrix for Four-Loop Operation: APEX	5 - 20
Table 5.4	Numerical Values of Inertia Matrix for Four-Loop Operation: SPES	5 - 20
Table 5.5	Numerical Values of Inertia Matrix for Two-Loop Operation: ROSA	5 - 21
Table 5.6	Inertia Matrix in Symbolic Form for AP600, APEX, and SPES During Phases 2 Through 4	5 - 21
Table 5.7	Inertia Matrix in Numerical Form for AP600 During Phase 2	5 - 22
Table 5.8	Impedance Matrix for Four-Loop Operation During Phase 1 of AP600, APEX, and SPES	5 - 25
Table 5.9	Impedance Matrix in Numerical Form for Four-Loop Operation of AP600, Phase 1	5 - 26
Table 5.10	Impedance Matrix in Numerical Form for Four-Loop Operation of APEX, Phase 1	5 - 26
Table 5.11	Impedance Matrix in Numerical Form for Four-Loop Operation of SPES, Phase 1	5 - 27
Table 5.12	Impedance Matrix in Numerical Form for Two-Loop Operation of ROSA, Phase 1	5 - 27
Table 5.13	Impedance Matrix in Symbolic Form for Seven-Loop Operation of AP600, APEX, and SPES (Phases 2, 3, and 4)	5 - 28
Table 5.14	Impedance Matrix in Numerical Form for Seven-Loop Operation of AP600 During Phases 2 Through 4	5 - 29
Table 5.15	Comparison of Estimated Reference Parameters with Experimental Data	5 - 37
Table 6.1	Causative Process Related Π -Groups for Depressurization During Subphase 1.1	6 - 25
Table 6.2	Fractional Π -Groups for Depressurization During Subphase 1.1	6 - 25
Table 6.3	Causative Process Related Π -Groups for Loss of Inventory During Subphase 1.1	6 - 26
Table 6.4	Fractional Π -Groups for Loss of Inventory During Subphase 1.1	6 - 27
Table 6.5	Causative process related Π -Groups for Change of Subcooled Liquid Temperatures During Subphase 1.1	6 - 28
Table 6.6	Fractional Π -Groups for Change of Subcooled Liquid Temperature During Subphase 1.1	6 - 29
Table 6.7	Causative Process Related Π -Groups of Dynamic Interaction Between Components During Phase 1	6 - 30

LIST OF TABLES (Cont'd.)

		Page
Table 6.8	Fractional Π -Groups of Dynamic Interaction Between Components During Phase 1	6 - 30
Table 6.9	Inertia Metric for Four-Loop Operation: AP600	6 - 31
Table 6.10	Inertia Metric for Four-Loop Operation: APEX	6 - 31
Table 6.11	Inertia Metric for Four-Loop Operation: SPES	6 - 31
Table 6.12	Inertia Metric for Two-Loop Operation of ROSA	6 - 32
Table 6.13	Impedance Metric for Four-Loop Operation of AP600, Phase 1	6 - 32
Table 6.14	Impedance Metric for Four-Loop Operation of APEX, Phase 1	6 - 33
Table 6.15	Impedance Metric for Four-Loop Operation of SPES, Phase 1	6 - 33
Table 6.16	Impedance Metric for Two-Loop Operation of ROSA, Phase 1	6 - 34
Table 6.17	Causative Process Related Π -Groups for Depressurization During Subphase 1.2	6 - 35
Table 6.18	Fractional Π -Groups for Depressurization During Subphase 1.2	6 - 36
Table 6.19	Causative Process Related Π -Groups for Loss of Inventory During Subphase 1.2	6 - 37
Table 6.20	Fractional Π -Groups for Loss of Inventory During Subphase 1.2	6 - 37
Table 6.21	Causative Process Related Π -Groups for Change of Subcooled Liquid Temperature During Subphase 1.2	6 - 38
Table 6.22	Fractional Π -Groups for Change of Subcooled Liquid Temperature During Subphase 1.2 . . .	6 - 39
Table 6.23	Causative process related Π -Groups for Depressurization During Phase 2.1	6 - 42
Table 6.24	Fractional Π -Groups for Depressurization During Phase 2.1	6 - 43
Table 6.25	Fractional Π -Groups for Depressurization of Secondary Side During Phase 2	6 - 43
Table 6.26	Causative Process Related Π -Groups for Depressurization During Phase 2.2, After Accumulator Trip	6 - 44
Table 6.27	Fractional Π -Groups for Depressurization During Phase 2.2, After Accumulator Trip	6 - 45
Table 6.28	Causative Process Related Π -Groups for Loss of Inventory During Phase 2.1, Before Accumulator Trip	6 - 46
Table 6.29	Fractional Π -Groups for Loss of Inventory During Subphase 2.1, Before Accumulator Trip . .	6 - 47
Table 6.30	Causative process related Π -Groups for CMT Draining During Subphase 2.1	6 - 49

LIST OF TABLES (Cont'd.)

		Page
Table 6.3	Fractional Π -Groups for CMT Draining During Subphase 2.1	6 - 51
Table 6.32	Causative Process Related Π -Groups for Loss of Inventory in Primary System During Phase 2.2, After Accumulator Trip	6 - 52
Table 6.33	Fractional Π -Groups for Loss of Inventory During Subphase 2.2, After Accumulator Trip	6 - 53
Table 6.34	Causative Process Related Π -Groups for Change of System Liquid Temperature During Subphase 2.1	6 - 54
Table 6.35	Causative Process Related Π -Groups for CMT Cooling During Subphase 2.1	6 - 55
Table 6.36	Causative Process Related Π -Groups for PRHR Cooling During Subphase 2.1	6 - 56
Table 6.37	Fractional Π -Groups for System Liquid Temperature Change During Subphase 2.1	6 - 58
Table 6.38	Fractional Π -Groups for CMT Cooling During Subphase 2.1	6 - 58
Table 6.39	Fractional Π -Groups for PRHR Cooling During Subphase 2.1	6 - 59
Table 6.40	Causative Process Related Π -Groups for System Liquid Temperature Change During Subphase 2.2	6 - 60
Table 6.41	Fractional Π -Groups for System Liquid Temperature During Subphase 2.2	6 - 61
Table 6.42	Causative Process Related Π -Groups of Dynamic Interaction Betwe	6 - 62
Table 6.43	Fractional Π -Groups of Dynamic Interaction Between Components During Phase 2	6 - 62
Table 6.44	Inertia Metric SI for Seven-Loop Operation During Phase 2, Passive Heat Rejection: AP600	6 - 63
Table 6.45	Inertia Metric SI for Seven-Loop Operation During Phase 2, Passive Heat Rejection: APEX	6 - 64
Table 6.46	Inertia Metric SI for Five-Loop Operation During Phase 2, Passive Heat Rejection: ROSA	6 - 65
Table 6.47	Inertia Metric SI for Seven-Loop Operation During Phase 2, Passive Heat Rejection: SPES	6 - 65
Table 6.48	Gravity Metric SG for Seven-Loop Operation During Phase 2, Passive Heat Rejection	6 - 66
Table 6.49	Impedance Metric S_p for Seven-Loop Operation of AP600 During Phases 2 through 4	6 - 66
Table 6.50	Impedance Metric S_p for Seven-Loop Operation of APEX During Phases 2 through 4	6 - 67
Table 6.51	Impedance Metric S_p for Five-Loop Operation of ROSA During Phases 2 through 4	6 - 68
Table 6.52	Impedance Metric S_p for Seven-Loop Operation of SPES During Phases 2 through 4	6 - 68
Table 6.53	Causative Process Related Π -Groups for ADS-123 Depressurization During Phase 3	6 - 71

LIST OF TABLES (Cont'd.)

		Page
Table 6.54	Fractional Π -Groups for Depressurization During Phase 3	6 - 72
Table 6.55	Causative Process Related Π -Groups for PRZ Inventory Change During Phase 3	6 - 74
Table 6.56	Fractional Π -Groups for PRZ Inventory Change During Phase 3	6 - 74
Table 6.57	Causative Process Related Π -Groups for CMT Inventory Change During Phase 3	6 - 76
Table 6.58	Fractional Π -Groups for CMT Inventory Change During Phase 3	6 - 76
Table 6.59	Causative Process Related and Fractional Π -Groups for ADS-4 Blowdown During Phase 4 . . .	6 - 79
Table 6.60	Causative Process Related Π -Groups for System Inventory Change During Phase 4	6 - 80
Table 6.61	Fractional Π -Groups for System Inventory Change During Phase 4	6 - 81
Table 6.62	Causative Process Related Π -Groups for RPV Inventory During Phase 4	6 - 83
Table 6.63	Fractional Π -Groups for RPV Inventory During Phase 4	6 - 84
Table 6.64	Causative Process Related Π -Groups for CMT Inventory Change During Phase 4	6 - 86
Table 6.65	Fractional Π -Groups for CMT Inventory Change During Phase 4	6 - 87
Table 6.66	Causative Process Related Π -Groups for PRZ Inventory Change During Phase 4	6 - 89
Table 6.67	Fractional Π -Groups for PRZ Inventory Change During Phase 4	6 - 89
Table 6.68	Π -Groups for Reactor Pressure Vessel Liquid Subcooling During Phase 4	6 - 91
Table 6.69	Causative Process Related Π -Groups for RPV Inventory Change During Phase 5	6 - 94
Table 6.70	Fractional Π -Groups for RPV Inventory Change During Phase 5	6 - 95
Table 6.71	Causative process related Π -Groups for PRZ Inventory Change During Phase 5	6 - 96
Table 6.72	Fractional Π -Group for PRZ Inventory Change During Phase 5	6 - 97
Table 6.73	Causative Process Related and Fractional Π -Groups for IRWST Inventory Change During Phase 5	6 - 98
Table 6.74	Causative Process Related Π -Groups for RPV Internal Energy Change During Phase 5	6 - 100
Table 6.75	Fractional Π -Groups for RPV Internal Energy Change During Phase 5	6 - 101
Table 6.76	Causative process related Π -Groups for RPV Subcooling Enthalpy (Temperature) Change During Phase 5	6 - 102
Table 6.77	Fractional Π -Groups for RPV Subcooling Enthalpy (Temperature) Change During Phase 5 . .	6 - 102

LIST OF TABLES (Cont'd.)

	Page
Table 6.78 Π -Groups for Global Flow Impedance During Phase 5	6 - 104
Table 6.79 Gravity Metric for Six-Loop IRWST Injection During Phase 5	6 - 104
Table 6.80 Impedance Metric for AP600 Six-Loop IRWST Injection During Phase 5	6 - 105
Table 6.81 Impedance Metric for APEX Six-Loop IRWST Injection During Phase 5	6 - 105
Table 6.82 Impedance Metric for ROSA Six-Loop IRWST Injection During Phase 5	6 - 106
Table 6.83 Impedance Metric for SPES Six-Loop IRWST Injection During Phase 5	6 - 106

EXECUTIVE SUMMARY

The objective of the scaling effort reported here is to assess the capability of the three test facilities APEX, ROSA, and SPES to simulate the *global system response* of the AP600, to the extent that global processes and phenomena taking place in the AP600 will also occur in the test facilities, and that the global system response in terms of component interactions is the same in AP600 and the test facilities. The scaling analysis has been carried out for the 1-inch diameter Cold Leg break, to develop the similarity criteria for *global system response* and for the *dynamic interaction between system components* and

- (1) to identify the *leading processes and phenomena* responsible for maintaining the *reactor coolant inventory* high enough to keep the reactor core covered and cooled.
- (2) to quantify the *scale distortions*, if any, for the leading phenomena and to interpret the significance of the scale distortion with regard to minimum coolant inventory and the prediction of minimum inventory by computer code.

The assessment of relative importance and of scale distortion is needed to ascertain that transport phenomena take place in the same heat transfer and flow regimes in the test facilities as in the full-size plant. This assessment is not possible with any computer code, unless the computer code is programmed to evaluate scaling criteria. Without the assessment, one cannot use test data to determine whether or not the closure relations in a computer code are applicable to the full-size plant. All three test facilities are required for assessing the capability of a code to predict AP600 transients, as each facility is limited to the simulation of selected phases and phenomena, as identified in the matrices of Π -Groups in Section 6.2 and summarized in Section 6.3.

Approach. The AP600 thermohydraulic system is described (Figure 1.1). The transient is subdivided into five phases, some of which are further subdivided into subphases (Figure 3.1). The events occurring in each phase are described (see summary in Table 3.1). The global systems, or top-down, scaling methodology of Wulff [17] is followed. Scaling criteria and their relation to scaling or Π -Groups are introduced and two scaling principles are restated [17]; both are needed to establish the relation between Π -Groups, plant-specific characteristics, importance of phenomena, and scale distortion.

The scaling criteria are expressed through scaling or Π Groups and derived by normalizing mass, momentum, and energy conservation equations which are applied to clearly identified control volumes. The conservation equations are combined with thermal and caloric equations of state to form the model description. Every scaled equation produces one fewer scaling criterion than the number of terms in the equation, and one Π -Group that equals 1; only the scaling groups which differ from unity impose scaling requirements. The rules for selecting reference parameters for normalizing the conservation equations are dictated by the above-mentioned modeling principles; reference parameters are estimated only from specified geometric data, specified initial conditions, and specified trip set points, they are constants and selected or estimated for every phase of the transient. The estimation of reference parameters introduces modeling assumptions and uncertainties. The reference parameters were, therefore, confirmed to the extent possible with available test data (Table 5.15).

A working definition of *importance of phenomena* has been introduced in Section 4.5 on the basis of scaling groups. A scaling criterion and its associated phenomenon are of first-order importance if its impact on the transient AP600 system response is of the same order of magnitude as the most important phenomenon, that is, if the corresponding scaling group is greater than 1/10 of the largest scaling group in its normalized conservation equation for AP600. A large number of first-order phenomena, which governing the depressurization transient, met this criterion and prompted an additional definition for phenomena of top priority importance whose corresponding scaling group is greater than 8/10 of the largest scaling group in its normalized conservation equation for AP600.

A working definition of *scale distortion* has been adopted in Section 4.6 on the basis of scaling groups. An important phenomenon is considered to be scale-distorted in a test facility if the associated scaling group differs from the cor-

responding scaling group of AP600 by more than the factor of 2, by being less than ½ or more than 2 times value of the AP600 scaling group. The factor 3 criterion has also been evaluated to establish the sensitivity of the distortion assessment to the criterion. Approximately half of the phenomena which met the factor 2 criterion met also the factor 3 criterion. A scale distortion is called *conservative* if the associated process has the tendency to produce lower minimum RPV inventory or less subcooling in the test facility than in the AP600 power plant. Otherwise, the scale distortion is called nonconservative.

Global scaling groups are arranged in a matrix (presented in Section 6.2 as one table for every conservation equation) with a column each for AP600, APEX, ROSA, and SPES, and with a row for every phenomenon of the transient. *Importance of phenomena* is then determined by comparing the matrix elements in the *column* of AP600 and by applying the above criterion of importance of phenomena (see Section 4.5). *Scale distortion* of a phenomenon in a test facility is determined by comparing the the matrix elements in the *row* of that phenomenon and by applying the above criterion of scale distortion of phenomena (see Section 4.6).

Two scaling methods were used in the work reported here. Each method has its distinct advantages. The first method produces the *causative process related* scaling groups or Π -Groups which scale, compare, and rank phenomena and processes relative to the *causative processes* of each phase. The causative process initiates the transient of a phase and is readily recognized as the break flow, the flows through the valves of the Automatic Depressurization System (ADS), all of which are responsible for the depressurization from initial full-load pressure to ambient containment pressure, and the discharge flow from the In-containment Refueling Water Storage Tank (IRWST) which initiates and dominates the long-term cooling of the reactor core.

The first method scales the capacitance terms individually, i.e., the terms with the time derivative, namely the volumetric capacitance, the thermal and caloric capacitances, and the inertia or dynamic capacitances. The scaling group of the capacitance term is the ratio of the characteristic response time of the specific change (e.g., of pressure, inventory, temperature, or flow rate) that is governed by the scaled equation (e.g., for depressurization, inventory draining, heating, or cooling, etc.) over the characteristic system reference time of the phase under consideration. If the scaling group of the capacitance term is much smaller than unity, then that specific change is completed very early in the phase. If it is much larger than unity, then the process is nearly a steady-state process relative to the overall system response. If the scaling group of the capacitance term is unity then the characteristic system response time is also the response time of the specific capacitance. Thus, *the causative process related method of scaling reveals with a single scaling group how close a particular change is to steady-state conditions*, and how important the source and flux-related processes, which bring about the change, are relative to the causative process. Finally, the first scaling method implies normalization with respect to a design-specific process, the causative process which turns out to be also controlled in the test facility.

The second scaling method produces the *fractional* scaling or Π -Groups which show the *fractional impact on the time-rate of change* for each source and flux-related process. Every scaling group equals the fractional contribution of the associated phenomenon to the total *time rate of change* of the system-defining state variables, such as pressure, mass inventory, temperature, and flow rate (see Figure 4.3). The fractional method scales, compares, and ranks phenomena directly on the basis of their importance on the system or component changes during a phase.

Both methods serve independently to meet the stated objectives of the reported work, namely to identify important phenomena and scale distortions. Only the fractional scaling method is used in this report for assessing importance and scale distortion because it gives directly the fractional change of state variables brought about by any flux or source-type phenomenon in the overall system and in major components. There is no difference between scaling groups from the two methods if the system reference time is equal to the system or component response time, because the capacity-related Π -Group is then unity. Westinghouse employed the first method in their scaling analysis [16], and INEL the second method [15].

The results are summarized in Section 6.3 and briefly stated here on the basis of the fractional scaling groups obtained from the *fractional* scaling method. Of the 127 *fractional* scaling or Π -Groups evaluated for the five phases with six subphases, and each for AP600, APEX, ROSA and SPES, 75 (or 59%) are found to be associated with *phenomena of*

first-order importance, 39 (or 30%) are of *top priority importance*. The phenomena of *first-order importance* for AP600 are identified by green numbers in the AP600 columns of the Π -Group matrices (tables) in Section 6.2; bold green is used for *top priority importance*. The number of evaluated important global scaling criteria or Π -Groups for any time period or subphase varies between 5 (Subphase 1.2) and 19 (Subphase 2.1).

All important global phenomena are scaled without distortion in at least one of the three test facilities, except for two phenomena:

(1) Flow inertia, or the ratio of inertia over pump forces during the Initial Depressurization Phase (this distortion has no impact on minimum reactor vessel inventory), and

(2) the effect of Reactor Pressure Vessel (RPV) Injection from the Pressurizer (PRZ), during the ADS-4 Blow-down Phase. This distortion does affect the RPV inventory at the beginning of Phase 5 during which the RPV inventory is expected to reach its minimum. APEX has a disproportionately high rate of injection from the PRZ into the RPV which causes also the ADS-4 flow at the PRZ side of the plant to attain low quality. The scale distortion may lead, therefore, to non-conservative simulation of AP600 minimum inventory by APEX, depending on whether the effect of lower-quality discharge through the ADS-4 valve on the PRZ side fails to cancel *during* Phase 4 the beneficial effect from the *initially* greater RPV injection rate from the PRZ. ROSA and SPES simulate the impact on RPV minimum inventory from PRZ injection into the RPV conservatively, because the PRZ injection is negative in ROSA and SPES at the beginning of Phase 4.

Of the 75 first-order important global scaling criteria, evaluated for the five phases with six subphases as fractional Π -Groups for each test facility, 23 (or 31%) show scale distortion for APEX, 21 (or 28%) for ROSA, and 11 (or 15%) for SPES. This assessment is based on the $\{1/2, 2\}$ or factor 2 criterion adopted in Section 4.6. If a lesser $\{1/3, 3\}$ or factor 3 criterion had been adopted, then only half as many scale distortions show for each facility.

APEX has the largest number of, namely 23, scale distortions, but 18 of the 23 scale distortions reduce to five common causes. The leading cause is inappropriate low-pressure scaling. All but 3 scale distortions in APEX are conservative. The most important scale distortion in SPES, which has the fewest distortions, is caused by its disproportionately large structural heat capacities. SPES has only one nonconservative scale distortion. Details on global scale distortions are found in Section 6.3.

The dynamic and quasi-static flow *distributions* in the system, or the *component interactions*, are scaled by the metrics of gravity, flow inertia and flow impedance, respectively. AP600, APEX, and SPES have 4 interconnected flow loops prior to the activation of CMT and PRHR systems (Phase 1), 7 loops prior to IRWST activation (Phases 2 through 4), and 6 loops after IRWST activation (Phase 5). None of the three test facilities simulates flow distribution without scale distortion, except ROSA for normal operation, prior to the break opening (Phase 1).

Section 6.2 presents for the first four phases the total of 158 metric elements of gravity, flow inertia, and flow impedance *distributions* for natural circulation.

While the passive systems, i.e., Core Make-up Tanks (CMT) and Accumulators, are active during Phases 2 to 4, only the gravity metrics are not scale-distorted. The inertia and important impedance metrics of all three facilities are distorted.

APEX has three *inertia* distortions of *minor consequence*. All *impedance* distortions imply greater flow resistance outside the reactor vessel of APEX than of AP600. This causes the coolant to prefer accumulation in the vessel of APEX more than in the reactor vessel of AP600, and the distortions are, therefore, *not conservative*.

ROSA has nineteen inertia distortions, five in the main loops, six in the CMT loops, three in the PRHR loop, two in the PRZ surge line, and three affecting the break flow. None of the inertia metric distortions affect the RPV inventory, even though *nine of the nineteen inertia* distortions in ROSA are, in principle, *nonconservative*. ROSA has greater

flow resistance in the reactor vessel than AP600, which retards the flow into the core and makes the *leading scale distortions* of flow impedance in ROSA *conservative*.

SPES has eight *inertia* distortions, none in the main loops, four *nonconservative* ones in the CMT loops, one *nonconservative* in the PRHR loop, and three *nonconservative* ones in the PRZ surge line. None of the inertia metric distortions affect the RPV inventory, because the flows respond in a very small fraction of the characteristic times of depressurization, inventory change, or thermal response. SPES has much lower resistance in the reactor vessel than AP600, which enhances the flow into the core and makes the leading scale distortions of flow *impedance* in SPES *nonconservative*.

During IRWST and Sump injection, i.e., during Phases 5, only impedance distributions are important because the flow is quasi-steady. The flow in APEX prefers, relative to AP600, to accumulate in the Steam Generators, to leave through the break, and it finds more resistance in the vessel. The ex-vessel impedance distortion is, therefore, *conservative*. However, the steam will vent more readily through the ADS-4 valves, reducing the Upper Plenum pressure and raising the mixture level in the Upper Plenum. The RPV-to-ADS-4 flow resistance in APEX is *nonconservatively* scale distorted. The flow in ROSA is retarded through the break and the ADS-4 valves, and finds it easier to get into the vessel due to five *nonconservative* scale distortions. ROSA loses PRZ inventory more readily through ADS-4. The associated scale distortions are *conservative*. For SPES, impedances are *nonconservatively* scale distorted, because the flows in SPES prefer to escape through ADS-4, to get into the vessel, and have difficulties escaping from the break. The flows prefer to accumulate in the Steam Generators, and have difficulties to drain from the PRZ. The impedances in these flow paths are *conservatively* distorted.

Inertia distortions are important only temporarily during dynamic flow transients, during flow oscillations, and when rapid condensation accelerates the flow. During monotonic depressurization, inertia scale distortions do not affect RPV minimum inventory, because inertia is so small that the flows in all loops respond to control functions and level changes in a very small fraction of the system response time. Impedance scale distortions, however, are important during dynamic flow transients, flow oscillations, and when rapid condensation accelerates the flow, *as well as during quasi steady-flow conditions*, because the flows seek the path of least resistance (impedance).

Previously published Scaling Analyses by INEL [15] and Westinghouse [16] show that they employ scaling methods similar to those in the analysis presented here and that all three scaling analyses are based on the normalization of governing conservation equations and the evaluation and comparison of the resulting scaling groups. However, the results of the INEL and Westinghouse scaling analyses cannot be expected to be equal to the results presented in Chapter 6 of this report, primarily because the first scaling principle stated in Section 4.3 of this report has not been satisfied in their scaling analyses. Consequently, (a) many scaling groups in [15] and [16] are not actually representative of their associated phenomena, and (b) the total number of scaling groups in [15] and [16] is too small as several phenomena are represented by a single scaling group; possible scale distortions remain undetected in [15] and [16].

Instead of demonstrating *quantitatively* what is unimportant, the INEL analysis implies many simplifications, based on *subjective* (unquantified) *assumptions* regarding the importance of phenomena. INEL and Westinghouse failed to account for the differences in coolant volume changes by heating of single- and two-phase fluids. The Westinghouse model has more primary state variables than conservation equations. This means also that INEL and Westinghouse end up with too few scaling groups. INEL used frequently postulated reference parameters and thereby replaced plant-specific design parameters in the scaling groups by numerical values of assumed reference parameters. Westinghouse used frequently experimental or code-computed data as reference parameters. This is shown in Chapter 7 to mislead and to delete plant-specific parameters from the scaling groups. INEL and Westinghouse did not confirm the reference parameters used for the calculation of scaling groups by test data.

Neither INEL nor Westinghouse defined “important” phenomena or “scale distortion.” INEL presents a “Summary of Important Nondimensional Groups by Transient Phase” on Page iv of [15] with the evaluation results of only 15 “important” groups for six phases or subphases. This summary lists groups that vary in magnitude by three orders of magnitude, and INEL does not state why *all* listed groups are considered important. INEL is in agreement with the

results of this report in stating that ADS flows (ADS-123 and ADS-4 flows) and line resistances in IRWST, CMT, and PRZ Surge lines are important. However, there are many more important phenomena (the 15 in the above Summary? [15]). INEL states that only the ratios of ADS-4 over CMT mass flow rates are distorted in APEX (OSU), ROSA, and SPES during the ADS-4 blowdown phase and the ADS-4 flow during the IRWST injection phase, and that otherwise there is no distortion during the IRWST injection and long-term cooling phases. However, the “Summary of Important Nondimensional Groups by Transient Phase” on Page iv of [15] shows significant differences in scaling groups: 4 for APEX, 1 for ROSA, and 3 for SPES. The results from this work, in contrast, indicate that there are 3 *global* distortions in APEX, 1 *global* distortion in ROSA and none in SPES; and that there are *force distribution* metrics distorted: 2 of gravity and 14 of impedance in APEX, 1 of gravity and 20 of impedance in ROSA, and 19 of impedance in SPES. Details of the INEL analysis are given in Section 7.1.4.

Westinghouse evaluated the total of 45 scaling groups. Of the 45 scaling groups evaluated, 31 (or 69%) appear to be important for AP600 by the criterion used in this report. Westinghouse agrees with the results of this report in stating that inertia is small and unimportant, that gravity and flow impedance are important, and that decay heating and steam generator heat transfer are important. By applying the criterion for scale distortion used in this report, one finds that in the Westinghouse analysis [16] 15 and 12 scaling criteria differ in SPES and APEX (OSU), respectively, by more than a factor of 2 from the corresponding AP600 scaling criteria. Details of the Westinghouse analysis are found in Section 7.2.4.

Neither INEL nor Westinghouse have scaled the local *flow distributions* in interconnected loops.

PREFACE

Scaling is essential for the design and operation of reduced-size test facilities for simulating experimentally large systems in nature and industry. Only by satisfying the same scaling criteria in the test facility and the large thermohydraulic system of a nuclear power plant, for example, can one claim that the phenomena occurring in the large and in the reduced-size systems occur in the *same regimes* of transport processes, i.e., of transfer of mass, momentum, and energy. Scaling is also indispensable for presenting in the most compact form possible, then correlating and generalizing, experimental data.

This report presents an application which extends scaling. Scaling is used here to rank the processes taking place in a large and complex nuclear reactor system in the order of their importance to the total system response. Normally, scaling is part of the facility design and done, to meet scaling criteria, prior to the selection of operating conditions. Scaling is used here after the completion of experiments to determine the extent to which scaling criteria had been met.

The scaling analysis presented here is the first application of the scaling methodology published earlier by Wulff [17] who introduced the matrix of scaling groups, the analogy between electric circuits and interconnected flow loops, and the matrices of gravity, flow inertia, and flow impedance forces. This report presents such matrices, but now of numerically evaluated global system scaling groups, and the first evaluation of the nondimensional metrics of gravity, flow inertia, and flow impedance. These metrics are needed to assure similarity of *flow distributions* in the interconnected flow loops of complex systems, as these metrics scale the inertia and impedance coupling between loops and, thereby, the global thermohydraulic interaction between the components in the system.

Scaling analysis is a powerful tool but it has limitations. Scaling provides otherwise unavailable and valuable insight about dynamic system behavior that is derived from comparing the order of magnitude of important nondimensional scaling groups, the magnitudes of characteristic frequencies, response times and fractional changes of system state variables. Scaling affords the *estimation* of trends in system transients and the comparison of different-size systems performances. But scaling is not a substitute for reliable dynamic systems simulation that *predicts* the transient behavior of a system.

ACKNOWLEDGMENTS

The work documented in this report was performed under the auspices of the United States Nuclear Regulatory Commission (USNRC). It was funded by the Reactor and Plant Systems Branch (RPSB), of the Division of Systems Technology (DST), in the Office of Nuclear Reactor Research (RES), under FIN Number W-6670. The program was monitored at the USNRC by David E. Bessette, whose support of this work is greatly appreciated.

The work was performed in the Safety and Risk Evaluation Division (SRED) of the Department of Advanced Technology (DAT) at Brookhaven National Laboratory (BNL). Wolfgang Wulff carried out the modeling in Chapter 5, the scaling analysis in Chapter 6 and Appendices 4 through 8, the assessment of previously published scaling analyses in Chapter 7, and drafted this report. Upendra S. Rohatgi collected and tabulated the plant-specific data in Appendices 1 through 3 and the data references in Appendix 9. The collection of data was an extremely tedious and frustrating effort because there is no single organized, comprehensive source available for consistent *global* system descriptions. The lesson learned from this work is that a national data bank is needed with general access to complete plant data of existing nuclear power plants and related test facilities.

In the course of the work reported here, the authors had the benefit of valuable advice offered during their presentations before the Subcommittee on Thermal Hydraulic Phenomena of the USNRC Advisory Committee on Reactor Safeguards (ACRS), primarily from Drs. N. Zuber, V. Schrock, and I. Catton. Their advice is deeply appreciated. Dr. Zuber's extremely helpful advice for the final editing of this report is acknowledged with great appreciation.

NOMENCLATURE

Symbols

Latin Symbols

A	flow cross-sectional area
C	constant coefficient of normalization
C_0	Zuber-Findlay distribution parameter
c	specific heat of solid
c_p	isobaric specific heat
c_v	isochoric specific heat
D/Dt	substantial (or LaGrangian) derivative
d_h	hydraulic diameter
\vec{E}	vector of directed kinetic energy, Eq. (5-45)
f_p	density function, Eq. (5-25)
f^*	general scaled property function
G	mass flux
g	gravitational constant
g^*	general scaled property function
\vec{g}	gravity vector
H	fixed elevation difference
\vec{H}	vector of directed kinetic energy
h	specific enthalpy
h_c	convective heat transfer coefficient
I	inertia, element of inertia matrix, Eq. (5-24)
\mathbf{I}	identity matrix
\vec{j}_m	vector of mixture volumetric flux
K	form loss coefficient, Eq. (5-23)
k	thermal conductivity
\hat{k}	unit vector in the direction of flow
L	length, moving mixture level elevation
$\mathbf{M} M_j$	loop momentum vector, component of loop momentum vector
MF	momentum flux, Eq. (5-24)
N_B	number of branch points in loop system
N_L	number of loops in loop system
P_{PP}	pumping power
p	pressure
p_1	pressure of the primary system
p_2	pressure of the secondary-side of Steam Generators
\dot{Q}	net rate of heat transfer (heating minus cooling)
\vec{q}	heat flux vector
S_G	nondimensional gravitational metric (vector), Eq. (6-63)
S_I	nondimensional inertia metric (matrix), Eq. (6-62)
$S_k(x)$	unit step function
S_M	momentum induced by phase change and phase separation

S_p	nondimensional impedance metric (matrix), Eq. (6-64)
S_Φ	fluid dilatation
R	resistance factor, Eq. (5-22)
T	temperature
T_l	liquid temperature
t	time
U	total internal energy
u	specific internal energy
V	volume
v	specific volume
$\langle\langle v_{gj} \rangle\rangle$	void fraction-weighted, area-averaged vapor drift velocity
\vec{v}	fluid velocity vector
W	mass flow rate
x	static quality, Eq. (5-61)
x_e	core exit quality
$Y(t)$	general dependent or independent variable
Y_{max}	maximal value of $Y(t)$
Y_{min}	minimal value of $Y(t)$
y^*	scaled general dependent or independent variable
z	axial coordinate
z_k	nonboiling length

Greek Symbols

A	admittance matrix primary block
α, α_v	vapor volume fraction
α_l	liquid volume fraction
α_v	vapor volume fraction
B	admittance matrix secondary block
β_T	isobaric thermal expansion coefficient
Γ_g	equilibrium vapor generation rate
γ	specific heat ratio, isentropic expansion exponent
Δh_{sub}	subcooling enthalpy
ΔMF	change of momentum flux
Δp	pressure difference
Δp_{pp}	pressure difference across a pump
ΔY	range of variable $Y(t)$
$\Delta \rho$	difference between liquid and vapor saturation densities
$\Delta \Phi$	volume dilation, Eq. (5-26)
δp	difference between primary-side and secondary-side pressures
E	impedance matrix primary block
Z	impedance matrix secondary block
ζ	form loss factor, Eq. (5-23)
H	admittance matrix
η	dynamic viscosity
I	inertia matrix, Eq. (5-37)

κ	isothermal compressibility coefficient
Λ	matrix of inertia of primary flow rates
Π	scaling group
\mathbf{P}	impedance matrix
ρ	density
\mathbf{Y}	dilatation vector in terms primary flow rates
\mathbf{X}	matrix of inertia of secondary flow rates
χ_V	mechanical compliance of volume V
Ψ_α	volumetric compliance of two-phase mixture, Eq. (5-12)
Ψ_T	thermal compliance, Eq. (5-18)
Φ	volumetric flow rate
Φ_{j0}^2	two-phase friction multiplier
ω	response frequency

Subscripts

A	PRZ side of AP600
ACC	of Accumulators
ADS	of ADS valve
$ADS-123$	of ADS stages 1 through 3
$ADS-4$	of ADS stage 4
B	CMT side of AP600
b	at bottom of component
bk	break
CE	core entrance section
CL	of Cold Leg
CMT	of Core Make-up Tank
CR, cr	of reactor core
CRE	at core exit
CRI	at core inlet
c	compliance
chr	characteristic
cnd	condensation
$crit$	critical, choked flow
df	drift flux
dr	driving term
drn	draining
e	equilibrium
f	saturated liquid
fg	equilibrium phase change
$form$	form loss
fr	friction
$fuel$	of fuel
G	gas
GR	gravitational
GR, P	gravitational, under forced-flow condition
g	saturated vapor

<i>HEM</i>	homogeneous equilibrium
<i>HL</i>	of Hot Leg
<i>IN, G</i>	inertia, under natural-circulation condition
<i>IN, P</i>	inertia, under forced-circulation condition
<i>IRWST</i>	of IRWST system
<i>i, j</i>	counting indices
<i>inj</i>	injection
<i>LP</i>	Lower Plenum
<i>l</i>	liquid
<i>loop</i>	of loop
<i>k</i>	phase index, $k = l, v$
<i>MC</i>	mechanical compliance
<i>m</i>	two-phase mixture
<i>max</i>	maximum
<i>mean</i>	arithmetic mean
<i>min</i>	minimum
<i>N₂</i>	nitrogen, inert gas
<i>net</i>	net, heating minus cooling
<i>PBL</i>	of Pressure Balance Line
<i>PP</i>	of pumping power
<i>PRHR</i>	of Passive Residual Heat Rejection
<i>PRZ</i>	of, in Pressurizer
<i>p, q</i>	dummy counting indices
<i>pbl-A</i>	pressure balance line on PRZ side
<i>pbl-B</i>	pressure balance line on CMT side
<i>pr</i>	primary, state variable
<i>ps</i>	of flow from primary system to CMT, PRHR
\dot{p}	of depressurization, time rate of change related
\dot{Q}	of heating
<i>q</i>	dummy counting index
<i>RPV</i>	of Reactor Pressure Vessel
<i>RS,G</i>	impedance, under natural-circulation conditions
<i>RS, P</i>	impedance, under forced-circulation conditions
<i>r</i>	rank-reduced
<i>ref</i>	reference parameter
<i>res</i>	fluid residence
<i>sat</i>	saturation
<i>sn</i>	secondary
<i>str</i>	storage
<i>sub</i>	subcooling
<i>T</i>	for temperature change
<i>TC</i>	of thermal compliance
\dot{T}	for temperature change, time rate of change related scaling
<i>th</i>	thermal response
<i>thrcnt</i>	of thermal center
<i>tot</i>	total
<i>UP</i>	Upper Plenum
<i>V</i>	for system volume, inventory
<i>VC</i>	volumetric compliance

v	vapor
w	wall
0	initial, reference
1	primary side
1.2	for Subphase 1.2
1A	from Upper Plenum to PRZ side
1B	from Upper Plenum to CMT side
1 ϕ	single-phase
2	secondary side
2 ϕ	two-phase
$\dot{\alpha}$	of inventory, time rate of change related
Δp	of depressurization
Φ	of volumetric flow rate

Superscripts

\bar{a}	arithmetic mean of a
*	scaled
\dot{a}	time derivative of a
'	derivative with respect to pressure, along the saturation line

Acronyms

ACC	Accumulator
ADS	Automatic Depressurization System
ADS-123	Automatic Depressurization System, Stages 1 through 3
ADS	Automatic Depressurization System, Stage 4
APEX	Advanced Plant Experiment
AP600	Advance Pressurized Water Reactor (600 MW)
BNL	Brookhaven national Laboratory
CMT	Core Make-up Tank
CR	Reactor Core
cl1, 2-A	Cold Legs on Side A
cl1, 2-B	Cold Legs on Side B
DC	Downcomer
DVI	Direct Vessel Injection
hl-A, B	Hot Leg
INEL	Idaho National Engineering Laboratory
IRWST	In-containment Refueling Water Storage Tank
LDC	Lower Downcomer
LPL	Lower Plenum
OSU	Oregon State University
PBL	Pressure Balance Line
PRHRS	Passive Residual Heat Rejection System
PRZ	Pressurizer
RCP	Reactor Circulation Pump
ROSA	Rig of Safety Assessment
RPV	Reactor Pressure Vessel
SG-A, B	Steam Generators (on Side A, B)
SPES	Simulatore per Esperienze di Sicurezza
SRL	Surge Line of Pressurizer
UDC	Upper Downcomer
UHD	Upper Head
UPL	Upper Plenum
US NRC	US Nuclear Regulatory Commission

1. INTRODUCTION

1.1 Background

Westinghouse has designed and submitted for certification the new, simplified 600 MW nuclear power plant with passive safety features: the AP600 [1]. The AP600 is a pressurized water reactor. It utilizes gravity for high- and low-pressure injection of emergency coolant, respectively, from two Core Make-up Tanks (CMT), and from the In-containment Refueling Water Storage Tank (IRWST), and for the passive cooling of the containment building by natural circulation and natural convection. The AP600 relies also on condensation of primary-system steam in a heat exchanger that is submerged in the IRWST. Ultimately, the decay heat is transferred to the atmosphere outside of the containment building, via condensation at the containment shell and via natural circulation in the annular gap of the containment wall. Therefore, the new AP600 contains new safety systems, consisting of new components which are interconnected with conventional components of pressurized water reactors. The new components with their connections are a new challenge to the AP600 accident analysis by currently used computer codes for thermohydraulic systems.

Westinghouse conducted integral system testing for the nuclear steam supply system in *two* integral test facilities to provide experimental data for validating the computer codes which they use for analyzing the performance of the AP600 design, namely in the Simulatore per Esperienze di Sicurezza (Simulator for Safety Experimental Analysis, **SPES-2**) located in Piacenza, Italy [2, 3, 4, 5], and in the Advanced Plant Experiment (**APEX**) facility located at Oregon State University (OSU) at Corvallis [6, 7, 8, 9].

To support the design certification effort, the Division of Systems Research in the Office of Nuclear Regulatory Research (RES) of the US Nuclear Regulatory Commission is conducting independent testing programs at *two* facilities, namely at the Rig of Safety Assessment (**ROSA**) Large Scale Test Facility located in Tokai-mura, Japan [10, 11, 12], and at OSU in the **APEX** test facility.

The coolant volumes of APEX, ROSA, and SPES are 1/192, 1/30.5, and 1/395, respectively, of the AP600 coolant volume. ROSA and SPES have the same height as AP600, while APEX has 1/4-height. Reactor power, flow areas, and flow rates were designed to have the same ratios as the volume ratios for ROSA and SPES. This means, at least in principle, isochronicity for *flow responses* in AP600, ROSA, and SPES. In APEX, however, the reactor power, flow areas, and flow rates were designed to have, respectively, the ratios of 1/96, 1/48, and 1/96. The flow response in APEX is expected to be twice as fast as in AP600, ROSA, and SPES.

There was no comprehensive scaling analysis published for ROSA or SPES prior to the simulation of AP600. Bessette, DiMarzo, and Griffith [13] have analyzed the experimental results from APEX, ROSA and SPES, using selective *local* scaling analysis. The APEX facility design and testing program were based on the scaling analysis by Reyes, Hochreiter, Lau, and Lafi [7].

It must be demonstrated, by a combination of experiment and analysis, that the AP600 safety systems meet the design specification. The certification is, therefore, to be supported by analysis with the RELAP5/MOD3 computer code [14] the capabilities of which are to be assessed by comparison with test results from the three facilities APEX, ROSA, and SPES.

1.2 Objectives of Scaling Analysis

The objective of the scaling effort reported here is to assess the capability of the three facilities APEX, ROSA, and SPES to simulate the *global system response* of the AP600, to the extent that global processes and phenomena taking place in the AP600 will also occur in the test facilities in the same flow and heat transfer regimes as in the AP600, and

1. Introduction

that the global system response in terms of component interactions is the same in AP600 and the test facilities. The scaling analysis concentrates, therefore, on developing the similarity criteria for *global system response* and for the *dynamic interaction between system components*. APEX and SPES have been scaled by OSU and Westinghouse but without consideration of the dynamic component interaction. There is no documentation of global system scaling for ROSA in support of AP600.

The scaling effort reported here had been initiated after the completion of the testing programs of Westinghouse and of the USNRC. Consequently, the results of the this scaling effort had no impact on the design and execution of the testing program, and the scaling objectives are therefore limited here:

- (1) to the identification of the *leading processes and phenomena* responsible for maintaining the *reactor coolant inventory* high enough to keep the reactor core covered and cooled.
- (2) to the quantification of the *scale distortions*, if any, for the leading phenomena and the interpretation of the significance of the scale distortion with regards to minimum coolant inventory and the prediction of minimum inventory by computer code.

The three facilities are to be independently evaluated in terms of their system level scaling to address the issues of relevance, completeness, and possible scale distortion with respect to AP600 of the integral system data base that has been or might be available from the test facilities APEX, ROSA, and SPES. The scaling analysis reported here covers the following 1-inch cold-leg break tests:

Facility:	Test No.:		
APEX of OSU	SB05	conducted on	June 21, 1994 [8, Vol. II],
ROSA	AP-CL-03	conducted on	April 14, 1994 [12],
SPES	S00401	conducted on	May 6, 1994 [5, Vol. I].

The 1-inch break is postulated to appear in Cold Leg B1, between the Reactor Pressure Vessel (RPV) and the Pressure Balance Line (PBL) of the Core Make-up Tank on the side of the plant that does not have the Pressurizer (PRZ), as shown in Figure 1.1.

The US NRC had OSU repeat the 1-inch Cold-Leg Break Test SB05 with the break diameter revised from 0.160 inch in Test SB05 to 0.106 inch in Test NRC-22, the S-signal for tripping natural circulation flow delayed, and the ADS-3 valve size changed to reflect the AP600 conditions better than with Test SB05. When on March 12, 1997 the results of Test NRC-22 were transmitted to BNL, it was decided by the NRC not to restart the evaluation of the scaling groups for APEX, and instead to complete the scaling analysis with the original Westinghouse Test SB05.

The US NRC had contracted earlier a global system scaling analysis for AP600 and the related test facilities APEX, ROSA, and SPES. The analysis was carried out at the Idaho National Engineering Laboratory (INEL) [15]. It concentrated mainly on the last two phases of the transient, namely on the automatic depressurization by the fourth stage of the Automatic Depressurization System (ADS-4), and on the long-term cooling by gravity injection from the In-containment Refueling Water Storage Tank (IRWST) and from the containment sump. Westinghouse performed an AP600 scaling analysis [16] and evaluated the scaling groups for APEX of OSU and for SPES.

It is also the objective of the work reported here to identify the similarities and differences in the methodology and the results of the INEL and Westinghouse analyses, relative to the scaling analysis presented here.

1.3 Organization of Report

This report on System Scaling for The Westinghouse AP600 Pressurized Water Reactor and Related Test Facilities describes generically the system and transient scenario, and presents the results of the scaling analysis but no proprietary information about the AP600 system. The data base for the system scaling report has been submitted to the NRC in a separate document, which contains appendices with the plant-specific information of AP600 and the related test facilities APEX, ROSA, and SPES.

Chapter 2 describes the AP600 System to the extent necessary for the understanding of its global response and of the scaling analysis presented in this report. Chapter 3 presents the five phases of the transient following the appearance of a 1-inch break in the Cold Leg B. Chapter 4 introduces the general scaling methodology that was followed in the work presented here. In Chapter 5 are presented, in general form, the models which serve as the basis for the scaling analysis of all the phases of the transient. This includes the selection or computation of the reference parameters and their important validation on the basis of available test data. Chapter 6 presents first the scaled equations and the scaling groups in symbolic form, followed by the tabulation of their numerical values, arranged in the matrix of Π -Groups. The tabulation serves to identify the relevant processes for each phase and the scale distortions of the three test facilities relative to the AP600. We compare in Chapter 7 the methodology and the result presented in this report with those developed by Idaho National Engineering Laboratory [15] and by Westinghouse [16]. Chapter 8 presents the summary and conclusions.

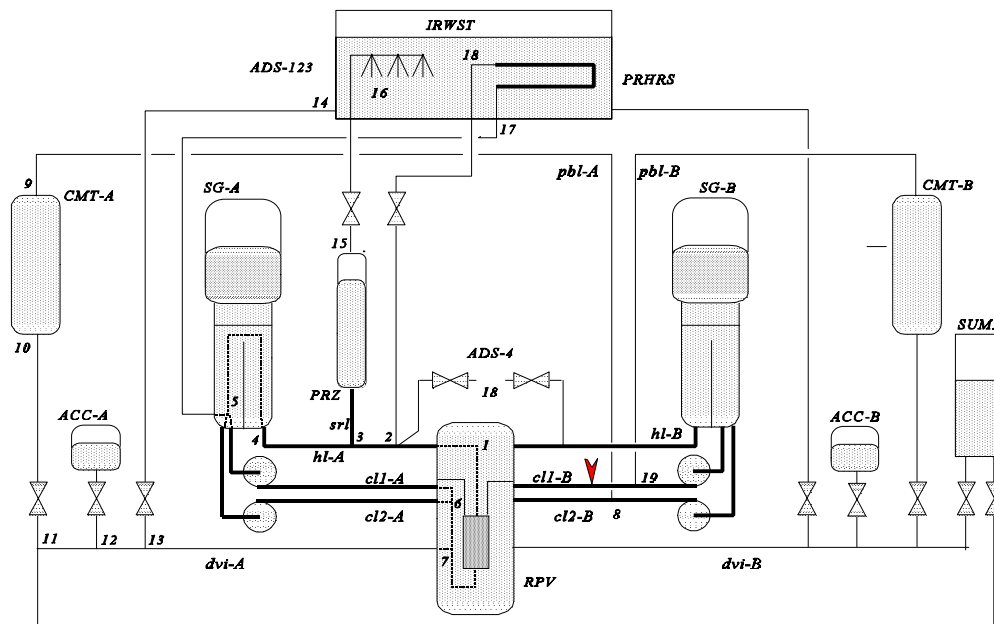


Figure 1.1 Schematic of AP600 Thermal Hydraulic System

1. Introduction

2. AP600 SYSTEM DESCRIPTION

The scaling analysis presented in this report addresses the primary system of the nuclear steam supply system, and the secondary-side of the Steam Generators to the extent that they affect the thermal response of the primary system. All passive safety systems affecting the primary system are modeled. The transient of the containment atmosphere is not modeled and scaled.

2.1 Primary System

The AP600 is a 600 MW(electric) pressurized water reactor power plant with two coolant loops [1]. Figure 1.1 shows the schematic of the AP600 system. The primary system consists of the Reactor Pressure Vessel (RPV), two Steam Generators (SG-A) and (SG-B) on Sides A and B, respectively, of the primary system, of one Hot Leg each between the RPV and each SG, (hl-A and hl-B), the total of four Cold Legs (cl1-A, cl2-A on Side A, and cl1-B, cl2-B on Side B), each with a Reactor Circulation Pump (RCP).

The A-Side of the primary system has the Pressurizer (PRZ), connected to hl-A via the Surge Line (srl). The solid lines in Figure 1.1 show the four loops of normal operation in the primary system, where fission heat is transported from the reactor core in the RPV to the SGs. Not shown in the diagram of Figure 1.1 are the feedwater lines and steam lines leading to and from, respectively, the SGs on the secondary system.

2.2 Safety Systems

2.2.1 Safety Injection Systems

The AP600 relies on *passive* injection of cooling water by *gravity* from elevated reservoirs, i.e., the two Core Make-up Tanks (CMT), the In-containment Refueling Water Storage Tank (IRWST), and the containment sump, and of cooling water from the two nitrogen-pressurized Accumulators (ACC).

At high system pressure (12.8 MPa or 128 bar), i.e., early in the transient and after loss of forced circulation, cold borated water is injected into the reactor core through the Direct Vessel Injection line (DVI), by natural circulation in the loops passing from the Pressure Balance Lines (PBL), through the CMTs and their drainage lines, the DVI lines, and then through the parallel passages either up through the downcomer, then through the Cold Legs and back to the PBL, or down through the downcomer, then through the core, the Hot Legs and Steam Generators (SG) and back through the Cold Legs and into the PBLs. Natural circulation is initiated by the Safety Signal (S-Signal at 12.8 MPa (128 bar)) on system pressure or collapsed liquid level elevation in the Pressurizer (PRZ). The passage through the SGs has the greater flow resistance and depends, therefore, much on the strong driving gravity forces caused by dense borated water and by cooling in the SGs. Of the two passages, the one leading through the core is the intended one because it is the purpose of the system to cool the core and to reduce the fission power by boron injection.

When the pressure has dropped, as the result of the actions from the Automatic Depressurization System (ADS), to the Accumulator pressure of 4.8 MPa (48 bar), borated water is injected by the expanding nitrogen cover gas in the Accumulators. When the pressure has further dropped to approximately 0.2 MPa (2 bar), water is injected from the elevated IRWST which is open to containment pressure. During all this time coolant escapes through interconnected paths out through the break and the valves of the ADS, i.e. the ADS-123 sparger in the IRWST, and the ADS-4 valves discharging directly into containment.

2. AP600 System Description

All safety injection flows from CMTs, Accumulators, and the IRWST must enter the RPV through the DVI lines; safety injection is impossible without at least one intact DVI line.

When break flow, containment condensate, and liquid discharge from the ADS have filled the containment sump to the elevation of the IRWST level, sump valves are opened to permit indefinitely recirculation through the core of containment condensate and liquid discharge from break and the ADS. Decay heat is rejected through the passive containment cooling system.

When IRWST injection begins, the coolant inventory is expected to reach its minimum in the reactor vessel. The issue is, therefore, whether or not there is sufficient coolant in the RPV covering the core. To reject 2% decay heat during the estimated 15 minute-long last stage of depressurization, it requires the complete evaporation of approximately 16,000 kg of water. Adiabatic flashing during the estimated 5 bar pressure reduction converts another 4,800 kg of water into steam. While the total of 20,800 kg of water is available at the beginning of the last depressurization stage, in the CMTs and the Upper Plenum, it must still be determined by experiment and analysis whether (1) the 19,000 m³ of steam being generated by the phase change can escape from the reactor vessel without entraining additionally too much liquid, but fast enough to free space for the liquid to enter and cover the core, and (2) the liquid available outside the vessel prefers to enter the core rather than to accumulate elsewhere in, or to escape from, the primary system.

2.2.2 Heat Rejection System

The S-Signal, which starts natural circulation through the CMTs, also trips the Reactor Coolant Pumps (RCP) and initiates natural circulation through the Passive Residual Heat Rejection System (PRHR). The PRHR accepts hot fluid from the Hot Leg at the A-Side of the primary system, cools or condenses the fluid and returns the cooled fluid or condensate at the exit plenum of SG-A to the A-Loop of the primary system.

2.2.3 Depressurization Systems

To utilize the cooling water in the Accumulators and in the IRWST, the primary system must be depressurized, first to 48.2 bar for Accumulator injection, and then to approximately 2 bar for IRWST injection. The initial depressurization is effected by the break flow. When the liquid inventory in one of the CMTs drops down to 67% of CMT volume ADS-123 is initiated and three sets of valves discharge steam at first and two-phase mixture later through the top of the PRZ, through the submerged spargers in the IRWST where at least partial condensation takes place.

Final depressurization is initiated as soon as the CMT liquid inventory is reduced to 20% of CMT volume in either tank. ADS-4 valves are opened to discharge two-phase mixture from the Hot Legs into the containment.

3. SCENARIO AND PARTITIONS OF SMALL-BREAK LOSS OF COOLANT ACCIDENT

The subject of this report is the postulated small-break loss of coolant transient in the AP600 which is initiated by a 1-inch diameter break in the Cold Leg c11-B as shown in Figure 1.1 on Page 1-3. The system is *depressurized*, first as the result of coolant discharge through the break, and then by discharge through four sets of ADS valves. Figure 3.1 shows schematically the depressurization of the primary system. The reactor is postulated to shut down through automatic scram at the pressure trip set point of 13.2 MPa (132 bar), before the S-Signal occurs at 12.8 MPa (128 bar). Decay heat is removed during depressurization by *natural circulation* of cold water from the CMTs, and by cooling and condensation in the PRHR system. After depressurization, decay heat is removed by *gravity* injection of cold water from the IRWST, and later through heat transfer to the containment.

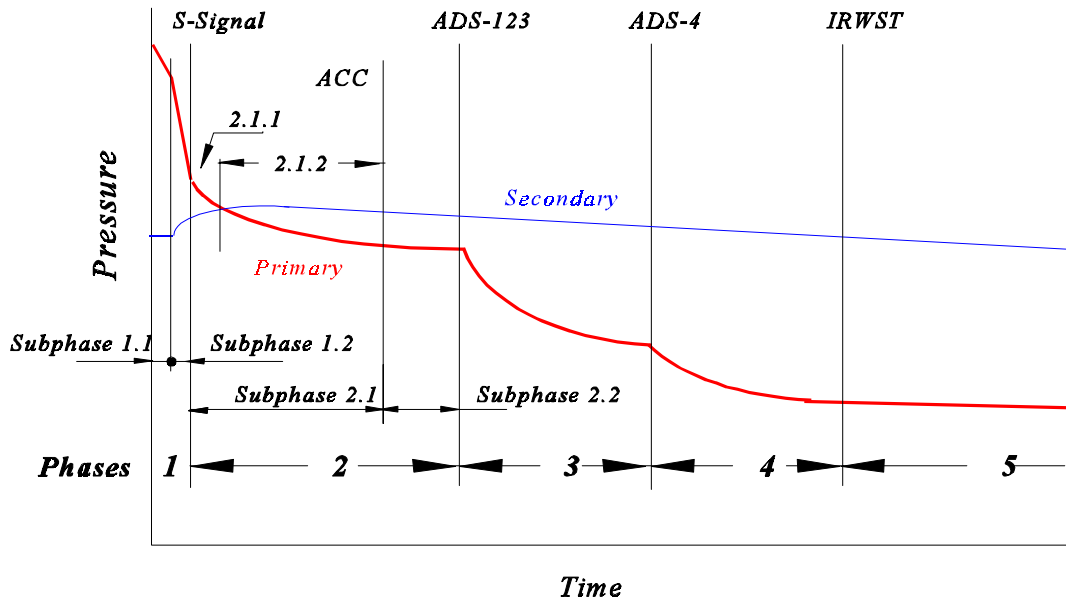


Figure 3.1 Schematic of Depressurization and Phase Sequence

The transient from the initial full-power to long-term heat rejection is divided into five time intervals, called Phases. Each Phase begins and ends at the occurrence of a control function at a designer-specified trip set point, and each Phase is dominated by a specific process or phenomenon [17]. The scaling analysis is carried out and repeated for each Phase, as explained later in Chapter 4. The five Phases are shown in Table 3.1. Table 3.1 presents in the first column the Phase Identification Number, and in the second and third columns the phase initiation and termination criteria. The fourth column lists the system control actions that take place at the beginning of, and possibly during, the respective phase. The fifth column shows the events that are reported by the Idaho National Engineering Laboratory [18, 19] in the Phenomena Identification and Ranking Table (PIRT). The sixth column lists the expected *dominant* processes that are listed in the PIRT.

3. Scenario and Partition of SBLOCA

Table 3.1 Event Summary

Phase	Phase Boundaries		Control Action	Events	Dominant Process	Control Volume Parts		
						Single Phase Liquid	Two-Phase	Single Phase Gas
1	Initial Depressurization							
	start at	155 bar	break flow	PRZ flashing	break flow	Prim. Syst.	PRZ	
				PRZ level dropping		CMT		
				pressure dropping		PRHR		
		132 bar	scram trip	Q_{cr} to 3%				
			turbine trip	temperature drop				
				stronger pressure drop				
				SG secondary pressure rise				
	end at	128 bar	S-Signal trip	PRZ filled with vapor				
2	Passive Heat Removal							
	start at	128 bar	S-Signal trip	PRZ is "empty"	SG Cooling			
			CMT activated	Flow transition to nat. circul.	PRHR natural circul.	Prim. Syst.		
			PRHR activated	pump coast-down		CMT	UHD	
			FW shut off	passive heat removal greater than Q_{cr}		PRHR		PRZ saturated vapor only
			Steam Lines isolated	Stored energy exch. betw. prim. side and isolated SG, SG press. rises over prim. press.			SG	
			RCP trip	CMT circulation disrupted,				
				CMT draining			CMT	
				PRHR goes from convection to condensation			PRHR	
				depressurization accelerates			Primary System	
		48.2 bar	ACC flow initiated			ACC H ₂ O (2/3)		ACC N ₂ (1/3)
	end at	CMT level @ 67%						

Table 3.1 Event Summary (continued)

Phase	Phase Boundaries		Control Actions	Events	Dominant Process	Control Volume Parts		
						Single Phase Liquid	Two-Phase Mixture	Single Phase Gas
3	ADS-123 Blowdown							
	start at	CMT level @ 67%	CMT level trip	rapid depressurization, break flow declining	ADS Flow	2/3 CMT, LPL, LDC	Rest = $V_r + V_g$	N_2
			ADS-1	2 x 4-in diam.		DVI		
		t_3+90 , 120 seconds	ADS-2, ADS-3	additl. 11-in diam opening				
				strong flow into HL				
	end at	CMT level @ 20%		PRZ fills				
4	ADS-4 Depressurization							
	start at	CMT level @ 20%	ADS-4	addl. 2 x 10-in diam orifices	gravity flow	CMT, DC, LPL		N_2
				depressurization				PRHR
	end at	$p = g \rho H_{IRWST}$					Rest of System	
5	Injection from IRWST and Sump							
	start at	$p = g \rho H_{IRWST}$		gravity draining from IRWST	natural circul.	LPL, DC, IRWST, DVI	CR, SRL, PRZ, CL, HL, ADS-4	N_2 : ACC vapor: UHD, SG, CMT, PBL, PRHR
	end at	IRWST & Sump @ same level		circulation through ADS-4 circulation through break				
				circulation through sump passive cooling via containment				

The PIRT ranks, according to expert opinion, all the processes perceived to appear in AP600 system, in the order of their relative importance. Each process evolving in every system component during each phase of the transient is compared with every other process unfolding in the same system component during the same transient phase. The more important process is given a higher rank, and the resulting ranking order is assembled in the Processes or Phenomena Identification and Ranking Table. The systematic ranking of phenomena in accordance with collective expert opinion provides a comprehensive basis for *starting* the analysis, but since the opinions are *subjective*, the ranking

3. Scenario and Partition of SBLOCA

must be *confirmed quantitatively* by the numerical evaluation of global scaling analysis as presented later in Chapter 6 of this report [17].

The last three columns of Table 3.1 indicate how the liquid and gaseous phases of the coolant and nitrogen gas was taken to be distributed throughout the system, using again the PIRT document as a guide.

Below is a description of the five Phases. The reader is referred to Table 3.1.

3.1 Phase 1. Initial Depressurization

Phase 1 begins at full power (nominally 600 MW) and normal operating pressure (15.5 MPa or 155 bar), with the *initiation of the break* flow and ends with the occurrence of the *S-Signal* at 12.8 MPa (128 bar). The break flow causes the depressurization. Phase 1 is subdivided into two Subphases, a phase each before and after reactor scram.

3.1.1 Subphase 1.1 Before Reactor Scram

Before scram, heating in the core and cooling in the steam generators are nearly balanced; there is no significant thermal contraction of the large subcooled liquid in the primary system. The break flow causes depressurization and flashing of the equilibrium two-phase mixture in the Pressurizer. Pressurizer heaters turn to full capacity to compensate for the pressure drop.

3.1.2 Subphase 1.2 After Reactor Scram

Reactor Scram is tripped at 13.2 MPa (132 bar, 1900 psig) [19] and turns off fission power. Core heating drops to decay heating at 3% of full power. The Steam Generators operate still at the normal temperature difference between primary and secondary sides. The resulting imbalance between normal-power cooling in the Steam Generators and the small decay heat of 3% of normal power causes the large volume of subcooled liquid in the primary system to shrink. This affects the system elasticity (by 11%, depending on the vapor volume in the Pressurizer) and increases the rate of depressurization and flashing in the Pressurizer. The liquid in the Pressurizer flashes and drains into the primary system, to compensate for liquid contraction and liquid loss through the break. Phase 1 and Subphase 1.2 terminate with the occurrence of the *S-Signal*.

3.2 Phase 2. Passive Heat Removal

Phase 2 begins when the *S-Signal* is tripped at the specified trip set point pressure of 12.8 MPa (128 bar, 1850 psig) [19] and it ends when the collapsed liquid level in at least one of the Core Make-up Tanks (CMT) reaches the designer-specified 67%-volume mark and thereby trips automatic depressurization.

At the *S-Signal*, valves are opened (see Figure 1.1) to permit natural circulation through the CMTs and the Passive Residual Heat Rejection System (PRHR), the Reactor Coolant Pumps (RCP) are tripped off, and the Steam Generators (SG) are isolated by closing off the steam lines and the feedwater lines. Passive heat rejection by natural circulation through CMTs and PRHR is the dominant process and described in Section 2.2.1. PRHR cooling power exceeds at first core heating. Before the initiation of ADS, the Accumulator valves open at the pressure set point of 4.82 MPa (48.2 bar, 700 psig) [19, p. H-5).

Phase 2 is subdivided into two Subphases of which the first one is subdivided again as follows:

3.2.1 Subphase 2.1 Before Accumulator Injection

This partition is needed because the system elasticity changes at the moment the Accumulator valves are opened at the pressure set point of 4.82 MPa (48.2 bar, 700 psig) [19, p. H-5], because of the addition of the nitrogen gas volume to the primary system volume. Subphase 2.1 is partitioned into two parts, according to the steam generator action, as follows:

3.2.1.1 Steam Generators as Heat Sink

The two-phase mixtures in the isolated Steam Generators (SG) are being pressurized by isochoric heating from the primary side and act, therefore, as intensive heat sinks of the primary system. This phase begins with Phase 2.1 and ends when the pressures of primary and secondary sides are equal at the “cross-over point” shown at the intersection of the blue and red curves in Figure 3.1.

3.2.1.2 Steam Generators as Heat Source

The Steam Generators remain, beyond the cross-over point, for the primary side a heat source through the duration of Phases 3, 4, and 5. The fluid on the SG secondary side undergoes isochoric depressurization due to cooling by heat transfer to the primary side and the containment.

3.2.2 Subphase 2.2 After Accumulator Injection

Subphase 2.2 starts at the design pressure set point of 4.82 MPa (48.2 bar, 700 psig) [19, p. H-5], when the pressures in Accumulator and primary system are almost equal, and it ends when the automatic depressurization is initiated at the beginning of Phase 3. Borated water is pushed out from the Accumulators, through the Direct Vessel Injection (DVI) lines (see Figure 1.1) into the primary system at the rate at which the break flow makes room; this means that the discharge rates from the break and the Accumulators differ only by the volume dilatation in the primary system and can be determined entirely without predicting the pressure drop across the Accumulator valves.

3.3 Phase 3. ADS-123 Blow-Down

The Automatic Depressurization System (ADS) is designed to reduce the primary system pressure until it is possible to drain water by gravity from the In-containment Refueling Water Storage Tank (IRWST) into the Reactor Pressure Vessel (RPV) (see Figure 1.1). The first three valve banks, ADS-123, discharge fluid from the top of the Pressurizer (PRZ) through submerged spargers into the IRWST.

The ADS-123 Blow-Down Phase begins when the collapsed liquid level in at least one of the Core Make-up Tanks (CMT) reaches the designer-specified 67%-volume mark and ends with the initiation of the fourth ADS stage when the collapsed liquid level in at least one of the CMTs reaches the designer-specified 20%-volume mark [19]. The flow rate through the ADS-123 valves dominates all other processes during Phase 3.

ADS-2 and ADS-3 valve banks are tripped open with a 90 and 210 second delay, respectively, after the opening of the ADS-1 bank. However, these three events are modeled in the scaling analysis as one event, since the 210 second time span is short compared to the 10^4 second long transient.

3. Scenario and Partition of SBLOCA

3.4 Phase 4. ADS-4 Depressurization

The ADS valve bank to be tripped last, the ADS-4 valves, discharge fluid from both Hot Legs through stand pipes directly into the containment (see Figure 1.1). The liquid portion of the ADS-4 (and break) flow ends up in the containment sump and becomes eventually available for recirculation through the RPV at the later part of Phase 5. The vapor portions from ADS-4 and break flows condense on the containment shell through the passive containment cooling system and return, via gutters, into the IRWST, from where the condensate is also available for long-term cooling.

Phase 4 begins when the collapsed liquid level in at least one of the CMTs reaches the designer-specified 20%-volume mark and it ends when the primary system pressure can be overcome by the gravity head in the IRWST to allow gravity draining from the IRWST via two DVI lines into the RPV (see Figure 1.1).

Fluid is being discharged during Phase 4 also from the break and through the ADS-123 valves. Near the beginning of Phase 4, the ADS-123 flow becomes subsonic, and the ADS-123 flow is approximated for the scaling analysis by the largest possible subsonic flow at the ADS-123 valves.

3.5 Phase 5. IRWST and Sump Injections

The IRWST and the Containment Sump provide in Phase 5 long-term cooling indefinitely. Water is supplied first from the elevated IRWST, passes via the DVI lines through the RPV and into the containment, primarily through the ADS-4 valves and the break. The CMTs and Accumulators are empty and isolated from the primary system by check valves. Vacuum breakers prevent back flow from the IRWST into the PRZ via the submerged spargers in the IRWST. The pressure at the PRZ top equals the containment pressure, and the PRZ provides water initially to the primary system.

Phase 5 begins when the primary system pressure can be overcome by the gravity head in the IRWST to allow gravity draining from the IRWST via two DVI lines into the RPV (see Figure 1.1). Phase 5 goes on indefinitely. Phase 5 is dominated by IRWST drainage. When the liquid levels in IRWST and sump are at the same elevation (above the elevation of the Hot Legs) then the sump valves open, making IRWST and sump one reservoir. Natural circulation continues indefinitely through the DVI lines, the RPV, and ADS-4 valves, thereby removing the decay heat.

3.6 Closing Remarks on Partitioning of Transient

It is important to realize the need for breaking up the transient in preparation for the scaling analysis. The development of PIRT [18] hinges on the partitioning of the complex transient into simpler time segments. Scaling requires this simplification also.

The first four phases are dominated by *depressurization* which, in turn, is caused by distinct processes: break flow, coolant thermal contraction, ADS-123 flow, and ADS-4 flow. The last phase is dominated by *gravity drainage*.

The partitioning is needed because the ranking of all the processes taking place during the entire transient must be achieved by comparing these with the dominant process in each phase and then the importance of the phases relative to each other [17]. Moreover, the conditions must be estimated for the beginning of each phase to obtain the reference parameter for normalizing the conservation equations. This estimation is possible only with reliable information about the changes that have taken place previously, information which is not accessible without having estimates for time segments which are governed by a single process in the previous phase.

3. Scenario and Partition of SBLOCA

The key issue is RPV coolant inventory, and it has been argued that Phase 4 with ADS-4 Depressurization is initiated by an *inventory signal*, i.e., the smaller inventory of the two Core Make-up Tanks, and that therefore (1) the system pressure at initiation of Phase 4 with ADS-4 Depressurization and (2) Phases 1 through 3 leading up to Phase 4 with ADS-4 Depressurization are unimportant for the RPV inventory at the end of Phase 4. However, the system pressure at the start of Phase 4 with ADS-4 Depressurization is affected by the heat transferred to the primary-side coolant during Phases 1 through 4, and then dominates the ADS-123 and ADS-4 valve discharge flows. Consequently, the system pressure prevailing at the start of Phase 4 is important.

3. Scenario and Partition of SBLOCA

4. SCALING METHODOLOGY

The scaling analysis for the AP600 presented in this report follows the methodology of thermohydraulic systems scaling presented earlier by Wulff [17]. This methodology serves to establish the scaling criteria of global system response and component interactions for relating integral, full-size industrial to reduced-size test facilities. It serves specifically the objectives of this work as stated in Section 1.2, namely (1) to identify the *leading processes and phenomena* that govern the system depressurization and long-term cooling of the AP600 (see Chapter 3), and (2) to quantify the *scale distortions*, if any, for the leading phenomena and to interpret the significance of the scale distortion with regard to core cooling, and to the capability of predicting the minimum coolant inventory by computer code.

4.1 Top-down and Global System Scaling

Scaling of the global system response is the first "top-down" step in the hierarchical two-tiered scaling methodology developed by Zuber [20]. The top-down scaling starts with scaling the *entire system as a whole*. Since no part of the system is excluded, top-down scaling provides the *comprehensiveness* of the scaling methodology. Since no part of the system is excluded, *no claims or assumptions about such exclusions need to be justified* by additional order-of-magnitude estimations, and top-down scaling provides therefore the *efficiency* of the scaling analysis.

As pointed out by Zuber [20, p.41], the top-down scaling approach in the hierarchical two-tiered scaling methodology proceeds from the whole system to the system components, to constituents, to phases, and fields. It yields one scaling group for every transfer process between media at every level in the system's hierarchy, such as system components, constituents, phases, or fields, etc. This report addresses the top-down scaling part of the hierarchical two-tiered scaling methodology on the global AP600 *system level* and on selected component levels for the primary system, the CMTs, PRHR, PRZ, the Accumulators, and the IRWST of the AP600 and its related three integral test facilities APEX, ROSA, and SPES. The results of the analysis provide the rational framework for the bottom-up or "traditional" component- and subcomponent-level scaling by directing it toward the components in which the most important processes evolve.

4.2 Scaling Criteria

Two facilities of different sizes are scaled and similar if *one* solution to a system of scaled equations describes the transient responses of *both* facilities in terms of the *same* scaled (normalized) time and scaled state variables. Scaled state variables (see Eq. (4-1) in Section 4.4.4), including initial and boundary conditions, and scaled times of the two facilities, and the constant coefficients in the scaled governing equations, which are the *nondimensional* scaling or Π -Groups, (see Eqs. (4-2) and (4-3) in Sections 4.4.5.1 and 2, respectively) must be common to both facilities. Similarity may exist between two facilities of different media, such as between a hydraulic system and its electrical analogue.

The scaling analysis yields for the AP600 and each test facility a separate set of numerical values from the evaluation of the Π -Groups. *Scaling criteria* are the requirement that for AP600 similitude of the APEX, ROSA, and SPES facilities their Π -groups must have nearly the same numerical values as the corresponding Π -Group of the AP600, at least for the dominant phenomena, and that scaled constitutive relations are the same for both systems (law of corresponding states).

In contrast to the *scaled time- and space-dependent variables*, y^* , scaling groups, Π , are *constants*, formed from specified fixed geometrical and controlled operating parameters, such as initial conditions and thermophysical properties at initial conditions. There is one and only one group for each transfer process or phenomenon taking place in the system. *Partial similitude* is achieved when the scaling groups of *dominant phenomena* are matched in AP600, APEX, ROSA, and SPES.

4. Scaling Methodology

4.3 Principles of Scaling

Scaling groups can be derived by several methods, as explained in Reference [20]. Here they are derived by normalizing the equations of the mathematical models for the system and its components. The equations are the mass, energy, and momentum conservation equations, the thermal and caloric equations of state for the *global system* and selected components, and constitutive relations for heat transfer, wall friction, form losses, and phase change. The normalization meets two important principles of scaling [17]:

- (1) The governing equations are *normalized* such that the *normalized variables, y^* , and their derivatives with respect to normalized time and space coordinates are of order unity* and the *magnitude* of each term of the normalized conservation equation is *measured by its constant, normalizing factor, C* . The factors, C , are storage rates (of mass, momentum, or energy) on the left-hand side (factored out from the time-derivative term) and flow rates (of mass, momentum, or energy) on the right-hand side of the conservation equation; all factors, C , in an equation have the same dimension. This fundamental principle of normalization renders the magnitude of the constant normalizing factors, C , and, consequently, of the resulting scaling groups, or Π -Groups, representative of the magnitude of their respective terms.
- (2) The governing equations are then *scaled* by dividing the equations through one of their constant normalizing factors. The division produces for an equation of m terms ($m - 1$) nondimensional scaling or Π -Groups which, being different from unity, form the ($m - 1$) *scaling criteria* of the scaled equation. The second principle affords simplicity and flexibility, i.e., the largest number of design and operating parameters in the smallest number of potential scaling requirements, and it provides a basis for convenient interpretation.

One could, in principle, divide, and scale, an equation by anyone of its constant normalizing factors as reference. The choice of reference is determined by the purpose of interpreting the resulting Π -Groups. The choice has no impact on the ranking of processes and the assessment of scale distortions. Two choices were made in this scaling analysis because of their specific advantages.

The first choice is to divide the governing equation by the constant normalizing factor of the *causative term*. This choice renders the Π -Group of the causative process to be unity ($\Pi = 1$ for the causative or reference term) and provides for all the other terms in the equation Π -Groups which *measure the magnitudes of their respective terms relative to the causative term*, and therewith the importance of the associated transfer processes relative to the causative process. See Eq. (4-2) for the form of a governing equation scaled by the causative term.

The causative term represents the *causative process*, that transfer process appearing on the right-hand side of the conservation equation which initiates the change for its control volume during a phase of the transient. Typically, the break flow, the valve discharge flow through the Automatic Depressurization System, or the heat transfer at the Passive Residual Heat Rejection System are causative processes.

The change in a control volume is, in general, described by a set of mass, energy, and momentum conservation equations. The causative process will affect the storage of mass, energy, and momentum. The *causative process* will be the *dominant process* for the change of mass, energy, or momentum in a control volume, but it does not have to be the dominant process for all changes.

The *dominant process* must be scaled with top priority. The dominant process is the transfer process the term of which is on the right-hand side of the equation and has the largest normalizing factor and therefore the largest Π -Group on the right-hand side of the scaled equation. The dominant process causes, at least initially in a phase, the greatest change for a state variable of the control volume. It is the most important process, unless it lasts only a short fraction of the characteristic time of the phase (causing a short, insignificant spike) and is overpowered by a lesser but longer-lasting transfer process. Scaling analysis provides information only for the start of a phase. Simulation (integration of the conservation equations) is needed to determine rapidly changing trends. The process dominance is decided, therefore, on the basis of Π -Groups only.

One could scale every conservation equation with the normalizing factor of its dominant term, or one could scale the set of governing equations with their common causative term for the phase of the transient. The ranking of processes and the assessment of scale distortion would be *the same* for either choice, if only the same choice is used for all facilities. In the scaling analysis reported here, we have used the causative term and we call the method the causative process related scaling method. Since the experiments in the AP600 related test facilities had been completed before the start of the scaling analysis, it was found that the causative processes are more than other transfer processes controlled by design and operation of the test facilities, and therefore suitable as the reference for comparing and ranking processes, and for assessing scale distortions.

For a single conservation equation, one obtains its characteristic response time by defining the Π_c -Group of the equation's time-derivative (capacitance term) as unity. Thus, the number of *causative term*-related scaling criteria can be reduced further to $(m - 2)$, but only if there is no need to refer to a common system response time for *all* the governing equations. This is discussed in Section 4.4.5.1. The specific advantage of the causative-process related scaling method is described in Section 4.4.5.1.

The second choice is to divide the governing equation by the *constant normalizing factor of the capacitance term* (or storage term, i.e., the time-derivative term) on the left-hand side of the conservation equation. This provides for all the other terms (on the right-hand side) in the equation Π -Groups which *measure directly the fractional contributions of their respective processes to the time-rate of change* of that state variable (pressure, mass inventory, temperature, or flow rate) which is governed by the equation. Each Π -Group in the scaled equation is the fraction of the total change in the control volume that is caused by the corresponding source within, or the corresponding flux across, the boundaries of the control volume. Thus, the second method is called the *fractional scaling method* and produces the *fractional scaling* or Π Groups. See Eq. (4-3) for the form of a governing equation scaled by the fractional scaling method. The magnitude of the fractional Π Groups also exhibit the importance of the associated transfer processes. The specific advantage of the fractional scaling method is described in Section 4.4.5.2.

The two scaling principles yield scaling groups which characterize their respective processes with the smallest possible number of potential scaling requirements. At the same time, by combining the largest possible number of design and operating parameters into each scaling group, they provide to the experiment designer and the experimenter the greatest flexibility for meeting the scaling requirements. As demonstrated in [17], the two important principles explained above are indispensable for associating *relative importance* of phenomena or transfer processes with the *magnitude of their respective nondimensional Π -Groups*. The consequences of not heeding these principles are very serious:

- (a) Every rate of change (*storage process*) and transfer of mass, momentum, and energy (*transport process*) is associated with a normalized variable, y^* , or a product of normalized variables, and a Π -Group.

Unless all the terms in the equation are *individually* normalized such that *every* normalized variable, y^* , and its derivative, are of order unity (reaching, without exceeding, during the phase of a transient the limits between -1 and +1), the associated Π -Groups fail to represent the magnitudes, and cannot characterize the significance, of *all* its corresponding processes (see [15], pp. 24-26; 28, 29, 32).

- (b) Processes which are not scaled *individually* so as to satisfy the above scaling principle cannot be assessed regarding their relative importance (for examples see [15], pp. 24-26; 28, 29, 32).

The success of satisfying the requirements of Scaling Principle (1) depends entirely on one's capability to estimate reliable reference parameters for normalizing the terms in the conservation equations. Fortunately, the large majority of reference parameters is secured directly by design specifications and specified operating conditions. Some estimations of reference parameters require assumptions about heat transfer and flow regime modes. When there are no experimental data available, one may have to normalize a term with two or more potentially valid reference parameters, each representing a different but unknown flow or heat transfer mode. One may then have to continue the scaling analysis and its application conditionally with all alternatives until later all but one alternative are

4. Scaling Methodology

eliminated, most likely through subsequent experimentation or possibly by analysis. In the work presented here, we have taken advantage of available test data to confirm the estimation of reference parameters.

4.4 Scaling Approach

The scaling analysis presented in this report addresses the AP600 global system response and component interactions that follow a Cold-Leg break. The transient scenario is divided into five phases and six subphases, as explained before in Chapter 3. Up to two pressures, two liquid inventory levels, three liquid temperatures (or enthalpies), and seven flow rates, are used as state variables to describe the global system and its component interactions in a (sub)phase. The state variables are:

for Phase 1, initial depressurization:

the pressure p_1	of the primary system (consisting of all the components communicating during Phase 1, and their connecting lines), each before and after scram,
the liquid volume fraction α_l	in primary system (i.e., in Pressurizer (PRZ)),
the liquid temperature T_l	of subcooled liquid in primary system, and
the mass flow rates W	in each cold leg (4);

for Phase 2, passive heat rejection:

the pressure p_1	of the primary system (consisting of all the components communicating during Phase 2, and their connecting lines), each before and after accumulator injection,
the pressure p_2	of the secondary side of the isolated steam generators,
the liquid volume fraction α_l	in primary system (primary system inventory),
the liquid temperatures T_l	of subcooled liquid in primary system and, individually, in Core Make-up Tanks (CMT), and in Passive Residual Heat Rejection (PRHR) system, and
the mass flow rates W	in each cold leg (4), in CMT (2), and PRHR system;

for Phase 3, ADS-123 blow-down:

the pressure p_1	of the primary system (consisting of all the components communicating during Phase 3, and their connecting lines), each before and after accumulator injection, and
the liquid volume fraction α_l	in primary system (Pressurizer and Core Make-up Tank) inventory;

for Phase 4, ADS-4 depressurization:

the pressure p_1	of the primary system (consisting of all the components communicating during Phase 4, and their connecting lines), each before and after accumulator injection,
the liquid volume fractions α_i	in primary system (primary system inventory), Reactor Pressure Vessel (RPV), CMTs, and PRZ, and
the subcooling enthalpy Δh_{sub}	at the core entrance;

for Phase 5, IRWST and sump injections:

the liquid inventory (level L)	in RPV, PRZ, and IRWST,
the liquid enthalpy hl	of the Downcomer (DC) and Lower Plenum (LPL),
the mixture enthalpy h	at the reactor core exit, and
the mass flow rates W	from IRWST, PRZ, ADS-4/A and B and the break.

The method of scaling is consistently applied to all five phases of the transient. It is described here in the following five steps which are common to the scaling for each phase:

4.4.1 Identification of Control Volume

It was pointed out in Section 4.3 that the scaling criteria are derived in the present work by normalizing the mass, momentum, and energy conservation equations. The first step of the scaling process for a phase of the transient is to identify the control system and to apply it consistently for every conservation equation. For mass and energy conservation, the control system is a volume, called the *control volume*. For the momentum equations, the control system is a link of momentum control volumes, called the *loop* or *loop system*. Forces are first balanced on control volumes of constant cross-sections, and the forces exerted by the fluid channels on the fluid are introduced in the links between the momentum control volumes as described in detail in [17]. Inertia, gravitational, and flow resistance forces are expressed as pressure differences. Internal fluid pressures at component interfaces cancel out in the resulting loop momentum balance. Flow velocities are replaced by volumetric flow rates because these are continuous across flow area discontinuities.

As stated in Section 4.1 the control system (volume or loop system) encloses the entire primary system for the global system scaling. This includes, for the depressurization equation derived from mass and energy balances, all the components that can communicate (by pressure signal) even where closed valves disallow through flows. Specifically, the volumes of the CMTs and the PRHR system are part of the control volume of the primary system for mass and energy conservation even before the S-Signal activates natural circulation through CMT and PRHR. On the other hand, the flow passages through CMTs and PRHR are not part of the loop system for the momentum balance until the CMT and PRHR valves are open.

The entire boundary and interior of the control system is scrutinized to include all fluxes and every storage of mass, momentum, or energy. The specific control systems are presented in Figures 5.2 through 5.4 of Section 5.4.1 for mass and energy conservation, and in Figures 5.5 through 5.7 of Section 5.4.2 for momentum conservation. There are no simplifying assumptions implied in the definition of control systems or in the application of the conservation equations. Assumptions are implied only in the distribution, over the control volume and at the beginning of a phase, of subcooled liquid, two-phase mixture, superheated vapor, and noncondensable gases, and in the estimation of reference parameters.

4. Scaling Methodology

4.4.2 Model Derivation

The modeling technique used for the global scaling analysis presented here is the same as published earlier by Wulff [17]. With the control system identified, the second step is to write the global conservation equations, either directly for the system, or first for parts of the system which are then combined for the system. The conservation equations are written for parts of the system if it consists of regions of differing fluids, such as regions of subcooled liquid, superheated vapor, equilibrium two-phase mixture, or perfect gas. The identification of regions and the associated selection of intrinsic constitutive relations for material properties introduces the first kind of modeling assumptions which are amenable to confirmation by experiments. Specific model descriptions and assumptions are presented later in Section 5.4.

4.4.3 Selection, Calculation, and Validation of Reference Parameters

The great importance of selecting or estimating reliable reference parameters which render the normalized variables, y^* , to be of order unity was explained in Section 4.3(b). It is also important to note that only *fixed and known*, or *fixed and controllable* parameters, Y_{max} and Y_{min} , or ΔY , may be used as reference parameters (see Eq. (4-1) below) for normalizing the variables. The parameters used in this work are only those known from the given *geometric design*, the given selection of materials and their *properties*, from given *initial* and *operating conditions*, such as the specification of trip set points.

The third step in the process of scaling, that is, the collection of plant-specific design parameters (for geometry, initial and operating conditions) turned out to be an extraordinary chore because there is no single comprehensive source available for consistent *global* system descriptions. Many data are reported in different documents and in conflict with related published data (see the variation of reported ADS valve size specifications in Appendix 9). Global data, primarily for form losses, had to be assembled from local (detailed) data. Data are needed that are specific to the system topology, as determined by the location of branch points, but data are reported invariably specific to the location of instrumentation. Cooperation is needed in the future between analysts and experimenters who reduce and report data.

Reference parameters which are not specified by design and, therefore, not known directly, are determined either for initial conditions from the steady-state balance equations, or for the starting conditions of the second and later phases from the transient modeling equations that are also used for scaling. In any case, reference parameters are expressed in terms of directly known design parameters since they must characterize appropriately the AP600 or the respective test facility.

This determination of reference parameters introduces the second kind of modeling assumptions which are amenable to confirmation by experiments. Experience showed that, in general, computed reference parameters failed to agree with test results, not because of modeling errors, but because of errors in reported data. These errors had to be resolved before agreement could be achieved with test data. Specific model descriptions and assumptions are presented in Section 5.4. Table 5.15 in Section 5.5.5 presents the parameter comparison with available experimental data to confirm the reference parameters by experiments.

4.4.4 Normalization of Modeling Equations

The global conservation equations for the AP600 system are normalized, in the fourth step of the scaling process, first according to Principle (1) stated in Section 4.3: each variable $Y(t)$ in the equations is normalized with the aid of the reference parameters obtained in Step 3 above. More specifically, each variable is reduced by an estimate of its expected minimum Y_{min} , and then divided by an estimate of its range $Y_{max} - Y_{min} = \Delta Y$, so that the scaled variable

$$y^* = \frac{Y(t) - Y_{min}}{Y_{max} - Y_{min}} = \frac{Y(t) - Y_{min}}{\Delta Y} \quad (4-1)$$

measures the *fraction* of the expected change of Y , between approximately 0 and 1¹. For monotone (depressurization) transients, Y_{max} is for most variables their initial value Y_0 , and Y_{min} may be the estimated (asymptotic) end value, or 0. Should the variable exceed its initial value, Y_{max} is the highest set point of the variable that causes the reversal of the rising trend of the variable. We point out that the normalized variable, y^* , does not have to reach the magnitude of 1 exactly, but only sufficiently close to pass the magnitude of the respective term on to the constant normalizing normalizing factor.

It must be recognized that *normalization of the governing (conservation) equations does not affect their validity, even if the normalization fails to meet Scaling Principle (1)* as stated in Section 4.3. From this follows as important corollary that the display of agreement (collapsing of data) between scaling groups or normalized variables from different experimental facilities cannot reveal whether or not the *correct* reference parameters for scaling have been chosen which render the normalized variables of order of magnitude 1. For this purpose, one must confirm that the history $y^*(t)$ of the scaled *variables* spans the entire range from 0 to 1, but does not exceed it. One can also test the *model* with test data, either in scaled or in unscaled form but not the *scaling process*.

While the global conservation equations are universally valid, the need to estimate *parameter magnitudes* and to select reference parameters Y_{max} and Y_{min} for their normalization is the compelling reason for the need to distinguish between different operating modes or phases of a transient.

4.4.5 Scaling of Conservation Equations and Scaling Criteria

The fifth and final step in the scaling process is the scaling of the conservation equations according to Principle (2) in Section 4.3. Two useful methods of scaling the conservation equations are described in Section 4.3 and have been employed in this work. The methods differ in the use of the reference term for scaling the equation. The reference term is crucial for the comparison of facilities. Each scaling method provides its distinct advantages for interpreting the scaling groups. These are described in the next two subsections.

4.4.5.1 Conservation Equations Scaled on the Basis of the Causative Process

The first method explained in Section 4.3 is the scaling method *by causative processes* and provides the *causative process related, scaled conservation equations* with the *causative process related Π -Groups*. The first scaling method is called the *causative process related* method because the causative term in the equation, which represents the causative process, is the reference for assessing the importance of all other terms in the equation. The causative process initiates the transient of a phase. The causative process dominates some but not all changes during the phase of a the transient. The associated causative term is the dominant term in some but not every governing equation for the phase. The processes causing the system depressurization are the flows through the break, through the first three Automatic Depressurization System (ADS) valves, and the fourth-stage ADS valves. The discharge flow from the In-containment Refueling Water Storage Tank (IRWST) is the causative process during long-term cooling.

The form of the conservation equations scaled on the basis of its *causative process* is

$$\Pi_c f^*(y^*) \frac{dy^*}{dt^*} = \sum \Pi_i g_i^*(y^*) y_i^* + y_{cs}^* \quad (4-2)$$

¹In scaling for analogue computers or digital computers with fixed-point arithmetic, one scales often for the range of $-1 \leq y^* \leq +1$. This option is not used here because of additional complexity for the scaling groups.

4. Scaling Methodology

where f^* and g^* are, in general, scaled material property functions (some of which may be unity), and the summation is over all terms but the causative term (subscript cs) of the conservation equation. The magnitude of each *causative process related* Π -Group reflects the importance of the associated process relative to the causative process whose Π -Group has the value of 1. The identification of the causative process and the associated *causative term* for each equation has been discussed in Section 4.3.

The *causative process related* Π -Groups on the right-hand side of Eq. (4-2) are ratios of flow rates or of fluxes, namely: of volumetric flow rates for the depressurization equation, mass flow rates for the inventory balance equation, energy flow rates for the energy conservation equation (to describe temperature changes), and momentum fluxes (pressure differences) for the system of loop momentum balances. The electrical analogue to the flow rates and fluxes would be the current proportional to the reciprocal of Ohmic resistance.

The time-derivative term on the left-hand side of Eq. (4-2) is the storage term for the control volume of the scaled equation. It is associated with the volumetric, mechanical, or thermal, compliance or dynamical inertia, depending on whether the equation describes the rate of change, respectively, of mass inventory, pressure, temperature, or flow rate. The corresponding scaling group is the Π -Group of compliance, Π_c , in Eq. (4-2).

By setting Π_c in Eq. (4-2) equal to $\Pi_c = 1$, one determines the characteristic response time, t_{chr} , of the control volume for which the scaled equation is written. The characteristic response time is the characteristic drainage time, the thermal re-
sponse time, or the characteristic depressurization time, depending on whether the equation describes the change of inventory, stored energy, or pressure, respectively. Figure 4.1 shows the initial slope of the monotonic decrease of the scaled state variable from $y^* = 1$, in the scaled characteristic response time, $t_{chr}^* = t/t_{chr}$, of the control volume. Every control volume has one characteristic response time each for depressurization, and for the changes of inventory, temperature, and flow rate. To unify all responses during a phase, a single reference time, t_{ps} , of primary system response is used in the scaling analysis reported here. The scaled system time $t^* = t/t_{ps} = t_{chr}^* \cdot t_{chr}/t_{ps}$ is the abscissa in Figure 4.2, and the ratio $\Pi_c = t_{chr}/t_{ps}$ of the characteristic time for the change of y^* (storage) in the *control volume*, over the characteristic *system* response time is the capacitance scaling group in Eq. 4-2. Characteristic times are defined in Section 5.5.1. $\Pi_c = 1$ if the characteristic time of change is also the characteristic time of system response (e.g., if Π_c is from the depressurization equation and if depressurization is the characteristic process of the phase of interest, which makes the system characteristic time equal to the characteristic time for depressurization). As shown in Figure 4.2, when $\Pi_c > 1$ then y^* changes only fractionally during the phase and approaches steady-state conditions for $\Pi_c \gg 1$. Conversely, when $\Pi_c \ll 1$, then y^* completes its change very early in the transient.

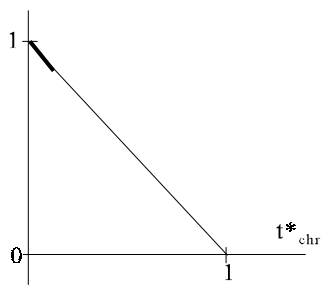


Figure 4.1 Initial Rate of Change in Scaled Time of Specific State Variable

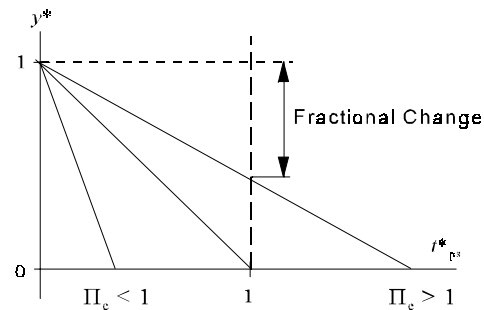


Figure 4.2 Initial Rate of Change in Scaled Time of Overall System

This demonstrates the two advantages of the *causative process* related scaling method: (1) the magnitude of the *causative process* related scaling groups indicate the importance of their associated processes relative to the well-known causative process which initiates and sustains, and is therefore responsible for, the changes, and (2) the method

of scaling reveals with a *single* scaling group, namely Π_c in Eq. (4-2), how close a particular change is to steady-state conditions relative to the overall system change.

4.4.5.2 Fractional Scaling of the Conservation Equations

The second scaling method explained in Section 4.3 is designed to exhibit the time-rate of change contribution by each process (flow, flux, and source terms) taking place in, and on the boundary of, the control volume of interest. The second method is called the *fractional scaling method* and provides the *fractional* form of the scaled conservation equations with the *fractional* Π -Groups. The *fractional* scaled conservation equation is obtained either directly by dividing the normalized equation by the constant normalizing factor of its time-derivative term, or by dividing Eq. (4-2) by the capacitance scaling group Π_c of its time-derivative term. Neither the constant normalizing factor nor the capacitance scaling group is zero.

The conservation equation scaled by the *fractional* method has this form:

$$f^*(y^*) \frac{dy^*}{dt^*} = \sum \Pi_i g_i(y^*) y_i^* \quad (4-3)$$

The *fractional* Π -Groups on the right-hand side of Eq. (4-3) are ratios of characteristic times or frequencies, or equivalently, products of characteristic times and characteristic frequencies [20]. These time or frequency ratios reveal the extent (fraction or multiple) to which the corresponding storage or transport process is being completed during the characteristic time of the entire system.

The important advantage of the second scaling method is that the *fractional* Π -Groups measure directly the fractional rate of change of the respective process on the total rate of change, as shown in Figure 4.3 for two processes with two Π -Groups, Π_1 and Π_2 . The magnitude of the *fractional* Π -value indicates how much the tangent on the curve $y^*(t^*)$ is turned by the respective process at the initial time. The second method of scaling the conservation equations allows one also to rank the processes represented in the conservation equation in the order of their importance for a given facility. Additionally, it serves to estimate the changes brought about by each process and all processes combined. In fact, equations in the form of Eq. (4-3) were used to estimate starting conditions for a phase from the starting conditions of the previous phase.

Capacitance-related design specifications (fluid volumes and heat capacities, for example) are inherent to, and fixed for, a completed facility and difficult to change in comparison to the adjustable design specifications which control the causative processes (valve settings and flow orifices, for example). Since in the second scaling method the

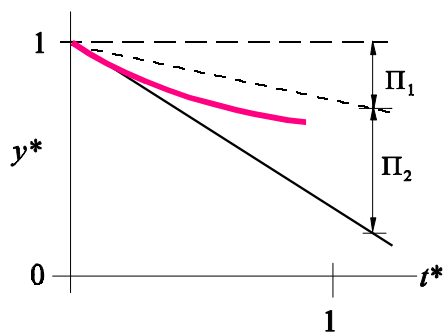


Figure 4.3 Fractions of Total Change Rate

capacitance term serves as the basis for comparing different facilities and for identifying scale distortions, and since the capacitance term affects all scaling groups on the right-hand side of Eq. (4-3), the second method produces sometimes more distorted scaling criteria than the first method. It must be recognized that the capacitance term plays an important role in either scaling method, even though it is represented by only a single scaling group in the first method.

Results from both scaling methods are reported in Chapter 6.2 for all conservation equations except for the quasi-steady loop momentum balances of Phase 5, i.e., the long and nearly steady IRWST and sump injection phase, for which the inertia scaling groups would have been of order 10^{-4} . The

4. Scaling Methodology

ranking of phenomena and the assessment of scaling distortions are based in this report on the *fractional scaling groups*, as obtained by the second scaling method, for all but the processes affecting the steady-state momentum balances of Phase 5.

4.4.6 Scaling of Loop System

The dynamic interaction between components of the thermohydraulic system is through forced or free circulation of liquid, vapor, or two-phase mixture. The interaction is modeled [17, 21] by the system of loop momentum balances. The loop momentum balances are combined into a single vector equation (see Eq. (5-49) on Page 5-25) with one vector component for each closed loop in the thermohydraulic system. The scalar scaling equations, Eqs. (4-2) and (4-3) must be extended to vector equations.

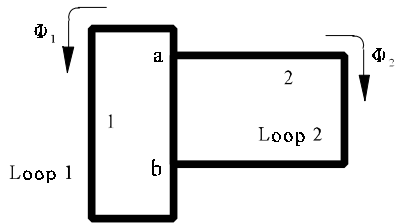


Figure 4.4 Schematic of Two-Loop System

The derivation of the loop momentum balances for general flow conditions is found in Reference [21] and summarized in Section 5.4.2 of this report. The loop momentum balances are scaled in Section 6.1.4. The *scaling methodology* for vector equations is explained below for the loop momentum balances of single-phase flow in the simple, two-loop system shown schematically in Figure 4.4.

Figure 4.4 shows a system of two closed loops: Loop 1, starting from Branch Point a, going on passed 1 to Branch Point b, and returning back to Branch Point a; and Loop 2, starting also from Branch Point a, going on passed 2 to Branch Point b, and back to Branch Point a. Each loop consists of components having straight flow channels, bends, expansions and contractions. The

two loops have three loop sections: Section a1b, Section ab, and Section a2b. The state variables of Loops 1 and 2 are the volumetric flow rates Φ_1 and Φ_2 , respectively, of the flows leaving Branch Point a.

Section 5.4.2 explains below Eq. (5-20) on Page 5-12 that, when forces acting on a loop system are replaced by pressures, and fluid velocities by volumetric flow rates, then the familiar inertia (mass) of $\rho V = \rho LA$ of the fluid with density ρ in a component with volume V , length L , and cross-sectional area A is replaced by $\rho L/A$, and the flow resistance in a component with loss coefficient K , Darcy friction factor f , and hydraulic diameter d_h is $\rho/2[(K + fL/d_h)/A^2] \Phi|\Phi|$. With this nomenclature, the two loop momentum balances for the system shown in Figure 4.4 are given by this vector equation:

$$\begin{bmatrix} \oint_{Loop1} \rho \frac{dz}{A} & \int_a^b \rho \frac{dz}{A} \\ \int_a^b \rho \frac{dz}{A} & \oint_{Loop2} \rho \frac{dz}{A} \end{bmatrix} \begin{bmatrix} \frac{d\Phi_1}{dt} \\ \frac{d\Phi_2}{dt} \end{bmatrix} = \begin{bmatrix} \vec{g} \cdot \oint_{Loop1} \hat{k} \rho dz \\ \vec{g} \cdot \oint_{Loop2} \hat{k} \rho dz \end{bmatrix} + \begin{bmatrix} (\Delta p_{PP})_{Loop1} \\ (\Delta p_{PP})_{Loop1} \end{bmatrix} - \begin{bmatrix} R_{a1b} & 0 & R_{ab} \\ 0 & R_{a2b} & R_{ab} \end{bmatrix} \begin{bmatrix} \Phi_1 |\Phi_1| \\ \Phi_2 |\Phi_2| \\ (\Phi_1 + \Phi_2) |\Phi_1 + \Phi_2| \end{bmatrix}. \quad (4-4)$$

On the left-hand side of Eq. 4-4 is the product of the 2×2 inertia matrix, \mathbf{I} , times the 2-dimensional vector of time derivatives of the state variables, $d\vec{\Phi}/dt$, i.e., of the flow rates leaving Branch Point a. On the right-hand side of Eq. 4-4 are first the two 2-dimensional vectors of pressure differences, $\vec{\Delta p}_{GR}$ and $\vec{\Delta p}_{PP}$, caused by gravitational and pumping forces, respectively. The last term of Eq. 4-4 is the flow impedance term and the product of the 2×3 impedance matrix, \mathbf{P} , times the 3-dimensional vector of the so-called directed kinetic energy, \vec{H} . \vec{H} is called the vector of directed kinetic energy, because its elements change sign with changing flow directions and represent the kinetic energy which governs irreversible pressure losses. The number of columns of \mathbf{P} equals the number of loop sections. The number of rows in \mathbf{I} and \mathbf{P} must equal the number of closed loops in the system, and \mathbf{I} is always a square matrix.

- Notice that each *diagonal* element of the *inertia matrix* \mathbf{I} is the closed-loop inertia of the loop associated with the row of the element.
- Loops 1 and 2 have Section ab in common. Section ab couples the two loops dynamically because any pressure difference caused by the flow Φ of one loop imposes itself on the flow in the other loop. The coupling by inertia and impedance is evident directly from Eq. 4-4, the coupling by gravity and pumping can be recognized when Eq. 4-4 is solved explicitly for the two time derivatives.
- Equation 4-4 shows that the acceleration of Φ_1 is coupled to the acceleration of Φ_2 , and vice versa, by virtue of the *off-diagonal* elements in the *inertia matrix* \mathbf{I} . The coupling is the stronger the larger the off-diagonal terms are.
- Any two loops which have the same impedance matrix element in a column of the impedance matrix \mathbf{P} are impedance-coupled via the loop section that pertains to the column. See the last column of \mathbf{P} in Eq. 4-4: both loops are impedance-coupled through Loop Section ab.

Normalization. Equation 4-3 shows that when a *vector equation* is normalized according to the first principle of scaling presented in Section 4.3 (normalization is the fourth step of the scaling methodology described in Section 4.4.4), the scalar constant normalizing factors, C , of the scalar conservation equation, must become matrices. Every time-dependent element of the $\vec{\Delta p}_{GR}$ and $\vec{\Delta p}_{PP}$ vectors and of the \mathbf{I} and \mathbf{P} matrices must be normalized and then scaled to render every time-dependent element of the scaled variable arrays of order unity. The vectors and matrices are normalized with respect to the main-loop reference parameters and each array element is normalized with its maximum (or initial) value. The normalization with respect to the main-loop reference parameters provides the global system scaling and serves as the basis for scaling the distribution of inertia, gravity, and impedance. The distribution of inertia, gravity, and impedance determines the flow distribution and the individual loop response times.

The left-hand side of Eq. 4-4 is normalized with the reference volumetric flow rate, Φ_{ref} , the system characteristic response time, t_{ref} , and the initial inertia of the main (i.e., reference) loop.

$$\begin{aligned} \mathbf{I}_{ij} \frac{d\Phi_j}{dt} &= \frac{I_{ref} \Phi_{ref}}{t_{ref}} \left(\frac{\Phi_0}{\Phi_{ref}} \right)_j \odot \left(\frac{I_0}{I_{ref}} \right)_{ij} \odot \mathbf{I}_{ij}^* \frac{d\Phi_j^*}{dt^*} \\ &= \frac{I_{ref} \Phi_{ref}}{t_{ref}} (S_I)_{ij} \odot \mathbf{I}_{ij}^* \frac{d\Phi_j^*}{dt^*} = \frac{I_{ref} \Phi_{ref}}{t_{ref}} (S_I \mathbf{I}^*)_{ij} \frac{d\Phi_j^*}{dt^*}, \end{aligned} \quad (4-5)$$

where $\mathbf{I}_{ij}^* = (I/I_0)_{ij}$ and $\Phi_j^* = (\Phi/\Phi_0)_j$. Repeated indices indicate summation, except where \odot denotes term-by-term multiplication without summation. The specific reference parameters and the selection of the main loop are discussed in Section 6.2 for the individual phases.

The first factor on the right-hand side of Eq. 4-5 is the scalar normalizing factor C which relates inertia to the system response and becomes, after scaling, the *global* Π -Group of inertia, Π_{IN} . The term-by-term multiplication of the second

4. Scaling Methodology

and third factors on the right-hand side of the top line of Eq. 4-5 yields the Inertia Metric S_I shown as the second factor in the bottom line of Eq. 4-5. The Inertia Metric S_I scales the effects of loop system geometry on *local inertia distribution*. The scaled inertia matrix, \mathbf{I}_{ij}^* , scales the local density variations (caused by changes of void fraction and void distribution parameter); it equals the identity matrix unless the fluid density changes with time.

Scaling. The gravity and impedance terms on the right-hand side of Eq. (4-4) are normalized in the same manner as the term on the left-hand side for the time rate of momentum change. For natural circulation, the pumping term is omitted and the normalized equation is divided by the constant normalizing factor of the gravity term. The result that corresponds to Eq. (4-2), i.e., the scalar conservation equation scaled by the causative process related method, is for the scaled vector equation, Eq. (4-4), written here in indicial notation:

$$\Pi_{IN,GR} \left(S_I \mathbf{I}^* \right)_{ij} \frac{d\Phi_j^*}{dt^*} = \left(S_G G^* \right)_i - \Pi_{RS,G} \left(S_P P^* \right)_{ik} E_k^*, \quad (4-6)$$

where $i = 1, 2$ and is the loop and equation index, the summation over j covers the loops, and the summation over k covers the loop sections. S_G and S_P are the gravity and impedance metrics

$$S_{G_j} = \frac{\left[\left(\Delta H_{GR} \beta_T \Delta T_{GR} \right)_0 \right]_j}{\left(\Delta H_{GR} \beta_T \Delta T_{GR} \right)_{ref}}, \quad S_{P_{jk}} = \frac{\left(\frac{\Phi_{j,0}}{\Phi_{ref}} \right)^2 \left(R_0 \right)_{jk}}{\sum_{i \in loop_{ref}} \left(\frac{\Phi_{i,0}}{\Phi_{ref}} \right)^2 R_{ref,i}}. \quad (4-7)$$

ΔH_{GR} is the elevation difference of gravity center points, β_T the isobaric expansion coefficient, and ΔT_{GR} is the driving temperature difference for natural circulation. The resistance coefficients R are the same as the elements of the impedance matrix in Eq. (4-4). The Π -Groups in Eq. (4-6) are the global scaling groups of inertia and impedance.

The vector equation of momentum balances is scaled by the *causative process* related method and the *fractional* method, except for the nearly quasi-steady conditions of Phase 5 where only the causative process related method is used. The scaled loop momentum balance, i.e., Eq. (6-56) for forced, and Eqs. (4-6) and (6-68) for natural circulation, has the form of Eq. (4-2), except that the state variables are *vectors* and the scaling groups are *arrays*. Each array of scaling groups is factored into a scalar Π -Group for characterizing the *global* system dynamics (main loops), and into the S -Metric, for scaling the local variations of inertia, gravity, and impedance, and for characterizing the dynamic flow distribution.

4.4.6.1 Global System Dynamics

The *global* scalar Π -Groups in Eq. (4-6) are presented for the more general momentum balances, Eqs. (6-56) and (6-68), in Section 6.2 for each one of the five phases. The *global* scalar Π -Groups scale the inertia, gravity, mechanical pumping, and flow resistance forces in the main loop of the system. The main loop is taken for Phases 1 through 4 to be one of the reactor coolant loops of normal operations (CMT Side B, Cold Leg 1 in Figure 1.1), since these loops are active for all phases. The main loop for Phase 5 is the loop from containment through the IRWST tank, the reactor vessel, the ADS-4 valves, and back to the containment, because the IRWST flow dominates the flows during Phase 5.

The *causative process* is the action of the reactor coolant pump for forced circulation, and the action of gravity due to density differences for natural circulation. The associated *causative process* related scaling groups are unity in, respectively, Eq. (6-56) for forced circulation, and Eq. (6-68) for natural circulation. A small value of the capacitance group, Π_c in Eq. (4-2), of the loop momentum balance indicates a fast response of flow rates in the main loop to the

tripping of pumps, or any changes in valve settings or level elevations. The flows in AP600 respond quickly, as can be seen from the small value of $\Pi_C = \Pi_{I,N,P}$ for forced flow in Table 6.7 and $\Pi_C = \Pi_{I,N,GR}$ for natural circulation in Table 6.42. An imbalance among the *causative process* related or the *fractional* scaling groups on the right-hand side of the momentum balance indicates an imminent large change in main-loop flow rates at the beginning of the phase.

4.4.6.2 Distribution and Interaction of Flows

The S_I , S_G , and S_P -Metrics in the scaled momentum balance, Eqs. (4-6) above and for the actual AP600 system Eqs. (6-56) and (6-68) are the two-, one-, and two-dimensional arrays, respectively, that measure the *distribution* of inertia, gravity, and flow resistance (impedance) relative to those of the main loop. The arrays apply to the causative term related and to the fractional scaling methods, and for forced and natural circulation modes.

All metrics have as many *rows* as there are closed loops in the thermohydraulic system and equations in the system of momentum balances. The S_I -Metric of inertia is a square matrix since there is one independent branch exit flow in every closed loop; all other branch exit flows are related to the former by mass conservation. The S_G -Metric of gravity force distributions has only one column. Its elements are the ratios of initial specific loop over main loop gravity forces. The S_P -Metric of flow impedance has as many columns as there are loop segments between branch points.

The Inertia Metric, S_I , is shown schematically for the two-loop system in Figure 4.4, as the 2x2 matrix in the last three rows and columns of Figure 4.5. The first column in Figure 4.5 identifies the loops shown in Figure 4.4, one row for each loop. The two independent branch exit flows are indicated in the column header, one column for each exit flow.

	Φ_1	Φ_2
Loop 1	$(S_I)_{Loop1}$	$(S_I)_{ab}$
Loop 2	$(S_I)_{ab}$	$(S_I)_{Loop2}$

The general inertia elements are derived in Section 5.4.2.1 and defined by Eq. (5-24), which shows that inertia is governed by $\rho L/A$, the length over area aspect ratio, multiplied by density (see Eq. (4-3)), and that inertia is concentrated in long pipe segments with small cross-sectional areas, rather than in vessels with large cross-sectional areas. The scaled elements, S_I , of inertia are defined by Eq. (4-5) or (6-62).

Figure 4.5 Inertia Metric for Two-Loop System of Fig. 4.4

It is explained in Section 6.1.4.1 that:

- The diagonal S_I -elements (printed in **boldface**) show the magnitude of the *loop inertia* associated with the loop of the row, relative to the main loop.
- The magnitude of the off-diagonal S_I -elements is a measure of the *cross-coupling between the loops by inertia*. The elements printed in **blue** measure the coupling between *adjacent loops on the same side* of the system. The elements printed in Tables 6.9 through 11 for four-loop systems (Chapter 6.1) in **magenta** measure the coupling between *separated loops, on opposite sides* of the system.
- The element-by-element multiplication of the S_I and I^* matrices provide the time-dependent normalized inertia matrix which is, along with the impedance matrix, needed to compute the eigenvalues and time constants of Eqs. (6-56). The Inertia Metric reveals how quickly the flow readjusts to changes in flow conditions: the larger the S_I -elements of a row are, the slower responds the fluid in the loop associated with that row, and relative to the responses in other loops.

4. Scaling Methodology

The Impedance Metric, S_p , is shown schematically for the two-loop system of Figure 4.4, as the 2x3 matrix in the last two rows and three columns of Figure 4.6. The first column in Figure 4.6 identifies the two loops in Figure 4.4. The three segments of the system are identified in the column header: each loop segment has a column in the Impedance Metric.

	a1b	a2b	ab
Loop 1	$(S_p)_{a1b}$	0	$(S_p)_{ab}$
Loop 2	0	$(S_p)_{a2b}$	$(S_p)_{ab}$

Figure 4.6 Impedance Metric for Two-Loop System in Fig. 4.4

The elements of the general impedance metric for the AP600 system are derived in Section 5.4.2.4 and defined by Eq. (5-41). These equations show that the elements of the Impedance Metric, S_p , are governed by form losses, i.e., the *geometry, of primarily the connecting pipes* in the system where the flows are largest. The scaled elements, S_p , of impedance are defined for the system in Figure 4.4 by Eq. (4-7), and for the general AP600 system by Eq. (6-64).

It is explained in Section 6.1.4.1 that:

- The magnitude of the S_p -elements in a row show the *distribution of flow impedances* in the loop associated with the row. Emerging from a branch point, the flow prefers downstream the loop segment with the lowest scaled impedance values. The Impedance Metric determines the flow distribution in the system, particularly as the steady state is being approached.
- Repeated S_p -elements in a *column* indicate *cross-coupling by impedance* between the loops that are associated with the rows containing the repeated S_p -elements. The S_p -elements are repeated because the same loop segment is common to more than one loop. The last column in Figure 4.6 belongs to the common Loop Section ab in Figure 4.4, and therefore couples, both loops in Figure 4.4. In the case of four loops in Tables 6.13 through 6.15, the last column has equal values in every row because the reactor core couples all four loops.
- The element-by-element multiplication of the S_p and P^* matrices, shown in Eq. (4-6), provides the time-dependent scaled impedance matrix with is needed to compute the ratios of specific over main loop characteristic frequencies.

We demonstrate the importance of impedance and inertia with the expression of dynamic response frequency for the following simple case of a single loop. For a single, horizontal loop with single-phase fluid and no pumps, the characteristic frequency of flow response is, from Eq. (5-49), equal to twice the ratio of flow impedance over flow inertia (a linearized approximation).

$$\omega_{ref} = \frac{W_0 \sum_i \frac{K_i + f_i \frac{L_i}{d_{h_i}}}{A_i^2}}{\oint \rho \frac{dz}{A}} \quad (4-4)$$

Here, W_0 , ρ , K , and f denote, respectively, the initial mass flow rate, fluid density, form loss coefficient, and Darcy friction factor. L , d_h , and A stand for length, hydraulic diameter, and flow cross-sectional area, respectively. Equation

(4-4) reduces to $\omega_{ref} \rightarrow fv/ d_h$ for a loop of uniform flow cross-sectional area and no form losses. Equation (4-4) is a simple case that shows the importance of the inertia and impedance matrices for the determination of dynamic loop response (via the calculation of eigenvalues in the case of coupled loop systems).

4.5 Criterion of Relevant Phenomenon

Since the magnitude of each Π -Group carries the magnitude of its respective term in an equation, the magnitude of the Π -Group’s numerical value signifies the importance of the term *quantitatively*. In fact, the numerical value of the causative process-related Π -Group (for its definition see Section 4.4.5.1) indicates directly how much larger or smaller its respective term is in comparison to the causative term whose Π -Group is unity. For assessing importance (later in Section 6.2) on the basis of the fractional Π -Groups (Section 4.4.5.2), one needs to compare the magnitudes of the Π -Groups in the scaled fractional equations. Since there are five main phases and the changes of inventory, pressure, temperature and flow rates of the primary system and its major components, it is quite evident that a single criterion for relevance should serve to judge consistently what is important.

The working criterion for importance is that the phenomena and processes are considered *important* for a facility if the associated Π -Group is greater than 1/10 of the largest Π -Group in the equation and evaluated for that facility. This choice is based on the common engineering standard of keeping under consideration first-order terms and ignoring second-order terms. It should be recognized that the adoption of this convention affects the total number of important scale distortions, which is one of the major results of this report.

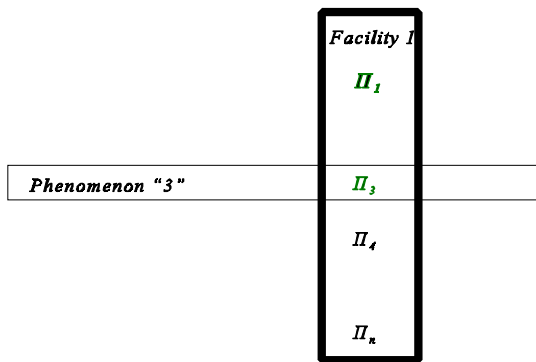


Figure 4.7 Phenomenon Importance in Column of Π -Group Matrix

For assessing very important scale distortions, phenomena and processes are said in this report to have top-priority importance if their associated AP600 scaling groups differ by less than 20% from the largest Π -Group in the same equation.

Importance of phenomenon in any facility is recognized in the matrix of Π -Groups. The matrix is broken up in individual tables, one table for each conservation equation, as shown in Section 6.2. Each facility has its own column.

AP600 has the leading column of numerical Π -Group values. Importance is determined by comparing the magnitude of the Π -Groups in the *column* of the respective facility. The phenomena are arranged in the rows of the tables in Section 6.2 in the order of their importance for AP600, with top priority of importance in the top row. Scaling groups of important phenomena in AP600 are highlighted in **green**. Scaling groups of AP600 phenomena with top priority importance are highlighted in **bold green**, as indicated in Figure 4.7.

4.6 Criterion of Scale Distortion

The ratio of two Π -Groups from two different facilities, but corresponding to the same term in the equation, are a measure of similarity or scale distortion for the phenomenon which is represented by the term in the equation. The ratio of 1 implies similarity, or no scale distortion.

A phenomenon or process is taken to be distorted in a test facility, relative to the same phenomenon or process in the AP600 if the ratio of test facility over AP600 Π -Groups is less than 1/2 or greater than 2. This implies a difference of

4. Scaling Methodology

the order of 100%. It should be recognized that the adoption of this convention also affects the number of important scale distortions, which is one of the major results of this report. The count of important scale distortions has been repeated, however, with the criterion of “less than 1/3 or greater than 3,” to indicate the sensitivity of the assessment to the thresholds of 1/2 and 2.

Scale distortions are recognized in the matrix of Π -Groups by observing the magnitude of the numerical values of Π -Groups in the row of a phenomenon. In the tables of Section 6.2, the Π -Groups of important phenomena whose numerical value is less than 1/2 or greater than twice the value of the corresponding AP600 Π -Group is highlighted in red as shown in Figure 4.8.

The scale distortion in a test facility is considered to be *conservative* if the associated process reduces the minimum coolant inventory or the subcooling temperature in the reactor vessel of the test facility more than in the AP600.

This completes the description of the scaling process used in the present analysis. The next chapter presents the models, i.e., the conservation equations, and the thermal and caloric state equations which serve as the basis for scaling. The scaled conservation equations and the scaling criteria are presented in Chapter 6.

	<i>Facility 1</i>	<i>Facility 2</i>
	Π_1	Π_1
Phenomenon "3"	Π_3	Π_3
	Π_4	Π_4
	Π_n	Π_n

Figure 4.8 Phenomenon Distortion in Row of Π -Group Matrix

5. MODELING EQUATIONS

In this chapter are presented all the conservation equations and their combinations with thermal and caloric equations of state which are common to two or more phases of the thermohydraulic transient.

5.1 Model Selection

The models are selected to describe the global system response and the component interactions within the system. Global conservation equations for the system control volume are written in terms of volume-averaged variables for recognized portions of the system, and in terms of transfer processes that are taking place at the control volume boundary.

The system response is dominated by *depressurization* in Phases 1 through 4. Pressure has been identified in Section 4.4 as an important state variable characterizing the primary system during Phases 1 through 4 and the secondary system during Phase 2. The time rate of pressure change is modeled by combining the total system mass and energy balances with the thermal equation of state as described in [17] but extended here to a system whose control volume, V , is occupied by any combination of subvolumes V_l , $V_{2\phi}$, V_v , and V_{N_2} , of, respectively, subcooled liquid, saturated two-phase mixture, single-phase vapor, or noncondensable nitrogen gas, where $V = V_l + V_{2\phi} + V_v + V_{N_2}$. All subvolumes are permitted to change size with time, but the total volume, V , is constant. The subvolumes may interchange mass and energy. Each subvolume exchanges heat with the environment. The subvolumes encompass the fluid either in components (Pressurizer (PRZ), Core Make-up Tank (CMT), etc.), or in portions of components or in the primary system. The primary side of the Steam Generators (SG) (U-tube and plenum volumes) is part of the primary-side system volume; the secondary SG volume is separate, $V = V_{SG}$.

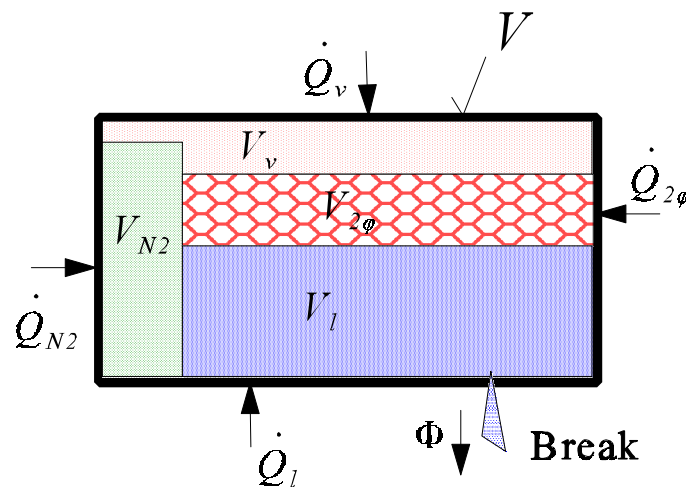


Figure 5.1 General Subvolume Assembly

The overall system volume discharges subcooled liquid or two-phase mixture to the environment (break flow, ADS flow). Figure 5.1 shows schematically the assembly of subvolumes with the heat exchange rate terms \dot{Q} and break flow for Phases 1 and 2.

5. Modeling Equations

5.2 Modeling Assumptions and Limitations

We list below the modeling assumptions. The prefixes of the cardinal Roman numerals indicate the model for which the simplification has been introduced: p, T, and W for time-rate of pressure, temperature, and momentum change equations.

- (p-i) The two-phase mixture is always in thermal equilibrium at the pressure p .
- (p,T-ii) The volume average of a thermophysical property function equals the function evaluated with volume-averaged state variables.
- (p,T-iii) The kinetic energy and dissipation of viscous energy are ignored relative to the thermal energy transport.
- (p-iv) The momentum balance is decoupled from the energy balance because the flow rates are subsonic everywhere except at the break or at a valve with critical flow. The region of steep pressure gradients in the vicinity of choked flow is excluded from the control volume, and the volumetric flow rate of critical flow is computed from quasi-steady critical mass flow rate correlations and the mean density upstream of the break (or valve). In the subsonic interior of the control volume $\nabla p \approx 0$, the pressure gradient is ignored relative to the absolute pressure and the temporal change of pressure [21].
- (p,T-v) The nitrogen temperatures in both accumulators are the same.
- (W-vi) The flow in lines between vessels, in RPV, and in SG primary side is turbulent.
- (W-vii) The *change* in momentum flux is caused by phase change and unimportant: in adiabatic piping (high-velocity flows) with primarily single-phase fluid, in vessels with little phase change (after scram) but low velocities.

It must be recognized that the purpose of scaling is not the precise prediction of the AP600 plant response but, instead, a comparison of the magnitude of terms representing the processes which evolve during the postulated transient. None of the above simplifying assumptions introduces a limitation in the achievement of this objective.

5.3 Validation of Models

Under normal circumstances, a scaling analysis is performed before the design of a test facility is completed, and before there is any opportunity for comparing those reference parameters that are needed for scaling but cannot be specified by the designer. Examples of such parameters would be reference flow and heat transfer rates. The scaling analysis must, therefore, be performed normally for all the possible heat transfer and flow regimes (natural or forced circulation, etc.) that cannot be ruled out prior to the design and operation of test and prototype facilities.

The scaling uncertainty arises from *modeling* uncertainty in general. The models used for scaling consist of conservation equations, thermophysical material properties (*intrinsic* closure relations) and correlations for mass, energy, and momentum transport (*extrinsic* closure relations) across the boundaries which surround the control system, and which separate subsystems inside the system. The scaling uncertainties arise from three sources: (1) from the assumptions listed in Section 5.2 above, (2) from the assumptions made regarding those of the volumes listed in Section 4.4 for which it is not specified by design how they are occupied by subcooled liquid, saturated two-phase mixture, superheated vapor, or inert gases, and (3) from the extrinsic closure relations which are needed to estimate reference parameters for scaling that cannot be specified by the designer. Therefore, *the most important need for validation in support of scaling analysis is the experimental confirmation of estimated reference parameters and of fluid distribution* in the system. The simplifying assumptions of Section 5.2 and the distribution of fluids in the system determine the mechanical, volumetric, and thermal capacities and, therefore, the rates of temperature, volume, and pressure change. There is no need, however, to confirm conservation equations by experiment since no

5. Modeling Equations

uncertainties arise from drawing specified system and component control volumes and writing down global conservation equations.

Since *this* scaling analysis is being carried out after the completion of experiments in APEX, ROSA, and SPES, and since selected experimental data are available from these experiments, we have compared estimated reference parameters and mechanical, volumetric, and thermal capacities with *available* experimental data. *This comparison gives the only assurance that the scaling analysis presented here complies with Scaling Principle (1) explained in Section 4.3, namely with the requirement that all scaled variables must be of order unity.* It was explained in Section 4.3 that without this assurance, ranking of phenomena or processes and an assessment of scaling distortion are not possible.

The equations for estimating the reference parameters are given in Sections 5.5.1, 2, 3, and 4 for time, pressure, volumetric flow rates, and mass flow rate, respectively, and the comparison of estimated parameters and experimental data is presented in Section 5.5.5.

It is important to realize that scaling in itself consists only of algebraic operations which do not alter the validity of the equations and, as mathematical operations, these cannot be effectively confirmed by experiment.

It is also important to realize that the purpose of scaling is not to predict events, but to determine that similitude exists between prototype and test facilities so that the same important phenomena and processes occur in prototype and test facilities. It was explained in Section 4.2 that this requires only that the facilities are governed by the same equations, i.e., that the leading Π -Groups and the scaled initial conditions are the same for the facilities. The prediction of events would require the solution to the governing equations. Scaling requires the estimation of parameters only at a single instant at the beginning of each phase.

5.4 Conservation Equations

Conservation equations are the basis for the scaling analysis [17]. The transient *mass and energy* conservation equations are written for the fluid in the entire primary system *volume* and the *volumes* of its components, in terms of ordinary differential equations in time, to obtain the rate of change for pressures p_1 and p_2 of primary and secondary systems, respectively, for liquid volume fraction α_l (inventory), and temperatures T in single-phase portions of the system. Specific control volumes for mass and energy balances are given in Figures 5. 2, 3, and 4 for each time phase of the transient. The global mass and energy balances are applied in this scaling analysis to control volumes in standard form. The momentum balance application is special because of the complexity of the system with arbitrary orientations in three directions and the dependence on the local geometric detail and global system topology.

The transient *momentum* balance is written here, in contrast to the familiar global, three-dimensional form for a volume, in *scalar form* for the fluid in every *closed loop* [17, 21], namely either the four (4) or seven (7) loops internal to the system, as shown in Figure 1.1, for Phases 1 through 4, or through five (5) loops that are open to the containment for Phase 5. The four-loop system consists of the two double loops leading from the Upper Plenum through two Steam Generators on Sides A and B, each double loop passing through a separate Cold Leg, cl1 and cl2, respectively. All four loops are closed through the Reactor Pressure Vessel. The seven-loop system consists of the four-loop system plus two CMT and one PRHR loops. Specific loop diagrams are given in Figures 5.5, 6, and 7. The transient momentum balance is derived from the local, one-dimensional form, which is integrated along sectionally straight loop segments. The results are joined with standard form loss models, summed up over a closed loop, and written to obtain the transient or steady-state volumetric flow rates in the system [17].

This formulation of the loop momentum balance determines the form in which the forces appear in the momentum balance. The conventional global momentum balance produces the time rate of change of the three-dimensional, volume-averaged fluid *velocity*, \vec{v} , in terms of three-dimensional body and contact *forces* acting on the fluid in the volume. While such a formulation is relatively simple for a component with one-dimensional flow, it is entirely impractical to assemble the momentum balance for a system of many arbitrarily oriented components, by using the component momentum balances and eliminating all internal (three-dimensional) forces at component interfaces while

5. Modeling Equations

accounting for all reaction forces from the solid structures. One could scale, instead, all the individual momentum balances of all the vessels and all the straight sections of all the connecting pipes between vessels but this alternative is also impractical because it gives an unmanageably large number of scaling criteria. The (system of) loop momentum balance(s), on the other hand, combines the system characteristics of all the vessels and pipe segments located between branch points in the loop into a single loop segment characteristic. The result is simplicity without any loss of generality for the description of the *fluid* dynamics.

The *conventional momentum balance* contains (for the sake of simplicity, we consider here single-phase flow) fluid velocity v , inertia $\rho V = \rho AL$, pressure forces $F_p = pA$ at inlet and exit cross-sections, and flow resistance forces $F_\tau = \tau A_w$ at the walls. In the *loop momentum balance*, fluid velocity v is replaced by fluid volumetric flow rate Φ , forces F_p at inlet and exit cross-sectional areas are replaced by pressures p , and wall shear is replaced by resistance forces per unit of flow cross-sectional area. As a consequence, inertia ρAL is replaced and represented by $\rho L/A$, and forces by forces per unit of flow area.

It is shown later in Section 5.4.2.1 that integration of a simple scalar momentum balance for each loop, combined with the integral of the volumetric flux divergence equation, suffices to describe the transient flow everywhere in the system of loops [21]. The first step in the simplification of the momentum balance for one-dimensional flow is the replacement of the directed forces by scalar pressures. The forces exerted by solid structures on the fluid are completely accounted for by the introduction of pressure differences due to form losses. All internal pressures except the pressure rise due to pumps are eliminated by utilizing the fact that for pressure, as for any state variable, the closed-contour integral $\oint dp = 0$ around every closed loop in the system.

This first step changes the representation of inertia from $\rho V = \rho AL$ to ρL . This is the inertia per unit of cross-sectional flow area. This step replaces also forces by forces per unit of flow area.

The fluid velocity v can vary spacially at any given instant in a component or a loop segment between two loop branch points by as much as two orders of magnitude, simply on account of flow cross-sectional area variations. It is, therefore, impractical to represent and *scale* the flow in a component or a loop segment between two loop branch points by a single velocity, without violating the scaling requirement that all variables be scaled to be of order unity. In contrast to the fluid velocity, the fluid volumetric flow rate is of the same order of magnitude everywhere between two loop branch points, except in the rare instance when a condensation shock or intensive boiling occurs. The fluid volumetric flow rate is the natural kinematic state variable for analyzing or simulating the fluid flow in networks of pipes and vessels [17, 21]. Thus, the second step in the simplification of the momentum balance for one-dimensional flow is the replacement of the volume-averaged, directed fluid velocity by the scalar fluid volumetric flow rate at the entrance to a loop segment.

This second step changes the representation of inertia in the loop momentum balance from ρL to $\rho L/A$. It is the inertia per square of cross-sectional flow area and represents inertia in the loop momentum balance, as shown in Section 5.4.2.1. The traditional inertia is the ratio of force over acceleration. The inertia in the loop momentum balance is the ratio of pressure over the time rate of change of volumetric flow rate. The inertia in the loop momentum balance encompasses all the geometric effects; the scaling groups representing loop inertia also contain all geometric effects related to inertia.

5.4.1 Mass and Energy Conservation

The mass and energy conservation equations are combined with the caloric equation of state to yield the ordinary differential equation for the time rate of pressure change. The scaling of this equation leads to the characteristic time of depressurization in terms of system total elasticity and volumetric break flow rate, the scaling criterion for mechanical system compliance, and the scaling criteria for all the heat transfer to and from the system.

5. Modeling Equations

5.4.1.1 Control Volumes for Mass and Energy Balance Equations

Figure 5.1 shows schematically the assembly of subvolumes with the heat exchange rate terms \dot{Q} . The subvolumes are separated by movable or rigid interfaces and may exchange mass and energy. The overall system volume $V = V_l + V_{2\phi} + V_v + V_{N_2}$ is fixed. Figures 5.2, 3, and 4 show the specific primary system control volumes for Phases 1, 2 (and 3), and 4, respectively. The primary system control volumes consist of the components in solid boxes and the connecting lines. For Phase 1, Pressurizer (PRZ) and Surge Line (SRL) are filled with two-phase mixture in thermal equilibrium at primary system pressure p_1 , the rest of the primary system, the Core Make-up Tanks (CMT), and the Passive Residual Heat Rejection (PRHR) system are filled with subcooled liquid.

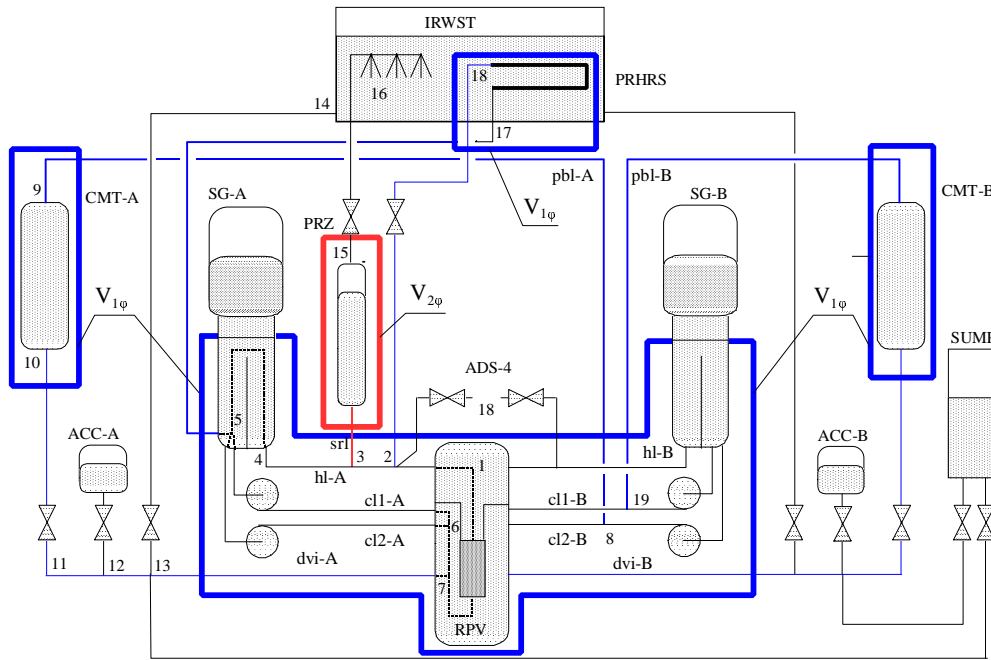


Figure 5.2 Primary System Control Volume for Phase 1; Initial Depressurization:
 blue lines and components in blue boxes are filled with subcooled liquid,
 red line (SRL) and component in red box (PRZ)
 is filled with saturated two-phase mixture.

For Phase 2, the Passive Heat Rejection phase (see Figure 5.3), the primary-system control volume consists of the Pressurizer (PRZ) and Surge Line (SRL) which are filled with vapor, the Upper head (UHD) and Steam Generators which are filled with two-phase mixture in thermal equilibrium at primary system pressure p_1 , the rest of the primary system, the Core Make-up Tanks (CMT), and the Passive Residual Heat Rejection (PRHR) system are filled with subcooled liquid. After the Accumulator valves are opened (second subphase, see Figure 3.1 on Page 3-1), the primary-system control volume is extended to include the nitrogen gas and fluid in the Accumulators (ACC).

For Phase 3, the ADS-123 Blow-Down phase, the primary-system control volume is the same as for the second subphase of Phase 2; except that it includes the nitrogen gas and liquid in the Accumulators. The nitrogen gas has expanded isothermally during the last part of Phase 2.

5. Modeling Equations

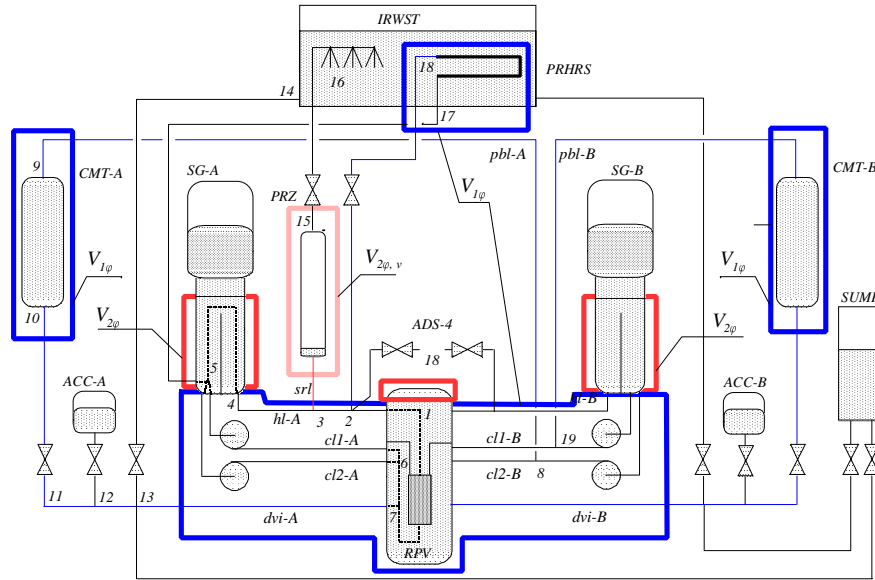


Figure 5.3 Primary System Control Volume for Phase 2; Passive Heat Rejection:
 blue lines and components in blue boxes are filled with subcooled liquid,
 components in dark red boxes are filled with saturated two-phase mixture
 pale red indicates vapor-filled PRZ and SRL (same, with ACC, for Phase 3).

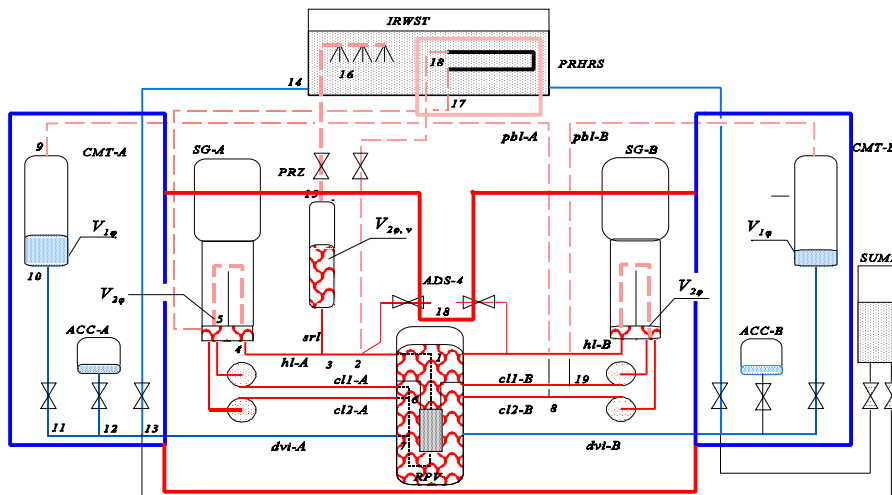


Figure 5.4 Primary System Control Volume for Phase 4; ADS-4 Depressurization:
 blue areas in blue boxes denote subcooled liquid, red box, pattern and solid lines
 saturated two-phase mixture, PRHR and dashed lines are vapor-filled.

5. Modeling Equations

For Phase 4, the ADS-4 Depressurization phase, the primary-system control volume is shown in Figure 5.4. The control volume is filled with saturated two-phase mixture and vapor, except for the subcooled liquid in CMTs, ACCs and RPV Downcomer (DC).

For Phase 5, the IRWST injection, depressurization is not modeled because the primary system is open to the containment atmosphere, and the system pressure is dictated by fluid elevations.

5.4.1.2 Time Rate of Pressure Change

For *single-phase fluid* in volumes V_l and V_v shown in Figure 5.1, the *mass balance* is written, for convenience, first as the local mass balance

$$\begin{aligned}\nabla \cdot \vec{v} &= -\frac{1}{\rho} \frac{D\rho}{Dt} \\ &= -\frac{1}{\rho} \left[\left(\frac{\partial \rho}{\partial p} \right)_u \frac{Dp}{Dt} + \left(\frac{\partial \rho}{\partial u} \right)_p \frac{Du}{Dt} \right],\end{aligned}\quad (5-1)$$

where v , ρ , p , and u stand for velocity, density, pressure, and internal energy, respectively; t is time, and D/Dt is the substantial derivative. By virtue of simplifying assumption (p,T-iii) listed in Section 5.2, the energy balance for single-phase fluid is

$$\rho \frac{Du}{Dt} = -\nabla \cdot \vec{q} - p \nabla \cdot \vec{v}. \quad (5-2)$$

\vec{q} is the heat flux vector. After invoking simplifying assumptions (p,T-ii) and (p-iv) listed in Section 5.2, and after substituting Eq. (5-2) into Eq. (5-1), one finds, with the aid of differential calculus and standard thermodynamic property identities, the volumetric flux divergence equation for single-phase fluids (subcooled and saturated liquids (in V_l), superheated and saturated vapors (in V_v))

$$V_{l,v} : \quad \nabla \cdot \vec{v} = \frac{c_v \kappa}{c_p} \dot{p} - \frac{\beta_T}{\rho c_p} \nabla \cdot \vec{q}, \quad (5-3)$$

where c_v , c_p , β_T , and κ are the isochoric and isobaric specific heats, the isobaric thermal expansion coefficient, and the isothermal compressibility. The superscripted dot means differentiation with respect to time. For nitrogen, modeled as a *perfect gas*, Eq. (5-3) reduces to

$$V_{N_2} : \quad \nabla \cdot \vec{v} = -\frac{1}{\gamma p} \dot{p} - \frac{\gamma - 1}{\gamma p} \nabla \cdot \vec{q}. \quad (5-4)$$

For two-phase mixture in control subvolume $V_{2\phi}$ of Figure 5.1, the mixture volumetric flux divergence equation, simplified on account of assumptions (p-i) and (p-iv) listed in Section 5.2, is

$$\nabla \cdot \vec{j}_m = v_{fg} \Gamma_g - \frac{dp}{dt} \sum_{k=f,g} \alpha_k \frac{\rho'_k}{\rho_k}, \quad (5-5)$$

5. Modeling Equations

where j_m , v_{fg} , and α are the mixture volumetric flow rate, the specific volume change due to phase change, and the volume fraction, respectively. Subscripts f and g denote saturated liquid and vapor, respectively. The superscripted prime means differentiation with respect to pressure along the saturation line. Γ_g is the rate of equilibrium phase change. The expression for Γ_g is derived from the mass and energy balances to yield the contributions from heating and cooling (boiling and condensing) and from pressure variations (flashing and condensing) as follows:

$$\Gamma_g = \frac{-\nabla \cdot \vec{q}}{h_{fg}} + \frac{dp}{dt} \frac{1 - \sum_{k=g,f} \alpha_k \rho_k h'_k}{h_{fg}}, \quad (5-6)$$

where h stands for enthalpy. By combining Eqs. (5-5) and (5-6) one gets the mixture volumetric flux divergence equation for the two-phase mixture in subvolume $V_{2\phi}$ of Figure 5.1

$$V_{2\phi} : \quad \nabla \cdot \vec{j}_m = - \left\{ \sum_{k=g,l} \alpha_k \left[\frac{v_{fg}}{h_{fg}} (\rho_k h'_k - 1) + \frac{\rho'_k}{\rho_k} \right] \right\} \dot{p} - \frac{v_{fg}}{h_{fg}} \nabla \cdot \vec{q}. \quad (5-7)$$

Equations (5-3), (5-4), and (5-7) show that the single- and two-phase fluid dilatation depends only on two processes, namely on heat addition and depressurization. For two-phase fluid, this is a consequence of the equilibrium assumption (Assumption p-i in Section 5.2). Conversely, the rate of depressurization can depend only on volume changes due to volume discharge and volume expansion or contraction caused by heating or cooling, respectively, which may include phase change.

By integrating Eqs. (5-3), (5-4), and (5-7) over the total volume V in Figure 5.1, by using the divergence theorem to convert volume into area integrals, the mean-value theorem of integral calculus for volume averaging, simplifying assumption (p,T-ii) presented in Section 5.2, and the fact that $V = V_i + V_v + V_{2\phi} + V_{N2}$ is rigid, one obtains the very important equation for the time rate of pressure change in the total volume V of Figure 5.1.

$$\dot{p} = \frac{1}{V \chi_V} \left[- \sum_{bk, ADS} \Phi + \frac{v_{fg}}{h_{fg}} (\dot{Q}_{2\phi})_{net} + \sum_{l,v} \frac{\beta_T}{\rho c_p} \dot{Q}_{net} + \left(\frac{\beta_T}{\rho c_p} \right)_l P_{PP} + \frac{\gamma-1}{\gamma P} \dot{Q}_{N2} \right]. \quad (5-8)$$

Each term in the square bracket is a rate of volume change. The first term is the sum of volumetric flow rates, Φ , leaving the control volume V through break and valve openings. The second term is the volume generation or annihilation by phase change, the third and fourth terms are the volume generation or annihilation by thermal expansion or contraction by net heating or cooling, \dot{Q}_{net} , and by the pumping power, P_{PP} , in single-phase regions. The denominator of Eq. (5-8) is the total system *elasticity* or mechanical compliance, $V \chi_V$, where the system isentropic compressibility (volumetric mechanical compliance) is given by

$$\chi_V = \sum_i \chi_i = \sum_{j=l,v} \left(\frac{c_v \kappa}{c_p} \right)_j \frac{V_j}{V} + \left\{ \sum_{k=g,f} \alpha_k \left[\frac{v_{fg}}{h_{fg}} (\rho_k h'_k - 1) + \frac{\rho'_k}{\rho_k} \right] \right\} \frac{V_{2\phi}}{V} + \frac{1}{\gamma P} \frac{V_{N2}}{V}. \quad (5-9)$$

Equation (5-9) shows that the total system elasticity is a series of up to four subvolume-fraction-weighted, *isentropic* compressibilities, namely, $\chi_i = V_i/V [-1/v (\partial v/\partial p)_i]$, one each for single-phase liquid, single-phase vapor, ideal gas (each subvolume having its own averaged temperature), and two-phase mixture, regardless of their distribution within the

5. Modeling Equations

system. Equation (5-9) is derived for the cases prevailing at the beginnings of all the phases analyzed, namely for continuous volumetric flow rates at the interfaces between subvolumes. Should there be phase change (due to mixing of vapor with subcooled liquid, for example) associated with the mass flow rate from some region (1) to region (2) then $\chi_1 V_1(1 - \rho_1/\rho_2)/V$ would have to be added to χ_V .

Equation (5-8) demonstrates also the important fact that a given amount of heat exchanged with any control subvolume has profoundly differing effects on the system pressure, depending on whether the subvolume contains single or two-phase fluids. Moreover, the equation shows that a large volume (such as the primary system volume) of liquid being heated or cooled strongly (by fission power, or SG cooling) can affect the pressure as much as a small volume of two-phase mixture (in Pressurizer, with a small heater). Equation (5-8) shows also that pressure changes only because of volume changes caused by volume discharge or injection and by heat transfer.

5.4.1.3 Time Rate of Inventory Change

The loss of liquid inventory in the system with fixed control volume, V , and the component volume $V_{2\phi}$ containing a two-phase mixture is modeled as the gain of vapor. See Figure 5.1. The vapor mass balance gives the rate of change of vapor volume fraction, α , in $V_{2\phi}$ and is, on account of Assumption (p-i) in Section 5.2, given, for the prevailing cases that $V_{2\phi}$ is rigid or that the void fractions at the moving boundary equals the volume-averaged void fraction, by

$$\text{For } V_{2\phi}: \quad V_{2\phi} \rho_g \frac{d\alpha}{dt} = \sum_{in} W_G + V_{2\phi} (\Gamma_g - \alpha \rho_g' \dot{p}), \quad (5-10)$$

where the time rate of vapor generation per unit of volume, Γ_g , is given by Eq. (5-6), and the rate of change of pressure, \dot{p} , is given by Eq. (5-8). W_G is the vapor mass flow rate, counted positive when entering $V_{2\phi}$, and ρ_g is the vapor density. The volumetric flow rates between components are computed by integrating, over the component volume, and with the pressure derivative from Eq. (5-8), the volumetric flux divergence equation, Eqs.(5-3), (5-4), or (5-5), depending on which type of fluid occupies the component.

After substituting Eqs. (5-6) and (5-8) into Eq. (5-10), one obtains the time rate of change of vapor fraction in terms of transfer processes taking place at the system boundary, namely in terms of the volumetric flows at the break, Φ_{bk} , and at the ADS valves (discharging from subcooled regions), Φ_{ADS} , the direct vapor discharge (if any) from $V_{2\phi}$, the heat transfer to two-phase regions, $\dot{Q}_{2\phi}$, to single-phase regions of liquid, $\dot{Q}_{1\phi,l}$, and pumping power P_{PP} to single-phase liquid, and heat transfer to single-phase regions of vapor, $\dot{Q}_{1\phi,v}$ and to the noncondensable gas \dot{Q}_{N_2} , all contained in the system volume, V . The general expression for the vapor conservation equation is

$$\begin{aligned} \frac{V \chi_V}{\Psi_\alpha} \frac{d\alpha}{dt} = & \sum_{bk, ADS} \Phi + \frac{V \chi_V}{V_{2\phi} \Psi_\alpha} \Phi_g - \dot{Q}_{2\phi} \left(\frac{v_{fg}}{h_{fg}} - \frac{V \chi_V}{\Psi_\alpha \rho_g h_{fg} V_{2\phi}} \right) \\ & - \left(\frac{\beta_T}{\rho c_p} \right)_l (\dot{Q}_{1\phi} + P_{PP})_l - \left(\frac{\beta_T}{\rho c_p} \right)_v (\dot{Q}_{1\phi})_v - \frac{\gamma - 1}{\gamma P} \dot{Q}_{N_2}, \end{aligned} \quad (5-11)$$

where obviously not all the terms are appropriate for every phase, and where the rate of volume expansion per unit of energy, in the two-phase region is

5. Modeling Equations

$$\Psi_{\alpha} = \frac{\alpha(\rho_g h_g' + h_{fg} \rho_g') + (1 - \alpha)\rho_f h_f' - 1}{\rho_g h_{fg}} \quad (5-12)$$

The elasticity of the system, χ_V , is given by Eq. (5-9). The right-hand side of Eq. (5-11) shows rates of volume displacements, as show the terms in the square bracket of Eq. (5-8).

5.4.1.4 Time Rate of Temperature Change

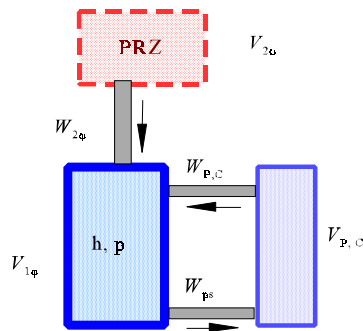


Figure 5.5 Schematic Control Volume for Primary System. (dark blue box; P for PRHR, C for CMT)

The scaling analysis deals with heat transfer between, and temperatures of, saturated two-phase mixture (Assumption (p-i) in Section 5.2), subcooled liquid, and structures. The energy balance below is written to predict the temperature change in the *subcooled liquid*. The temperature in the two-phase regions of the system volume, V , is the saturation temperature (Assumption (p-i) in Section 5.2) at the system pressure given by the integral of Eq. (5-8). With heat transfer *to the fluid* counting positive, structural temperatures are predicted by integrating the energy balance of structures, given by

$$(c_p M)_{stc} \frac{dT_{stc}}{dt} = -\dot{Q}_{stc}.$$

The energy balance for the fixed volume $V_{1\phi}$ of the reactor cooling system (subscript ps), that is filled with subcooled liquid and connected to the Pressurizer (PRZ), the Core Make-up Tank (CMT), the Passive Residual heat Rejection (PRHR) system, and (possibly) the Accumulators (ACC), is combined with the mass balance for the same control volume to give

$$V_{1\phi} \frac{d}{dt} \left[\rho \left(h - \frac{p}{\rho} \right) \right]_{ps} = (\dot{Q}_{net})_{1\phi} + P_{PP} + \sum_{inj,i} W_i (h_i - h) - W_{bk} h_{ps} \quad (5-13)$$

$$V_{1\phi} \frac{d\rho}{dt} = \sum_{inj,i} W_i - W_{bk}, \quad (5-14)$$

where the summations are taken over PRZ, CMT, PRHR, and ACC, with the mass flow rates, W , counting positive when entering the primary system (see dark blue heavy box in Figure (5.5)). The flow rates, W , through the CMT and PRHR system are driven by buoyancy and, therefore, computed from the coupled loop momentum balances. The mass flow rate, $W_{2\phi}$, from the pressurizer to the primary system is driven entirely by the fluid expansion in the PRZ, and computed from the flux divergence equation, Eq. (5-7).

$$W_{2\phi} = \rho_{2\phi} \left(\frac{v_{fg}}{h_{fg}} \dot{Q}_{2\phi} - \chi_{2\phi} V \dot{p} \right), \quad (5-15)$$

where the pressure derivative is given by Eq. (5-8), $\dot{Q}_{2\phi}$ is the (electrical) heating power supplied to the two-phase region (PRZ), and the elasticity (or mechanical volumetric compliance) of the two-phase region is, as in Eq. (5-9),

5. Modeling Equations

$$\chi_{2\phi} = \left\{ \sum_{k=f,g} \alpha_k \left[\frac{v_{fg}}{h_{fg}} (\rho_k h_k' - 1) + \frac{\rho_k'}{\rho_k} \right] \right\} \frac{V_{2\phi}}{V}. \quad (5-16)$$

After expanding the enthalpy derivative in Eq. (5-13) in terms of temperature and pressure, and after substituting Eqs. (5-14), (5-15) and (5-8), into Eq. (5-13), one finds for the time rate of temperature change in the *reactor cooling system* (or primary system of normal operation), as before in terms of transfer processes taking place at the global system's boundary, namely in terms of the volumetric flows at the break and at the ADS valves, Φ_{bk} , the heat transfer to two-phase regions, $\dot{Q}_{2\phi}$, to single-phase regions of liquid, $\dot{Q}_{1\phi}$ and P_{PP} , and to the noncondensable gas \dot{Q}_{N_2} , all contained in the system volume, V .

$$\begin{aligned} V_{1\phi} \rho c_p \frac{dT}{dt} = & \sum_{CMT, PRHR} W_i (h_i - h) + (\dot{Q}_{1\phi} + P_{PP}) \left(1 + \frac{\beta_T}{\rho c_p} \frac{\Psi_T}{\chi_V V} \right) \\ & + \dot{Q}_{2\phi} \frac{v_{fg}}{h_{fg}} \left[\frac{\Psi_T}{\chi_V V} + \rho_{2\phi} (h_{2\phi} - h) \right] - \frac{\Psi_T}{\chi_V V} \left(\Phi_{bk} - \frac{\gamma-1}{\gamma p} \dot{Q}_{N_2} \right), \end{aligned} \quad (5-17)$$

where

$$\Psi_T = V_{1\phi} \beta_T T - V \chi_{2\phi} \rho_{2\phi} (h_{2\phi} - h). \quad (5-18)$$

Obviously, not all the terms in Eq. (5-17) apply for every phase. Equation (5-17) is general, however, and is modified and used also for the temperature prediction of liquid in components CMT and PRHR.

5.4.2 Momentum Balance

The momentum balance is used to scale the dynamic component interaction in the primary system of the AP600, and to estimate the reference flow rates which are needed to normalize the mass, momentum, and energy balances. The local, one-dimensional momentum balance is integrated, as explained by Wulff [17] to obtain the loop momentum balance for every closed loop of the system in terms of the loop momentum M , which is a scalar momentum per unit of area. Its rate of change is derived in terms of scalar pressure differences, rather than in terms of vectorial resultant forces.

For Phases 1 through 4, i.e., the time before the depressurization of the system establishes communication (by *subcritical* flow through break and ADS valves) with the containment atmosphere, the seven loops (five for ROSA) are contained inside the primary system. For Phase 5, the quasi-steady IRWST and sump injection phase, there are five loops that are closed with segments of constant pressure in the containment atmosphere. The special formulation for Phase 5 is described in Section 5.5.4. Figures 5.6, 7, 8, and 9 show the loops for normal operation and Phases 1, 2, 3, 4, and 5, respectively. ROSA has two loops fewer than AP600 for Phases 1 through 4.

5.4.2.1 System Momentum Balance

There is a loop momentum balance written for every closed loop. The loop momentum balances are then combined into a vector equation of first-order ordinary differential equations for scaling as a single vector equation. The vector equation is the global momentum balance of the system. The j^{th} element of that vector equation is given by

5. Modeling Equations

$$\frac{dM_j}{dt} = \vec{g} \cdot \oint_j \hat{k} \rho_m dz + \Delta p_{PP,j} - \sum_j (\Delta MF) - \sum_j RW_m |W_m|, \quad (5-19)$$

where the j^{th} loop momentum is defined by

$$\begin{aligned} M_j &= \oint_j W_m \frac{dz}{A} = \sum_{i \in j} \int_0^{L_i} W_m \frac{dz}{A} \\ &= \sum_{i \in j} \left[(\Phi_m)_i(0) \int_0^{L_i} f_\rho \frac{dz}{A} + \int_0^{L_i} f_\rho \Delta \Phi_m \frac{dz}{A} - \int_0^{L_i} \alpha \Delta \rho \langle v_{gj} \rangle dz \right]. \end{aligned} \quad (5-20)$$

The loop momentum balance, Eq. (5-19), is derived by summing up the *pressure differences* across the segments of the loop, i.e., by utilizing the fact that the contour integral of pressure gradient around every loop, $\oint dp$, equals the sum of the pump-induced pressure increases in that loop. The summation eliminates *all* internal pressures from Eq. (5-19). Internal pressures are scalars (akin to voltages in electrical circuits) and more natural to eliminate than internal forces (which are vectors, involving fluid-to-structure interactions). The important consequence of formulating the momentum balance for a loop segment in terms of *pressure difference*, instead of resultant forces, and in terms of volume flow rate instead of the familiar velocity, is that one obtains in the case of single-phase fluid, not the familiar fluid mass (ρV , i.e., density times segment volume), but rather the inertia per area squared, ($\rho L/A$), as the inertia representation (analogous to capacitance in electrical circuits) of the loop segment, where L and A are the segment length and cross-sectional area, respectively. For two-phase flow, ($\rho L/A$) becomes the first integrand in the bracket of Eq. (5-20), with f_ρ given by Eq. (5-25). The associated integral is, for this report, the so-called inertia of the loop segment, which leads to the loop inertia and inertia matrix of the system. Equation (5-19) demonstrates that flow rates in a closed-loop system can be predicted without computing pressures.

As seen in Eq. (5-20), the defining contour integral is replaced, in the first line, by the sum of i integrals taken along a loop segment of constant flow cross-section. In the second line, the mixture mass flow rate is expressed by its drift-flux identity, in terms of the liquid mass flow rate at the entrance to the segment, times the density function, f_ρ given by Eq. (5-25), and then the contributions from momentum flux change due to phase change, and from the vapor drift.

The second term in Eq. (5-19) is the driving pressure due to gravity, with the unit vector, \hat{k} , pointing in the normal flow direction. The third term in Eq. (5-19) is the pressure induced by the Reactor Coolant Pumps. The fourth term accounts for the change, ΔMF , along the i^{th} segment in the j^{th} loop, of the momentum flux, MF , where

$$\begin{aligned} MF &= \frac{W_v \Phi_v (1 - \alpha) + W_l \Phi_l \alpha}{\alpha (1 - \alpha) A^2} \quad \text{for } \alpha \neq 0, 1 \\ MF &= \frac{W_l \Phi_l}{A^2} \quad \text{for } \alpha = 0 \\ MF &= \frac{W_v \Phi_v}{A^2} \quad \text{for } \alpha = 1. \end{aligned} \quad (5-21)$$

5. Modeling Equations

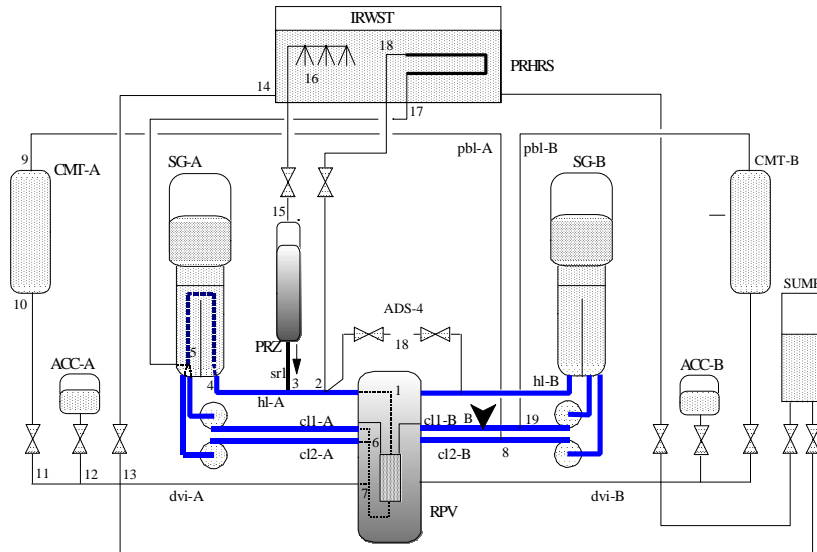


Figure 5.6 Four-Loop Control Volume for Normal Operation and for Phase 1, Initial Depressurization.

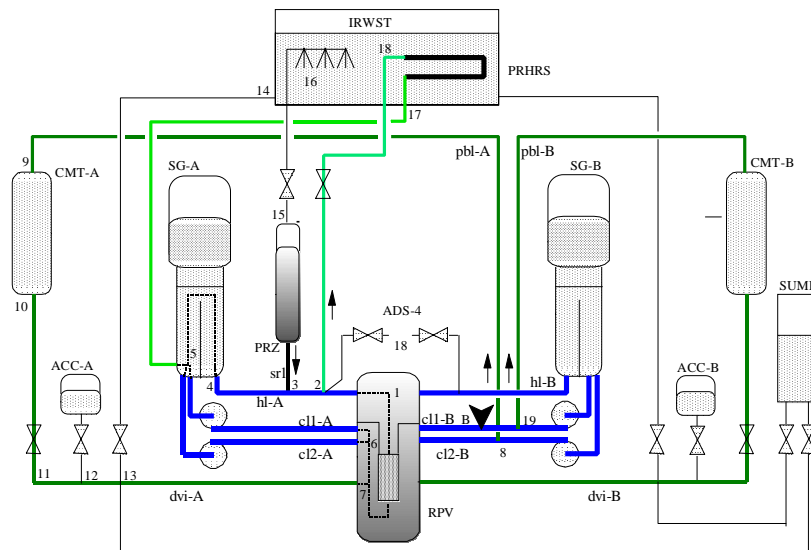


Figure 5.7 Seven-Loop Control Volume for Phase 2, Passive Heat Removal.
Green loops are closed on shortest connection.

5. Modeling Equations

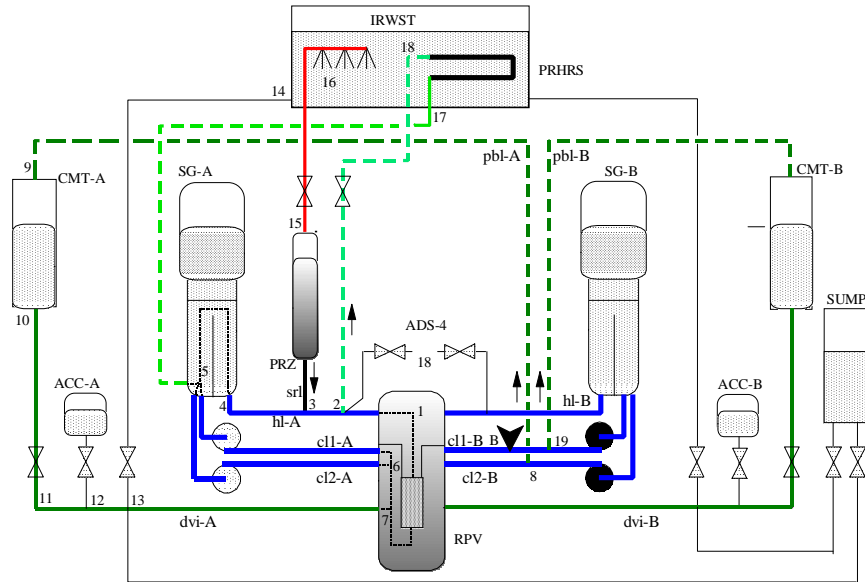


Figure 5.8 Seven-Loop Control Volume for Phase 3, ADS-123 Blowdown.

Green loops are closed by shortest connections.

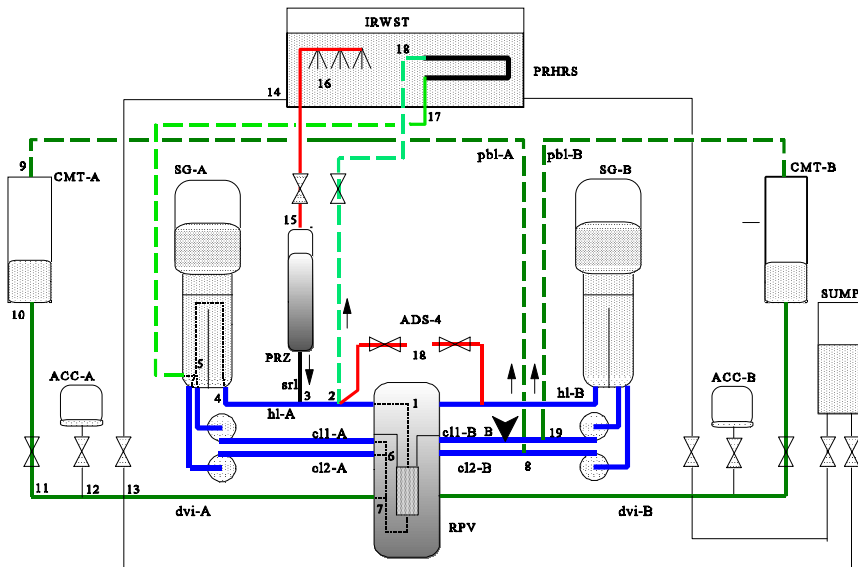


Figure 5.9 Seven-Loop Control Volume for Phase 4, ADS-4 Depressurization.

Green loops are closed by shortest connections.

5. Modeling Equations

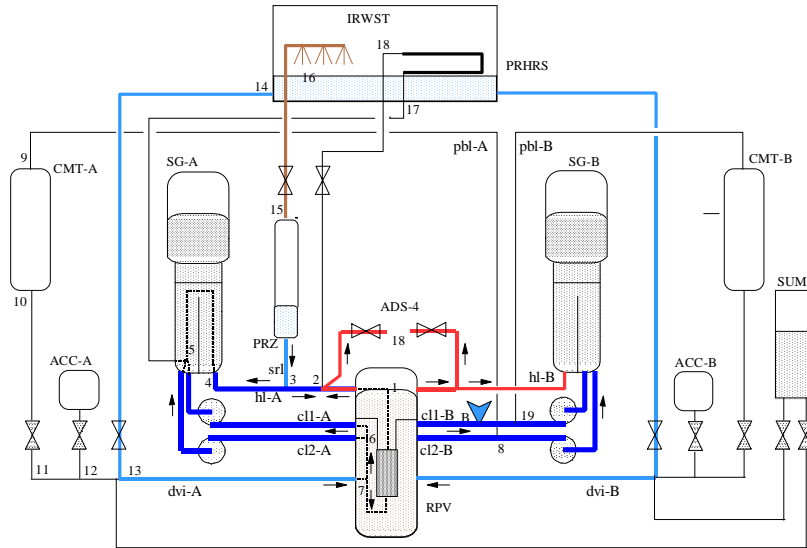


Figure 5.10 Six-Loop Control Volume for Phase 5, IRWST Injection.

Loops in color are closed by shortest connections.

The last term in Eq. (5-19) is the pressure drop due to wall shear and form losses. Its detailed derivation is found in [17]. The flow resistance, R , is

$$R = \frac{K + (\varphi_{i0}^2 f) \frac{L}{d_h}}{2\rho_l A^2}, \quad (5-22)$$

where f , φ_{i0}^2 , L , d_h , and A denote, respectively, the Darcy friction factor, the two-phase friction multiplier, the length of the i^{th} duct segment in the j^{th} loop, and K is the form loss coefficient for the exit of the segment and defined in terms of the standard form loss factor, ζ ,

$$K = \zeta \left(\frac{A}{A_{\min}} \right)^2 - \left[1 - \left(\frac{A^-}{A^+} \right)^2 \right] \quad (5-23)$$

$$\zeta = S_0(W) (\zeta_{fd} - \zeta_{bd}) + \zeta_{bd}$$

$$S_k(x) = 0 \quad \text{for } x < k$$

$$= 1 \quad \text{for } x \geq k .$$

$S_k(x)$ is the unit step function. The prediction of ζ is described in Idelchick [23], the subscripts fd and bd indicate forward and backward directions, respectively.

5. Modeling Equations

The first term in the last line of Eq. (5-20) dominates the momentum M_j ; it contains the so-called inertia of the i^{th} segment, i.e., the “inertia” related to the volumetric flow rate, $\Phi_m(0)$, at the entrance to the loop segment, and to the pressure difference in Eq. (5-19), rather than the traditional inertia of segment mass which is related to velocity and resultant force (see also the final form of the momentum balance, Eq. (5-36), below). The inertia of the loop segment is

$$I = \int_0^{L_i} f_\rho \frac{dz}{A}, \quad (5-24)$$

where the density function is

$$f_\rho(z) = (\rho_l - \alpha(z) \Delta\rho C_0) \quad (5-25)$$

and equals ρ_l for single-phase liquid, and ρ_v for single-phase vapor. The second term in the last line of Eq. (5-20) is the momentum induced by phase and phasic density changes. Here

$$\Delta\Phi_m = \frac{\Delta\rho}{\rho_f \rho_g} \Gamma_g - \dot{p} \sum_{k=l,g} \alpha_k \frac{\rho'_k}{\rho_k}, \quad (5-26)$$

and the pressure derivative is given by Eq. (5-8). The last term in the last line of Eq. (5-20) is the momentum induced by phase separation; $\langle v_{gj} \rangle$ is the void fraction-weighted, area-averaged vapor drift velocity.

There are $N_L = 4, 7, 7,$ and 6 closed loops, respectively, with $N_B = 5, 9, 9,$ and 7 branch points in Figures 5.6, 7, 8, and 9. The loops have been described in Section 5.4 on Page 5-3. The branch points in the four-loop system are shown in Figure 5.6 as Points 1, 5A, 5B, and 6. For the seven-loop system, the four additional branch points are given in Figure 5.7 as Points 2, 7, 8, and 19. Wulff [23] has shown that a system of N_L closed loops and N_B branch points calls for $(N_L + N_B - 1)$ linearly independent equations for the $(N_L + N_B - 1)$ transient volumetric flow rates, $\Phi_m(0, t)$ in Eq. (5-20), at branch exits (i.e., where $z = 0$ for the associated loop segment). These flow rates are needed to evaluate the last line in Eq. (5-20) and to calculate the transient local mass flow rates anywhere in the system. Open injection or discharge points or connections to dead-ended components are not counted as branch points because their associated flow rates are, respectively, imposed, computed from critical flow or quasi-steady valve flow models, or from the appropriate volumetric flux divergence equation, Eqs. (5-3), (5-4), or (5-7); see Eq. (5-15) as an example. Therefore, the loop momentum balances provide N_L volumetric flow rates in the role of state variables from which all the linearly independent $(N_L + N_B - 1)$ flow rates can be computed for the branch point exits and, from that the flow for any time and any location in the system [23].

N_L of these equations are given by the loop momentum definitions Eqs. (5-20), for which the momenta are obtained by integrating Eqs. (5-19). We associate with each loop (with index j) a *conveniently selected primary* loop segment (subscript pr) that has the primary volumetric flow rate $\Phi_{m,pr}(0, t)$ (or state variable) at the entrance. We call all other branch point exit volumetric flow rates secondary flow rates $\Phi_{m,sn}(0, t)$. Correspondingly, we decompose the loop inertia defined by the first sum in the last line of Eq. (5-20) by associating with the ji -element of the $(N_L \times N_L)$ matrix, Λ_{ji} , the inertia of the primary loop segment i in loop j , and with the elements of the $[N_L \times (N_B - 1)]$ matrix \mathbf{X}_{jq} the flow inertia contributions of the secondary loop segments. We use the Einstein summation convention: repeated indices imply summation. Thus, by rewriting the definition of the loop momentum given in the last line of Eq. (5-20), now with the sum of primary and secondary volumetric flow rates for the first and important inertia term, and with S_M for the combination of phase change- and phase separation-induced momenta, one finds

$$M_j = \oint_j W_m \frac{dz}{A} = \Lambda_{ji} [\Phi_{m,pr}(0, t)]_i + \mathbf{X}_{jq} [\Phi_{m,sn}(0, t)]_q + S_{Mj}, \quad j = 1, \dots, N_L. \quad (5-27)$$

5. Modeling Equations

These N_L equations are combined with $(N_B - 1)$ linearly independent equations of volumetric flow rate continuity at branch points (l).

$$\sum_{k \in l} \left(\Phi_m(0, t) \right)_k + \left(S_\Phi \right)_k = 0, \quad (5-28)$$

where $l = 1, \dots, N_{B-1}$. Flows leaving the branch count positive, and the S_Φ 's represent the dilatation of incoming flows along the upstream segment and are defined from the integral of Eq. (5-5):

$$\Phi_m(z, t) = \Phi_m(0, t) + \int_0^z \Delta \Phi_m dz = \Phi_m(0, t) + S_\Phi. \quad (5-29)$$

Eqs. (5-27) and (5-28) form a system of $(N_L + N_B - 1)$ equations, implicit in the $(N_L + N_B - 1)$ unknown volumetric flow rates at branch exits that are needed in Eq. (5-20). This system of equations was solved to obtain the inertia and impedance matrices for AP600, APEX, ROSA, and SPES by use of the mathematical software package MATHCAD. The formal solution was obtained by specifying first the *admittance matrix* which characterizes the system connectivity.

5.4.2.2 System Admittance Matrix

For most system topologies, one can derive the inertia matrix and impedance matrix by inspection and manual matrix inversion. It was found, however, to be more convenient to follow Reference [21] and to use the admittance matrix shown in Appendix 6 and the available mathematical software package MATHCAD for obtaining the matrices in Eq. (5-32) below and for arranging the inertia and impedance matrices. Below we explain the admittance matrix and the linear algebra performed with MATHCAD to obtain the inertia and impedance matrices.

One finds that all the signs of $\Phi_m(0, t)$ in the summation of Eq. (5-28) are represented by either -1 (for flows approaching the junction l), 0 (for all flows through segments that are not directly connected to the junction l), or 1 (for flows leaving the junction l). The coefficients $\{-1, 0, +1\}$ are organized in the $N_B \times (N_L + N_B - 1)$ system *admittance matrix* \mathbf{H} in which each *branch point* is represented by a *row* and each *unknown branch exit flow rate*, $\Phi_m(0, t)$, by a *column* (see Appendix 6).

$$\mathbf{H}_{pq} = (\mathbf{A} \mathbf{B})_{pq} \quad (5-30)$$

The first $(N_B - 1)$ columns in \mathbf{H} are associated with the secondary branch exit flows $[\Phi_m(0, t)]_{sn}$, and form the $N_B \times (N_B - 1)$ matrix \mathbf{A} . The last N_L columns are associated with the primary branch exit flows, $[\Phi_m(0, t)]_{pr}$ and form the $N_B \times N_L$ matrix \mathbf{B} . The columns in \mathbf{H} are to be arranged in the same order as the vector elements $\{[\Phi_m(0, t)]_{sn}\}_1$ and $\{[\Phi_m(0, t)]_{pr}\}_q$ in Eq. (5-27). The elements in every column of \mathbf{H} sum up to 0 (as seen in Appendix 6). Next, the system admittance matrix \mathbf{H} is augmented with the $N_B \times N_B$ identity matrix \mathbf{I} to yield the augmented admittance matrix \mathbf{H}_A

$$(\mathbf{H}_A)_{pq} = (\mathbf{A} \mathbf{B} \mathbf{I})_{pq}. \quad (5-31)$$

By performing elementary row reductions on the augmented admittance matrix, (\mathbf{H}_A) , one obtains its row-reduced echelon matrix whose rank is $(N_B - 1)$, because only $(N_B - 1)$ conservation equations of branch points are linearly independent; the N_B^{th} secondary exit flow satisfies the mass balance automatically because the global mass balance, Eq. (5-8), is satisfied (see Appendix 6). After removal of the last row (with $(N_L + N_B - 1)$ 0s, followed by N_B 1s) and the $(N_L + N_B)^{\text{th}}$ column of zeroes, the row-reduced echelon matrix has this block structure,

$$\left[\mathbf{I}_r \left(\mathbf{A}_r^{-1} \mathbf{B}_r \right) \mathbf{A}_r^{-1} \right] \quad (5-32)$$

5. Modeling Equations

and yields *simultaneously*, in addition to the $(N_B - 1) \times (N_B - 1)$ identity matrix in first position, the $(N_B - 1) \times N_L$ reduced matrix $(\mathbf{A}_r^{-1} \mathbf{B}_r)$, and the reduced $(N_B - 1) \times (N_B - 1)$ square matrix \mathbf{A}_r^{-1} in second and third positions, respectively. The inverse \mathbf{A}_r^{-1} and the product $(\mathbf{A}_r^{-1} \mathbf{B}_r)$ are constants (having -1, 0, 1 as elements) and characterize the topology of the system. Both matrices need to be extracted only once for a given system from the row-reduced echelon matrix given by Eq. (5-32).

By replacing all positive elements of the system admittance matrix \mathbf{H} by zeroes and by removing its last row, one obtains the $(N_B - 1) \times (N_L + N_B - 1)$ reduced admittance matrix \mathbf{H}_r . Finally, with all the elements $(S_{\Phi})_j$ of dilation (shown in Eq. (5-28) but defined in Eq. (5-29)) ordered in accordance with their associated volumetric flow rates $\{[\Phi_m(0, t)]_{sn}\}_p$ and $\{[\Phi_m(0, t)]_{pr}\}_q$, we form the dilatation vector

$$\mathbf{Y}_i = (\mathbf{H}_r)_{ij} (S_{\Phi})_j, \quad i = 1, \dots, N_B - 1, \quad j = 1, \dots, N_L + N_B - 1 \quad (5-33)$$

and write the volumetric flow continuity equation, Eq. (5-28), for a branch point (i),

$$(\mathbf{A}_r)_{ip} [(\Phi_m(0, t))_{sn}]_p + (\mathbf{B}_r)_{iq} [(\Phi_m(0, t))_{pr}]_q + \mathbf{Y}_i = 0. \quad (5-34)$$

By pre multiplying Eq. (5-34) with the inverse \mathbf{A}_r^{-1} from Eq. (5-32), by solving then the result for the unknown *secondary* branch exit flow rates, $\{[\Phi_m(0, t)]_{sn}\}_p$

$$\left[(\Phi_m(0, t))_{sn} \right]_p = - (\mathbf{A}_r^{-1})_{pi} \left\{ (\mathbf{B}_r)_{iq} [(\Phi_m(0, t))_{pr}]_q + \mathbf{Y}_i \right\} \quad (5-35)$$

and by substituting the solution of $\{[\Phi_m(0, t)]_{sn}\}_p$ into Eq. (5-27) one finds the vector equation for the system loop momentum *explicit* in terms of only the *primary branch exit flow rates*, i.e., the dynamic state variable flow rates, $\{[\Phi_m(0, t)]_{pr}\}_p$, the known dilatation vector, \mathbf{Y}_p , and the known momenta induced by phase change and phase separation, S_{M_i} .

$$M_i = \mathbf{I}_{ip} [(\Phi_m(0, t))_{pr}]_p - \mathbf{X}_{iu} (\mathbf{A}_r^{-1})_{up} \mathbf{Y}_p + S_{M_i}, \quad i = 1, \dots, N_L. \quad (5-36)$$

5.4.2.3 Inertia Matrix

The $N_L \times N_L$ square matrix \mathbf{I}_{ip} in Eq. (5-36) is the *global system inertia matrix* [17] and given by

$$\mathbf{I}_{ip} = \mathbf{A}_{ip} - \mathbf{X}_{iu} (\mathbf{A}_r^{-1})_{ut} (\mathbf{B}_r)_{tp}. \quad (5-37)$$

It is recognized as the inertia matrix because it reduces for the simple case of single-phase flow the equations of system momentum balance, Eq. (5-19) to

$$\mathbf{I}_{ji} \frac{d[(\Phi_m)_{pr}]_i}{dt} = \bar{g} \cdot \oint_j \hat{k} \rho_m dz + \Delta p_{PP,j} - \sum_j R W_m |W_m|, \quad (5-38)$$

5. Modeling Equations

since ΔMF in Eq. (5-19) and Y and S_M in Eq. (5-36) are 0. Figure A.6.1 in Appendix A.6 shows the admittance matrix and the row-reduced, augmented matrix for AP600 in *Phase 1*, i.e., the Initial Depressurization (*normal conditions*). The volumetric flow rates shown in Figure A.4.1 refer to the branch point designations in Figure 5.6.

Equation (5-24) defines the inertia, I , for two-phase flow in a *component*, i.e., the contributions to the elements of the inertia matrix, \mathbf{I} , representing the inertia of the *loop segment* between branch points. Appendix A.1.4 lists under “Aspect Ratios” the numerical values of the geometric inertia coefficients, L/A , for the components AP600, APEX, ROSA, and SPES. These aspect ratios were computed from the flow cross-sectional areas of the components, as given in Appendix A.1.2, and from the channel lengths, L , listed in Appendix A.1.3. The density function, f_ρ defined by Eq. (5-25), is evaluated, with density and void fractions occurring at the beginning of every phase, as an average for every loop segment.

Figure A.6.1 in Appendix A.6 shows the admittance matrix, \mathbf{H} , i.e., the combination of the two parts \mathbf{A} and \mathbf{B} , which are associated with the secondary and primary flow rates, respectively, and the row-reduced, augmented matrix, all for the AP600, APEX, and SPES during *Phases 1*. The volumetric flow rates shown in Figure A.6.1 on Page A.6-2 refer to the branch point designations in Figure 5.6.

Table 5.1 presents the inertia matrix with symbol entries, I , of the loop segments for the four-loop systems AP600, APEX, and SPES at normal operating conditions and for Phase 1, i.e., the phase of Initial Depressurization. The subscripts of I denote the segment endpoints shown in Figure 5.6. Tables 5.2, 3, and 4 have the inertia symbols, I , replaced by the corresponding numerical values in kg/m^4 , and serve to compare the inertia matrices of normal operation for AP600, APEX, and SPES in numerical form.

Table 5.1 Inertia Matrix for Four-Loop Operation of AP600, APEX, and SPES under Normal Conditions and Phase 1, Initial Depressurization.

Loop		Flow Rate leaving from			
on Side	through	SG Exit of Loop _{B1}	SG Exit of Loop _{B2}	SG Exit of Loop _{A1}	SG Exit of Loop _{A2}
B	Cold Leg 1	$I_{\text{loop-B1}}$	$I_{\text{B6-1-5}}$	$I_{\text{G-1}}$	$I_{\text{G-1}}$
B	Cold Leg 2	$I_{\text{B6-1-5}}$	$I_{\text{loop-B2}}$	$I_{\text{G-1}}$	$I_{\text{G-1}}$
A	Cold Leg 1	$I_{\text{G-1}}$	$I_{\text{G-1}}$	$I_{\text{loop-A1}}$	$I_{\text{B6-1-5}}$
A	Cold Leg 2	$I_{\text{G-1}}$	$I_{\text{G-1}}$	$I_{\text{B6-1-5}}$	$I_{\text{loop-A2}}$

Each row in Tables 5.1 through 5.7 represents a loop as indicated in the first two columns. Each column represents the primary flow rate (state variable) of the loop, as noted in the heading of the matrix. The Cold-Leg flow rates at the Steam Generator exits are the primary flow rates for the coolant loops, as shown in Figure 5.6. Diagonal (**bold**) symbols represent the whole loop, off-diagonal **blue** and **magenta** symbols, respectively, neighboring and opposite-side loop segments.

For normal operation and during Phase 1, all flows are positive around the loop. Therefore, the diagonal elements of the inertia matrix in Tables 5.1 through 5.5 (bold-face symbols) represent the *loop inertia*. The magnitude of the off-diagonal elements shown in **blue** is a measure of the cross coupling by inertia between loops on the same side of the reactor, while the magnitude of the off-diagonal elements shown in **magenta** is a measure of the cross coupling by inertia between loops on opposite sides of the reactor. Coupling by inertia is through Hot Leg, Steam Generator, and Reactor Vessel for loops on the same side of the reactor. Loops on opposite sides are inertia-coupled only through the Reactor Vessel.

5. Modeling Equations

Table 5.2 Numerical Values of Inertia Matrix for Four-Loop Operation: AP600
under Normal Conditions and Phase 1, Initial Depressurization (kg m^{-4})

Loop		Flow Rate leaving from			
on Side	through	SG Exit of Loop _{B1}	SG Exit of Loop _{B2}	SG Exit of Loop _{A1}	SG Exit of Loop _{A2}
B	Cold Leg 1	5.25×10^4	3.11×10^4	3.83×10^3	3.83×10^3
B	Cold Leg 2	3.11×10^4	5.25×10^4	3.83×10^3	3.83×10^3
A	Cold Leg 1	3.83×10^3	3.83×10^3	5.25×10^4	3.11×10^4
A	Cold Leg 2	3.83×10^3	3.83×10^3	3.11×10^4	5.25×10^4

Table 5.3 Numerical Values of Inertia Matrix for Four-Loop Operation: APEX
under Normal Conditions and Phase 1, Initial Depressurization (kg m^{-4})

Loop		Flow Rate leaving from			
on Side	through	SG Exit of Loop _{B1}	SG Exit of Loop _{B2}	SG Exit of Loop _{A1}	SG Exit of Loop _{A2}
B	Cold Leg 1	5.56×10^5	3.33×10^5	3.48×10^4	3.48×10^4
B	Cold Leg 2	3.33×10^5	5.56×10^5	3.48×10^4	3.48×10^4
A	Cold Leg 1	3.48×10^4	3.48×10^4	5.56×10^5	3.33×10^5
A	Cold Leg 2	3.48×10^4	3.48×10^4	3.33×10^5	5.56×10^5

Table 5.4 Numerical Values of Inertia Matrix for Four-Loop Operation: SPES
under Normal Conditions and Phase 1, Initial Depressurization (kg m^{-4})

Loop		Flow Rate leaving from			
on Side	through	SG Exit of Loop _{B1}	SG Exit of Loop _{B2}	SG Exit of Loop _{A1}	SG Exit of Loop _{A2}
B	Cold Leg 1	8.25×10^6	7.42×10^6	1.30×10^6	1.30×10^6
B	Cold Leg 2	7.42×10^6	8.25×10^6	1.30×10^6	1.30×10^6
A	Cold Leg 1	1.30×10^6	1.30×10^6	8.25×10^6	7.42×10^6
A	Cold Leg 2	1.30×10^6	1.30×10^6	7.42×10^6	8.25×10^6

5. Modeling Equations

For ROSA which has only two Cold Legs and only two reactor cooling loops, the inertia matrix was derived by the same method as described for AP600. For the two-loop system of ROSA, the 2x2 inertia matrix is shown in Table 5.5 below.

Table 5.5 Inertia Matrix for Four-Loop Operation of ROSA
under Normal Conditions and Phase 1, Initial Depressurization.

Loop		Flow Rate leaving from	
on Side	through	SG Exit of Loop _B	SG Exit of Loop _A
B	Cold Leg B	6.63×10^5	5.48×10^4
A	Cold Leg A	5.48×10^4	6.63×10^5

Table 5.6 presents the inertia matrix with symbol entries for the 7-Loop operation of AP600, APEX, and SPES during Phases 2 through 4. The indices of the *I*-elements refer to the flow diagrams in Figures 5.7 through 5.9. The inertia matrix is derived from Eq. (5-37), using the row-reduced echelon matrix in Figure A.6.2 of Appendix A.6, and then numerically evaluated with the data listed in Appendix A.1.4 and with the fluid densities listed in Appendices A.4.3 through A.4.4.

Table 5.6 Inertia Matrix in Symbolic Form for AP600, APEX, and SPES During Phases 2 Through 4

Loop		Flow Rate leaving from							Flow Rate from	
on side	through	CMT Branch of Loop _{B1} to RPV	CMT Branch of Loop _{B2} to CMT _A	SG Exit of Loop _{A1}	SG Exit of Loop _{A2}	CMT Branch of Loop _{B1} to CMT _B	CMT Branch of Loop _{B2} to RPV	PRHR Branch of Loop _A to PRHR	Surge Line to Hot Leg of Loop _A	Break in Loop _{B1}
B	Cold Leg 1	$I_{loop-B1}$	$I_{B,7-1-5}$	I_{6-1}	I_{6-1}	$I_{B,7-1-19}$	$I_{B,6-1-5}$	0	0	$(-I_{6-1})$
A	CMT _A	$(-I_{6-7})$	$I_{cmtA,8-9-7}$	$(-I_{6-7})$	$(-I_{6-7})$	0	$(-I_{6-7})$	0	0	I_{6-7}
A	Cold Leg 1	I_{6-1}	I_{7-1}	$I_{loop-A1}$	$I_{A,6-1-5}$	I_{7-1}	I_{6-1}	$(-I_{A,2-5})$	$(-I_{A,1-3})$	$(-I_{7-1})$
A	Cold Leg 2	I_{6-1}	I_{7-1}	$I_{A,6-1-5}$	$I_{loop-A2}$	I_{7-1}	I_{6-1}	$(-I_{A,2-5})$	$(-I_{A,1-3})$	$(-I_{7-1})$
B	CMT _B	$(-I_{B,19-7})$	0	$(-I_{6-7})$	$(-I_{6-7})$	$I_{cmtB,19-9-7}$	$(-I_{6-7})$	0	0	I_{6-7}
B	Cold Leg 2	$I_{B,6-1-8}$	$I_{B,7-1-8}$	I_{6-1}	I_{6-1}	$I_{B,7-1-8}$	$I_{loop-B2}$	0	0	$(-I_{6-1})$
A	PRHR	I_{6-1}	I_{7-1}	$I_{A,5-6-2}$	$I_{A,6-1-2}$	I_{7-1}	I_{6-1}	$I_{rhr,2-5}$	$(-I_{A,1-2})$	$(-I_{6-1})$

5. Modeling Equations

Table 5.7 shows the numerical values of the elements of the inertia matrix for the 7-Loop operation of AP600 during Phase 2. The I -elements in Table 5.6 are evaluated according to Eq. (5-37), using the data listed in Appendix A.1.4 and with the fluid densities listed in Appendices A.2.3 through A.2.4. The negative elements in the inertia matrix indicate that the flow corresponding to the column of the matrix is, in the common segment of the loop corresponding to the row of the matrix, in the direction opposite of the normal flow in that loop.

Table 5.7 Inertia Matrix in Numerical Form for AP600 During Phase 2
(All lines being filled with single-phase liquid, kg/m⁴)

Loop		Flow Rate leaving from							Flow Rate from	
on Side	through	CMT Branch of Loop _{B1} to RPV	CMT Branch of Loop _{B2} to CMT _A	SG Exit of Loop _{A1}	SG Exit of Loop _{A2}	CMT Branch of Loop _{B1} to CMT _B	CMT Branch of Loop _{B2} to RPV	PRHR Branch of Loop _A to PRHR	Surge Line to Hot Leg of Loop _A	Break in Loop _{B1}
B	Cold Leg ₁	5.21·10⁴	3.04·10 ⁴	3.81·10 ³	3.81·10 ³	3.76·10 ⁴	3.09·10 ⁴	0	0	-3.81·10 ³
A	CMT _A	-5.29·10 ²	1.49·10⁶	-5.29·10 ²	-5.29·10 ²	0	-1.46·10 ⁴	0	0	5.29·10 ²
A	Cold Leg ₁	3.81·10 ³	3.28·10 ³	5.21·10⁴	3.09·10 ⁴	3.28·10 ³	3.81·10 ³	-2.09·10 ⁴	-3.39·10 ⁴	-3.28·10 ³
A	Cold Leg ₂	3.81·10 ³	3.28·10 ³	3.09·10 ⁴	5.21·10⁴	3.28·10 ³	3.81·10 ³	-2.09·10 ⁴	-3.39·10 ⁴	-3.28·10 ³
B	CMT,B	-1.46·10 ⁴	0	-5.29·10 ²	-5.29·10 ²	1.66·10⁶	-5.29·10 ²	0	0	5.29·10 ²
B	Cold Leg ₂	3.81·10 ⁴	3.76·10 ⁴	3.81·10 ³	3.81·10 ³	3.76·10 ⁴	5.21·10⁴	0	0	-3.81·10 ³
A	PRHR	3.81·10 ³	3.28·10 ³	3.12·10 ⁴	1.00·10 ⁴	3.28·10 ³	3.81·10 ³	1.38·10⁶	-6.21·10 ³	-3.81·10 ³

Appendix A.7 shows the numerical values of the elements of the inertia matrix for the 7-Loop operation of APEX and SPES, and for the five-loop configuration of ROSA during Phases 2. For Phases 3 and 4, the elements were evaluated the same way as for Phase 2, but with different density in some of the loop segments. No inertia matrix was evaluated for the long lasting, quasi-steady Phase 5.

Inertia, I , is defined in Eq. (5-24) for two-phase flow in a *component*. It is the principal part of the inertia, accounting for the geometric effects, mixture density and void distribution. The effects on inertia of phase change and local vapor drift are accounted for by $\Delta\Phi_m$ given in Eq. (5-26). As seen from Eq. (5-25), I reduces for single-phase flows to the familiar inertia, $\rho L/A$, which is the reason for calling I “inertia.”

Equation (5-37) defines the global inertia matrix of loop system. The elements of the global system inertia matrix of two-phase flow, \mathbf{I} , in Eq. (5-37) also reduce for single-phase flow to the familiar $\rho L/A$ -combinations of the system. The diagonal elements of \mathbf{I} for loops with a single primary flow in its closed contour are the loop momenta if, in the definition of loop flows, only positive flows are encountered around the closed contour, and if none of the branch exit

5. Modeling Equations

flows selected as primary flow is of a collecting branch (e.g., plenum exit flow). Only under these conditions are the *off-diagonal elements* a measure of the *cross-coupling between loops by inertia*, since every pressure difference induced in a common loop segment by acceleration in one loop exerts the same pressure difference in the other loop(s).

A final note on the importance of the inertia matrix: the eigenvalues of the system of momentum balances, Eqs. (5-19), are obtained from its Jacobian with respect to the primary volumetric flow rates which, by the chain rule of differentiation applied to Eq. (5-27), involves the inertia matrix. The inertia matrix and the impedance matrix determine, therefore, system stability in the vicinity of a point in time (linear stability criterion).

5.4.2.4 Impedance Matrix

The global momentum balances, Eqs. (5-19), for a system of loops contain the flow resistance terms of friction, and form loss as expressed by Eq. (5-22). The friction (wall shear) term is proportional to the mass flow rate, $|W|$, only at low Reynolds numbers. Form losses are always proportional to the square of the mass flow rate. For the purpose of scaling, however, the flow is taken to be always turbulent (simplifying assumption W-vi listed in Section 5.2), and both friction and form losses are proportional to $W|W|$ and depend always on the direction of the flow.

By using the integral of Eqs. (5-19) to get the loop momenta, by solving the linear system of equations, Eqs. (5-36), for the primary volumetric flow rates, and by using Eqs. (5-35) for the secondary volumetric flow rates, one obtains all the mixture volumetric flow rates at the entrance of every flow segment in every loop of the system. With the volumetric and mass flows predicted, one evaluates first the mass flow rate, W_i , at the entrance of each loop segment

$$W_{m,i} = \left[f_p (\Phi_m)(0) - \alpha \Delta p \ll v_{gj} \gg \right]_i \quad (5-39)$$

and then *directly* the irreversible dissipation in terms of the resistance of each component (index i), in each loop segment (with index k and entrance mass flow rate W_i) between branch points of a loop (with index j)

$$\sum_{i \in k} (\Delta p_{fr} + \Delta p_{form})_i = R_{jk} (W|W|)_k \quad (5-40)$$

$$R_{jk} = \sum_{i \in k} \frac{1}{2\rho l_i} \left(\frac{K_i + (\phi_{l0}^2 f)_i \frac{L_i}{d_{h,i}}}{A_i^2} \right), \quad (5-41)$$

where the repeated indices in Eq. (5-40) do not imply summation, and all the symbols are defined below Eq. (5-22). Equation (5-23) shows that the form loss coefficient, K , depends on flow direction.

A single flow resistance coefficient, R_{kj} , combines in Eq. (5-40) the flow resistances of all components in a loop segment. This implies not only a reduction of the very large number of local resistance coefficients associated with all the discontinuities of flow cross-sectional areas in a hydraulic system, but also flexibility for controlling flow resistances to achieve hydraulic similarity between different facilities.

As for the inertia matrix, the irreversible dissipation of the system is expressed in terms of only the primary mass flow rates, $(W_m)_{pr,j}$, one for each loop with index j . This is achieved by expressing all the secondary mass flow rates in terms of primary mass flow rates, using Eq. (5-35). As a result, the resistance vector in Eq. (5-19) becomes the product of the flow impedance matrix \mathbf{P} and the kinetic energy vector, \vec{H} , [17].

The distribution of flow resistance in a loop system determines the flow distribution under steady-state conditions and, along with the inertia matrix discussed in Section 5.4.2.3, the transient redistribution of flow in the system during a transient [17]. The flow impedance matrix \mathbf{P} displays, therefore, perspicuously the *combination* of resistance coefficients that governs the distribution of flow in a loop system and the cross coupling between loops by *impedance*.

5. Modeling Equations

The flow impedance matrix \mathbf{P} displays the resistance characteristics related to *system topology*, whereas the *dynamic state* of the system is represented by the vector \vec{H} of kinetic energy. The flow impedance matrix \mathbf{P} changes weakly with time as the fluid density and possibly the Reynolds number change (at low Reynolds numbers).

The central idea is to express the resistance vector in Eq. (5-19) in terms of only the same N_L primary mass flow rates that are associated with the N_L primary volumetric flow rates, as obtained, according to Eq. (5-36), from the known N_L loop momenta. For this purpose, the total of $(N_L + N_B - 1)$ independent mixture mass flow rates $W_m(0, t)$ of the loop system are grouped into N_L primary, $W_{m,pr}(0, t)$, and $(N_B - 1)$ secondary, $W_{m,sn}(0, t)$, flow rates and arranged in the *same order as the volumetric flow rates* in Eq. (5-27). The primary mass flow rates, $W_{m,pr}(0, t)$, are given by Eqs. (5-36) and (5-37), while the $(N_B - 1)$ secondary mass flow rates are given by

$$\left[\left(W_{m,sn}(0, t) \right) \right]_p = - \left(\mathbf{A}_r^{-1} \right)_{pi} \left(\mathbf{B}_r \right)_{iq} \left[\left(W_{m,pr}(0, t) \right) \right]_q. \quad (5-42)$$

The j^{th} loop resistance vector in Eq. (5-19) is broken up in the same way as the loop inertia in Eq. (5-27), that is

$$\sum_{k \in j} \left(\Delta p_{fr} + \Delta p_{form} \right)_k = \mathbf{E}_{jp} \left[W_{m,pr}(0, t) \mid W_{m,pr}(0, t) \right]_p + \mathbf{Z}_{jq} \left[W_{m,sn}(0, t) \mid W_{m,sn}(0, t) \right]_q, \quad j = 1, \dots, N_L, \quad (5-43)$$

where the indices p and q imply summation, \mathbf{E} is the $N_L \times N_L$ matrix of resistance elements, R_{jp} , defined in Eq. (5-41) and associated with the loop segments of the *primary* flow rates, $W_{m,pr}$, and \mathbf{Z} is the $N_L \times (N_B - 1)$ matrix of resistance elements, R_{jq} , also defined in Eq. (5-41) but associated with the loop segments of the *secondary* flow rates, $W_{m,sn}$. The matrices \mathbf{E} and \mathbf{Z} are obtained by simply replacing the inertia elements in $\mathbf{\Lambda}$ and \mathbf{X} , respectively, by the resistance elements of the associated loop segments. The $N_L \times (N_L + N_B - 1)$ flow impedance matrix \mathbf{P} is then \mathbf{E} , augmented by \mathbf{Z}

$$\mathbf{P} = \left(\mathbf{E} \mathbf{Z} \right) \quad (5-44)$$

and to be multiplied with the $(N_L + N_B - 1) \times 1$ column vector of directed kinetic energy,

$$\vec{H} = \left(\vec{H}_{pr} \mid \vec{H}_{sn} \right)^T, \quad (5-45)$$

to produce the elements (see Eq. (5-43)) of the resistance vector in Eq. (5-19). The first N_L elements of \vec{H} are given by

$$\vec{H}_{pr} = \left[\left(W_{m,pr}(t) \mid W_{m,pr}(t) \right) \Big|_1, \dots, \left(W_{m,pr}(t) \mid W_{m,pr}(t) \right) \Big|_{N_L} \right]^T, \quad (5-46)$$

and the last $(N_B - 1)$ elements of \vec{H} are given by

$$\vec{H}_{sn} = \left[\left(W_{m,sn}(t) \mid W_{m,sn}(t) \right) \Big|_1, \dots, \left(W_{m,sn}(t) \mid W_{m,sn}(t) \right) \Big|_{N_B-1} \right]^T, \quad (5-47)$$

where each vector element is given by Eq. (5-42). Indexical notation defines the matrix algebra for generating the resistance vector in Eq. (5-19)

5. Modeling Equations

$$\mathbf{P}_{ij} H_j = \mathbf{Z}_{ip} (H_{pr})_p + \mathbf{E}_{iq} (H_{sn})_q. \quad (5-48)$$

With the above matrix-vector product substituted into Eq. (5-43) and the result substituted for the friction term in the global momentum balance, Eq. (5-19), this equation is written, with indicial notation, to show the impedance matrix \mathbf{P} of the form loss and friction term.

$$\frac{dM_j}{dt} = \bar{g} \cdot \oint_j \hat{k} \rho_m dz + \Delta p_{pp,j} - \sum_j (\Delta MF) - \mathbf{P}_{jk} H_k. \quad (5-49)$$

Wulff [17] introduced earlier a more complicated matrix multiplication of a simpler, more compact form of the impedance matrix with a more complicated *matrix* of directed kinetic energies. The standard matrix-vector multiplication, adopted from [21] and presented here in Eq. (5-48) is preferred, however, because the directed kinetic energy appears as the simple vector, \mathbf{H} .

\mathbf{P} displays clearly the impedance coupling between loops, and we arrive at the following interpretation of \mathbf{P} : The relative magnitudes of the elements in each *row* of \mathbf{P} in Eqs. (5-44) and (5-48) reveal the flow *resistance distribution* in the loop associated with that row. Loops which share a common element in one or more *columns* are *impedance-coupled*, the stronger the larger the common element is relative to the other elements in the respective row.

Table 5.8 shows the impedance matrix in symbolic form for the four-loop systems of AP600, APEX, and SPES, for normal operating conditions and for Phase 1, i.e., before the occurrence of the S-Signal. The resistance coefficients, R , are defined by Eq. (5-41). The subscripts denote the end points of loop segments, as shown in Figure 5.6. Each row is labeled to show the loop of the system, and each column is labeled to show the loop segment to which the resistance coefficient belongs.

Table 5.8 Impedance Matrix for Four-Loop Operation During Phase 1 of AP600, APEX, and SPES.
(for subscripts of R , see Fig. 5.6)

Loop		Resistance Coefficients of Loop Sections between Branch Points:		
on Side	through	RPV to Exit of SG 1 - 5	SG Exit to RPV	Interior of RPV
B	Cold Leg 1	$R_{B,1-5}$	$R_{B1,5-6}$	R_{61}
B	Cold Leg 2	$R_{B,1-5}$	$R_{B2,5-6}$	R_{61}
A	Cold Leg 1	$R_{A,1-5}$	$R_{A1,5-6}$	R_{61}
A	Cold Leg 2	$R_{A,1-5}$	$R_{A2,5-6}$	R_{61}

The numerical values of the impedance matrices for AP600, APEX, and SPES are shown in Tables 5.9 through 5.11. Actually shown are the geometric parameters $2\rho R$ in 1/(m kg), where R is defined by Eq. (5-41). Consequently, the

5. Modeling Equations

tables are used to cover Phases 2 through 4: the values of the elements of the impedance matrix listed are to be multiplied with twice the fluid density, that is, for scaling purposes with twice the fluid density at the beginning of the respective phase. Tables 5.9 through 5.11 serve to compare, in absolute values, the impedance-related geometry of the three facilities. It is obvious that the form loss and friction factors of the test facilities differ by three orders of magnitude from those of the AP600. However, what counts are the comparison of scaled system impedance and scaled impedance matrices shown in Chapter 6.

Table 5.9 Impedance Matrix in Numerical Form for Four-Loop Operation of AP600, Phase 1.
(Shown is $2\rho_l R$, in $1/(m \text{ kg})$, for identification of values see Table. 5.8)

Loop		Resistance Coefficients ($\times 2\rho$) of Loop Sections between Branch Points:		
on Side	through	RPV to Exit of SG 1 - 5	SG Exit to RPV	Interior of RPV
B	Cold Leg 1	18.404	3.469	3.386
B	Cold Leg 2	18.404	3.469	3.386
A	Cold Leg 1	18.404	3.469	3.386
A	Cold Leg 2	18.404	3.469	3.386

Table 5.10 Impedance Matrix in Numerical Form for Four-Loop Operation of APEX, Phase 1.
(Shown is $2\rho_l R$, in $1/(m \text{ kg})$, for identification of values see Table. 5.8)

Loop		Resistance Coefficients ($\times 2\rho$) of Loop Sections between Branch Points:		
on Side	through	RPV to Exit of SG 1 - 5	SG Exit to RPV	Interior of RPV
B	Cold Leg 1	$2.06 \cdot 10^4$	$2.50 \cdot 10^4$	$2.38 \cdot 10^3$
B	Cold Leg 2	$2.06 \cdot 10^4$	$2.50 \cdot 10^4$	$2.38 \cdot 10^3$
A	Cold Leg 1	$2.06 \cdot 10^4$	$2.50 \cdot 10^4$	$2.38 \cdot 10^3$
A	Cold Leg 2	$2.06 \cdot 10^4$	$2.50 \cdot 10^4$	$2.38 \cdot 10^3$

5. Modeling Equations

Table 5.11 Impedance Matrix in Numerical Form for Four-Loop Operation of SPES, Phase 1.
 (Shown is $2\rho_l R$, in $1/(m\ kg)$, for identification of values see Table. 5.8)

Loop		Resistance Coefficients ($\times 2\rho$) of Loop Sections between Branch Points:		
on Side	through	RPV to Exit of SG 1 - 5	SG Exit to RPV	Interior of RPV
B	Cold Leg 1	$3.01 \cdot 10^6$	$7.46 \cdot 10^5$	$3.53 \cdot 10^5$
B	Cold Leg 2	$3.01 \cdot 10^6$	$7.46 \cdot 10^5$	$3.53 \cdot 10^5$
A	Cold Leg 1	$3.01 \cdot 10^6$	$7.46 \cdot 10^5$	$3.53 \cdot 10^5$
A	Cold Leg 2	$3.01 \cdot 10^6$	$7.46 \cdot 10^5$	$3.53 \cdot 10^5$

The impedance matrix for the two-loop system of ROSA was developed by the same method as those for AP600, APEX, and SPES. Table 5.12 presents the geometric parameters $2\rho_l R$ in $1/(m\ kg)$, where R is defined by Eq. (5-41), for ROSA. Thus, the values in Table 5.12 are the impedance-related geometric parameters for ROSA and can also be compared with the values given in Tables 5.9 through 5.11 to see that the form loss and friction factors of ROSA differ by two orders of magnitude from those of the AP600. However, for assessing similitude, one must compare the scaled system impedance and scaled impedance matrices shown in Chapter 6.

Table 5.12 Impedance Matrix in Numerical Form for Two-Loop Operation of ROSA, Phase 1. (Shown is $2\rho_l R$, in $1/(m\ kg)$)

Loop		Resistance Coefficients ($\times 2\rho$) of Loop Sections between Branch Points:	
on Side	through	Hot-Leg Entrance to Cold-Leg Exit	Interior of RPV
B	Cold Leg	$3.82 \cdot 10^3$	$11.76 \cdot 10^3$
A	Cold Leg	$3.82 \cdot 10^3$	$11.76 \cdot 10^3$

After the S-Signal has occurred, for Phases 2, 3 and 4, AP600, APEX, and SPES have seven interacting loops. The impedance matrix for AP600, APEX, and SPES during Phases 2, 3 and 4 is given, in symbolic form, in Table 5.13. The resistance coefficients, R , are defined by Eq. (5-41). The subscripts denote the end points of loop segments, as shown in Figure 5.7, 5.8, and 5.9. Each row is labeled to show the loop of the system, and each column is labeled to show the loop segment to which the resistance coefficient belongs.

5. Modeling Equations

Table 5.13 Impedance Matrix in Symbolic Form for Seven-Loop Operation of AP600, APEX, and SPES (Phases 2, 3, and 4).
(for subscripts of R , see Fig. 5.7, 8, and 9)

Loop		Resistance Coefficients of Loop Sections between Branch Points:								
on Side	through	RPV to PRHR of Loop _A	PRHR to SRL of Loop _A	(Remainder of) Hot Leg and SG	SG to CMT Branch in Loop _B	(Remainder of) Cold Leg	Upper Downcomer	Vessel from DVI to Upper Plenum	CMT from Cold Leg to DVI	PRHR from Hot Leg to SG in Loop _A
B	Cold Leg ₁	0	0	$R_{B,1-5}$	$R_{B1,5-19}$	$R_{B1,19-6}$	R_{6-7}	R_{7-1}	0	0
A	CMT _A	0	0	0	0	$R_{B2,8-6}$	R_{6-7}	0	$R_{B2,8-9-7}$	0
A	Cold Leg ₁	$R_{A,1-2}$	$R_{A,2-3}$	$R_{A,3-5}$	0	$R_{A1,5-6}$	R_{6-7}	R_{7-1}	0	0
A	Cold Leg ₂	$R_{A,1-2}$	$R_{A,2-3}$	$R_{A,3-5}$	0	$R_{A2,5-6}$	R_{6-7}	R_{7-1}	0	0
B	CMT _B	0	0	0	0	$R_{B1,19-6}$	R_{6-7}	0	$R_{B1,19-9-7}$	0
B	Cold Leg ₂	0	0	$R_{B,1-5}$	$R_{B2,5-8}$	$R_{B2,8-6}$	R_{6-7}	R_{7-1}	0	0
A	PRHR	$R_{A,1-2}$	0	0	0	$R_{A1,5-6}$	R_{6-7}	R_{7-1}	0	$R_{A,2-17-5}$

The numerical values of the impedance matrix elements for AP600 are shown in Table 5.14 on the next page. Actually shown are again the geometric parameters $2\rho R$, in $1/(m \text{ kg})$ where R is defined by Eq. (5-41). Consequently, the tables are used to cover Phases 2 through 4: the values of the elements of the impedance matrix listed are to be multiplied with twice the fluid density, that is, for scaling purposes with twice the fluid density at the beginning of the respective phase. Corresponding tables for APEX, ROSA, and SPES, and the impedance matrices for Phase 5 are given in Appendix 8.

5.5 Reference Parameters

In this section are defined the reference parameters as obtained in accordance with the rules that were explained in Section 4.4.3. All reference parameters were expressed in terms of design-specified geometric quantities and in terms of specified initial and operating conditions. Where a reference parameter could not be computed directly from design specifications, steady-state or transient conservation equations had to be used to estimate characteristic reference parameters. There is no need for precise predictions of indirectly obtained reference parameters; instead, reliable estimates are needed which can serve to normalize the system variables such that their order of magnitude is one.

5. Modeling Equations

Table 5.14 Impedance Matrix in Numerical Form for Seven-Loop Operation of AP600 During Phases 2 Through 4. (Shown is $2\rho_l R$, in 1/(m kg), for identification of R , see Fig. 5.12)

Loop		Resistance Coefficients ($\times 2\rho$) of Loop Sections between Branch Points:								
on Side	through	RPV to PRHR of Loop _A	PRHR to SRL of Loop _A	(Remainder of) Hot Leg and SG	SG to CMT Branch in Loop _B	(Remainder of) Cold Leg	Upper Downcomer	Vessel from DVI to Upper Plenum	CMT from Cold Leg to DVI	PRHR from Hot Leg to SG in Loop _A
B	Cold Leg ₁	0	0	18.404	0.496	2.973	-0.026	3.412	0	0
A	CMT _A	0	0	0	0	2.973	0.026	0.000	$7.48 \cdot 10^4$	0
A	Cold Leg ₁	0.124	0.635	17.646	0	3.469	-0.026	3.412	0	0
A	Cold Leg ₂	0.124	0.635	17.646	0	3.469	-0.026	3.412	0	0
B	CMT _B	0	0	0	0	2.973	0.026	0	$8.04 \cdot 10^4$	0
B	Cold Leg ₂	0	0	18.404	0.496	2.973	-0.026	3.412	0	0
A	PRHR	0.124	0	0	0	3.469	-0.026	3.412	0	$5.12 \cdot 10^4$

5.5.1 Time References

Reference times are estimates of the time taken by the system for passing through a phase or a subphase. Their selection is important for obtaining time derivatives of order of unity. The reference time is a common factor in all scaling criteria obtained by the *fractional* scaling method (Sect. 4.4.52) but it does not affect the ranking of phenomena. In the scaling method related to the *causative-process* (Section 4.4.5.1) the reference time has no impact on either the ranking of phenomena or on the assessment of scaling distortions, except for scaling the capacitance term in transient conservation equations.

The reference (or characteristic response) time, t_{ref} , is found for a phase by setting the capacitance scaling group Π_c of Eq. (4-2) equal to 1, in that equation which describes the important process during the phase. For Phases 1 and 2, the important process is the draining of the pressurizer and drainage time is the reference time. The characteristic times of ADS-123 and 4 depressurizations were used for Phases 3 and 4, respectively. For Phase 5, the time of draining the IRWST was taken as the characteristic time. Below are the generic definitions of characteristic or reference times, t_{ref} .

The *characteristic drainage time* for the fluid in volume V is

$$t_{dm} = \frac{V}{\Phi_0}, \quad (5-50)$$

where Φ_0 is the initial volumetric break flow rate (cf. Section 5.5.3) for Phases 1 and 2, or, for Phase 5, the volumetric flow rate at the IRWST drain line (cf. Section 5.5.3).

5. Modeling Equations

The *characteristic fluid residence time* for the fluid in the loop of specified volume V_{loop} is

$$t_{res} = \frac{V_{loop}}{\Phi_{0, loop}}, \quad (5-51)$$

where $\Phi_{0, loop}$ is the design-specified initial volumetric flow rate of the fluid entering the loop.

The *characteristic time of depressurization* is an estimate of the time that the system, having the system elasticity or mechanical compliance $V \chi_{v,0}$, requires to pass through the pressure range Δp_0 , as the result of fluid leaking from a break or discharge valve at the volumetric flow rate Φ_0 (cf. Section 5.5.3). It is

$$t_{\Delta p} = \frac{\Delta p_0 \chi_{v,0} V}{\Phi_0}. \quad (5-52)$$

5.5.2 Pressure References

For **Phase 1**, the first phase which begins at break initiation and ends at the S-Signal initiation, the reference pressure difference equals the difference between the specified initial pressure and the S-Signal pressure trip set point, as recorded for each facility in the EXCEL Spreadsheet Section Phase 1 of Appendices 4.1 (for the time before scram) and 4.2 (for the time after scram). The initial pressure and the pressure trip set point for the S-Signal are given in Appendix 4.1.

For **Phase 2**, the phase which begins at the S-Signal pressure trip set point and ends when the liquid level elevation reaches the 67% mark in one of the Core Make-Up Tanks, the reference pressure difference equals the difference between specified S-Signal pressure trip set point and the pressure trip set point for Accumulator flow initiation. The pressure trip set point for Accumulator flow initiation was selected because it is the only design-specified pressure that is approximately equal to the system pressure at the time when one of the liquid levels in the CMT's reaches the 67% mark.

The S-Signal trip and the Accumulator trip pressures are recorded in Appendix 4.3 for each facility. The reference pressures are computed in the EXCEL Spreadsheet Section for Phase 2 of Appendix 5.2.

For **Phase 3**, The ADS-123 Blowdown phase, the reference pressure difference equals the difference between the design-specified pressures of trip set point for Accumulator flow and of the containment. Both pressures are listed for the four facilities in Appendix 4.4, and the pressure difference is computed in the Phase 3 section of the EXCEL worksheet that is reproduced in Appendix 5.3.

For **Phase 4**, The ADS-4 Depressurization Phase, the reference pressure difference, Δp_0 , is computed as the difference between the estimated starting pressure of Phase 4 and the hydrostatic pressure upstream of the closed IRWST shut-off valve in the Direct Vessel Injection (DVI) line. The starting pressure of Phase 4 is estimated from the estimated time for draining the Core Make-up Tanks from the 67% to the 20% elevation marks, and from the integral of the depressurization equation, Eq. (5-8). For integrating Eq. (5-8), the ADS-123 discharge volumetric flow rate is taken to be a function of pressure. The integral of Eq. (5-8), evaluated with only the causative term of ADS discharge, yields for Δp_0 ,

$$\Delta p_0 = p_0 \left[1 - e^{\left(\frac{\Phi_{ADS-123}}{\chi_v V p_0} \right)_0 \Delta t_{drn}} \right], \quad (5-53)$$

5. Modeling Equations

where p_0 is the initial pressure of Phase 3, $\Phi_{ADS-123}$ is the causative discharge volumetric flow rate (cf. Section 5.5.3), χ_V is the system isentropic compressibility, Eq. (5-9), and the time, Δt_{dm} , for CMT draining is estimated from Eq. (5-50)

$$\Delta t_{dm} = \frac{V_{CMT} \Delta \alpha_l}{\bar{\Phi}_{CMT} - \Phi_{cnd}}, \quad (5-54)$$

where $\Delta \alpha_l = 0.47$ is the liquid volume fraction that drains from the CMT during Phase 3. The mean flow rate, $\bar{\Phi}_{CMT}$, is obtained as the average of the draining volumetric flow rates, Φ_{CMT} , estimated with the initial and final level elevations, L_{CMT} , in the CMT. The volumetric flow rate, Φ_{CMT} , is computed from the steady-state momentum balance for the CMT loop, Eq. (5-19), with the time derivative and the momentum flux change terms set equal to zero, and with the resistance coefficients, R , defined by Eq. (5-41)

$$\Phi_{CMT} = \sqrt{\frac{g(L_{CMT} - H_{HL}) \left(1 - \frac{\rho_g}{\rho_f}\right)}{\sum_{i \in CMT} \rho_i R_i}}. \quad (5-55)$$

In Eq. (5-55), g and H_{HL} stand for, respectively, the gravitational constant and the elevation of the Hot Leg centerline. The CMT draining by gravity is counteracted by the condensation-induced volumetric hold-up rate

$$\Phi_{cnd} = \frac{\dot{Q}_{cnd, CMT}}{\rho_g h_{fg}} = \frac{\bar{A}_w \Delta T_w}{\rho_g h_{fg}} \sqrt{\frac{4 (k \rho c)_w}{\pi \Delta t_{\Delta p}}}, \quad (5-56)$$

where the heat flux is limited by conduction (thick-walled CMT), the depressurization time, $\Delta t_{\Delta p}$, is computed from Eq. (5-52), and the driving temperature difference, ΔT_w , is the initial difference between hot-leg and CMT temperatures. The wall area is the average between initial and final wall areas.

The accuracy of estimating the starting pressure of Phase 4 suffers from the uncertainties in estimating the starting pressure for Phase 3, the condensation heat transfer, and the duration of the ADS-123 blowdown phase. The estimated starting pressure of Phase 4, and the estimated duration of the ADS-123 phase are compared with experimental data in Table 5.15. The comparison shows that the reference starting pressure is accurate enough to meet the scaling requirement for getting normalized pressures and normalized pressure derivatives of order of unity. The estimations of starting pressure for Phase 4 are shown in the EXCEL worksheet Section for Phase 3 in Appendix 5.4.

For **Phase 5**, there was no depressurization equation to be scaled since the pressures are governed by the constant containment pressure and gravity heads.

The compressibility (or mechanical compliance) of nitrogen gas in Eqs. (5-8), (5-9), (5-11), and (5-17) is scaled with the absolute pressure that exists at the beginning of the respective phase.

5.5.3 Volumetric Flow Rate References

Reference values for normalizing *individually* all volumetric flow rates are computed either from steady mass and momentum balances for HEM critical flow through the break and ADS valves, or from quasi-steady correlations for choked flow of subcooled liquid, or from the steady form of the loop momentum balance, Eq. (5-19) for subcritical flow (cf. Eq. (5-55)).

5. Modeling Equations

For **Phase 1**, the first phase which begins at break initiation and ends at S-Signal initiation, the reference volumetric flow rate is the critical break flow rate, estimated from the critical mass flux in Appendix 4.1 for initial conditions of Phase 1. The critical mass flux of subcooled liquid is computed from the expression by Bestion [22], using the equilibrium quality, x_e , the system pressure, p_0 , and the saturation pressure, p_{sat} , corresponding to the cold-leg temperature

$$G_{crit,0} = (1 - 0.544 x_{e,0}) \sqrt{2 \rho_{l,0} [p_0 - 0.9 (1 - x_{e,0}) p_{sat}]} \quad (5-57)$$

and then multiplied with the specified break area and divided by the average liquid density in the Cold Leg, to yield the reference volumetric flow rate, i.e., the break flow rate

$$\Phi_{bk,0} = \frac{G_{crit,0}}{\rho_{l,0}} A_{bk} \quad (5-58)$$

Since $\nabla p = 0$ (Assumption p-iv in Section 5.2) is implied in the derivation of the depressurization equation, Eq. (5-8), one must use the cold-leg density on Eq. (5-58) instead of the the fluid density at the throat section of the break. The estimated break mass flow rates, $G_{crit,0} A_{bk}$, are compared with experimental data in Table 5.16. For ROSA the estimate is 14% low, for SPES estimate and test data agree, but there are no data for APEX because APEX does not model Phase 1.

For **Phase 2**, the phase which begins at the S-Signal initiation and ends with the 33% liquid inventory depletion in the CMT, the reference volumetric flow rate for time scaling is also the critical break flow rate, estimated from the critical mass flux in Appendix 4.3 for initial conditions of Phase 2. Equations (5-57) and (5-58) are evaluated again for Phase 2.

For Phase 2, the reference volumetric flow rates are needed also for the natural circulation flows through the Core Make-up Tanks (CMT) and the Passive Residual Heat Rejection (PRHR) system. These flow rates are estimated from the steady form of the loop momentum balance, Eq. (5-19)

$$\Phi_{CMT, PRHR} = \left(\sqrt{\frac{\Delta H_{thrcnt} g \beta_T \rho_0 (T_{min} - T_{max})}{\sum_{i \in loop} R_i}} \right)_{CMT, PRHR} \quad (5-59)$$

Here, ΔH_{thrcnt} , g , β_T , ρ_0 , T_{max} , and T_{min} denote, respectively, the elevation difference between the thermal centers, gravitational constant, isobaric thermal expansion coefficient, mean fluid density, and maximum and minimum fluid temperatures. The minimum temperature of the fluid is the initial CMT and PRHR temperature and equals the initial containment temperature; the maximum temperature equals the hot-leg temperature for the PRHR, and the cold-leg temperature for the CMT. The resistance coefficients, R , are defined by Eq. (5-41).

The estimated CMT and PRHR flow rates are compared with test data in Table 5.16 of Section 5.5.5. For APEX and ROSA the estimates are less than 7% too small, for SPES, however, the estimate is about 50% too large.

For **Phase 3**, the ADS-123 blowdown phase, the reference volumetric flow rate is estimated as the critical homogeneous equilibrium (HEM) flow rate through the ADS-123 valve. The critical HEM flow was computed with the aid of MATHCAD, using HTFS polynomial fits to saturation properties of water [24]. The mass flux, G , satisfies the steady-state energy and mass balances

$$G(p) = \frac{\sqrt{2(h_0 - h(p))}}{v(p)} \quad (5-60)$$

5. Modeling Equations

and reaches a maximum $G_{crit,0}$, for which $dG/dp = 0$, as the pressure drops isentropically along a path through the ADS-123 valves. To establish isentropic expansion, one needs to satisfy

$$x = \frac{s_0 - s_f(p)}{s_{fg}(p)} \quad (5-61)$$

$$h = h_f(p) + x h_{fg}(p) \quad (5-62)$$

$$v = v_f(p) + x v_{fg}(p), \quad (5-63)$$

where s_0 is the upstream stagnation entropy, x , h , s , and v , are, respectively, equilibrium quality, enthalpy, entropy, and specific volume, and subscripts f and fg denote, respectively, saturated liquid and phase change. The maximum $G_{crit,0}$ is found by solving

$$\frac{h' + G^2 v' v}{v^2 G} = 0, \quad (5-64)$$

where the prime means differentiation with respect to pressure along the saturation line. The solution $G_{crit,0}$ to Eq. (5-64) is transferred from MATHCAD to EXCEL, as shown in Appendices A.2.4 for ADS-123 flow at the start of Phase 3, and in Appendix A.4.5 for ADS-4 flow at the beginning of Phase 4. ADS-123 flow at the start of Phase 3 is from the vapor-filled Pressurizer ($\alpha = 1$). The HEM critical mass flux, G_{crit} , is multiplied with the respective flow area and divided by the *upstream* fluid density, to obtain the reference volumetric flow rate as shown in Eq. (5-58).

The flow rate estimates are compared with test data in Table 5.16 of Section 5.5.5. The estimates are for APEX, ROSA, and SPES, respectively, 23% too high, 3% too low, and 14% too high. This is sufficiently accurate to assure order of unity for the scaled flow rates.

For **Phase 4**, the ADS-4 depressurization phase, the reference volumetric flow rates through the break, the ADS-123 and ADS-4 valves are computed by MATHCAD from the HEM model given by Eqs. (5-60) through (5-64), evaluated with the quality of, respectively, $x = 0$ at the break, $x = 1$ at the ADS-123 valves, and $x = x_{df}$, where x_{df} is the core exit quality computed from the equilibrium quality at the core exit

$$x_{CRE,HEM} = \frac{\dot{Q}_{CR} - W_{CR}(h_f - h)}{W_{CR} h_{fg}} \quad (5-65)$$

and the drift-flux correlation to give

$$x_{df} = \frac{1}{1 + \frac{A_{CR} \rho_f v_{gj}}{x_{CRE,HEM} W_{CR}} + C_0 \left(\frac{1}{x_{CRE,HEM}} - 1 \right) + (C_0 - 1) \frac{\rho_f}{\rho_g}}. \quad (5-66)$$

The core heating power, \dot{Q}_{CR} , is the decay heat, the core flow, W_{CR} , is computed as the sum of the draining flows from the Pressurizer (PRZ) and Core Make-up Tank, both being mass flow rates, W_{PRZ} and W_{CMT} , estimated from the steady form of the momentum balance, (see Eq. (5-55) for the volumetric flow rate), evaluated with the respective level elevations in PRZ and CMT at the beginning of Phase 4. The subcooling enthalpy flow rate in Eq. (5-65) equals the

5. Modeling Equations

sum of subcooling enthalpy flow rates of the flows from the PRZ and CMT. C_0 and v_{gj} are the standard Zuber-Findlay distribution parameter and void-fraction weighted, area-averaged vapor drift velocity for bubbly flow.

The flow rate estimates are computed by EXCEL as shown in Appendix 4.5 and compared with test data in Table 5.16 of Section 5.5.5. The estimates are for APEX, ROSA, and SPES, respectively, 40% too high, 30% too high, and by a factor of 2 too high. Except for SPES, this is sufficiently accurate to assure order of unity for the scaled flow rates.

For **Phase 5**, the IRWST and sump injection phase, the normalization of flow rates was carried out on the basis of Mass flow rates which are defined in Section 5.5.4 below. All volumetric flow rates were computed by dividing mass flow rates by fluid density.

5.5.4 Mass Flow Rate References

Mass flow rates were normalized *individually*. For Phases 1 through 4 the subcritical flows were normalized with the product of volumetric flow rates times fluid density. The volumetric flow rate estimations are described in Section 5.5.3 above.

For Phase 5, the IRWST and sump injection phase, the flow rates are governed by gravity, and therefore all reference mass flow rates were computed by solving, with MATHCAD, simultaneously six coupled steady-state loop momentum and three junction mass balances, to obtain these nine mass flow rates: $W_{ADS-4,A}$, the ADS-4 flow on the Pressurizer side; $W_{ADS-4,B}$, the ADS-4 flow on the CMT side; W_{IRWST} , the flow from the IRWST; W_{SRL} , the flow from the PRZ surge line; W_{bk} , the break flow; $W_{34,A}$ and $W_{34,B}$, the flows toward the steam generators on, respectively, the PRZ and CMT sides; W_{1A} , the flow from the Upper Plenum toward the PRZ; and $W_{CL,A}$, $W_{CL,B}$, the cold-leg flows from the steam generators on, respectively, the PRZ and CMT sides. The reader is referred to Figure 5.10.

Six loop contours are formed, namely, (1) and (2) through Loops A and B, the primary-side coolant loops; (3) through the loop from the containment through the PRZ to the ADS-4 valve on the PRZ side and back to the containment; (4) through the loop from the containment through the PRZ to the ADS-4 valve on the CMT side and back to the containment; (5) through the loop from the containment through the IRWST to the break and back to the containment; and (6) through the loop from the containment through the IRWST to the ADS-4 valve on the PRZ side and back to the containment. The six loop momentum balances are

for Loop A:

$$\begin{aligned}
 & \left[\Delta\rho (L_{SGI} - L_{SGE}) \right. \\
 & \left. + (\rho_l - \bar{\rho}) L_{PRV} \right] g = -R_{34,A} (W_{SRL} + W_{1A} - W_{ADS-4,A}) |W_{SRL} + W_{1A} - W_{ADS-4,A}| \\
 & \quad - R_{56} W_{CL,A} |W_{CL,A}| \\
 & \quad - R_{67} (W_{CL,A} + W_{CL,B} + W_{bk}) |W_{CL,A} + W_{CL,B} + W_{bk}| \\
 & \quad + R_{71} (2W_{IRWST} - W_{CL,A} - W_{CL,B} - W_{bk}) |2W_{IRWST} - W_{CL,A} - W_{CL,B} - W_{bk}| \\
 & \quad + R_{12,A} W_{1A} |W_{1A}|.
 \end{aligned} \tag{5-67}$$

5. Modeling Equations

for Loop B:

$$\begin{aligned}
 & \left[\Delta\rho (L_{SGE} - L_{SGI}) \right. \\
 & \left. + (\rho_l - \bar{\rho}) L_{PRV} \right] \mathcal{G} = +R_{24,B} (W_{BI} - W_{ADS-4,B}) |W_{BI} - W_{ADS-4,B}| \\
 & \quad - R_{5-bk} W_{CL,B} |W_{CL,B}| - R_{bk-6} (W_{CL,B} + W_{bk}) |W_{CL,B} + W_{bk}| \\
 & \quad - R_{67} (W_{CL,A} + W_{CL,B} + W_{bk}) |W_{CL,A} + W_{CL,B} + W_{bk}| \\
 & \quad + R_{71} (2W_{IRWST} - W_{CL,A} - W_{CL,B} - W_{bk}) |2W_{IRWST} - W_{CL,A} - W_{CL,B} - W_{bk}| \\
 & \quad + R_{12,B} W_{1B} |W_{1B}|.
 \end{aligned} \tag{5-68}$$

for the loop from the containment through the PRZ to the ADS-4 valve on the PRZ side and back to the containment:

$$\begin{aligned}
 \mathcal{G} \left[\rho_l (H_{PRZ,b} + L_{PRZ} - H_{HL}) - \rho_{CRE} (H_{ADS-4,A} - H_{HL}) \right] = & +R_{SRL-2} W_{SRL} |W_{SRL}| \\
 & - R_{ADS-4} W_{ADS-4,A} |W_{ADS-4,A}|.
 \end{aligned} \tag{5-69}$$

for the loop from the containment through the PRZ to the ADS-4 valve on the CMT side and back to the containment:

$$\begin{aligned}
 \mathcal{G} \left[\rho_l (H_{PRZ,b} + L_{PRZ} - H_{HL}) - \rho_{CRE} (H_{ADS-4,A} - H_{HL}) \right] = & +R_{SRL-2} W_{SRL} |W_{SRL}| \\
 & - R_{1-23,A} W_{1A} |W_{1A}| \\
 & + R_{1-2,B} W_{1B} |W_{1B}| \\
 & + R_{ADS-4,B} W_{ADS-4,B} |W_{ADS-4,B}|.
 \end{aligned} \tag{5-71}$$

for the loop from the containment through the IRWST to the break and back to the containment

$$\begin{aligned}
 \mathcal{G} \rho_l (H_{IRWST} + L_{IRWST} - H_{HL}) = & +R_{IRWST} W_{IRWST} |W_{IRWST}| \\
 & + R_{67} (W_{CL,A} + W_{CL,B} + W_{bk}) |W_{CL,A} + W_{CL,B} + W_{bk}| \\
 & + R_{6-bk} (W_{CL,B} + W_{bk}) |W_{CL,B} + W_{bk}| \\
 & + R_{bk} W_{bk} |W_{bk}|.
 \end{aligned} \tag{5-72}$$

5. Modeling Equations

For the loop from the containment through the IRWST to the ADS-4 valve on the PRZ side and back to the containment:

$$\begin{aligned}
 \rho_l (H_{IRWST,b} + L_{IRWST}) - \bar{\rho} L_{RPV} \\
 - \rho_{CRE} (H_{ADS-4,A} - H_{HL}) \Big] g = & + R_{IRWST} W_{IRWST} |W_{IRWST}| \\
 & + R_{1-23,A} W_{1A} |W_{1A}| \\
 & + R_{71} (2W_{IRWST} - W_{CL,A} - W_{CL,B} - W_{bk}) |2W_{IRWST} - W_{CL,A} - W_{CL,B} - W_{bk}| \\
 & + R_{ADS-4,B} W_{WADS-4,B} |W_{ADS-4,B}|.
 \end{aligned} \tag{5-73}$$

In Eqs. (5-67) through (5-73), the symbol g stands for the gravitational constant, H for fixed and design-specified component elevations found in Appendix 1.5, L for the elevations of moving liquid levels as found in Appendix 1.5 for the design-specified levels and in Appendix 4.6 for the computed elevations, ρ is the density and $\Delta\rho$ the difference between the densities of saturated liquid and vapor. The over-bar denotes core average (arithmetic mean of inlet and exit densities). The resistance coefficients, R , are defined by Eq. (5-41); their subscripts are shown in Figure 5.10, and their numerical values were computed from the listing in Appendix 1.7 and are shown in Appendix 8. The resistance coefficients for cold-leg pipes and valve passages in parallel are combined by

$$R_{ab} = \frac{R_a R_b}{(\sqrt{R_a} + \sqrt{R_b})^2} \tag{5-74}$$

The six momentum balances, Eqs. (5-67) through (5-73), are supplemented with three mass balances, one for the RPV, one for the Hot Leg at the PRZ side, and the third for the Hot Leg on the CMT side:

$$\begin{aligned}
 W_{1A} + W_{1B} &= 2W_{IRWST} - W_{CL,A} - W_{CL,B} - W_{bk} \\
 W_{SRL} &= W_{ADS-4,A} + W_{cnd,SGA} - W_{CL,A} - W_{1A} \\
 W_{1B} &= W_{ADS-4,B} - W_{CL,B} + W_{cnd,SG.B}
 \end{aligned} \tag{5-75}$$

The nine coupled equations, Eqs. (5-67) through (5-73) and (5-75) were solved with the aid of MATHCAD. The results are listed in Appendix 5.5, the reproduction of the EXCEL Worksheet for the reference parameters for Phase 5. The comparison between reference mass flow estimates and available test data is shown in Table 5.15 of the next section.

5.5.5 Comparison of Reference Parameters with Test Data

Where a reference parameter could not be computed directly from design specifications, steady-state or transient conservation equations had to be used to estimate characteristic reference parameters. It was explained in Section 5.3 that the estimates need to be confirmed to ascertain scaled variables of order of unity. This Section presents in Table 5.15 the comparison of estimated with available experimental data. *This comparison gives the assurance that the scaling analysis presented here complies with Scaling Principle (1) explained in Section 4.3, namely with the*

5. Modeling Equations

requirement that all scaled variables must be of order unity. It was also explained in Section 4.3 that the ranking of phenomena or processes and the assessment of scaling distortion depend on the compliance with this principle.

Table 5.15 covers all phases of the transient. There are two rows for every compared parameter, the first one presenting the estimates, the second row the data from the test facility. Each facility is represented in a column, as indicated in the top row of the table. The estimated reference parameter for AP600 may be of interest and are, therefore, included even though there are no test data available for AP600. The table shows that the accuracy of the reference parameters is for most facilities sufficient to support the scale distortion criterion described in Section 4.6.

Table 5.15 Comparison of Estimated Reference Parameters with Experimental Data

		AP600	APEX	ROSA	SPES
PHASE 1, Depressurization, before scram					
PRZ Fluid Residence Time, t_{ref}	estim.	303	not applicable	268	279
	test	not available		220	285
Depressurization Time, break	estim.	178		168	249
	test	not available		203	300
Surge line Ref. Mass Flow Rate	estim.	41.7		1.45	0.10
	test	not available		not available	not available
Break Mass Flow Rate (kg/s)	estim.	55.2		1.81	0.13
	test	not available		2.10	0.13
PHASE 2, Passive Decay Heat Removal					
CMT-B nat. circul. ref. mass flow rate, W_{ns} (kg/s)	estim.	44.26	0.22	1.09	0.11
	test	not available	0.20	0.68	0.05
CMT draining ref. mass flow rate, W_{ps} (kg/s)	estim.	54.51	0.44	1.53	0.13
	test	not available	0.20	0.55	0.06
PRHR nat. circul. ref. mass flow rate, W_{ns} (kg/s)	estim.	135.47	0.58	3.92	0.30
	test	not available	0.53	2.80	0.29
Time for primary & secondary-side pressures cross-over (s)	estim.	252	61	242	312
	test	not available	70	213	490
Cross-over pressure, primary & secondary-side pressures (MPa)	estim.	6.27	2.07	6.60	6.30
	test	not available	2.2	7.00	5.93

5. Modeling Equations

Table 5.15 Comparison of Estimated Reference Parameters with Experimental Data (continued)

		AP600	APEX	ROSA	SPES
PHASE 3, ADS-123 Blowdown					
ADS-123 Mass Flow Rate (HEM) (kg/s)	estim.	361.0	1.7	10.1	0.8
	test	not available	1.3	10.4	0.6
CMT Draining, Volumetric Flow Rate (m ³ /s)	estim.	5.59e-02	4.2e-04	1.3e-03	1.4e-04
	test	not available	4.4e-04	1.4e-03	9.1e-05
Duration of ADS-123 Phase (s), CMT draining from	estim.	723	465	869	988
	test	not available	485	917	1037
Depressurization Rate at ADS-123 Trip (Pa/s)	estim.	-2.0e+04	-9.8e+03	-1.6e+04	-1.3e+04
	test	not available	-1.8e+04	-2.6e+04	-7.9e+03
PHASE 4, ADS-4					
Starting Pressure	estim.	2.73e+05	1.37e+05	3.03e+05	3.66e+05
	test	not available	1.24e+05	3.31e+05	3.67e+05
ADS-4 Mass Flow Rate, both sides (kg/s)	estim.	200.6	2.00	6.80	1.46
	test	not available	1.43	5.30	0.65
CMT Draining, Volumetric Flow Rate (m ³ /s)	estim.	4.0e-02	3.23e-04	9.41e-04	9.81e-05
	test	not available	3.91e-04	1.22e-03	6.80e-05
PRZ Level above bottom of PRZ	estim.	10.57	1.51	8.34	4.76
	test	not available	2.10	7.40	3.00
ADS-4 Depressurization Time (s)	estim.	672	243	674	282
	test	not available	356	528	142

5. Modeling Equations

Table 5.15 Comparison of Estimated Reference Parameters with Experimental Data (continued)

		AP600	APEX	ROSA	SPES
PHASE 5, IRWST Injection					
IRWST Mass Flow Rate (kg/s)	estim.	90.4	0.6	1.5	0.2
	test	not available	1.2	1.4	0.4
ADS-4 Mass Flow Rate (kg/s)	estim.	399	0.61	6.52	1.47
	test	not available	not available	5	1
PRZ Draining Mass Flow Rate (kg/s)	estim.	707	461	858	987
	test	not available			
Break Mass Flow Rate (kg/s)	estim.	5.28	0.07	0.19	0.01
	test	not available			0.02

5. Modeling Equations

6. SCALING GROUPS

The conservation equations were derived in Chapter 5. This chapter presents the scaled conservation equations and the scaling groups with their definitions, their numerical evaluation for every phase, and their interpretations.

6.1 Scaled Equations and Scaling Groups

In this section are presented the scaled equations and the scaling groups in symbolic form, along with their general definitions. For phase and component-specific interpretations of the scaling groups, see Section 6.2.

It was explained in Section 4.4.5 that two useful scaling methods have been employed in this work, one is the *causative process* related scaling method as shown in Eq. (4-2), the other is the fractional scaling method shown in Eq. (4-3). The respective advantages of the two methods are described in Sections 4.4.5.1 and 4.4.5.2. We present both methods here in the same order as in Section 4.4.5.

6.1.1 Depressurization

Equation (5-8) for the time-rate of depressurization is the global mass balance of the primary system. It is scaled with the specified geometric parameters listed in Appendix 1, the specified initial conditions listed in Appendices 4.1 through 4.5 for Phases 1 through 4, and with the computed reference parameters described in Section 5.5.

6.1.1.1 Causative-Process Related Scaling of Depressurization

The scaling of the depressurization equation, Eq. (5-8), is given first following the *causative-process* related scaling method, i.e., according to Eq. (4-2). The *causative-process related* scaling exhibits the scaling group Π_{MC} of the *system's elasticity or mechanical compliance*. The equation scaled by the *causative-process related* method is written for use with two types of discharge volumetric flow rates: one for the reference flow, Φ_{ref}^* , (i.e., break flow for Phases 1 and 2, ADS-123 flows for Phase 3, ADS-4 flow for Phase 4) and the second for additional discharge flows (break flow for Phases 3, and 4, ADS-123 flows for Phase 4). The reference flow is the causative process for depressurization. According to Eq. (4-2), the scaling group of the reference flow is, therefore, unity. The scaling of Eq. (5-8) yields this depressurization equation, scaled by the *causative-process related* method:

$$\begin{aligned} \Pi_{MC} \chi_{V_{tot}}^* \dot{P}^* &= \Phi_{ref}^* + \sum_i \Pi_{\Phi, i} \Phi_i^* + \Pi_{\dot{Q}_{2\phi}} \left(\frac{v_{fg}}{h_{fg}} \right)^* \dot{Q}_{2\phi}^* + \sum_{v,l} \Pi_{\dot{Q}, 1\phi} \left(\frac{\beta_T}{\rho c_p} \right)^* (\dot{Q}_{1\phi})_{net}^* \\ &+ \Pi_{PP} \left(\frac{\beta_T}{\rho c_p} \right)^* P_{PP}^* + \Pi_{\dot{Q}_{N_2}} \frac{\dot{Q}_{N_2}^*}{p^* + \frac{p_{min}}{\Delta p_0}} \end{aligned} \quad (6-1)$$

All terms in the depressurization equation, and their respective processes, are compared against the term of the causative process: the break or ADS discharge (therefore $\Pi_{\phi, break} = 1$, or $\Pi_{\phi, ADS} = 1$). In Eq. (6-1), all the starred quantities are the scaled quantities of the unstarred quantities in the original depressurization equation, Eq. (5-8), they are formed according to Eq. (4-1). In Eq. (6-1)

6. Scaling Groups

$$\Pi_{MC} = \frac{\Delta p_0 \chi_{V,0} V}{\Phi_0 t_{ref}} \quad (6-2)$$

is the scaling group of the system's *mechanical compliance*, where the reference parameters Δp_0 , $\chi_{V,0}$, Φ_0 , and t_{ref} , are, respectively, the difference between initial and end pressures of the phase, the initial system mechanical volumetric compliance or elasticity, the reference discharge (break) volumetric flow rate, and the *system* reference time. The smaller the system's mechanical compliance group, Π_{MC} , is the faster will the pressure change in time, and the more quasi-statically will the pressure adjust to external agents acting on the system. In physical terms, Π_{MC} is the ratio of the *characteristic time for the pressure change* over the *characteristic system time*. Characteristic times have been defined previously in Section 5.5.1. $\Pi_{MC} = 1$, if the characteristic time for pressure change is the characteristic time of system response.

In Eq. (6-1), $\Pi_{\phi_i} = \phi_{0i} / \phi_0$ are the scaling groups of *secondary discharge* or injection volumetric flow rates, with $\phi_{0,i}$ denoting the individual initial secondary discharge or injection volumetric flow rates. These are zero during Phases 1 and 2, they stand for the break flow when the ADS-123 flows are the dominating discharges, and they stand for the break and ADS-123 flows when the ADS-4 flows are the dominating discharges.

In Eq. (6-1), the scaling group of mechanical energy addition by *Reactor Coolant Pumps* is

$$\Pi_{PP} = (\Delta p_{PP})_0 \frac{(\Phi_{cr})_0}{\Phi_0} \left(\frac{\beta_T}{\rho c_p} \right)_0 \quad (6-3)$$

where $(\Delta p_{PP})_0$ is the initial pressure rise in the Reactor Coolant Pumps, $(\Phi_{cr})_0$ is the initial total core volumetric flow rate, Φ_0 the initial (reference) volumetric flow rate at the break, and the thermophysical properties β_T , ρ , and c_p , are the isobaric thermal expansion coefficient, density, and isobaric specific heat, respectively. Π_{PP} is the ratio of volume expansion rate due to thermal expansion over break volumetric flow rate.

In Eq. (6-1), the scaling group of thermal expansion by *heating of single-phase fluid* is

$$\Pi_{\dot{Q},1\phi} = \frac{(\dot{Q}_{1\phi})_0}{\Phi_0} \left(\frac{\beta_T}{\rho c_p} \right)_0, \quad (6-4)$$

where $(\dot{Q}_{1\phi})_0$ is the initial heating power applied to the single-phase fluid, Φ_0 the initial (reference) volumetric flow rate at the break, and the thermophysical properties β_T , ρ , and c_p , are the isobaric thermal expansion coefficient, density, and isobaric specific heat, respectively. $\Pi_{\dot{Q},1\phi}$ is the ratio of volume expansion rate due to thermal expansion, caused by heating the single-phase fluid, over break volumetric flow rate.

In Eq. (6-1), the scaling group of *phase change by heating of two-phase fluid* is

$$\Pi_{\dot{Q},2\phi} = \frac{(\dot{Q}_{2\phi})_0}{\Phi_0} \left(\frac{v_{fg}}{h_{fg}} \right)_0, \quad (6-5)$$

where $(\dot{Q}_{2\phi})_0$ is the initial heating power applied to the regions of two-phase mixture, Φ_0 is the initial (reference) volumetric flow rate at the break, and the thermophysical properties v_{fg} and h_{fg} are the specific volume change and enthalpy of phase change, respectively. $\Pi_{\dot{Q},2\phi}$ is the ratio of volume expansion or contraction rate due to phase change, resulting from net heating or cooling of the two-phase mixture anywhere in the system, over break volumetric flow rate.

In Eq. (6-1), the scaling group of *thermal expansion due to heating of noncondensable gas* is

$$\Pi_{\dot{Q},N_2} = \frac{(\dot{Q}_{N_2})_0}{\Phi_0 \Delta p_0} \left(\frac{\gamma}{\gamma-1} \right)_0 \quad (6-6)$$

where $(\dot{Q}_{N_2})_0$ is the initial heating power applied to the regions of nitrogen gas, Φ_0 is the initial (reference) volumetric flow rate at the break, Δp_0 is the difference between initial and end pressures of the phase, and γ is the specific heat ratio of (the noncondensable gas) nitrogen. $\Pi_{\dot{Q},N_2}$ is the ratio of volume expansion or contraction rate due to net heating or cooling of the inert gas in the system, over break volumetric flow rate (cf. assumption p,T-v in Section 5.2).

Equation (6-1) shows that the phenomenon of system elasticity and every transfer process of the control volume has a term. All but the reference flow have a scaling group. Depressurization is scaled by up to six scaling groups. Equation (6-1) is the scaled depressurization obtained from the *causative process* related scaling method and has, as explained in Section 4.4.5.1, two advantages: (1) the magnitude of the *causative process* related scaling groups indicates the importance of their associated processes relative to the well-known *causative* processes of break and ADS discharge flows which are responsible for the depressurization, and (2) the method of scaling reveals with a *single scaling group*, namely Π_{MC} in Eq. (6-2), how close the depressurization is to steady-state conditions relative to the overall system change.

6.1.1.2 Fractional Scaling of Depressurization

The fractional scaling method of the scaling is explained in Section 4.4.5.2 to provide the *fractional* scaling groups as in Eq. (4-3). The *fractional* scaling groups have the advantage of displaying for every transfer of mass and energy across the boundary of the control volume the effect that the process has on the time rate of change of *pressure*. Each *fractional* scaling group shows the *fractional contribution* of its respective transfer process to the total time rate of pressure change. The largest *fractional* scaling groups are the most important ones as they bring about the largest changes.

The *fractional* form of the scaled depressurization equation is obtained by dividing the causative-process related, scaled depressurization equation, Eq. (6-1), by the scaling group of the system's mechanical compliance, Π_{MC} . The result is

$$\begin{aligned} \chi_{V_{tot}}^* \dot{p}^* = & \sum_{bk,ADS} \Pi_{\dot{p},\Phi,i} \Phi_i^* + \Pi_{\dot{p},\dot{Q},2\phi} \left(\frac{v_{fg}}{h_{fg}} \right)^* \dot{Q}_{2\phi}^* + \sum_{v,l} \Pi_{\dot{p},\dot{Q},1\phi} \left(\frac{\beta_T}{\rho c_p} \right)^* (\dot{Q}_{1\phi})_{net}^* \\ & + \Pi_{\dot{p},\dot{Q},N_2} \frac{\dot{Q}_{N_2}^*}{p^* + \frac{p_{min}}{\Delta p_0}} \end{aligned} \quad (6-7)$$

Corresponding Π -Groups in Eqs. (6-1) and (6-7) have the same subscripts, except that the subscripts of *fractional* Π -Groups in Eq. (6-7) for depressurization have the prefix of \dot{p} .

6. Scaling Groups

The *fractional scaling group of flow discharge* that appears in Eq. (6-7) is

$$\Pi_{\dot{p}, \Phi, i} = t_{ref} \frac{(\Phi_i)_0}{\Delta p_0 (\chi_V)_0 V} \quad (6-8)$$

and equals the ratio of volume displaced through port i over the system volume expansion due to depressurization.

The *fractional scaling group of thermal expansion due to pumping power* appearing in Eq. (6-7) is

$$\Pi_{\dot{p}, PP} = \left(\frac{\beta_T}{\rho c_p} \right)_0 t_{ref} \frac{(\Delta p_{PP} \Phi_{cr})_0}{\Delta p_0 (\chi_V)_0 V} \quad (6-9)$$

and equals the ratio of volume displaced by thermal expansion, due to pumping of single-phase fluid, over the system volume expansion due to depressurization.

The *fractional scaling group of thermal expansion or contraction due to net heating or cooling of single-phase fluid* that appears in Eq. (6-7) is

$$\Pi_{\dot{p}, \dot{Q}_{1\phi}} = \left(\frac{\beta_T}{\rho c_p} \right)_0 t_{ref} \frac{(\dot{Q}_{1\phi, net})_0}{\Delta p_0 (\chi_V)_0 V} \quad (6-10)$$

and equals the ratio of volume displaced by thermal expansion or contraction of single-phase fluid over the system volume expansion due to depressurization.

The *fractional scaling group of phase change due to heating or cooling of two-phase mixture* that appears in Eq. (6-7) is

$$\Pi_{\dot{p}, \dot{Q}_{2\phi}} = \left(\frac{v_{fg}}{h_{fg}} \right)_0 t_{ref} \frac{(\dot{Q}_{2\phi, net})_0}{\Delta p_0 (\chi_V)_0 V} \quad (6-11)$$

and equals the ratio of volume displaced by boiling or condensing due to heat transfer (not flashing!) over the system volume expansion due to depressurization.

The *fractional scaling group of thermal expansion due to heating or cooling of inert nitrogen* in Eq. (6-7) is

$$\Pi_{\dot{p}, \dot{Q}_{N_2}} = \left(\frac{\gamma - 1}{\gamma} \right)_0 t_{ref} \frac{(\dot{Q}_{N_2})_0}{\Delta p_0^2 (\chi_V)_0 V} \quad (6-12)$$

and equals the ratio of volume displaced by expansion or contraction of inert gas, caused by heat transfer, over the system volume expansion due to depressurization.

The *fractional scaling group of volume expansion due to break flow* that appears in Eq. (6-7) is

$$\Pi_{\dot{p}, bk} = \frac{\Phi_0 t_{ref}}{\Delta p_0 \chi_{V,0} V} = \frac{1}{\Pi_{MC}} \quad (6-13)$$

and equals the ratio of the *characteristic system time* over the *characteristic time for the pressure change*. Characteristic times have been defined previously in Section 5.5.1. The system elasticity or mechanical compliance group, Π_{MC} , is defined by Eq. (6-2).

Notice that every *fractional* scaling group has $t_{ref}/t_{\Delta p}$ as a factor. Consequently, the ranking of processes is not affected by the choice of reference time, t_{ref} , nor the characteristic time of depressurization, $t_{\Delta p}$ (see also Eq. (5-52) in Section 5.5.1), but the assessment of scaling distortion is affected because the timing could be distorted in a test facility. Numerical evaluations of the Π -Groups are shown in Section 6.2.

6.1.2 Inventory

Equation (5-11) for the time-rate of vapor volume fraction is the vapor mass balance of the system control volume, V . It is used to determine liquid volume fraction, or liquid inventory, and it is scaled with the specified geometric parameters listed in Appendix 1, the specified initial conditions listed in Appendices 4.1 through 4.6 for Phases 1 through 5, and with the computed reference parameters described in Section 5.5.

6.1.2.1 Causative-Process Related Scaling of Liquid Inventory Loss

The scaling of Eq. (5-11) for the time rate of inventory change is given first following the *causative-process* related scaling method (see Eq. (4-2)). The *causative-process* related scaling exhibits the scaling group Π_{VC} of the *system's volumetric compliance*. The inventory equation scaled by the *causative-process related method* is written also for the use with two types of discharge volumetric flow rates: one for the reference flow, Φ_{ref}^* , of Eq. (6-14) (i.e., break flow for Phases 1 and 2, ADS-123 flows for Phase 3, ADS-4 flow for Phases 4 and 5) and the second for direct vapor discharge flows, Φ_g^* (discharge from PRZ). The scaling of Eq. (5-11) yields the vapor inventory equation, as scaled by the causative-process related method:

$$\begin{aligned} \Pi_{VC} \left(\frac{\chi_V}{\Psi_\alpha} \right)^* \frac{d\alpha}{dt^*} = & - \sum_{l,v} \Pi_{\dot{Q},1\phi} \left(\frac{\beta_T}{\rho c_p} \right)^* \dot{Q}_{1\phi}^* \\ & - \Pi_{PP} \left(\frac{\beta_T}{\rho c_p} \right)^* P_{PP}^* \\ & - \Pi_{V,\dot{Q},2\phi} \left(\frac{v_{fg}}{h_{fg}} - \frac{\chi_V V}{\Psi_\alpha \rho_g h_{fg} V_{2\phi}} \right)^* \dot{Q}_{2\phi}^* \\ & + \Phi_{bk,ADS}^* + \Pi_{\Phi_g} \Phi_g^* - \Pi_{\dot{Q}_{N_2}} \frac{\dot{Q}_{N_2}^*}{p^* + \frac{P_{min}}{\Delta p_0}} \end{aligned} \quad (6-14)$$

All terms in the scaled “inventory” equation, Eq. (6-14) and their respective processes are compared against the term of the causative process: the break or ADS discharge flow (therefore $\Pi_{\phi,break} = 1$, or $\Pi_{\phi,ADS} = 1$). In Eq. (6-14), all the starred quantities are the scaled quantities of the unstarred quantities in the original vapor mass conservation equation, Eq. (5-11), they are formed according to Section 4.4.5.1 and Eq. (4-2). In Eq. (6-14)

$$\Pi_{VC} = \frac{\chi_{V,0} V}{\Psi_{\alpha,0} \Phi_0 t_{ref}} \quad (6-15)$$

6. Scaling Groups

is the scaling group of the system's *volumetric compliance*, where the reference parameters $\Psi_{\alpha,0}$, $\chi_{V,0}$, Φ_0 , and t_{ref} are, respectively, the initial value of the saturation property function given by Eq. (5-12), the initial volumetric system mechanical compliance or specific elasticity, the reference discharge (break) volumetric flow rate, and the system reference time. V is the primary system volume. The smaller the system's volumetric compliance group, Π_{VC} , is the faster will the liquid inventory deplete. In physical terms, Π_{VC} is the ratio of the *characteristic time for liquid depletion* over the *characteristic system time*, t_{ref} . Characteristic times have been defined previously in Section 5.5.1. $\Pi_{VC} = 1$, if the characteristic time for liquid draining is selected to be the characteristic time of system response.

In Eq. (6-14), $\Pi_{\Phi_g} = \Phi_{g,0} / \Phi_0$ is the scaling group of *direct vapor discharge*, with Φ_0 denoting the reference volumetric flow rate. The direct vapor discharge occurs during Phases 3 and 4, when ADS-123 steam flows from the PRZ.

In Eq. (6-14), the scaling groups Π_{pp} , $\Pi_{\dot{Q},1\phi}$, and $\Pi_{\dot{Q},N_2}$ of mechanical energy addition, net heating of single-phase regions, including the noncondensable nitrogen, are the same as defined by Eqs. (6-3), (6-4), and (6-6) for Eq. (6-1). Thus, there are only three new scaling groups introduced by Eq. (6-14). The scaling group for heating of the two-phase region is

$$\Pi_{V,\dot{Q},2\phi} = \left(\frac{\dot{Q}_{2\phi}}{\Phi_{bk,ADS}} \right)_0 \left| \frac{v_{fg}}{h_{fg}} - \frac{\chi_V V}{\Psi_{\alpha} \rho_g h_{fg}} \right|_0 \quad (6-16)$$

and is the ratio of vapor volume expansion or liquid volume reduction rate due to phase change, resulting from net heating or cooling of the two-phase mixture anywhere in the system, over break volumetric flow rate.

Equation (6-14) shows that the loss of inventory is caused not only by volume discharge but it is also influenced by heating and cooling on the primary system boundary, and that it is scaled by at most three new scaling groups. Equation (6-14) is the scaled equation for inventory loss obtained from the *causative process* related scaling method. Section 4.4.5.1, explains the two advantages of this method: (1) the magnitude of the *causative process* related scaling groups indicates the importance of their associated processes relative to the break and automatic depressurization flows which are responsible for the inventory changes, and (2) this method of scaling reveals with a single scaling group, namely Π_{VC} in Eq. (6-15), how far the inventory draining is from steady-state conditions relative to the overall system change.

6.1.2.2 Fractional Scaling of Inventory Loss

Section 4.4.5.2 presents the *fractional* scaling method according to Eq. (4-3) and provides the *fractional* scaling or Π -Groups for the liquid inventory equation. These Π -Groups display for every transfer of mass and energy across the boundary of the primary system control volume the fractional contribution of the respective transfer process to the time rate of change of vapor volume, or, equivalently, to the rate of change of liquid inventory. The *fractional* scaled inventory equation is obtained by dividing Eq. (6-14) by the scaling group of the system's volumetric compliance, Π_{VC} in Eq. (6-15). The result is

$$\begin{aligned}
\left(\frac{\chi_V}{\Psi_\alpha}\right)^* \frac{d\alpha}{dt^*} &= - \sum_{l,v} \Pi_{\dot{\alpha},\dot{Q},1\phi} \left(\frac{\beta_T}{\rho c_p}\right)^* \dot{Q}_{1\phi}^* \\
&\quad - \Pi_{\dot{\alpha},PP} \left(\frac{\beta_T}{\rho c_p}\right)^* P_{PP}^* \\
&\quad - \Pi_{\dot{\alpha},\dot{Q},2\phi} \left(\frac{v_{fg}}{h_{fg}} - \frac{\chi_V V}{\Psi_\alpha \rho_g h_{fg} V_{2\phi}}\right)^* \dot{Q}_{2\phi}^* \\
&\quad + \Pi_{\dot{\alpha},bk} \Phi_{bk}^*
\end{aligned} \tag{6-17}$$

Corresponding Π -Groups in Eqs. (6-14) and (6-17) have the same subscripts, except that the subscripts of fractional Π -Groups in Eq. (6-17) have the prefix of $\dot{\alpha}$.

The fractional *scaling group* that represents in Eq. (6-17) the *vapor volume contraction or expansion due to net heating or cooling, $\dot{Q}_{1\phi}$, of single-phase fluid* in the control volume is

$$\Pi_{\dot{\alpha},\dot{Q},1\phi} = \left(\dot{Q}_{1\phi}\right)_0 \left(\frac{\beta_T}{\rho c_p}\right)_0 \left(t_{ref} \frac{\Psi_\alpha}{\chi_V V}\right)_0 \tag{6-18}$$

and it equals the ratio of volume displaced by thermal expansion or contraction of single-phase fluid over the system volume expansion due to depressurization, times the ratio of system reference time over reference time for liquid volume depletion.

The *fractional scaling group* representing in Eq. (6-17) the *vapor volume contraction or expansion due to boiling or condensation* as a result of the net heat transfer rate $\dot{Q}_{2\phi}$ in the two-phase fluid regimes is

$$\Pi_{\dot{\alpha},\dot{Q},2\phi} = \left(\dot{Q}_{2\phi}\right)_0 \left|\frac{v_{fg}}{h_{fg}} - \frac{\chi_V V}{\Psi_\alpha \rho_g h_{fg}}\right|_0 \left(t_{ref} \frac{\Psi_\alpha}{\chi_V V}\right)_0 \tag{6-19}$$

and it equals the ratio of volume displaced by phase change over the system volume expansion due to depressurization, times the ratio of system reference time over reference time for liquid volume depletion.

The *fractional scaling group of vapor volume contraction or expansion due to mechanical (pumping) power added to single-phase fluid* that appears in Eq. (6-17) is

$$\Pi_{\dot{\alpha},PP} = \left(\Delta P_{PP} \frac{\Phi_{cr}}{\Phi_{bk}}\right)_0 \left(\frac{\beta_T}{\rho c_p}\right)_0 \left(t_{ref} \Phi_{bk} \frac{\Psi_\alpha}{\chi_V V}\right)_0 \tag{6-20}$$

and it equals the ratio of volume displaced by thermal expansion due to mechanical power addition over the system volume expansion due to depressurization, times the ratio of system reference time over reference time for liquid volume depletion.

6. Scaling Groups

The *fractional scaling group of vapor volume expansion due to break flow* that appears in Eq. (6-17) is

$$\Pi_{\alpha,bk} = \left(t_{ref} \Phi_{bk} \frac{\Psi_{\alpha}}{\chi_V V} \right)_0 = \frac{1}{\Pi_{VC}} \quad (6-21)$$

and it equals the ratio of system reference time over reference time for liquid volume depletion.

Notice again that every *fractional* scaling group has t_{ref} as a factor. Consequently, the ranking of processes is not affected by the choice of reference time, t_{ref} , (see also Section 5.5.1), but the assessment of scaling distortion is affected because the timing could be distorted in a test facility. Whereas there are common Π -Groups in Eqs. (6-1) and (6-14), there is no such correspondence between Eqs. (6-7) and (6-17). The numerical evaluations of the Π -Groups in Eqs. (6-18) through (6-21) are shown in Section 6.2.

6.1.3 Temperatures

Equation (5-17) for the time-rate of temperature change is the liquid energy balance for the system control volume, V . It could be used to predict the liquid temperature, and it is used here for scaling. It is scaled with the specified geometric parameters listed in Appendix 1, the specified initial conditions listed in Appendices 4.1 through 4.6 for Phases 1 through 5, and with the computed reference parameters described in Section 5.5.

6.1.3.1 Causative-Process Related Scaling of Temperature Change

The scaling of Eq. (5-17) for the time rate of primary-system liquid temperature change is given first given for the *causative-process* related scaling method represented by Eq. (4-2). Equation (5-17) is scaled for Phases 1 and 2 of the transient, for the primary system, with and without passive CMT and PRHR circulation, and for two types of discharge flows: one for the reference flow, Φ_{ref}^* , (i.e., break flow Φ_{bk}^* for Phases 1 and 2, ADS-123 flows $\Phi_{ADS-123}^*$ for Phase 3, ADS-4 flow Φ_{ADS-4}^* for Phases 4 and 5), and the second for direct vapor discharge flows, Φ_g^* , from PRZ. Equation (5-17) is scaled for the subphases in which core heating and SG cooling, or PRHR cooling dominate, and for the subphase starting after accumulator injection. The liquid energy balance is also scaled for temperature changes in the CMT and PRHR control volumes.

The *causative-process* related scaling method yields the scaling group Π_{TC} of the *system's heat capacity or thermal compliance* and has, as explained in Section 4.4.5.1, two advantages: (1) the magnitude of the *causative process* related scaling group indicates the importance of the associated process relative to the energy flow through the break when heating and cooling are balanced, and otherwise relative to the dominant cooling rate (by SG or PRHR); and (2) the *causative process* related method of scaling reveals with a single scaling group, namely Π_{TC} in Eq. (6-22), how far the thermal response of the system or a component is from steady-state conditions relative to the overall system change.

Primary-System Temperature Change, Break Flow Dominating

The scaling of Eq. (5-17) yields the scaled equation for the time rate of temperature change during Phase 1 in which the liquid temperature change is governed by break flow, Φ_{bk}^* , and when there is no CMT or PRHR circulation:

$$\begin{aligned}
\Pi_{TC}(\rho c_p)^* \frac{dT^*}{dt^*} &= \left(\Pi_{T,\dot{Q},1\phi} \dot{Q}_{1\phi}^* + \Pi_{T,PP} P_{PP}^* \right) \left(1 + \frac{\beta_T}{\rho c_p} \frac{\Psi_T}{\chi_V V} \right)^* \\
&+ \Pi_{T,\dot{Q},2\phi} \dot{Q}_{2\phi}^* \left\{ \frac{v_{fg}}{h_{fg}} \left[\frac{\Psi_T}{\chi_V V} + \rho_f (h_f - h) \right] \right\}^* \\
&- \left(\frac{\Psi_T}{\chi_V V} \right)^* \left(\Phi_{bk}^* - \Pi_{T,\dot{Q},N_2} \frac{\dot{Q}_{N_2}^*}{p^* + \frac{P_{\min}}{\Delta p_0}} \right)
\end{aligned} \tag{6-22}$$

All terms in the energy equation for the liquid temperature, and the processes associated with these terms, are compared against the term of the causative process: the break discharge (therefore $\Pi_{T,break} = 1$). In Eq. (6-22), all the starred quantities are the scaled quantities of the unstarred quantities in the original energy conservation equation for the subcooled liquid, Eq. (5-17), they are formed according to Eq. (4-1). In Eq. (6-22)

$$\Pi_{TC} = \frac{V_{1\phi} (\rho c_p \Delta T)_0 (\chi_V)_0 V}{t_{ref} (\Phi_{bk})_0 (\Psi_T)_0} = \frac{V_{1\phi} (\rho c_p \Delta T)_0 (\chi_V)_0 V}{(V_{l,PRZ})_0 (\Psi_T)_0} \tag{6-23}$$

is the scaling group of the system's *heat capacity* or *thermal compliance*, where the reference parameters ΔT_0 , $\Psi_{T,0}$, $\chi_{V,0}$, $\Phi_{bk,0}$, and t_{ref} , are, respectively, the driving temperature difference, the initial value of the thermal expansion function defined by Eq. (5-18), the mechanical volumetric compliance (Eq. (5-9)), the initial (reference, break) discharge volumetric flow rate, and the system reference time. The smaller the system's thermal compliance group, Π_{TC} , is the faster will the liquid temperature change. In physical terms, Π_{TC} , is the ratio of the *characteristic time for thermal response* over the *characteristic system time*, multiplied by the ratio of thermal heat over mechanical work capacities, $(M_i \Delta h_i) / (\Delta V_i \Delta p)$, where ΔV_i is the thermal expansion or contraction of the subcooled liquid volume. Characteristic times have been defined previously in Section 5.5.1. The second of Eqs. (6-23) is written for Phase 1, the initial depressurization phase, where the Pressurizer drain time is the characteristic time (cf. Eq. (5-50)).

In Eq. (6-22), the causative-process related scaling group for *subcooled liquid temperature change due to heating or cooling of the liquid* is

$$\Pi_{T,\dot{Q},1\phi} = \left| 1 + \frac{\beta_T}{\rho c_p} \frac{\Psi_T}{V \chi_V} \right| \left(\frac{V \chi_V \dot{Q}_{1\phi}}{\Psi_T \Phi_{bk}} \right)_0, \tag{6-24}$$

where $(\dot{Q}_{1\phi})_0$ is the initial net heating power applied to the single-phase fluid, Φ_0 the initial (reference) volumetric flow rate at the break, and the thermophysical properties β_T , ρ , and c_p , are the isobaric thermal expansion coefficient, density, and isobaric specific heat, respectively. $\Pi_{TQ,1\phi}$ is the ratio of net cooling power over the rate of mechanical work discharge at the break.

In Eq. (6-22), the causative-process related scaling group for *subcooled liquid temperature change due to mechanical energy addition to the liquid* by the recirculation pumps is

6. Scaling Groups

$$\Pi_{T,PP} = \Pi_{TQ,1\phi} \left(\frac{P_{PP}}{\dot{Q}_{1\phi}} \right)_0 \quad (6-25)$$

and equals the ratio of RCP pumping power over the rate of mechanical work discharge at the break.

In Eq. (6-22), the causative-process related scaling group for *subcooled liquid temperature change due to heating or cooling the two-phase mixture* is

$$\Pi_{T,Q,2\phi} = \left| \frac{v_{fg}}{h_{fg}} \left[\frac{\Psi_T}{\chi_V V} + \rho_{2\phi} (h_{2\phi} - h) \right] \right|_0 \left(\frac{V \chi_V \dot{Q}_{2\phi}}{\Psi_T \Phi_{bk}} \right)_0 \quad (6-26)$$

and equals the ratio of the effect of heating or cooling of the two-phase mixture (e.g., in PRZ) on subcooled liquid temperature, over the effect on that temperature from mechanical work discharge at the break. When saturated liquid crosses from the two-phase into the subcooled liquid region the $\rho_{2\phi}$ and $h_{2\phi}$ are to be replaced by ρ_f and h_f , respectively, in Eq. (6-26) and in Eq. (5-18) for Ψ_T .

Primary-System Temperature Change, Dominated by Wall Heating or Cooling

When the change of liquid temperature is governed by the net cooling due to the imbalance between full-power Steam Generator cooling and reduced core heating after scram, as is the case during Phase 1.2, then the scaling of Eq. (5-17) yields, for the time prior to the initiation of CMT and PRHR circulation,

$$\begin{aligned} \Pi_{TC} (\rho c_p)^* \frac{dT^*}{dt^*} &= (\dot{Q}_{1\phi}^* + \Pi_{T,PP} P_{PP}^*) \left(1 + \frac{\beta_T}{\rho c_p} \frac{\Psi_T}{\chi_V V} \right)^* \\ &+ \Pi_{T,Q,2\phi} \dot{Q}_{2\phi}^* \left\{ \frac{v_{fg}}{h_{fg}} \left[\frac{\Psi_T}{\chi_V V} + \rho_{2\phi} (h_{2\phi} - h) \right] \right\}^* \\ &- \Pi_{T,bk} \left(\frac{\Psi_T}{\chi_V V} \right)^* \Phi_{bk}^* . \end{aligned} \quad (6-27)$$

Equation (6-27) applies only to Subphase 1.2, the second part of Phase 1, after scram. For this subphase the power of the mechanical work at the break, which is the reference energy in Eq. (6-22), is replaced by the net cooling by the Steam Generators. The scaling group of the system's *heat capacity* or *thermal compliance* in Eq. (6-27) for Subphase 1.2 is

$$\Pi_{TC,1.2} = \frac{V_{1\phi} (\rho c_p \Delta T \Phi_{bk})_0}{(V_{l,PRZ})_0 \dot{Q}_{1\phi} \left| 1 + \frac{\beta_T}{\rho c_p} \frac{\Psi_T}{\chi_V V} \right|_0}, \quad (6-28)$$

which equals the ratio of the rate of thermal energy release from the subcooled liquid over the net cooling power.

The causative-process related scaling group for heat transfer to the single-phase fluid regions is equal to one for Eq. (6-22) for Subphase 1.1. For Eq. (6-27) of Subphase 1.2 the effect of the *break flow* is represented by the causative-process related scaling group

$$\Pi_{T,bk,1.2} = \frac{\left(\frac{\Psi_T}{\chi_V} \Phi_{bk} \right)_0}{\left| 1 + \frac{\beta_T}{\rho c_p} \frac{\Psi_T}{\chi_V V} \right|_0 \left(\dot{Q}_{1\phi} \right)_0}. \quad (6-29)$$

It is the ratio of mechanical power discharged through the break over the cooling power in the Steam Generators.

In Eq. (6-27), the causative-process related scaling group for *subcooled liquid temperature change due to mechanical energy addition to the liquid* by the recirculation pumps equals

$$\Pi_{TPP,1.2} = \left(\frac{P_{PP}}{\dot{Q}_{1\phi}} \right)_0 \quad (6-30)$$

and is the ratio of RCP pumping power over the cooling power in the Steam Generators.

In Eq. (6-27), the causative-process related scaling group for *subcooled liquid temperature change due to heating or cooling the two-phase mixture* is

$$\Pi_{TQ,2\phi,1.2} = \frac{\left| \frac{v_{fg}}{h_{fg}} \left[\frac{\Psi_T}{\chi_V V} + \rho_{2\phi} (h_{2\phi} - h) \right] \right|_0 \left(\frac{\dot{Q}_{2\phi}}{\dot{Q}_{1\phi}} \right)_0}{\left| 1 + \frac{\beta_T}{\rho c_p} \frac{\Psi_T}{\chi_V V} \right|_0} \quad (6-31)$$

This is the ratio of the effect of heating or cooling of the two-phase mixture (e.g., in PRZ) on subcooled liquid temperature, over the cooling power in the Steam Generators.

Primary-System Temperature Change, Domination by PRHR Cooling

PRHR cooling dominates the liquid temperature change at the beginning and during the early part of Phase 2. For this phase, Eq. (5-17) is scaled after the inclusion of the CMT-A and CMT-B circulation flows and yields these causative-process related scaling groups:

The system's thermal compliance group, Π_{TC} , for Phase 2,

$$\Pi_{TC,2} = \frac{V_{1\phi} (\rho c_p \Delta T)_0}{t_{ref} (W_{PRHR})_0 (h - h_{PRHR})_0} \quad (6-32)$$

6. Scaling Groups

is the causative-process related scaling group of the system's *heat capacity*. All the symbols are as defined above. The smaller the system's thermal compliance group, Π_{TC} , is the faster will the liquid temperature change. $\Pi_{TC,2}$ is the ratio of the *characteristic time for liquid cool-down* by PRHR cooling over the *characteristic system time*. Characteristic times have been defined previously in Section 5.5.1.

The causative-process related scaling group for *subcooled liquid temperature change due to heating or cooling of the single-phase liquid* is

$$\Pi_{TQ,1\phi,2} = \left| 1 + \frac{\beta_T}{\rho c_p} \frac{\Psi_T}{\chi_V V} \right|_0 \left(\frac{\dot{Q}_{1\phi}}{W_{PRHR} (h - h_{PRHR})} \right)_0, \quad (6-33)$$

which is the ratio of net wall cooling power over PRHR cooling power.

The causative-process related scaling group for *subcooled liquid temperature change due to mechanical energy addition to the liquid* by the recirculation pumps is, as in Eq. (6-25)

$$\Pi_{TPP,2} = \Pi_{TQ,1\phi,2} \left(\frac{P_{PP}}{\dot{Q}_{1\phi}} \right)_0 \quad (6-34)$$

and equals the ratio of RCP pumping power over PRHR cooling power.

The causative-process related scaling group for *subcooled liquid temperature change due to heating or cooling the two-phase mixture* during Phase 2 is

$$\Pi_{TQ,2\phi,2} = \left| \frac{v_{fg}}{h_{fg}} \left[\frac{\Psi_T}{\chi_V V} + \rho_{2\phi} (h_{2\phi} - h) \right] \right|_0 \left(\frac{\dot{Q}_{2\phi}}{W_{PRHR} (h - h_{PRHR})} \right)_0 \quad (6-35)$$

and equals the ratio of the heating or cooling power of the two-phase mixture, over the PRHR cooling power.

The effect of the *break flow* on the change of liquid temperature is represented by the causative-process related scaling group

$$\Pi_{Tbk,2} = \frac{\left(\frac{\Psi_T}{\chi_V} \Phi_{bk} \right)_0}{W_{PRHR} (h - h_{PRHR})_0}. \quad (6-36)$$

It is the ratio of mechanical power discharged through the break over the PRHR cooling power. $\Pi_{PRHR} = 1$, because the PRHR cooling is the reference transport process. The representative, causative-process related scaling groups for the effects of CMT circulation on the change of the liquid temperature in the primary system are, for CMTs on the Pressurizer side (A), and CMT side (B)

$$\Pi_{T,CMT;A,B} = \left(\frac{W_{CMT;A,B}}{W_{PRHR}} \right)_0 \left(\frac{h - h_{CMT;A,B}}{h - h_{PRHR}} \right)_0. \quad (6-37)$$

Equation (6-37) is the ratio of CMT over PRHR cooling power. The reference mass flow rates, W , are computed from the steady momentum balance, and the initial enthalpies in Eq. (6-37) are computed from the specified initial temperatures.

Temperature Change in Core Make-up Tank

Equation (5-17) reduces for the Core Make-up Tank, at the beginning of Phase 2 when CMT circulation is initiated, to

$$V_{1\phi} \rho c_p \left. \frac{dT}{dt} \right|_{CMT_{A,B}} = W_{CMT_{A,B}} (h_{CMT_{A,B}} - h) + \dot{Q}_{1\phi, CMT_{A,B}}, \quad (6-38)$$

where \dot{Q} is the heating power passing from the CMT tank walls to the single-phase liquid in the CMT. Equation (6-32) implies that the mass flows entering through the Pressure Balance Lines and leaving through the Direct Vessel Injection Lines are equal. Scaling of this equation yields the equation scaled by the causative-process related method (see Section 4.4.5.1)

$$\Pi_{TC, CMT} \frac{dT_{CMT}^*}{dt^*} = W_{CMT}^* (h^* - h_{CMT}^*) + \Pi_{TQ, CMT} \dot{Q}_{CMT}^* \quad (6-39)$$

with two causative-process related scaling groups, the first one representing the *thermal capacity* of the fluid in the CMT

$$\Pi_{TC, CMT} = \frac{(\rho c_v V)_{CMT} (T_l - T_{CMT})_0}{t_{ref} (W_{CMT})_0 (h_l - h_{CMT})_0} = \frac{\left(\rho \frac{c_v}{c_p} V \right)_{CMT}}{t_{ref} (W_{CMT})_0}, \quad (6-40)$$

which is the ratio of the CMT's thermal response time over the system reference time, t_{ref} , with the CMT's response time being the time it takes to raise the initial CMT temperature, T_{CMT} , to the initial mean temperature, T_b , of the liquid in the primary system. $\Pi_{TC, CMT}$ is also the ratio of the heat capacity of the liquid in the CMT over the heat capacity of the liquid circulating through the CMT during the system reference time. The difference between the Cold-Leg and mean fluid temperatures is neglected in Eq. (6-40) because the difference is less than 1°C after scram. The CMT volume, V_{CMT} , includes the volumes of the Pressure Balance Line (PBL) and the Direct Vessel Injection Line (DVI). The reference mass flow rate, $(W_{CMT})_0$ is computed from the steady momentum balance equation, Eq. (5-56), as shown in Appendix 5.2. All initial conditions are found in Appendix 4.3.

The second causative-process related scaling group for the CMT temperature equation scales the effect of *wall heating*

$$\Pi_{\dot{Q}, CMT} = \frac{(\dot{Q}_{CMT})_0}{(W_{CMT})_0 (h_{CL} - h_{CMT})_0}, \quad (6-41)$$

where the wall heating power, $(\dot{Q}_{CMT})_0$, is computed for Phase 2 in Appendix 5.2, using the Dittus-Boelter correlation for convective heat transfer. The initial enthalpies are listed in Appendix 4.3.

6. Scaling Groups

Temperature Change in Passive Residual Heat Rejection System

Equation (6-38) is applied to the fluid in the tube-side volume of the Passive Residual Heat Rejection System, with the subscript *CMT* replaced by *PRHR*, and scaled to yield the two causative-process related scaling groups that are similar to those defined by Eqs. (6-39) and (6-40) for the CMT, the first one representing the *thermal capacity* of the fluid in the PRHR

$$\Pi_{TC,PRHR} = \frac{(\rho c_v V)_{PRHR} (T_l - T_{PRHR})_0}{t_{ref} (W_{PRHR})_0 (h_l - h_{PRHR})_0} = \frac{\left(\rho \frac{c_v}{c_p} V \right)_{PRHR}}{t_{ref} (W_{PRHR})_0}, \quad (6-42)$$

where the difference between the Hot-Leg and mean fluid temperatures is neglected because the difference is less than 1 °C after scram.

The second causative-process related scaling group for the PRHR temperature equation scales the effect of *wall heating* during natural circulation

$$\Pi_{\dot{Q},PRHR} = \frac{(\dot{Q}_{PRHR})_0}{(W_{PRHR})_0 (h_{CL} - h_{PRHR})_0}, \quad (6-43)$$

where the wall heating power, $(\dot{Q}_{PRHR})_0$ is computed for Phase 2 in Appendix 5.2, using the Dittus-Boelter correlation for convective heat transfer. The initial enthalpies are listed in Appendix 4.3. The scaling groups given by Eqs. (6-42) and (6-43) for the PRHR have the same interpretations as the scaling groups given by Eqs. (6-40) and (6-41) for the CMT temperature.

Primary System Temperature Change after Start of Accumulator Injection

The mass flow rate from the Accumulators is needed in the energy balance, Eq. (5-17). It is computed from the volumetric flux divergence equation, Eq. (5-4), which produces the volumetric flow rate of the Accumulators for pressures below the specified pressure trip set point for opening the accumulator valves:

$$\frac{W_{ACC}}{\rho_l} = \Phi_{ACC} = \frac{\gamma - 1}{\gamma} \frac{\dot{Q}_{ACC}}{p} - \frac{V_{N_2}}{\gamma p} \dot{p}, \quad (6-44)$$

where the pressure derivative, \dot{p} , is given by Eq. (5-8) and the pressure, p , from the integral of that equation. The first term accounts for the thermal expansion that the nitrogen gas experiences as it is being heated by the wall; the second term accounts for the expansion due to depressurization. The mean liquid temperature in the primary system decreases as cold water from the Accumulators mixes with the coolant in the Direct Vessel Injection (DVI) Lines. Thus, after scaling Eq. (5-17) one obtains for Phase 2, with PRHR cooling being dominant, the energy conservation equation for the liquid in the primary system, scaled according to the causative-process related method (see Section 4.4.5.1)

$$\begin{aligned}
\Pi_{TC}(\rho c_p)^* \frac{dT^*}{dt^*} &= \Pi_{T\dot{Q}, 1\phi, 2} \dot{Q}_{1\phi}^* \left(1 + \frac{\beta_T}{\rho c_p} \frac{\Psi_{T,ACC}}{\chi_V V} \right)^* \\
&+ \Pi_{T,\dot{Q}, 2\phi, 2} \dot{Q}_{2\phi}^* \left\{ \frac{v_{fg}}{h_{fg}} \left[\frac{\Psi_{T,ACC}}{\chi_V V} + \rho_{2\phi} (h_{2\phi} - h) \right] \right\}^* \\
&- \sum_{A,B} \Pi_{T,CMT} W_{CMT}^* (h - h_{CMT})^* \\
&- \Pi_{T,bk, 2} \left(\frac{\Psi_{T,ACC}}{\chi_V V} \right)^* \Phi_{bk}^* - W_{PRHR}^* (h - h_{PRHR})^* \\
&+ \Pi_{T,ACC} \frac{\dot{Q}_{N_2}^*}{p^* + \frac{p_{min}}{\Delta p_0}} \left[\frac{\Psi_{T,ACC}}{\chi_V V} + \rho_l (h_{ACC} - h) \right]^* .
\end{aligned} \tag{6-45}$$

Notice that Ψ_T in Eq. (6-27), and defined in Eq. (5-18), is now replaced for Eq. (6-45) by

$$\Psi_{T,ACC} = V_{1\phi} \beta_T T - \chi_{2\phi} \rho_{2\phi} (h_{2\phi} - h) + \frac{V_{N_2}}{\gamma p} \rho_l (h_{ACC} - h), \tag{6-46}$$

and that the mechanical compliance defined by Eq. (5-9) must now include the term proportional to the gas volume V_{N_2} . Equation (6-45) has one causative-process related scaling group in addition to those defined by Eqs. (6-32) through (6-37). The additional scaling group characterizes the effects from Accumulator injection on the temperature of the subcooled liquid in the primary system and is defined by

$$\Pi_{T,ACC} = \left(\frac{\dot{Q}_{N_2}}{W_{PRHR} (h - h_{PRHR})} \right)_0 \frac{\gamma - 1}{\gamma (P_{ACC})_0} \left| \rho_l (h_{ACC} - h) + \frac{\Psi_{T,ACC}}{\chi_V V} \right|_0 \tag{6-47}$$

and represents the ratio of heating and thermal convection power from the Accumulator over the PRHR cooling power.

6.1.3.2 Fractional Scaling of Energy Equation

The *fractional* scaling of the energy conservation equation is explained in detail in Section 4.4.5.2. It is of the form of Eq. (4-3). When scaled by the fractional scaling method, the energy conservation equation has the advantage of displaying *directly* for every transfer of energy across the boundary of the primary system control volume the fraction that the corresponding transfer contributes to the time rate of change of the primary-system liquid temperature. The *fractional* form of the scaled energy equation is obtained by dividing the causative-process related, scaled energy equation, Eq. (6-27), by the scaling group of the system's thermal compliance, Π_{TC} . The result is

6. Scaling Groups

$$\begin{aligned}
 (\rho c_p)^* \frac{dT^*}{dt^*} &= \left(\Pi_{\dot{T}, \dot{Q}, 1\phi} \dot{Q}_{1\phi}^* + \Pi_{\dot{T}, PP} P_{PP}^* \right) \left(1 + \frac{\beta_T}{\rho c_p} \frac{\Psi_{T, ACC}}{\chi_V V} \right)^* \\
 &+ \Pi_{\dot{T}, \dot{Q}, 2\phi} \dot{Q}_{2\phi}^* \left\{ \frac{v_{fg}}{h_{fg}} \left[\frac{\Psi_{T, ACC}}{\chi_V V} + \rho_f (h_f - h) \right] \right\}^* \\
 &- \Pi_{\dot{T}, bk} \Phi_{bk}^* \left(\frac{\Psi_{T, ACC}}{\chi_V V} \right)^* \\
 &+ \Pi_{\dot{T}, PRHR} W_{PRHR}^* (h_{PRHR} - h)^* + \sum_{A, B} \Pi_{\dot{T}, CMT} W_{CMT}^* (h_{CMT} - h)^* \\
 &+ \Pi_{\dot{T}, ACC} \frac{\dot{Q}_{N_2}^*}{p^* + \frac{p_{min}}{\Delta p_0}} \left[\frac{\Psi_{T, ACC}}{\chi_V} + \rho_l (h_{ACC} - h) \right]^* \tag{6-48}
 \end{aligned}$$

and shows that every causative process related scaling group in Eq. (6-27), i.e., the scaling groups defined in Eqs. (6-29) through (6-31) need to be divided by Π_{TC} , as defined by Eq. (6-28).

For Eq. 6-48 the effect of the *break flow* is represented by the scaling group

$$\Pi_{\dot{T}, bk} = \frac{\left(\frac{\Psi_{T, ACC}}{\chi_V} \Phi_{bk} \right)_0 t_{ref}}{V_{1\phi} (\rho c_p \Delta T)_0} \tag{6-49}$$

It is the fraction of thermal energy change in the liquid that is caused by mechanical work discharged through the break.

In Eq. (6-48), the scaling group for *subcooled liquid temperature change due to mechanical energy addition to the liquid* by the recirculation pumps is

$$\Pi_{\dot{T}, PP} = \frac{(P_{PP})_0 \left| 1 + \frac{\beta_T}{\rho c_p} \frac{\Psi_{T, ACC}}{\chi_V} \right|_0 t_{ref}}{V_{1\phi} (\rho c_p \Delta T)_0} \tag{6-50}$$

and represents the fraction of thermal energy change in the liquid that is caused by mechanical work supplied by the Reactor Coolant Pumps (RCP).

In Eq. (6-48), the fractional scaling group for *subcooled liquid temperature change due to wall heat transfer to or from the liquid* is

$$\Pi_{\dot{T}, \dot{Q}_{1\phi}} = \frac{(\dot{Q}_{1\phi})_0 \left| 1 + \frac{\beta_T}{\rho c_p} \frac{\Psi_{T,ACC}}{\chi_V} \right|_0 t_{ref}}{V_{1\phi} (\rho c_p \Delta T)_0} \quad (6-51)$$

and represents the fraction of thermal energy change in the liquid that is caused by wall heat transfer experienced by the subcooled liquid.

In Eq. (6-48), the scaling group for *subcooled liquid temperature change due to heating or cooling the two-phase mixture* is

$$\Pi_{\dot{T}, \dot{Q}_{2\phi}} = \frac{(\dot{Q}_{2\phi})_0 \left| \frac{v_{fg}}{h_{fg}} \left[\frac{\Psi_{T,ACC}}{\chi_V} + \rho_f (h_f - h) \right] \right|_0 t_{ref}}{V_{1\phi} (\rho c_p \Delta T)_0} . \quad (6-52)$$

This is the fraction of thermal energy change in the liquid that is caused by phase change due to wall heat transfer to or from the two-phase region in the system volume V .

In Eq. (6-48), the fractional scaling group for *subcooled liquid temperature change due to CMT circulation* is

$$\Pi_{\dot{T}, CMT} = \frac{(W_{CMT})_0 (h - h_{CMT})_0 t_{ref}}{V_{1\phi} (\rho c_p \Delta T)_0} . \quad (6-53)$$

This is the fraction of total thermal energy change in the liquid that is caused by CMT circulation.

In Eq. (6-48), the scaling group for *subcooled liquid temperature change due to PRHR circulation* is

$$\Pi_{\dot{T}, PRHR} = \frac{(W_{PRHR})_0 (h - h_{PRHR})_0 t_{ref}}{V_{1\phi} (\rho c_p \Delta T)_0} . \quad (6-54)$$

This is the fraction of total thermal energy change in the liquid that is caused by PRHR circulation.

In Eq. (6-48), the fractional scaling group for *subcooled liquid temperature change due to heat transfer to the nitrogen gas in the Accumulators* is

$$\Pi_{\dot{T}, ACC} = \frac{(\dot{Q}_{N_2})_0 t_{ref}}{V_{1\phi} (\rho c_p \Delta T)_0} \frac{\gamma - 1}{\gamma (p_{ACC})_0} \left| \rho_l (h_{ACC} - h) + \frac{\Psi_{T,ACC}}{\chi_V} \right|_0 \quad (6-55)$$

6. Scaling Groups

and represents the fraction of total thermal energy change in the liquid that is caused by coolant injection from the Accumulators.

Corresponding Π -Groups in Eqs. (6-45) and (6-48) have the same subscripts, except that the subscripts of the *fractional* Π -Groups in Eq. (6-48) have the prefix T instead of T . Equation (6-48) applies to all phases. However, the volumetric mechanical compliance, χ_V , and the thermal expansion, $\Psi_{T, ACC}$, must be evaluated for each phase, without any non-participating subvolume. Notice that all fractional scaling groups of Eq. (6-48) are proportional to the reference time, and the reference time, therefore, does not affect the ranking of the terms in that equation.

6.1.4 Flow Rates, Inertia and Impedance

In this section are derived, defined, and interpreted the scaling metrics (scaled arrays) S_i , S_G , and S_p which characterize the *distributions* of inertia, gravity, and flow resistance (impedance) in the system and the global scaling groups, or Π -Groups, which characterize the *relative importance* of inertia, gravity, and flow resistance. The concept of the scaling metrics S_i , S_G , and S_p , and of the global Π -Groups of the momentum balances have been introduced in Section 4.4.6 for a simple two-loop system with single-phase flow. Here, we scale the momentum balances for general two-phase flow in the AP600 system.

The set of loop momentum balances is derived in Section 5.4.2 and given by Eq. (5-49). The equation accounts for the inertia, gravity, pump, and flow resistance forces, and also for the change in momentum flux. The scaling of momentum flux changes by using the Zuber and Subcool Numbers is described by Wulff [17] but omitted here on account of Assumption (W-vii) explained in Section 5.2. The elements of the inertia, gravity, pump, and flow resistance vectors are normalized with the reference values of the main loop, and the inertia and impedance matrices are normalized so that the scaled and time-dependent gravity force element, G_j^* , the scaled and time-dependent element, P_{jk}^* , of the impedance matrix, the scaled and time-dependent element of the directed kinetic energy vector, E_j^* , and the scaled and time-dependent element of the inertia matrix, I_{ji}^* , in the scaled form of the momentum equation, Eq. (5-49), are of order unity.

6.1.4.1 Forced Circulation

For the Phase 1 with forced circulation, the pumping by the Reactor Coolant Pumps is the causative and driving process, and the scaled momentum balances are given by

$$\Pi_{IN,P} \frac{dM_j^*}{dt^*} = \Pi_{GR,P} \left(S_G G^* \right)_j + \Delta p_{PP_j}^* - \Pi_{RS,P} \left(S_p P^* \right)_{jk} E_k^*, \quad (6-56)$$

where repeated indices imply summation. The products in the subscripted brackets of Eqs. (6-56) and (6-57) imply element-by-element multiplication. All the scaled *variables* of the vector equation, namely the scaled and time-dependent loop momentum vector element, M_j^* , the scaled and time-dependent gravity force element, G_j^* , the scaled and time-dependent element, P_{jk}^* , of the impedance matrix, the scaled and time-dependent element of the directed kinetic energy vector, E_j^* , and the scaled and time-dependent element of the inertia matrix, I_{ji}^* , are defined by

$$M_j^* = \frac{M_j}{M_{ref}} = \left(S_I I^* \right)_{ji} \Phi_i^* \quad (6-57)$$

$$G_j^* = \hat{g} \cdot \oint_j \hat{k} \rho_m^* dz^* \quad (6-58)$$

$$P_{ji}^* = \frac{R_{ji}(t)}{R_{ji}(0)} \quad \text{for } R_{ji}(0) > 0 \quad (6-59)$$

$$E_i^* = \frac{E_i(t)}{E_i(0)} \quad \text{for } E_i(0) > 0 \quad (6-60)$$

$$I_{ji}^* = \frac{I_{ji}(t)}{I_{ji}(0)} \quad \text{for } I_{ji}(0) > 0. \quad (6-61)$$

Here, \hat{g} and \hat{k} are the unit vectors of, respectively, the gravitational force and the positive flow direction, $z^* = z/L_j$, and ρ_m^* is the mixture density normalized by the reference mixture density as listed in Appendices A.4.3.2, A.4.4.2, A.4.5.2, and A.4.6.2. The non-zero scaled elements P_{jk}^* , E_j^* , and I_{ji}^* are initially equal to 1. The nondimensional *Inertia Metric*, S_I is defined by its elements

$$S_{I_{ji}} = \frac{(\Phi_0)_j (I_0)_{ji}}{\sum_{i \in loop_{ref}} (\Phi_0)_{ref} (I_0)_{ref,i}} \quad (\text{no summation in numerator}) \quad (6-62)$$

and displays the *distribution of relative inertia* in the integrated hydraulic system. It is computed from the inertia matrix presented in Figures 5.1 through 5.7. Φ_0 stands for initial or nominal volumetric flow rate. Subscripts j and ref denote, respectively, the j^{th} and main or reference loops. The initial inertia I_0 is evaluated with initial conditions and the LA ratios in Appendix 1.4 according to Eq. (5-24). The elements of the nondimensional *Gravitational Metric*, S_G are defined by

$$S_{G_j} = \frac{\left[(\Delta H_{GR} \beta_T \Delta T_{GR})_0 \right]_j}{(\Delta H_{GR} \beta_T \Delta T_{GR})_{ref}} \quad (6-63)$$

where ΔH_{GR} , β_T , and ΔT_{GR} denote, respectively, the elevation difference of the thermal center, the isobaric thermal expansion coefficient, and the driving temperature difference, all at the initial time, and with subscripts j and ref for the j^{th} and reference loops, respectively. The nondimensional *Gravitational Metric*, S_G , is a vector that gives the *relative distribution of gravitational forces* in the integrated system. The nondimensional *Impedance Metric* has the elements

$$S_{P_{jk}} = \frac{\left(\frac{W_{j,0}}{W_{ref}} \right)^2 (R_0)_{jk}}{\sum_{i \in loop_{ref}} \left(\frac{W_{i,0}}{W_{ref}} \right)^2 R_{ref,i}} \quad (6-64)$$

6. Scaling Groups

and represents *relative distribution of flow resistance forces* in the integrated system. Equation (6-64) is evaluated from the matrices given in Tables 5.8 through 5.14. W stands for mass flow rate, the resistance coefficients are defined by Eq. (5-41), subscript 0 denotes initial value, and subscript *ref* shows association with the reference or main loop.

S_I , S_G , and S_P are the two-, one-, and two-dimensional arrays, respectively, that characterize the distribution of inertia, gravity, and flow resistance (impedance) in a most compact form. The arrays apply to forced and natural circulation modes.

The elements of the **Inertia Metric**, S_I , are governed by the aspect ratios, i.e., the *geometry, of the connecting pipes* in the system (see Appendix 1.4 for aspect ratios).

- (1) Each row of the S_I -matrix is associated with a loop, each column with the primary flow rate of a loop.
- (2) The diagonal S_I -elements show the relative magnitude of the *loop inertia* associated with the loop of the row, if the flows are defined so as to be positive in the positive sense around the loop, and if none of the primary flows is a plenum branch exit flow.
- (3) The magnitude of the off-diagonal S_I -elements are a measure of the *cross-coupling between the loops by inertia*.
- (4) The element-by-element multiplication of the S_I and I^* matrices provide the time-dependent normalized inertia matrix with all the properties described in Items (1) through (3).
- (5) The sum of the S_I -elements in the row of the reference loop add up to one, as a consequence of the scaling (Eq. (6-62)).
- (6) The Inertia Metric reveals how quickly the flow re-adjusts to changes in flow conditions: the larger the S_I -elements of a row are, the slower responds the fluid in the loop associated with that row, and relative to the responses in other loops.

The elements of the **Gravitational Metric**, S_G , are governed by the elevation differences *of the thermal centers* in, i.e., the *geometry* of, the system (see Appendix 1.5 for elevation differences).

- (1) Each row of the S_G column vector is associated with a loop.
- (2) The magnitude of each S_G -element in a row of the column vector shows the importance of gravity effects in the loop associated with that row, relative to the gravity effects in the main or reference loop.
- (3) The element-by-element multiplication of the S_G and G^* vectors provide the time-dependent normalized gravity vector with all the properties described in Items (1) through (3).

The elements of the **Impedance Metric**, S_P , are governed by form losses, i.e., the *geometry, of primarily the connecting pipes* in the system (see Appendix 1.7 for flow resistance factors).

- (1) Each row of the S_P -matrix is associated with a loop, each column with the directed kinetic energy in a segment of the loop. The first N_L columns are associated with the kinetic energy of the primary flows, the remaining columns with those of the secondary flows which are expressed in terms of the primary flows (see Eq. (5-42)).
- (2) The magnitude of the S_P -elements in a row show the *distribution of flow impedances* in the loop associated with the row.
- (3) Repeated S_P -elements in a column indicate *cross-coupling by impedance between the loops* that are associated with the rows containing the repeated S_P -elements.

- (4) The element-by-element multiplication of the S_p and P^* matrices provide the time-dependent normalized impedance matrix with all the properties described in Items (1) through (3).
- (5) The sum of the S_p -elements in the row of the reference loop add up to one, as a consequence of the scaling (Eq. (6-64)).
- (6) The Impedance Metric determines the flow distribution in the system, particularly as the steady state is being approached.

The *scaling arrays* S_i , S_G , and S_p in Eq. (6-56) characterize the *distribution* of inertia, gravity, and flow resistance (impedance). The *scaling groups*, or Π -Groups, in Eq. (6-56), on the other hand, characterize the relation between *global forces* of inertia, gravity, and flow resistance. The ratio of inertia over Reactor Coolant Pump (RCP) forces yields the causative process related scaling group of *system inertia* (or dynamic capacitance) *for forced circulation*

$$\Pi_{IN,P} = \left(\frac{\Phi_{ref}}{t_{ref} \Delta P_{PP}} \right)_0 \sum_{i \in loop_{ref}} \frac{(\Phi_0)_i}{\Phi_{ref}} (I_0)_i. \quad (6-65)$$

Since the *pumping* of the Reactor Coolant Pumps is the causative and dominant phenomenon, $\Pi_{pp} = 1$. The retarding phenomenon is the friction and scaled by the Π -Group of *system impedance*, of flow resistance, i.e., the ratio of frictional pressure drop over pumping pressure rise

$$\Pi_{RS,P} = \frac{W_{ref}^2}{(\rho \Delta P_{PP})_0} \sum_{i \in loop_{ref}} \left(\frac{W_{i,0}}{W_{ref}} \right)^2 R_{ref,i}, \quad (6-66)$$

which is, under steady-state conditions, also of order of unity. The causative process related Π -Group of *system gravity* in Eq. (6-56) for forced circulation is defined, for the case of density change due to thermal expansion or contraction by heating or cooling of single-phase fluid, by

$$\Pi_{GR,P} = \frac{g \Delta H_{GR} (\beta_{TP} \dot{Q}_{1\phi})_0}{W_{ref} (c_p \Delta P_{PP})_0}, \quad (6-67)$$

which is the ratio of gravitational over pumping forces.

6.1.4.2 Natural Circulation

For Phases 2, 3, 4, and 5, gravity drives and dominates the flow. The pumping term is zero and deleted. All terms are compared with the gravity term of the reference loop representing the causative phenomenon, and the causative process related scaling of the momentum balances, Eqs. (5-49) gives, for natural circulation

$$\Pi_{IN,GR} \frac{dM_j^*}{dt^*} = (S_G G^*)_j - \Pi_{RS,GR} (S_P P^*)_{jk} E_k^*, \quad (6-68)$$

where repeated indices imply summation, and the products in subscripted brackets imply element by element multiplication. The scaled *variables* of Eq. (6-68), namely the scaled and time-dependent loop momentum vector element, M_j^* , the scaled and time-dependent gravity force element, G_j^* , the scaled and time-dependent element, P_{jk}^* , of the impedance matrix, the scaled and time-dependent element of the directed kinetic energy vector, E_j^* , and the

6. Scaling Groups

scaled and time-dependent element of the inertia matrix, I_{ji}^* , all are identical to those defined by Eqs. (6-57) through (6-61) for forced convection.

The *scaling arrays* S_i , S_G , and S_p in Eq. (6-68) for natural circulation are also identical to those defined by Eqs. (6-62), (6-63), and (6-64) for forced convection. They characterize the *distribution* of inertia, gravity, and flow resistance (impedance).

The *causative process related scaling groups*, or Π -Groups, in Eq. (6-68) characterize the relation between *global forces* of inertia, gravity, and flow resistance. The ratio of inertia over gravity forces yields the scaling group of *system inertia for natural circulation*

$$\Pi_{IN, GR} = \frac{\Phi_{ref}}{t_{ref} g \Delta H_{GR} (\beta_T \rho \Delta T_0)_0} \sum_{i \in loop_{ref}} \frac{(\Phi_0)_i}{\Phi_{ref}} (I_0)_i, \quad (6-69)$$

where the symbols have the same meaning as for Eqs. (6-62) and (6-63), and where the reference temperature difference is either known directly from initial conditions or computed from the reference heating or cooling power by

$$\Delta T_0 = \frac{\dot{Q}_{1\phi, 0}}{(c_{p,l})_0 W_{ref}}. \quad (6-70)$$

The ratio of flow resistance (impedance) over gravity forces yields the scaling group of *system impedance for natural circulation*

$$\Pi_{RS, GR} = \frac{W_{ref}^2}{g \Delta H_{GR} (\beta_T \rho \Delta T)_0} \sum_{i \in loop_{ref}} \left[\frac{(W_0)_i}{W_{ref}} \right]^2 (R_0)_{ref, i}. \quad (6-71)$$

6.2 Evaluation of Scaling Groups, Ranking and Scale Distortions

This section presents the results of the numerical evaluation of the Π -Groups that were derived and defined in Section 6.1. The numerical evaluation of the Π -Groups was carried out with the specified geometric parameters listed in Appendix 1, the specified initial conditions listed in Appendices 4.1 through 4.6 for Phases 1 through 5, and with the computed reference parameters described in Section 5.5 and evaluated in Appendix 5 of the proprietary database that was transmitted separately to the NRC.

The numerical values of the Π -Groups are arranged in a matrix of Π -Groups that is similar to the one introduced by Wulff [17]. This report has a matrix (or a table) of Π -Groups for each conservation equation and each phase. Each table is explained and interpreted in the section of its presentation, with references to the general interpretations of causative process related and of fractional scaling groups given in Section 4.4.5, and to the identification of relevant processes, as well as of important scale distortions presented in Sections 4.5 and 4.6.

There are two types of matrices presented each for depressurization (mass and energy balances), inventory change (phasic mass balance), and temperature change (phasic energy balance), as it was explained in Section 4.4.5, to give the results from two useful methods of scaling the conservation equations. One method leads to the causative process related scaling groups, as represented in Eq. (4-2), the other to the *fractional* scaling groups as in Eq. (4-3).

The first two columns of the Π -Group tables present the physical definitions and the symbols of the Π -Groups, as introduced either in Section 6.1, or just prior to the table presentation. The *third column* of either type of matrix of Π -Groups shows the numerical values of the Π -Groups for the *AP600 nuclear power plant*. Each third-column entry in the matrix of *causative process related scaling groups* shows the fraction or multiple that the respective process effect has on the AP600, relative to the effect from the causative process. Each third-column entry in the matrix of *fractional scaling groups* shows the extent to which the process associated with the row of the matrix rotates the slope of the time plot, thereby affecting the rate of change, as shown in Figure 4.3.

As explained in Section 4.5, the **vertical scan of the third column reveals**, from the magnitude of its entries, **which phenomena and processes are important** for the AP600. The rows in the Π -Group matrix are ordered such that the AP600 entries in a column end up in the order of decreasing values, with the maximum value at the top. The criteria of relevance adopted for this report were defined in Section 4.5: all phenomena and processes are considered *important* if the associated Π -Group is greater than 1/10 of the largest Π -Group in the equation represented by the table. The values of important Π -Groups are printed in **green**, those of top priority in **bold-faced green**. The *vertical scans* of the fourth, fifth, and sixth columns reveal, also from the magnitude of their entries, which phenomena and processes are important for their respective facilities, namely APEX, ROSA, and SPES, but this matter is not pursued in this report because the focus is on AP600.

The *fourth, fifth, and sixth columns* show the numerical values of the Π -Groups for the AP600-related test facilities APEX, ROSA, and SPES. As explained in Section 4.6, the **horizontal scan of any row with important phenomena reveals**, by comparison of its entries, **which facility is similar or scale-distorted for the important phenomenon or process** associated with the row. Section 4.6 introduced the working definition for scale-distorted: a phenomenon or process is taken to be distorted in a test facility, relative to the same phenomenon or process in the AP600 if the ratio of test facility over AP600 Π -Groups is less than 1/2 or greater than 2. All Π -Groups indicating important scale distortions are printed in **red**.

6.2.1 Phase 1, Initial Depressurization

This section presents the results of the numerical evaluation of the Π -Groups for the initial depressurization phase. See Table 3.1 on Page 3-2 which shows that this phase lasts from the instant at which the break occurs, until the S-Signal is tripped. Presented are the scaling groups for depressurization, system inventory depletion, system temperature change, and flow rates. Flow rate scaling is the same for Subphases 1.1 and 1.2.

No results are presented for the APEX facility, since APEX of Oregon State University did not simulate this phase.

The reference time for this phase is the time it takes to empty the Pressurizer (PRZ), because a low PRZ level can trip the S-Signal. The time is computed according to Eq. (5-50) from

$$t_{ref} = t_{dm} = \frac{(V_{l, PRZ})_0}{(\Phi_{bk})_0}, \quad (6-72)$$

as the quotient of the specified initial liquid volume in the pressurizer over the computed initial break flow. The specified initial liquid volume is listed in the Volume Section of Appendix 1.1. The break flow is computed from the specified break area (specified in Appendix 1.2) and the critical mass flux according to Bestion [22] from Eq. (5-57), with the upstream equilibrium quality being $x_e = (h_0 - h_f)/h_{fg}$. The results for the critical mass flux, critical mass flow rate and critical volumetric flow rate are found in Appendix 4.1. The confirmation of the break mass flow rate is given in Table 5.15.

6. Scaling Groups

6.2.1.1 Phase 1.1, Before Scram

6.2.1.1.1 Depressurization Before Scram

Table 6.1 presents the numerical values of the *causative process related* Π -Groups. They are obtained from the *depressurization equation*, Eq. (6-1), applied to the control volume shown in Figure 5.2 for **Subphase 1.1** (see Figure 3.1 and Section 3.3.1 for the definition of Subphase 1.1). The *causative process related* Π -Groups show the significance of phenomena (system elasticity or system pressure response to volume changes) and processes (external heating and cooling) relative to the causative and dominant process of fluid discharge through the break.

By the methods and criteria described in Sections 4.5 and 4.6, and summarized at the beginning of Section 6.2 on Page 6-22, it is found that (1) the break flow is the dominant process, system elasticity (or mechanical compliance) and phase change are important; and (2) **there are no significant scale distortions** of depressurization during Subphase 1.1. APEX does not simulate this subphase.

Each Π -Group is interpreted in Section 6.1, next to the defining equation as indicated in the first column of Table 6.1. The second column shows the Π -Group symbol, the third through sixth columns list the numerical values of the Π -Groups, and the last column is provided for comments explaining distortions, if any. This table format is retained for all tables of Π -Groups in this report.

All geometric parameters appearing in the Π -Group definitions, Eqs. (6-2) through (6-5) are found in Appendix 1. The initial conditions and initial thermophysical properties are found in Appendix 4.1. The initial system compliance and computed reference parameters appearing in the Π -Group definitions were computed through EXCEL and are listed in Appendix 5.1.

The net initial cooling power applied to the subvolume occupied by single-phase fluid, $(\dot{Q}_{1\phi})_0$ (see Figure 5.1), is the difference between the specified Steam Generator cooling power, minus the core heating power. The difference is equal to the initial pumping power of the Reactor Coolant Pumps. The reference volumetric flow rate, Φ_0 , is the initial break flow rate, and the thermophysical properties β_T , ρ , c_p , v_{fh} , and h_{fg} are evaluated at initial conditions. The net initial heating power applied to the subvolume occupied by two-phase mixture, $(\dot{Q}_{2\phi})_0$, (see Figure 5.1) is the specified full heating power of the Pressurizer, that is turned on to compensate for the loss of pressure.

Table 6.2 presents the numerical values of the *fractional* Π -Groups. They are obtained from the *depressurization equation*, Eq. (6-7), applied to the same control volume as for Table 6.1 above. The *fractional* Π -Groups show the impact that processes (external heating and cooling) have on the time-rate of pressure change. As concluded from the *causative process related* Π -Groups by the methods and criteria described in Sections 4.5 and 4.6, and summarized at the beginning of Section 6.2 on Page 6-22, it is found that (1) the break flow causes the greatest fractional change of pressure, the flow and phase change are important; and (2) **there are no significant scale distortions** of depressurization during Subphase 1.1. APEX does not simulate this subphase.

Each *column* entry in Table 6.2 shows *how much* the tangent of the pressure vs. time curve in Figure 4.3 is rotated from the horizontal by the phenomenon associated with the row of the entry and, consequently, *how important* that phenomenon is during the respective phase. The rotation is downward for those terms in Eq. (6-7) whose signed product of scaled state variable and scaled property function is negative; for a positive product the tangent is turned upward. The larger the entry, the stronger is the effect on the slope of the depressurization equation.

Table 6.1 Causative Process Related Π -Groups for Depressurization During Subphase 1.1

Definition of Π -Group	Symbol of Π -Group	Π -Groups for				Comments
		AP600	APEX	ROSA	SPES	
Break Flow (reference)	Π_{bk}	1	-	1	1	
Elasticity or Mechanical Compliance, (Eq. (6-2))	Π_{MC}	0.59	-	0.63	0.89	
Phase Change (PRZ) (Eq. (6-5))	$\Pi_{\dot{Q}, 2\varphi}$	0.17	-	0.12	0.15	
Thermal Exp. by Pumping (Eq. (6-3))	Π_{PP}	0.04	-	$3 \cdot 10^{-4}$	0.04	
Thermal Exp. by Heating (Eq. (6-4))	$\Pi_{\dot{Q}, 1\varphi}$	0.04	-	$3 \cdot 10^{-4}$	0.04	

Differences between the entries in a row of Table 6.2 would imply differences in the system response, i.e., the fractional change in pressure, due to the phenomenon associated with that row and, consequently, the strength of *scale distortion* for that phenomenon. None of the relevant phenomena (green font) meet the criterion of distortion presented in Section 4.7.

Table 6.2 Fractional Π -Groups for Depressurization During Subphase 1.1

Definition of Π -Group	Symbol of Π -Group	Π -Groups for				Comments
		AP600	APEX	ROSA	SPES	
Break Flow (Eq. (6-13))	$\Pi_{p, bk}$	1.70	-	1.59	1.12	
Phase Change (PRZ) (Eq. (6-11))	$\Pi_{p, \dot{Q}, 2\varphi}$	0.29	-	0.19	0.17	
Thermal Exp. by Pumping (Eq. (6-9))	$\Pi_{p, PP}$	0.07	-	$4 \cdot 10^{-4}$	0.04	
Thermal Exp. by Heating (Eq. (6-10))	$\Pi_{p, \dot{Q}, 1\varphi}$	0.07	-	$4 \cdot 10^{-4}$	0.04	

6.2.1.1.2 Inventory Before Scram

Liquid inventory change is modeled as the compliment of vapor volume change. The model is presented in Section 5.4.1.3, the scaled inventory equation, Eq. (6-14), is scaled by the *causative process* related scaling method and shown in Section 6.1.2.1. The scaling groups are defined in Eqs. (6-3), (6-4), (6-15), and (6-16). Equation (6-14) is applied to the two-phase mixture in the Pressurizer and for Subphase 1.1 (defined in Figure 3.1 and Section 3.3.1).

6. Scaling Groups

Table 6.3 below presents the numerical values of the *causative process related* Π -Groups. The *causative process related* Π -Groups show the significance of phenomena (system volumetric compliance) and processes (external heating and cooling) relative to the process of fluid discharge through the break. By the methods and criteria described in Sections 4.5 and 4.6, and summarized at the beginning of Section 6.2 on Page 6-22, it is found that (1) the causative break flow is the dominant process, volumetric capacity (or volumetric compliance) and break flow make the draining a *transient*; and (2) **there are no significant scale distortions** of inventory depletion during Subphase 1.1 in ROSA and SPES. APEX does not simulate this subphase.

Table 6.3 is read as Table 6.1. The table description is found on Page 6-24. All geometric parameters appearing in the Π -Group definitions, Eqs. (6-3), (6-4), (6-15) and (6-16) are found in Appendix 1. The initial conditions and initial thermophysical properties are found in Appendix 4.1. The initial system compliance and computed reference parameters appearing in the Π -Group definitions were computed through EXCEL and are listed in Appendix 5.1.

Table 6.3 Causative Process Related Π -Groups for Loss of Inventory During Subphase 1.1

Definition of Π -Group	Symbol of Π -Group	Π -Groups for				Comments
		AP600	APEX	ROSA	SPES	
Volumetric Compliance (Eq. (6-15))	Π_{VC}	1.34	-	1.82	1.84	
Break Flow (reference) same as in Table 6.1	Π_{bk}	1	-	1	1	
Phase Change (PRZ) (Eq. (6-16))	$\Pi_{V, \dot{Q}, 2\phi}$	$6 \cdot 10^{-4}$	-	$3 \cdot 10^{-2}$	$3 \cdot 10^{-2}$	
Thermal Exp. by Pumping (Eq. (6-3), same as in Table 6.1)	Π_{PP}	0.04	-	$3 \cdot 10^{-4}$	0.04	
Thermal Exp. by Heating (Eq. (6-4), same as in Table 6.1)	$\Pi_{\dot{Q}, 1\phi}$	0.04	-	$3 \cdot 10^{-4}$	0.04	

As for the depressurization during Subphase 1.1 presented in Section 6.2.1.1, the net initial cooling power applied to the subvolume occupied by single-phase fluid, $(\dot{Q}_{1\phi})_0$ (see Figure 5.1), is the difference between the specified Steam Generator cooling power, minus the core heating power. The reference volumetric flow rate, Φ_0 , is the initial break flow rate, and the thermophysical properties β_T , ρ , c_p , v_{fg} , and h_{fg} are evaluated at initial conditions of Subphase 1.1. The net initial heating power applied to the subvolume occupied by two-phase mixture, $(\dot{Q}_{2\phi})_0$, (see Figure 5.1) is the specified full heating power of the Pressurizer.

Table 6.4 presents the numerical values of the *fractional* Π -Groups. They are obtained from the *vapor mass conservation equation*, Eq. (6.17), applied to the control volume of the two-phase mixture in the Pressurizer, for **Subphase 1.1** (see Figure 3.1 and Section 3.3.1 for the definition of Subphase 1.1). Each *column* entry in Table 6.4 shows the fractional contribution to the *vapor* inventory change by the phenomenon associated with the row of the entry and, consequently, *how important* that phenomenon is during the respective phase. The *fractional* Π -Groups show that (1) break flow has the greatest impact and external heating and cooling have only insignificant effects; and (2) there are **no significant scale distortions** observed from the *fractional* Π -Groups for inventory change during Subphase 1.1. APEX does not simulate this subphase.

Table 6.4 Fractional Π -Groups for Loss of Inventory During Subphase 1.1

Definition of Π -Group	Symbol of Π -Group	Π -Groups for				Comments
		AP600	APEX	ROSA	SPES	
Break Flow (reference) (Eq. (6-21))	$\Pi_{\dot{a}, bk}$	0.75	-	0.55	0.54	
Thermal Exp. by Pumping (Eq. (6-20))	$\Pi_{\dot{a}, PP}$	0.03	-	$2 \cdot 10^{-4}$	0.02	
Thermal Exp. by Heating (Eq. (6-18))	$\Pi_{\dot{a}, \dot{Q}, 1\phi}$	0.03	-	$3 \cdot 10^{-4}$	0.04	
Phase Change (PRZ) (Eq. (6-19))	$\Pi_{\dot{a}, \dot{Q}, 2\phi}$	$5 \cdot 10^{-4}$	-	0.03	0.03	

6.2.1.1.3 System Temperature Before Scram

The temperature change of the liquid in the primary system is modeled in Section 5.4.1.4 on the basis of energy conservation applied to the control volume of the single-phase liquid in the primary system, and for Subphase 1.1 (see Figure 3.1 and Section 3.3.1 for the definition of Subphase 1.1). The scaled temperature equation for change dominated by break flow, Eq. (6-22), is shown in Section 6.1.3.1. The reference temperature difference

$$\Delta T_0 = (T_0)_{ps} - T_{sat}(p_0)_{ss} \quad (6-73)$$

for Phase 1 equals the difference between the initial primary-side mean temperature and the saturation temperature corresponding to the initial pressure on the Steam Generator secondary side.

Table 6.5 below presents the numerical values of the *causative process related* Π -Groups for liquid temperature response. The *causative process related* Π -Groups show the significance of four phenomena (system thermal compliance) and processes (external heating and cooling) relative to the process of fluid energy discharge through the break. Table 6.5 is read in the same way as Table 6.1 and as explained on Page 6-24.

By the methods and criteria described in Sections 4.5 and 4.6, and summarized at the beginning of Section 6.2 on Page 6-22, it is found that (1) net cooling imbalance and mechanical pumping power are the dominant processes for primary system temperature change, break flow is the causative process and phase change effect is still of first-order significance; (2) the primary system temperature responds slowly because of its large heat capacity (or thermal compliance); and (3) **there are three significant scale distortions**, two in ROSA and one in SPES, affecting the change of subcooled liquid temperature during Subphase 1.1. The impact of the scale distortions is assessed on the basis of Table 6.6 below. The Π -Groups in Table 6.5 which reflect scale distortions beyond the $\{1/2, 2\}$ limits established in Section 4.6 are printed in **red** and explained in the comments column of the table. APEX does not simulate Subphase 1.1.

All geometric parameters appearing in the Π -Group definitions, Eqs. (6-23) and (6-26) are found in Appendix 1. The initial conditions and thermophysical properties are found in Appendix 4.1. The initial system thermal compliance and computed reference parameters appearing in the Π -Group definitions were computed through EXCEL and are listed in Appendix 5.1.

6. Scaling Groups

Table 6.5 Causative process related Π -Groups for Change of Subcooled Liquid Temperature During Subphase 1.1

Definition of Π -Group	Symbol of Π -Group	Π -Groups for				Comments
		AP600	APEX	ROSA	SPES	
Thermal Compliance of Subcooled Liquid (Eq. (6-23))	Π_{TC}	18.5	-	24.2	52.1	SPES: Relative low thermal response function Ψ_T
Heating of Single-Phase Liquid (Eq. (6-24))	$\Pi_{T\dot{Q}, 1\phi}$	1.19	-	8.4e-3	1.62	Low SG Cooling in ROSA; only 16% of full-power is rejected.
Thermal Effect of Pumping on Liquid Temperature (Eq. (6-25))	$\Pi_{T, PP}$	1.19	-	8.4e-3	1.62	
Break Flow (reference)	$\Pi_{T, bk}$	1	-	1	1	
Phase Change (PRZ) Effect on Liquid Temperature (Eq. (6-26))	$\Pi_{T\dot{Q}, 2\phi}$	0.24	-	0.20	0.46	

Table 6.6 presents the numerical values of the *fractional* Π -Groups for liquid temperature response. They are obtained, for Subphase 1.1 (see Figure 3.1 and Section 3.3.1 for the definition of Subphase 1.1), from the fractional of the scaled *liquid energy balance*, Eq. (6-48), for the single-phase liquid in the primary system. The *fractional* Π -Groups show the impact that processes (external heating and cooling, break flow, etc.) have on the time-rate of liquid temperature change.

Each *column* entry in Table 6.6 shows *how much* the tangent of the *temperature of the liquid* vs. time curve in Figure 4.3 is rotated from the horizontal by the phenomenon associated with the row of the entry and, consequently, *how important* that phenomenon is to liquid temperature change during the respective phase. The larger the table entry in a column, the stronger is the effect on the rate of change of the liquid temperature and the more important is it to scale the associated process well. Differences between the entries in a *row* of Table 6.6 imply differences in the system response due to the phenomenon associated with that row and, consequently, the strength of *scale distortion* for that phenomenon on liquid coolant temperature change. Important processes are high-lighted in **green**, top priority processes in **bold face**, and important scale distortions in **red**.

By the methods and criteria described in Sections 4.5 and 4.6, and summarized at the beginning of Section 6.2 on Page 6-22, it is found from the *fractional scaling groups* that (1) all fractional scaling groups are consistently small and indicate a slow, or a small fractional, liquid subcooling temperature change; net cooling, break flow, and pumping power are the leading transfer processes for the small temperature change, phase change due to depressurization during Subphase 1.1 has the smallest effect on liquid temperature change; and (2) **two and one** of the leading transfer processes are *nonconservatively distorted* in ROSA and SPES, respectively, but the distortion is small because the expected fractional subcooling temperature change in AP600 is small. APEX does not simulate Subphase 1.1.

Table 6.6 Fractional Π -Groups for Change of Subcooled Liquid Temperature During Subphase 1.1

Definition of Π -Group	Symbol of Π -Group	Π -Groups for				Comments
		AP600	APEX	ROSA	SPES	
Heating of Single-Phase Liquid (Eq. (6-51))	$\Pi_{T, \dot{Q}, 1\phi}$	6.5e-2	-	3.5e-4	3.1e-2	Low SG Cooling in ROSA; only 16% of full-power is rejected.
Thermal Effect of Pumping (Eq. (6-48))	$\Pi_{T, PP}$	6.5e-2	-	3.5e-4	3.1e-2	
Break Flow Effect on Liquid Temperature (Eq. (6-49))	$\Pi_{T, bk}$	5.4e-2	-	4.1e-2	1.9e-2	SPES: Relative low thermal response function Ψ_T
Phase Change (PRZ) Effect on Liquid Temperature (Eq. (6-52))	$\Pi_{T, \dot{Q}, 2\phi}$	1.3e-2	-	8.3e-3	8.8e-3	

6.2.1.1.4 Flow Rates, Inertia, and Impedance for Phase 1

The dynamic interaction between system components takes place in the connecting pipes and is modeled with the system momentum balance. The system momentum balance is the vector equation, Eq. (5-49), that is derived in Section 5.4.2 as the set of loop momentum balances which provide, via the loop momenta, M_j , the volumetric flow rates, Φ_m , according to the linear algebraic equations, Eqs. (5-36). The scaling of Eq. (5-49) leads to the scaled momentum balance for forced circulation in Phase 1, Eq. (6-56). The Π -Groups of that equation are defined in Eqs. (6-65) through (6-67) and scale the *global system response*. The transient splits and distribution of flows among the components are scaled by the three metrics, or *scaling arrays* S_I , S_G , and S_P in Eq. (6-56) characterizing, respectively, the *distribution* of inertia, gravity, and flow resistance (impedance). S_I , S_G , and S_P are conceptually introduced in Section 4.4.6 and defined in Eqs. (6-62), (6-63), and (6-64).

The specified core flow and the initial pressure rise in the Reactor Coolant Pumps are the reference parameters needed to evaluate Eqs. (6-62) through (6-67); symmetry is used to determine the reference flows in the two and four loops, respectively, of ROSA and of AP600 and SPES. The reference values are listed in Appendix 5.1.

Table 6.7 presents the numerical values of the causative process related Π -Groups of dynamic component interaction and shows that pumping from Reactor Coolant Pumps is the causative process and balances the system flow resistance (impedance); pumping and impedance are the only important transport phenomena. The extremely small inertia scaling group (representing dynamical capacitance) indicates small inertia forces and rapid flow adjustments in AP600 and even *much more rapid* adjustment in ROSA and SPES. By the criteria described in Sections 4.5 and 4.6, and summarized at the beginning of Section 6.2 on Page 6-22, it is found from the causative process related scaling groups that the inertia forces are insignificant and there are no significant scale distortions of global forces during Subphase 1.1. APEX does not simulate this subphase.

Table 6.8 By dividing the Π -Groups in the first three rows of Table 6.7, i.e., the scaling groups for pump, impedance, and gravity effects, through the Π -Groups for inertia shown in the last row of Table 6.7, one finds the *fractional* Π -Groups shown in Table 6.8. As a result of the small inertia Π -Groups in Table 6.7, one obtains very large Π -Groups reflecting very large rates of flow change (accelerations).

6. Scaling Groups

Table 6.8 shows that the flow rates in the system adjusts very quickly to any changes in RCP pressure rise or to impedance change, such as changes in valve settings. Table 6.8 shows also that the **dynamic response in the test facilities is distorted** by three and four orders of magnitude, respectively in ROSA and SPES. The global distortion is *conservative* because the faster response decelerates the flow faster and leads sooner to the loss of subcooling temperature.

Table 6.7 Causative Process Related Π -Groups of Dynamic Interaction Between Components During Phase 1

Definition of Π -Group	Symbol of Π -Group	Π -Groups for				Comments
		AP600	APEX	ROSA	SPES	
RCP Pumping (reference)	$\Pi_{PP,P}$	1	-	1	1	
System Impedance (Eq. (6-66))	$\Pi_{RS,P}$	0.99	-	0.96	1.00	
System Gravity (Eq. (6-67))	$\Pi_{G,P}$	0.02	-	0.07	0.02	
System Inertia (Eq. (6-65))	$\Pi_{IN,P}$	0.002	-	$2 \cdot 10^{-6}$	$3 \cdot 10^{-7}$	

Table 6.8 Fractional Π -Groups of Dynamic Interaction Between Components During Phase 1

Definition of Π -Group	Symbol of Π -Group	Π -Groups for				Comments
		AP600	APEX	ROSA	SPES	
RCP Pumping	$\Pi_{\dot{W}PP,P}$	556	-	$5 \cdot 10^5$	$4 \cdot 10^6$	low inertia in ROSA and SPES
System Impedance (Eq. (6-66))	$\Pi_{\dot{W}RS,P}$	552	-	$5 \cdot 10^5$	$4 \cdot 10^6$	low inertia in ROSA and SPES
System Gravity (Eq. (6-67))	$\Pi_{\dot{W}G,P}$	9.1	-	$3 \cdot 10^4$	$8 \cdot 10^4$	low inertia in ROSA and SPES

The Inertia Metric, S_i , is defined in Eq. (6-62) and obtained by applying that definition to the entries of Tables 5.2 through 5.5. As explained in section 6.1.4.1, the diagonal S_i -elements (**bold numbers**) show the relative magnitude of the *loop inertia* associated with the loop of the row. See Section 6.1.4.1. for the interpretation of the Inertia Metric. The Inertia Metric reveals how quickly the flow re-adjusts in a loop segment to changes in flow conditions (pressure, or setting of valves, etc. and conditions in parallel loops, such as the occurrence of a break): the larger the S_i -elements of a row are, the slower responds the fluid in the loop associated with that row, and relative to the responses in other loops.

Tables 6.9 through 6.12 show that SPES has 20% stronger cross coupling between the loops of the same plant side (**blue numbers**) than AP600, ROSA and SPES have twice the cross-coupling between loops of the opposite side (**magenta numbers**). The inertia distribution of APEX matches the distribution of AP600. The facilities' systems response is so fast, however, that the S_i distortions during Phase 1 will not affect minimum core coolant inventory and subcooling temperature.

Table 6.9 Inertia Metric for Four-Loop Operation: AP600
under Normal Conditions and Phase 1, Initial Depressurization (-)

Loop		Flow Rate leaving from			
on Side	through	SG Exit of Loop _{B1}	SG Exit of Loop _{B2}	SG Exit of Loop _{A1}	SG Exit of Loop _{A2}
B	Cold Leg 1	0.575	0.341	0.042	0.042
B	Cold Leg 2	0.341	0.575	0.042	0.042
A	Cold Leg 1	0.042	0.042	0.575	0.341
A	Cold Leg 2	0.042	0.042	0.341	0.575

Table 6.10 Inertia Metric for Four-Loop Operation: APEX
under Normal Conditions and Phase 1, Initial Depressurization (-)

Loop		Flow Rate leaving from			
on Side	through	SG Exit of Loop _{B1}	SG Exit of Loop _{B2}	SG Exit of Loop _{A1}	SG Exit of Loop _{A2}
B	Cold Leg 1	0.580	0.347	0.036	0.036
B	Cold Leg 2	0.347	0.580	0.036	0.036
A	Cold Leg 1	0.036	0.036	0.580	0.347
A	Cold Leg 2	0.036	0.036	0.347	0.580

Table 6.11 Inertia Metric for Four-Loop Operation: SPES
under Normal Conditions and Phase 1, Initial Depressurization (-)

Loop		Flow Rate leaving from			
on Side	through	SG Exit of Loop _{B1}	SG Exit of Loop _{B2}	SG Exit of Loop _{A1}	SG Exit of Loop _{A2}
B	Cold Leg 1	0.452	0.406	0.071	0.071
B	Cold Leg 2	0.406	0.452	0.071	0.071
A	Cold Leg 1	0.071	0.071	0.452	0.406
A	Cold Leg 2	0.071	0.071	0.406	0.452

6. Scaling Groups

Table 6.12 Inertia Metric for Two-Loop Operation of ROSA
under Normal Conditions and Phase 1, Initial Depressurization.

Loop		Flow Rate leaving from	
on Side	through	SG Exit of Loop _B	SG Exit of Loop _A
B	Cold Leg B	0.924	0.076
A	Cold Leg A	0.076	0.924

The Gravity Metric, S_G , defined by Eq. (6-31) has, for Phase 1, all elements equal to 1 because at the start of Phase 1 all loops are symmetric with regard to heating in the Core and cooling in the Steam Generators.

The Impedance Metric, S_p , is defined in Eq. (6-64) and obtained by applying that definition to the entries of Tables 5.9 through 5.12. Tables (6.13) through (6.16) present the numerical values of the impedance metric (scaled impedance matrix) for AP600, APEX, ROSA, and SPES, respectively.

As explained in Section 6.1.4.1, the S_p -elements in a row determine the *distribution of flow impedances* in the loop associated with that row, and, therefore, the flow distribution particularly as the steady state is being approached. Repeated S_p -elements in a column indicate *cross-coupling by impedance between the loops* that are associated with the rows containing the repeated S_p -elements. However, the the first two columns in Tables (6.13) through (6.16) have the same values because of loop symmetry. **Red** entries in Tables 6.14 and 6.16 indicate scale distortions of impedance distribution in APEX and ROSA, respectively (elements differ from corresponding elements in the APEX table, Table 6.13, by more than the factor of 2). Notice that the S_p -elements in the row of every loop add up to one, as a consequence of the scaling according to Eq. (6-64) and of the symmetry among the four loops.

Table 6.13 Impedance Metric for Four-Loop Operation of AP600, Phase 1.

Loop		Scaled Resistance Coefficients of Loop Sections between Branch Points:		
on Side	through	RPV to Exit of SG 1 - 5	SG Exit to RPV	Interior of RPV
B	Cold Leg 1	0.561	0.026	0.413
B	Cold Leg 2	0.561	0.026	0.413
A	Cold Leg 1	0.561	0.026	0.413
A	Cold Leg 2	0.561	0.026	0.413

Table 6.14 Impedance Metric for Four-Loop Operation of APEX, Phase 1.

Loop		Scaled Resistance Coefficients of Loop Sections between Branch Points:		
on Side	through	RPV to Exit of SG 1 - 5	SG Exit to RPV	Interior of RPV
B	Cold Leg 1	0.567	0.172	0.262
B	Cold Leg 2	0.567	0.172	0.262
A	Cold Leg 1	0.567	0.172	0.262
A	Cold Leg 2	0.567	0.172	0.262

Table 6.15 Impedance Metric for Four-Loop Operation of SPES, Phase 1.

Loop		Scaled Resistance Coefficients of Loop Sections between Branch Points:		
on Side	through	RPV to Exit of SG 1 - 5	SG Exit to RPV	Interior of RPV
B	Cold Leg 1	0.653	0.040	0.306
B	Cold Leg 2	0.653	0.040	0.306
A	Cold Leg 1	0.653	0.040	0.306
A	Cold Leg 2	0.653	0.040	0.306

The Impedance Metric for the two-loop system of ROSA was developed by the same method as those for AP600, APEX, and SPES, but from the entries of Table 5.12.

It was pointed out in Section 5.4.2.4 that the element-by-element comparison of the unscaled impedance matrices in Tables 5.9 through 5.12 for AP600, APEX, ROSA, and SPES shows order of magnitude differences. These differences do not necessarily reflect scale distortions. Instead, what is important are the Π_{RS} -Groups in Table 6.7 and the Impedance Metrics in Tables 6.13 through 6.16. It is neither necessary nor sufficient to match ratios of resistance coefficients locally, prototype over test facility.

Table 6.7 shows that there is no *global* impedance distortion in ROSA and SPES, but there is *local impedance distortion in ROSA* because there is relatively twice as much impedance in the reactor vessel of ROSA as in AP600,

6. Scaling Groups

which encourages the coolant in ROSA to bypass the vessel. The distortion of impedance in ROSA is conservative because it may decrease the coolant inventory and subcooling temperature in later phases.

Table 6.16 Impedance Metric for Two-Loop Operation of ROSA, Phase 1.

Loop		Scaled Resistance Coefficients of Loop Sections between Branch Points:	
on Side	through	Hot-Leg Entrance to Cold-Leg Exit	Interior of RPV
B	Cold Leg	0.074	0.926
A	Cold Leg	0.074	0.926

6.2.1.2 Phase 1.2, After Scram

Subphase 1.2 begins with the scram signal and ends with the S-Signal. The subphase is characterized by sudden net cooling due to reactor scram while the Steam Generators are still at full-power cooling. The coolant shrinking occurs in addition to break discharge, and depressurization accelerates. The turbines are tripped but the reactor coolant pumps are running.

6.2.1.2.1 Depressurization After Scram

Table 6.17 presents the numerical values of the *causative process related* Π -Groups for depressurization during Subphase 1.2. They are obtained from the scaled *depressurization equation*, Eq. (6-1), applied to the control volume shown in Figure 5.2 for Phase 1 (both subphases; see Figure 3.1 and Section 3.3.1 for the definition of Subphase 1.2). The *causative process related* Π -Groups show the significance of phenomena (system elasticity or system pressure response to volume changes) and processes (external heating and cooling) relative to the process of fluid discharge through the break.

Table 6.17 is read as explained on Page 6-24: each Π -Group is interpreted in Section 6.1 next to the equation that defines it, and the defining equation is indicated in the first column of Table 6.17. The second column shows the Π -Group symbol used in the scaled equation, the third through sixth columns list the numerical values of the Π -Groups, and the last column is provided for comments explaining distortions, if any.

By the methods and criteria described in Sections 4.5 and 4.6, and summarized at the beginning of Section 6.2 on Page 6-22, it is found that (1) the cooling in the Steam Generator is the dominant process (at least at the beginning of the subphase), the break flow is taken as the causative process, system elasticity (or mechanical compliance) is important; and (2) **there is one significant scale distortions** of depressurization during Subphase 1.2. in ROSA, because its starting power is only 16 % of the scaled-down value corresponding to its system volume. The distortion in ROSA is *conservative*. APEX does not simulate this subphase.

All geometric parameters appearing in the Π -Group definitions, Eqs. (6-2) through (6-5) are found in Appendix 1. The initial conditions and initial thermophysical properties are found in Appendix 4.2. The initial system mechanical

compliance and computed reference parameters appearing in the Π -Group definitions were computed through EXCEL and are listed in Appendix 5.1.

The net initial cooling power applied to the subvolume occupied by single-phase fluid, $(\dot{Q}_{1\phi})_0$ (see Figure 5.1), is the specified Steam Generator nominal cooling power. The reference volumetric flow rate, Φ_0 , is the initial break flow rate, and the thermophysical properties β_T , ρ , c_p , v_{fg} , and h_{fg} are evaluated at initial conditions of Subphase 1.1. The net initial heating power applied to the subvolume occupied by two-phase mixture, $(\dot{Q}_{2\phi})_0$, (see Figure 5.1) is the specified full heating power of the Pressurizer, that is still turned on to compensate for the loss of pressure.

Table 6.17 Causative Process Related Π -Groups for Depressurization During Subphase 1.2

Definition of Π -Group	Symbol of Π -Group	Π -Groups for				Comments
		AP600	APEX	ROSA	SPES	
Thermal Contr. by Cooling (Eq. (6-4))	$\Pi_{\dot{Q}, 1\phi}$	11.1	-	1.77	12.3	Reduced SG cooling in ROSA
Break Flow (reference)	Π_{bk}	1	-	1	1	
Mechanical Compliance (Eq. (6-2))	Π_{MC}	0.74	-	0.83	1.15	
Phase Change (PRZ) (Eq. (6-5))	$\Pi_{\dot{Q}, 2\phi}$	0.20	-	0.14	0.18	
Thermal Exp. by Pumping (Eq. (6-3))	Π_{PP}	0.04	-	$3 \cdot 10^{-4}$	0.04	

Table 6.18 presents the numerical values of the *fractional* Π -Groups (see Eq. (6-7)), for depressurization during Subphase 1.2 (see Figure 3.1 and Section 3.3.1 for the definition of Subphase 1.2). The *fractional* Π -Groups show the impact that transfer processes (external heating and cooling) have on the time-rate of pressure change. As concluded from the *causative process related* Π -Groups in Table 6.17, there is **one significant but conservative scale distortion** observed for ROSA from the *fractional* Π -Groups for Subphase 1.2, whereby “significant” is defined in Section 4.6. The distortion is conservative because ROSA will discharge ADS-123 flows at higher pressure and lower subcooling than AP600, due to less cooling in the Steam Generators. APEX does not simulate this subphase.

Each *column* entry in Table 6.18 shows *how much* the tangent of the pressure vs. time curve in Figure 4.3 is rotated from the horizontal by the phenomenon associated with the row of the entry and, consequently, *how important* that phenomenon is during the respective phase. The net cooling with attendant liquid shrinking dominates the depressurization. Differences between the entries in a *row* of Table 6.18 imply differences in the system response due to the phenomenon associated with that row and, consequently, the strength of *scale distortion* for that phenomenon.

6. Scaling Groups

Table 6.18 Fractional Π -Groups for Depressurization During Subphase 1.2

Definition of Π -Group	Symbol of Π -Group	Π -Groups for				Comments
		AP600	APEX	ROSA	SPES	
Thermal Contr. by Cooling (Eq. (6-10))	$\Pi_{p, \dot{Q}, 1\phi}$	14.96	-	2.15	10.69	Low SG Cooling. Only 16% of full power is rejected
Break Flow (Eq. (6-13))	$\Pi_{p, bk}$	1.35	-	1.21	0.87	
Phase Change (PRZ) (Eq. (6-11))	$\Pi_{p, \dot{Q}, 2\phi}$	0.27	-	0.17	0.15	
Thermal Exp. by Pumping (Eq. (6-9))	$\Pi_{p, PP}$	0.06	-	$3 \cdot 10^{-4}$	0.03	

6.2.1.2.2 Inventory After Scram

The change of liquid inventory is modeled as the compliment of vapor volume change. The model is presented in Section 5.4.1.3, the scaled inventory equation, Eq. (6-14), is shown in Section 6.1.2.1. As for the depressurization during Subphase 1.2 presented in Section 6.2.1.2.1, the net initial net cooling power applied to the subvolume occupied by single-phase fluid, $(\dot{Q}_{1\phi})_0$ (see Figure 5.1), is the specified Steam Generator cooling power. The reference volumetric flow rate, Φ_0 , is the initial break flow rate, and the thermophysical properties β_T , ρ , c_p , v_{fg} , and h_{fg} are evaluated at initial conditions of Subphase 1.2. The initial heating power supplied to the subvolume occupied by two-phase mixture, $(\dot{Q}_{2\phi})_0$, (see Figure 5.1) is the specified full heating power of the Pressurizer. Initial values are listed in Appendix 4.2.2 of the accompanying data base.

Table 6.19 below presents the numerical values of the *causative process related* Π -Groups. They are obtained from the *vapor mass conservation equation*, Eq. (6-14), scaled by the causative process related method and applied to the control volume of the two-phase mixture in the system for Subphase 1.2 (see Figure 3.1 and Section 3.3.1 for the definition of Subphase 1.2). The *causative process related* Π -Groups show the significance of phenomena (system volumetric compliance) and processes (external heating and cooling) relative to the causative process of fluid discharge through the break.

Table 6.19 is to be read as explained on Page 6-24 for Table 6.1. All geometric parameters appearing in the Π -Group definitions, Eqs. (6-15) and (6-16) are found in Appendix 1. The initial conditions and initial thermophysical properties are found in Appendix 4.2. The initial system compliance and computed reference parameters appearing in the Π -Group definitions were computed through EXCEL and are listed in Appendix 5.1.

By the methods and criteria described in Sections 4.5 and 4.6, and summarized at the beginning of Section 6.2 on Page 6-22, it is found that (1) thermal contraction is (at least initially and temporarily) the dominant process, break flow and system volumetric capacity (or volumetric compliance) are important; and (2) there is **one significant scale distortion** of inventory depletion during Subphase 1.2 observed for ROSA. The same low SG cooling in ROSA that produced the conservative distortion in system depressurization, produces nonconservative scale distortion by retarding inventory loss in ROSA. Both distortions cancel. This can be recognized by considering the rate of inventory over pressure losses. APEX does not simulate this subphase.

Table 6.19 Causative Process Related Π -Groups for Loss of Inventory During Subphase 1.2

Definition of Π -Group	Symbol of Π -Group	Π -Groups for				Comments
		AP600	APEX	ROSA	SPES	
Thermal Contr. by SG Cooling (Eq. (6-4), same as in Table 6.1)	$\Pi_{\dot{Q}, 1\phi}$	11.1	-	1.77	12.3	Low Cooling Power in SG of ROSA
Volumetric Compliance (Eq. (6-15))	Π_{VC}	1.43	-	1.60	1.62	
Break Flow (reference)	Π_{bk}	1	-	1	1	
Thermal Exp. by Pumping (Eq. (6-3), same as in Table 6.1)	Π_{PP}	0.03	-	2.0e-4	0.02	
Phase Change (PRZ) (Eq. (6-16))	$\Pi_{V, \dot{Q}, 2\phi}$	1.2e-3	-	3.6e-3	2.4e-3	

Table 6.20 presents the numerical values of the *fractional* Π -Groups for inventory drainage during Subphase 1.2, as they appear in the scaled *vapor mass conservation equation*, Eq. (6-17) (see Figure 3.1 and Section 3.3.1 for the definition of Subphase 1.1). The *fractional* Π -Groups show the impact that transfer processes (e.g., external heating and cooling) have on the time-rate of inventory change. Each *column* entry in Table 6.20 shows *how much* the tangent of the normalized *liquid* inventory vs. normalized time curve in Figure 4.3 is rotated from the horizontal by the phenomenon associated with the row of the entry and, consequently, *how important* that phenomenon is during Phase 1.2. Differences between the entries in a *row* of Table 6.20 imply *scale distortion* of the phenomenon associated with that row, for liquid draining.

Table 6.20 Fractional Π -Groups for Loss of Inventory During Subphase 1.2

Definition of Π -Group	Symbol of Π -Group	Π -Groups for				Comments
		AP600	APEX	ROSA	SPES	
Thermal Contr. by SG Cooling (Eq. (6-18))	$\Pi_{\dot{a}, \dot{Q}, 1\phi}$	7.75	-	1.11	7.62	Low Cooling Power in SG of ROSA
Break Flow (reference) (Eq. (6-21))	$\Pi_{\dot{a}, bk}$	0.70	-	0.62	0.62	
Thermal Exp. by Pumping (Eq. (6-20))	$\Pi_{\dot{a}, PP}$	0.02	-	2·10 ⁻⁴	0.01	
Phase Change (PRZ) (Eq. (6-19))	$\Pi_{\dot{a}, \dot{Q}, 2\phi}$	8·10 ⁻⁴	-	2·10 ⁻³	2·10 ⁻³	

By the methods and criteria described in Sections 4.5 and 4.6, and summarized at the beginning of Section 6.2 on Page 6-22, it is found from the fractional scaling method that (1) the loss of liquid *volume* in AP600 and SPES due to

6. Scaling Groups

thermal shrinking is (at least initially) ten times greater than the loss due to the break flow, and SG cooling dominates; and (2) as concluded from the *causative process related* Π -Groups in Table 6.19, there is also **one significant scale distortion for ROSA** observed from the *fractional* Π -Groups for inventory change during Subphase 1.2. However, the effect of this distortion in ROSA is canceled by the related distortion of depressurization. APEX does not simulate this subphase.

6.2.1.2.3 System Temperature After Scram

The temperature change of the liquid in the primary system is modeled in Section 5.4.1.4 on the basis of energy conservation which is applied to the control volume of the single-phase liquid in the primary system (see Figures 5.2 and 5.5), and for Subphase 1.2 (see Figure 3.1 and Section 3.3.1 for the definition of Subphase 1.2). The scaled temperature equation for change dominated by heat transfer, Eq. (6-27), is shown in Section 6.1.3.1. The reference temperature difference, ΔT_0 , is taken to be the same as for Subphase 1.1 and given by Eq. (6-73).

Table 6.21 below presents the numerical values of the *causative process related* Π -Groups for liquid temperature response during Subphase 1.2. The *causative process related* Π -Groups show the significance of phenomena (system thermal compliance) and processes (break flow, phase change, etc.) relative to the Steam Generator cooling power.

Table 6.21 is read as described on Page 6-24 for Table 6.1. All geometric parameters appearing in the Π -Group definitions, Eqs. (6-28) through (6-31) for Table 6.21 are found in Appendix 1. The initial conditions and initial thermophysical properties are found in Appendix 4.2. The initial system compliance and computed reference parameters appearing in the Π -Group definitions were computed through EXCEL and are listed in Appendix 5.1.

Table 6.21 Causative Process Related Π -Groups for Change of Subcooled Liquid Temperature During Subphase 1.2

Definition of Π -Group	Symbol of Π -Group	Π -Groups for				Comments
		AP600	APEX	ROSA	SPES	
Cooling of Single-Phase Liquid (reference)	$\Pi_{TQ, 1\phi}$	1	-	1	1	
Thermal Compliance of Subcooled Liquid (Eq. (6-28))	Π_{TC}	0.06	-	0.44	0.09	Low Cooling Power in SG of ROSA, relative to heat capacity.
Thermal Effect of Pumping on Liquid Temperature (Eq. (6-30))	$\Pi_{T, PP}$	$3.9 \cdot 10^{-3}$	-	$1.5 \cdot 10^{-4}$	2.810^{-3}	
Break Flow (Eq. (6-29))	$\Pi_{T, bk}$	$2.3 \cdot 10^{-3}$		$1.4 \cdot 10^{-2}$	$1.8 \cdot 10^{-3}$	
Phase Change (PRZ) Effect on Liquid Temperature (Eq. (6-31))	$\Pi_{TQ, 2\phi}$	$7.2 \cdot 10^{-4}$	-	$1.1 \cdot 10^{-2}$	$6.9 \cdot 10^{-4}$	

6. Scaling Groups

By the methods and criteria described in Sections 4.5 and 4.6, and summarized at the beginning of Section 6.2 on Page 6-22, it is found from the causative process-related scaling groups that (1) the Steam Generator cooling is the dominant process for liquid temperature change, system thermal capacity (or thermal compliance) is small to produce a fast temperature change; and (2) there is **one significant scale distortions** affecting the change of subcooled liquid temperature in ROSA during Subphase 1.2: the low starting power of causes the cooling power of the Steam Generators to be disproportionately small compared to the heat capacity of the liquid. The distortion is conservative, because the liquid temperature in ROSA remains higher than in AP600. APEX does not simulate Subphase 1.2.

Table 6.22 presents the numerical values of the *fractional* Π -Groups for liquid temperature response. They are obtained from the *liquid energy balance*, Eq. (6-48) scaled by the fractional scaling method (Section 4.4.5.2) for the single-phase liquid in the primary system, and evaluated for Subphase 1.2 (see Figure 3.1 and Section 3.3.1 for the definition of Subphase 1.2). The *fractional* Π -Groups in a *column* of Table 6.22 show the fractional changes that the external transfer processes have on the total liquid temperature change and, consequently, *how important* that phenomenon is to liquid temperature change during Subphase 1.2. Differences between the entries in a *row* of Table 6.22 imply differences in the temperature response due to the phenomenon associated with that row and, consequently, the strength of *scale distortion* for that phenomenon on liquid coolant temperature. The low starting power of ROSA distorts the liquid temperature response in ROSA by retarding the temperature drop.

The *fractional* Π -Groups for AP600 in Table 6-22 show that (1) the imbalance between Steam Generator cooling and heating by decay heat during Subphase 1.2 has the largest impact on the temperature drop of the liquid; and (2) as already concluded from the *causative process related* Π -Groups in Table 6.21, there is only **one significant scale distortion** observed from the *fractional* Π -Groups in Table 6.22 (red printing) for liquid temperature change in ROSA during Subphase 1.2. The fractional temperature drop of the liquid in the primary system of ROSA is less than in AP600. The scaling distortion is conservative, because the liquid temperature in ROSA remains higher than in AP600.

Table 6.22 Fractional Π -Groups for Change of Subcooled Liquid Temperature During Subphase 1.2

Definition of Π -Group	Symbol of Π -Group	Π -Groups for				Comments
		AP600	APEX	ROSA	SPES	
Cooling of Single-Phase Liquid (Eq. (6-51))	$\Pi_{T, \dot{Q}, 1\phi}$	16.83	-	2.26	11.06	Low SG Cooling in ROSA; only 16% of full-power is rejected.
Thermal Effect of Pumping (Eq. (6-48))	$\Pi_{T, PP}$	0.065	-	4e-4	0.031	
Break Flow Effect on Liquid Temperature (Eq. (6-49))	$\Pi_{T, bk}$	0.038	-	0.031	0.020	
Phase Change (PRZ) Effect on Liquid Temperature (Eq. (6-52))	$\Pi_{T, \dot{Q}, 2\phi}$	0.012	-	0.026	0.008	

In summary, Phase 1 reveals only one scale distortion in ROSA, i.e., its disproportionate initial power. The single scale distortion affects the rates of depressurization, inventory draining, and coolant temperature drop. The effects on inventory from the first two appear to cancel, while the last one is conservative with respect to liquid subcooling temperature.

6. Scaling Groups

6.2.2 Phase 2, Natural Circulation and Passive Decay Heat Removal

This section presents the results of the numerical evaluation of the Π -Groups for the phase of natural circulation through the Core Make-up Tanks (CMT) and passive heat removal through the Passive Residual Heat Rejection (PRHR) system. See Table 3.1 on Page 3-2 which shows that this phase lasts from the instant at which the S-Signal is tripped at the specified trip set point pressure of 12.8 MPa (128 bar, 1850 psig) [19] until it ends when the collapsed liquid level in at least one of the CMTs reaches the designer-specified 67%-volume mark, which trips the automatic depressurization. Presented are the scaling groups for depressurization, system inventory depletion, system temperature change, and flow rates. The APEX facility of Oregon State University is included in the evaluation for Phases 2 through 5, since these phases were simulated in APEX. It should be recalled that the AP600 scaling analysis is evaluated for OSU for the 1-inch Cold-Leg Break Test SB05 (see Section 1.2).

The S-Signal shuts off the Reactor Coolant Pumps; the corresponding term is deleted and $\Pi_{pp} = 0$. As shown in Figure 3.1, the Steam Generators (SG) act as a heat sink in Subphase 2.1 and as a heat source in Subphase 2.2. Therefore two Π -Groups are evaluated for each facility. The SG-heat transfer is computed with phase change on the primary side, but with the difference between initial Hot-Leg and secondary-side saturation temperatures as the driving temperature difference for Subphase 2.1, while for Subphase 2.2 the driving temperature difference was taken as the difference between the saturation temperature at the cross-over pressure, shown as the intersect of primary (red) and secondary-side (blue) pressure curves in Figure 3.1, and the saturation temperature at the Accumulator trip set point pressure.

The cross-over pressure, p_c , is computed by integrating simultaneously the depressurization equations for the primary and secondary sides, by solving for the time at which the difference, δp , between the primary- and secondary-side pressures is zero, and by evaluating either pressure for that time. The Steam Generator is closed up, feedwater and steam lines are closed, and the Steam Generator undergoes isochoric heating at first, then isochoric cooling, with the pressure passing through a maximum. The integration is carried out with constants of unity approximating the scaled property functions, the scaled decay heat, and the scaled break flow. The depressurization equations are obtained from Eq. (6-7), written in fractional form (see Section 4.4.5.2) specifically for the primary and secondary sides:

$$\chi_{V_{ps}} \dot{p}_{ps}^* = \Pi_{p, \dot{Q}_{1\phi}} \left(\frac{\beta_T}{\rho c_p} \right)^* \dot{Q}_{1\phi}^* - \Pi_{p, bk} \Phi_{bk}^* + \Pi_{p, \dot{Q}_{2\phi}} \left(\frac{v_{fg}}{h_{fg}} \right)^* \dot{Q}_{2\phi}^* \quad (6-74)$$

$$\chi_{V_{SG}} \dot{p}_{SG}^* = - \Pi_{p, SG} \dot{Q}_{2\phi}^*, \quad (6-75)$$

where

$$\dot{Q}_{2\phi}^* = \bar{h}_c^* \left(\frac{v_{fg}}{h_{fg}} T \right)^* (\dot{p}_{ps}^* - \dot{p}_{SG}^*). \quad (6-76)$$

The Π -Groups in Eq. (6-74) are defined in Section 6.1.1.2. The *Steam Generator depressurization* is scaled by the product, $\Pi_{p, SG}$, of the primary-system reference time, times the secondary-side response frequency.

$$\Pi_{p, SG} = \frac{1}{\Pi_{MC, SG}} = t_{ref} \frac{A_w (h_{cnv})_0}{M c_p + \left(\chi_{V_{SG}} \frac{h_{fg}}{T v_{fg}} \right)_0}. \quad (6-77)$$

Equations (6-74) and (6-75) are combined into a single differential equation for the time rate of change of the pressure difference ($p_{ps}^* - p_{SG}^*) = \delta p^*$. The integral of that differential equation is

$$\delta p^* = \left(\delta p_0^* + \frac{\Pi_{p, \dot{Q}1\phi} + \Pi_{p, bk}}{\Pi_{p, \dot{Q}2\phi} + \Pi_{p, SG}} \right) e^{-(\Pi_{p, \dot{Q}2\phi} + \Pi_{p, SG})t^*} - \frac{\Pi_{p, \dot{Q}1\phi} + \Pi_{p, bk}}{\Pi_{p, \dot{Q}2\phi} + \Pi_{p, SG}} \quad (6-78)$$

Equation (6-78) is solved for the time t_i^* that it takes for δp^* to become 0. That time is used to find the cross-over pressure, p_i^* , from the integral of Eq. (6-75). The absolute time, t_i , and the cross-over pressure, p_i , are confirmed by comparison with experimental data in Table 5.15.

The causative and reference process is the dominant PRHR cooling power. It is computed in Appendix 5.2 from the mass flow rate of natural circulation and the enthalpy difference of the fluids in the Cold Leg and the PRHR at the initial time of Phase 2. The flow rates of natural circulation for PRHR and CMTs are computed in Appendix 5.2, using the steady-state momentum balance according to Eq. (5-59).

The reference time for Phase 2 is taken to be the same as for Phase 1 since the reference time does not affect the ranking of phenomena or the assessment of scale distortion, and since using the same time provides time continuity for the comparison of estimated reference parameters with data. The numerical value of the reference time for Phase 2 is listed in Appendix 5.2.

The reference pressure difference, Δp_0 , is the difference between the specified trip set point pressure that trips the S-Signal and the pressure at which the Accumulator valves open. The Accumulator trip pressure is facility-related and the nearest specified pressure to the pressure at which the Automatic Depressurization System (ADS) trips and initiates Phase 3 (APEX tripped ADS very nearly at the Accumulator pressure). The selected Δp_0 assures the scaled pressure p^* to be of the order of unity. The values of Δp_0 are listed in Appendix 5.2.

The initial vapor, mixture, and liquid volumes determine the three initial system compliances for pressure, inventory, and temperature; they are identified in Table 3.1 and shown in Figure 5.3; their values are computed from the volumes listed in Appendix 1.1, and shown in Appendix 5.2.

The break flow is computed from the specified break area (specified in Appendix 1.2) and the critical mass flux according to Bestion [22] from Eq. (5-57), with the upstream equilibrium quality being $x_e = (h_0 - h_f)/h_{fg}$. The results for the critical mass flux, critical mass flow rate and critical volumetric flow rate are found in Appendix 4.3.

All initial data for Phase 2 are given in Appendix 4.3, Table A.4.3.1 shows the initial operating conditions, Table A.4.3.2 the thermophysical properties, and the computed reference parameters are found in Appendix 5.2.

6.2.2.1 Depressurization

Primary System Before Accumulator Trip

Table 6.23 presents the numerical values of the *causative process related* Π -Groups of depressurization. They are obtained from the scaled *depressurization equation*, Eq. (6-1), applied to the control volume shown in Figure 5.3 for **Phase 2.1** (see Figure 3.1 and Section 3.3.1 for the definition of Phase 2.1). The *causative process related* Π -Groups show the significance of phenomena (system elasticity or system pressure response to volume changes) and transfer processes (volumetric flow rates caused by external heating and cooling) relative to the process of fluid discharge through the break.

6. Scaling Groups

The explanation for Table 6.23 is the same as that given on Page 24 for Table 6.1. All geometric parameters appearing in the Π -Group definitions, Eqs. (6-2) through (6-5) and (6-10) through (6-13) for Tables 6.23 and 6.24 are found in Appendix 1. The initial conditions and initial thermophysical properties are found in Tables A.4.3.1 and A.4.3.2 of Appendix 4.3. The initial system compliance and computed reference parameters appearing in the Π -Group definitions were computed through EXCEL and are listed in Appendix 5.2.

By the methods and criteria described in Sections 4.5 and 4.6, and summarized at the beginning of Section 6.2 on Page 6-22, it is found that (1) phase change in the Steam Generators is the dominant process, thermal expansion of liquid due to core heating and the causative process of break discharge are equally *important*, and system elasticity (or mechanical compliance) is large, indicating slow depressurization; and (2) for depressurization during Phase 2.1, there are **three significant scale distortions: two in APEX and one in ROSA**.

Table 6.23 Causative process related Π -Groups for Depressurization During Phase 2.1

Definition of Π -Group	Symbol of Π -Group	Π -Groups for				Comments
		AP600	APEX	ROSA	SPES	
Mechanical Compliance (Eq. (6-2))	Π_{MC}	9.07	10.84	10.85	8.74	
Cooling by SG (Subphase 2.1.1) (Eq. (6-5))	$\Pi_{\dot{Q}, 2\phi, c}$	7.73	21.24	14.67	8.02	low pressure in APEX, v_{fg} is 4 times larger
Thermal Exp. by Decay Heating (Eq. (6-4))	$\Pi_{\dot{Q}, l}$	1.09	0.05	0.52	1.13	low PRHR power rel. to core power in ROSA, confirmed by test, no APEX data.
Break Flow (reference)	Π_{bk}	1	1	1	1	
Heating by SG (Subphase 2.1.2) (Eq. (6-5))	$\Pi_{\dot{Q}, 2\phi, h}$	0.66	0.11	1.25	0.50	
UHD Heating of vapor (Eq. (6-4))	$\Pi_{\dot{Q}, v}$	0.01	0.03	0.16	0.73	

Table 6.24 presents the numerical values of the *fractional* Π -Groups. They are obtained from the scaled fractional *depressurization equation*, Eq. (6-7), applied to the control volume shown in Figure 5.3 for Phase 2. The *fractional* Π -Groups in a *column* of Table 6.24 show directly the impact that corresponding processes (external heating and cooling) have on the time-rate of pressure change (see illustration in Figure 4.3). The larger the entry, the stronger is the effect on the slope of the depressurization curve. Differences between the entries in a *row* of Table 6.24 show *scale distortion* for the phenomenon associated with the row.

The *fractional* Π -Groups in Table 6.24 show, as the *causative process related* Π -Groups in Table 6.23, that (1) SG cooling, core heating and break flow are of first-order importance, with SG cooling being the dominant-leader process of depressurization during Phase 2; and (2) there are **two relevant scale distortions in APEX**, over-all **conservative**, and **one relevant, conservative scale distortion in ROSA** which affects the small but still first-order effect of thermal expansion due to core heating. The scale distortions are conservative because they speed up depressurization.

Table 6.24 Fractional Π -Groups for Depressurization During Phase 2.1

Definition of Π -Group	Symbol of Π -Group	Π -Groups for				Comments
		AP600	APEX	ROSA	SPES	
Cooling by SG (Subphase 2.1.1) (Eq. (6-11))	$\Pi_{\dot{p}\dot{Q}, 2\phi, c}$	0.85	1.96	1.35	0.92	low pressure in APEX, v_{fg} is 4 times larger
Thermal Exp. by Decay Heating (Eq. (6-10))	$\Pi_{\dot{p}\dot{Q}, l}$	0.12	0.005	0.048	0.13	low PRHR power rel. to core power in ROSA, confirmed by test, no APEX data.
Break Flow (Eq. (6-13))	Π_{pbk}	0.11	0.09	0.09	0.11	
Heating by SG (Subphase 2.1.2) (Eq. (6-11))	$\Pi_{\dot{p}\dot{Q}, 2\phi, h}$	0.07	0.01	0.11	0.06	
UHD Heating of vapor (Eq. (6-10))	$\dot{p}\Pi_{\dot{Q}, v}$	$8.5 \cdot 10^{-4}$	$2.4 \cdot 10^{-3}$	$1.5 \cdot 10^{-2}$	$4.8 \cdot 10^{-2}$	

Secondary System, Phase 2

The response of the Steam Generators (SG) after isolation is scaled by the ratio of system over SG response times, i.e., the single $\Pi_{\dot{p}, SG}$ -Group defined by Eq. (6-77) for the fractional scaled depressurization equation, Eq. (6-75). The evaluation of $\Pi_{\dot{p}, SG}$ is given in Table 6.25 below.

Table 6.25 Fractional Π -Groups for Depressurization of Secondary Side During Phase 2

Definition of Π -Group	Symbol of Π -Group	Π -Groups for				Comments
		AP600	APEX	ROSA	SPES	
Steam Generator Depressurization, secondary side, Eq. (6-77)	$\Pi_{\dot{p}, SG}$	0.28	1.65	0.27	0.25	low-pressure v_{fg} in APEX increases volume change 4 times

The heat capacities of the Steam Generators, $M c_p$, in Eq. (6-77) is computed from the structural mass listed in Appendix 3 and the specific heat in Table A.4.3.2 of Appendix 4. The convective heat transfer coefficient for the Steam Generators, h_{cv} , is computed in Appendix 5.2 from the initial power, the wall surface area, and the initial difference of hot-leg and secondary-side saturation temperatures.

Table 6.25 shows that **APEX has SG depressurization distorted** due to its low-pressure operation: the specific volume change of phase change outweighs the enthalpy change of phase change. The APEX steam generator secondary side depressurizes slower relative to the primary side. The secondary side maintains saturation temperature longer, allowing for more energy transfer to the primary side. The distortion is, therefore, considered to be conservative.

6. Scaling Groups

Primary System After Accumulator Trip

The scaling groups in Tables 6.23 and 6.24 have been re-evaluated for Phase 2.2 in which the Accumulator are communicating with the primary system. This means that the total system elasticity (or mechanical compliance) defined by Eq. (5-9) must now include the nitrogen gas volume. The liquid flow rate from the Accumulators is computed from the volume integral of Eq. (5-4), with the depressurization rate, \dot{p} , known from Eq. (5-8). The computation is shown in the Phase 2 section of Appendix 5.2.

Tables 6.26 and 6.27 show the results of the re-evaluation of the scaling groups in Tables 6.23 and 6.24, but now for Phase 2.2. The ranking of phenomena is unchanged by the Accumulator trip. The mechanical compliance of the AP600 is increased by 34 % due to the added elasticity of the nitrogen gas. The heat transfer from the Accumulator tank to the gas is unimportant for the pressure history of the primary system. The **scale distortions** remain also unaffected, except that the previous decay heat discrepancy of ROSA is now just above the adopted threshold of distortion.

Table 6.26 Causative Process Related Π -Groups for Depressurization During Phase 2.2, After Accumulator Trip

Definition of Π -Group	Symbol of Π -Group	Π -Groups for				Comments
		AP600	APEX	ROSA	SPES	
Mechanical Compliance (Eq. (6-2))	Π_{MC}	12.19	13.60	14.31	11.68	
Heating by SG (Subphase 2.1.1) (Eq. (6-5))	$\Pi_{\dot{Q}, 2\phi, c}$	2.15	25.41	4.08	1.64	low pressure in APEX, v_{fg} is 4 times larger
Thermal Exp. by Decay Heating (Eq. (6-4))	$\Pi_{\dot{Q}, l}$	1.22	0.06	0.70	1.11	low PRHR power rel. to core power in ROSA, confirmed by test, no APEX data.
Break Flow (reference)	Π_{bk}	1	1	1	1	
Accumulator Heat Transfer to Nitrogen Gas (Eq. (6-6))	$\Pi_{\dot{Q}, N_2}$	0.02	0.02	$2.1 \cdot 10^{-3}$	0.03	
UHD Heating of vapor (Eq. (6-4))	$\Pi_{\dot{Q}, v}$	0.01	0.06	0.30	1.40	Large UHD wall heat capacity in ROSA and SPES

Table 6.27 Fractional Π -Groups for Depressurization During Phase 2.2, After Accumulator Trip

Definition of Π -Group	Symbol of Π -Group	Π -Groups for				Comments
		AP600	APEX	ROSA	SPES	
Cooling by SG (Subphase 2.1.1) (Eq. (6-11))	$\Pi_{\dot{p}\dot{Q}, 2\phi}$	0.18	1.87	0.28	0.14	low pressure in APEX, v_{fg} is 4 times larger
Thermal Exp. by Decay Heating (Eq. (6-10))	$\Pi_{\dot{p}\dot{Q}, l}$	0.10	0.004	0.05	0.10	low PRHR power rel. to core power in ROSA, confirmed by test, no APEX data.
Break Flow (Eq. (6-13))	$\Pi_{\dot{p}bk}$	0.08	0.07	0.07	0.09	
Heating of Nitrogen by Accumulator Shell (Eq. (6-12))	$\Pi_{\dot{p}\dot{Q}, N_2}$	$2.0 \cdot 10^{-3}$	$1.5 \cdot 10^{-3}$	$1.5 \cdot 10^{-4}$	$2.9 \cdot 10^{-3}$	
UHD Heating of vapor (Eq. (6-10))	$\dot{p}\Pi_{\dot{Q}, v}$	$1.2 \cdot 10^{-3}$	$4.1 \cdot 10^{-3}$	$2.1 \cdot 10^{-2}$	0.12	Large UHD wall heat capacity in SPES

6.2.2.2 Inventory Change During Phase 2

Liquid inventory changes in the primary system and in the Core Make-up Tank are modeled as the compliment of vapor volume change, in the same manner as for Phase 1.

Primary System Inventory, Before Accumulator Trip, Phase 2.1

Table 6.28 below presents the numerical values of the *causative process related* Π -Groups which scale liquid inventory change in the primary system during Subphase 2.1. The model for primary system inventory is presented in Section 5.4.1.3. Section 6.1.2.1 presents the scaled inventory equation, Eq. (6-14), as obtained by the causative process related scaling method. Equation (6-14) applies to the control volume of the two-phase mixture in the primary system and contains the *causative process related* Π -Groups for Phase 2.1 (see Figure 3.1 and Section 3.3.1 for the definition of Phase 2.1). The *causative process related* Π -Groups are defined by Eqs. (6-4), (6-15) and (6-16) and show the significance of phenomena (system volumetric compliance) and processes (external heating and cooling) relative to the process of fluid discharge through the break.

To read Table 6.28, recall the description on Page 24 for Table 6.1: each Π -Group is interpreted in Section 6.1 in the text next to the equation that defines it, and the defining equation is indicated in the first column of Table 6.28. The second column shows the Π -Group symbol as in Eq. (6-14), the third through sixth columns list the numerical values of the Π -Groups, first for the AP600 and then for the three related facilities APEX, ROSA, and SPES, and the last column is provided for comments explaining distortions, if any. All geometric parameters appearing in the Π -Group definitions, Eqs. (6-4), (6-15) and (6-16) are found in Appendix 1. The initial conditions and initial thermophysical properties are found in Appendix 4.1. The initial system compliance and computed reference parameters appearing in the Π -Group definitions were computed through EXCEL and are listed in Appendix 5.2 of the separate data base document for this report.

6. Scaling Groups

The net initial cooling power applied to the subvolume occupied by single-phase fluid, $(\dot{Q}_{1\phi})_0$ (see Figure 5.1), is the absolute value of the difference between the combined cooling power of CMT and PRHR (computed in Appendix 5.2), minus the core heating power (specified decay heat, see Appendix 4.3). The reference volumetric flow rate, Φ_0 , is the initial break flow rate at the beginning of Phase 2, and the thermophysical properties β_T , ρ , c_p , v_{fg} , and h_{fg} are evaluated at initial conditions of Phase 2. The net initial heating power applied to the subvolume occupied by two-phase mixture, $(\dot{Q}_{2\phi})_0$, (see Figure 5.1) is the cooling power of condensation in the Steam Generator (see Appendix 5.2).

By the methods and criteria described in Sections 4.5 and 4.6, and summarized at the beginning of Section 6.2 on Page 6-22, it is found that (1) thermal expansion and phase change are of the same order of importance as the causative process of break flow, thermal expansion is the dominant process; and (2) there is **one significant scale distortion** of inventory depletion in the primary system of **APEX** during Phase 2.1: the relative low PRHR cooling retards inventory discharge in APEX less than in AP600. The distortion in APEX is, therefore, conservative.

Table 6.28 Causative Process Related Π -Groups for Loss of Inventory During Phase 2.1, Before Accumulator Trip

Definition of Π -Group	Symbol of Π -Group	Π -Groups for				Comments
		AP600	APEX	ROSA	SPES	
Volumetric Compliance (Eq. (6-15))	Π_{VC}	4.88	4.06	5.82	4.91	
Thermal Exp. by Net Heating in Core/PRHR (Eq. (6-4))	$\Pi_{\dot{Q}, 1\phi}$	1.23	0.41	0.74	1.13	low PRHR power in APEX and ROSA.
Break Flow (reference)	Π_{bk}	1	1	1	1	
Phase Change (PRZ, CMT, and SG) (Eq. (6-16))	$\Pi_{V, \dot{Q}, 2\phi}$	0.69	0.36	0.73	0.65	

Table 6.29 presents the numerical values of the *fractional* Π -Groups. They are obtained from the *vapor mass conservation equation*, Eq. (6-17), applied to the control volume of the two-phase mixture in primary system as defined in Table 3.1 for Subphase 2.1 (see Figure 3.1 and Section 3.3.1 for the definition of Subphase 2.1). The *fractional* Π -Groups show the impact that processes (external heating and cooling) have on the time-rate of liquid inventory change.

Each *column* entry in Table 6.29 shows *how much* the tangent of the *vapor* inventory vs. time curve in Figure 4.3 is rotated from the horizontal by the phenomenon associated with the row of the entry and, consequently, *how important* that phenomenon is during Subphase 2.1. The larger the entry, the stronger is the effect on the rate of change of the liquid inventory. Break flow, net heating and cooling in core, CMT, PRHR, and SG of subcooled liquid and two-phase mixture are equally important (of the same order of magnitude).

Differences between the entries in a *row* of Table 6.29 imply differences in the system response due to the phenomenon associated with that row and, consequently, the strength of *scale distortion* for that phenomenon on liquid draining. The fractional scaling leads to the same conclusion as the causative process related scaling: there is **one significant scale distortion** of inventory depletion in the primary system of **APEX** during Phase 2.1 because the relative low PRHR cooling retards inventory discharge in APEX less than in AP600. The distortion in APEX is, therefore, conservative.

Table 6.29 Fractional Π -Groups for Loss of Inventory During Subphase 2.1, Before Accumulator Trip

Definition of Π -Group	Symbol of Π -Group	Π -Groups for				Comments
		AP600	APEX	ROSA	SPES	
Thermal Exp. by Net Heating in Core, PRHR; (Eq. (6-18))	$\Pi_{\dot{\alpha}, \dot{Q}, 1\phi}$	0.25	0.10	0.13	0.23	Rel. to core power, PRHR power in APEX and ROSA are low; computed PRHR power is confirmed for ROSA and SPES, no data for APEX.
Break Flow (Eq. (6-21))	$\Pi_{\dot{\alpha}, bk}$	0.21	0.25	0.17	0.20	
Phase Change (PRZ, CMT, and SG) (Eq. (6-19))	$\Pi_{\dot{\alpha}, \dot{Q}, 2\phi}$	0.14	0.09	0.12	0.13	

Core Make-up Tank Inventory, Before Accumulator Trip, Phase 2.1

The loss of liquid inventory in the Core Make-up Tank (CMT), after disruption of liquid circulation in the pressure balance line, is modeled as the gain of vapor volume according to Eq. (5-10), with the time rate of pressure change given by Eq. (5-8) and the mass flow rate of the liquid leaving the CMT computed from the volumetric flow rate given by Eq. (5-55). Based on the definition given in Section 4.4.5.1, the inventory equation scaled by the causative process related method is

$$\Pi_{VC, CMT} \frac{d\alpha}{dt^*} = \Phi_{CMT}^* + \Pi_{V, \dot{Q}_{CMT}} \left(\frac{v_f}{h_{fg}} \right)^* \dot{Q}_{2\phi, CMT}^* - \left(\frac{\Psi_{\alpha, CMT}}{\chi_V} \right)^* \left[\Pi_{V, CMT, \dot{Q}_{1\phi}} \left(\frac{\beta_T}{\rho c_p} \right)^* \dot{Q}_{1\phi}^* - \Pi_{V, CMT, bk} \Phi_{bk}^* + \Pi_{V, CMT, \dot{Q}_{2\phi}} \left(\frac{v_{fg}}{h_{fg}} \right)^* \dot{Q}_{2\phi, SG}^* \right], \quad (6-79)$$

where χ_V is defined by Eq. (5-9), where the compressibility function of CMT is given by

$$\Psi_{\alpha, CMT} = \left(\alpha \frac{\rho_g'}{\rho_g} + \frac{\sum_{k=f, g} \alpha_k h_k' - 1}{\rho_g h_{fg}} \right)_{CMT} \quad (6-80)$$

and where the five causative process related scaling groups are (1) the *volumetric compliance of the CMT*, or the ratio of the CMT draining over the system response times

6. Scaling Groups

$$\Pi_{V,CMT} = \frac{V_{CMT}}{t_{ref}(\Phi_{CMT})_0}, \quad (6-81)$$

(2) the scaling group for *phase change in the CMT*, or the ratio of the rate of volume change due to phase change in the CMT over the rate of volume displaced by draining

$$\Pi_{V,\dot{Q}_{CMT}} = \frac{(\dot{Q}_{2\phi,CMT})_0}{(\Phi_{CMT})_0} \left(\frac{v_f}{h_{fg}} \right)_0, \quad (6-82)$$

and the last three scaling groups associated with the phenomena affecting the vapor formation in the CMT indirectly via flashing during depressurization, i.e., (3) the scaling group for the *effect on the CMT draining from flashing due to net cooling of the primary-side single-phase liquid*, or the ratio of the CMT reference time (draining time) over the CMT liquid volume response time to thermal expansion or contraction of the liquid in the primary system, i.e.,

$$\Pi_{V,CMT,\dot{Q}_{1\phi}} = \frac{V_{CMT}(\dot{Q}_{1\phi})_0}{(\Phi_{CMT})_0} \left(\frac{\beta_T}{\rho c_p} \right)_0 \left(\frac{\Psi_{\alpha,CMT}}{\chi_V V} \right)_0, \quad (6-83)$$

(4) the scaling group for the *effect on the CMT draining from flashing due to net phase change in the primary system*, or the ratio of the CMT reference time over the CMT liquid volume response time to evaporation or condensation on the primary side of the Steam Generators, i.e.,

$$\Pi_{V,CMT,\dot{Q}_{2\phi}} = \frac{V_{CMT}(\dot{Q}_{2\phi})_0}{(\Phi_{CMT})_0} \left(\frac{v_{fg}}{h_{fg}} \right)_0 \left(\frac{\Psi_{\alpha,CMT}}{\chi_V V} \right)_0, \quad (6-84)$$

and (5) the scaling group for the *effect on the CMT draining from flashing due to volume displacement through the break*, or the ratio of the CMT reference time over the CMT liquid volume response time to break flow, i.e.,

$$\Pi_{V,CMT,bk} = \frac{V_{CMT}(\Phi_{bk})_0}{(\Phi_{CMT})_0} \left(\frac{\Psi_{\alpha,CMT}}{\chi_V V} \right)_0. \quad (6-85)$$

Table 6.30 lists the *causative process related* Π -Groups defined by Eqs. (6-81) through (6-85). The fluid properties for the CMT which occur in Eqs. (6-80) through (6-85) are evaluated with the initial void fraction $(\alpha_{CMT})_0 = 0$. Reference parameters for the primary system which occur in Eqs. (6-81) through (6-84) are the same as for the scaling of the Phase 2 depressurization, as discussed in Section 6.2.2.1 and shown in Appendix 5.2. The CMT heat transfer rate, $(\dot{Q}_{2\phi,CMT})_0$, in Eq. (6-82) equals the conduction-limited, accumulated heat transferred from the (thermally thick) CMT walls divided by the system reference time

$$(\dot{Q}_{2\phi,CMT})_0 = 2 A_{w,CMT} \Delta T_0 \sqrt{\frac{(k \rho c)_{CMT}}{\pi t_{ref}}}, \quad (6-86)$$

with $A_{w,CMT}$ taken as the wall area being exposed to steam during Phase 2 and with the initial temperature difference, ΔT_0 , taken as the difference between specified initial CMT wall temperature and initial saturation temperature of the primary system at the beginning of Phase 2. The reference CMT flow rate is computed from the volumetric flow rate

according to Eq. (5-59). All geometric parameters appearing in the Π -Group definitions, Eqs. (6-81) through (6-84) are found in Appendix 1. The initial conditions and initial thermophysical properties are found in Appendix 4.3. The initial system compliance and computed reference parameters appearing in the Π -Group definitions were computed through EXCEL and are listed in Appendix 5.2.

To read Table 6.30, recall from the explanation for Table 6.1 on Page 6-24 that each Π -Group is interpreted in the text next to the equation that defines it, and the defining equation is indicated in the first column of Table 6.30. The second column shows the Π -Group symbol as in Eq. (6-79), the third through sixth columns list the numerical values of the Π -Groups for the AP600 and the three related facilities APEX, ROSA, and SPES, and the last column is provided for comments explaining distortions, if any.

By the methods and criteria described in Sections 4.5 and 4.6, and summarized at the beginning of Section 6.2 on Page 6-22, it is found that (1) phase change in the Steam Generator dominates the rate of CMT draining; and (2) **there are two significant scale distortions** affecting CMT inventory change in APEX during Subphase 2.1. Condensation in the Steam Generators causes faster CMT drainage in APEX than in AP600. The distortion in APEX is therefore conservative.

Table 6.30 Causative process related Π -Groups for CMT Draining During Subphase 2.1

Definition of Π -Group	Symbol of Π -Group	Π -Groups for				Comments
		AP600	APEX	ROSA	SPES	
CMT Volumetric Compliance (Eq. (6-81))	$\Pi_{VC, CMT}$	4.25	6.59	6.44	4.80	
SG Phase change effect on CMT drainage (Eq. (6-84))	$\Pi_{V, CMT, \dot{Q}_{2p}}$	2.69	26.40	5.19	2.54	low-pressure in APEX, large v_{fg} increases volume change by factor 4.
CMT Circulation (reference)	$\Pi_{V, \Phi_{CMT}}$	1	1	1	1	
CMT Phase Change (Eq. (6-82))	$\Pi_{V, \dot{Q}_{CMT}}$	0.28	0.16	0.57	0.28	
Break flow effect on CMT drainage (Eq. (6-85))	$\Pi_{V, CMT, bk}$	0.13	0.03	0.16	0.15	larger draining flow in APEX due to lower CMT-loop impedance
Primary-side heating effect on CMT drainage (Eq. (6-83))	$\Pi_{V, CMT, \dot{Q}_{1p}}$	0.07	0.01	0.18	0.10	

Table 6.31 presents the numerical values of the *fractional* Π -Groups for CMT drainage during Subphase 2.1 (see Figure 3.1 and Section 3.3.1 for the definition of Subphase 2.1). The *fractional* Π -Groups are introduced in Section 4.4.5.2. For CMT drainage during Phase 2.1, they are obtained by dividing the causative process related Π -Groups given in Eqs. (6-82) through (6-85) by the CMT volumetric compliance Π -Group given in Eq. (6-81). The CMT

6. Scaling Groups

inventory equation scaled by the *fractional scaling method* is derived by dividing Eq. (6-79) by the CMT volumetric compliance Π -Group given in Eq. (6-81). The result is

$$\begin{aligned} \frac{d\alpha}{dt^*} = & \Pi_{\dot{\alpha}, \Phi_{CMT}} \Phi_{CMT}^* + \Pi_{\dot{\alpha}, \dot{Q}_{CMT}} \left(\frac{v_f}{h_{fg}} \right)^* \dot{Q}_{2\phi, CMT}^* \\ - \left(\frac{\Psi_{\alpha, CMT}}{\chi_V} \right)^* & \left[\Pi_{\dot{\alpha}, CMT, \dot{Q}_{1\phi}} \left(\frac{\beta_T}{\rho c_p} \right)^* \dot{Q}_{1\phi}^* - \Pi_{\dot{\alpha}, CMT, bk} \Phi_{bk}^* + \Pi_{\dot{\alpha}, CMT, \dot{Q}_{2\phi}} \left(\frac{v_{fg}}{h_{fg}} \right)^* \dot{Q}_{2\phi, SG}^* \right], \end{aligned} \quad (6-87)$$

where the five *fractional* scaling groups are (1) the Π -Group of *CMT circulation* (vapor inflow), or the ratio of system response over CMT draining times

$$\Pi_{\dot{\alpha}, \Phi_{CMT}} = \frac{t_{ref} (\Phi_{CMT})_0}{V_{CMT}}, \quad (6-88)$$

(2) the scaling group for *phase change in the CMT*, or the ratio of system reference time over the time it takes to fill the CMT volume by condensation in the CMT, i.e.,

$$\Pi_{\dot{\alpha}, \dot{Q}_{CMT}} = \frac{t_{ref} (\dot{Q}_{2\phi, CMT})_0 \left(\frac{v_f}{h_{fg}} \right)_0}{V_{CMT}}, \quad (6-89)$$

(3) the scaling group for the *effect on the CMT draining from flashing due to net cooling of the primary-side single-phase liquid*, or the ratio of the system reference time over the CMT liquid volume response time to thermal expansion or contraction of the liquid in the primary system

$$\Pi_{\dot{\alpha}, CMT, \dot{Q}_{1\phi}} = t_{ref} (\dot{Q}_{1\phi})_0 \left(\frac{\beta_T}{\rho c_p} \right)_0 \left(\frac{\Psi_{\alpha, CMT}}{\chi_V V} \right)_0, \quad (6-90)$$

(4) the scaling group for the *effect on the CMT draining from flashing due to net phase change in the primary system*, or the ratio of the system reference time over the CMT liquid volume response time to evaporation or condensation at the primary side of the Steam Generators

$$\Pi_{\dot{\alpha}, CMT, \dot{Q}_{2\phi}} = t_{ref} (\dot{Q}_{2\phi})_0 \left(\frac{v_{fg}}{h_{fg}} \right)_0 \left(\frac{\Psi_{\alpha, CMT}}{\chi_V V} \right)_0, \quad (6-91)$$

and (5) the scaling group for the *effect on the CMT draining from flashing due to volume displacement through the break*, or the ratio of the system reference time over the CMT liquid volume response time to break flow

$$\Pi_{\dot{\alpha}, CMT, bk} = t_{ref} (\Phi_{bk})_0 \left(\frac{\Psi_{\alpha, CMT}}{\chi_V} \right)_0. \quad (6-92)$$

The association of Π -Groups with processes is the same in Eqs. (6-79) and (6-87); the subscript V in Eq. (6-79) is replaced by $\dot{\alpha}$ in Eq. (6-87).

As explained in Section 4.4.5.2, the *fractional* Π -Groups show directly the impact that processes (external heating and cooling, draining) have on the time-rate of CMT liquid inventory change. Each *column* entry in Table 6.31 shows *how much* the tangent of the vapor volume fraction vs. time curve in Figure 4.3 is rotated from the horizontal by the phenomenon associated with the row of the entry and, consequently, *how important* that phenomenon is during the respective phase.

As concluded above from the *causative process related* Π -Groups by the methods and criteria described in Sections 4.5 and 4.6, and summarized at the beginning of Section 6.2 on Page 6-22, it is found that (1) the condensation in the Steam generators causes the greatest fractional change of CMT liquid inventory; and (2) **there are two significant scale distortions** of CMT liquid inventory change in APEX during Subphase 2.1 (significant” is defined in Section 4.6). The explanation for the distortion is given in the last column of Table 6.31. The most important distortion is due to low-pressure operation in APEX, but conservative with regard to CMT inventory. The less important distortion is also caused by low-pressure operation and is nonconservative because the CMT liquid volume change in APEX is less than in AP600. However, the overall distortion of CMT inventory change in APEX is conservative because the conservative distortion of SG phase change effects more than compensates for the nonconservative distortion of CMT phase change.

Table 6.31 Fractional Π -Groups for CMT Draining During Subphase 2.1

Definition of Π -Group	Symbol of Π -Group	Π -Groups for				Comments
		AP600	APEX	ROSA	SPES	
SG Phase change effect on CMT drainage (Eq. (6-91))	$\Pi_{\dot{\alpha}, CMT, \dot{Q}_{2\phi}}$	0.63	4.01	0.81	0.53	low-pressure in APEX, large v_{fg} increases volume change by factor 4.
CMT Circulation (Eq. (6-88))	$\Pi_{\dot{\alpha}, \Phi_{CMT}}$	0.24	0.15	0.16	0.21	
CMT Phase Change (Eq. (6-89))	$\Pi_{\dot{\alpha}, \dot{Q}_{CMT}}$	0.07	0.02	0.09	0.06	low-pressure in APEX, large h_{fg} decreases volume change.
Break flow effect on CMT drainage (Eq. (6-92))	$\Pi_{\dot{\alpha}, CMT, bk}$	0.03	2e-3	0.02	0.03	
Primary-side heating effect on CMT drainage (Eq. (6-90))	$\Pi_{\dot{\alpha}, CMT, \dot{Q}_{1\phi}}$	0.02	5e-3	0.03	0.02	

Primary System Inventory, After Accumulator Trip, Subphase 2.2

Subphase 2.2 begins with the Accumulator trip at the primary system pressure of 48.2 bar. Opening of the Accumulator valves adds the volumes of the compressible nitrogen cover gas in the Accumulators to the system volume and alters thereby the system compliance. The model for primary system inventory change is presented in Section

6. Scaling Groups

5.4.1.3, the inventory equation, Eq. (6-14), obtained by the *causative process related* scaling method is shown in Section 6.1.2.1. The *causative process related* Π -Groups are obtained from the *vapor mass conservation equation*, Eq. (6-14), which is scaled by the causative process related method and applies to the control volume of the two-phase mixture in the primary system (see Figure 3.1 and Section 3.3.1 for the definition of Phase 2.2).

Table 6.32 below presents the numerical values of the *causative process related* Π -Groups which scale liquid inventory change in the primary system during Subphase 2.2. Table 6.32 is read according to the explanation for Table 6.1 on Page 6-24. All geometric parameters appearing in the Π -Group definitions, Eqs. (6-4) through (6-6), (6-15) and (6-16) are found in Appendix 1. The initial conditions and initial thermophysical properties are found in Appendix 4.1. The initial system compliance and computed reference parameters appearing in the Π -Group definitions were computed through EXCEL and are listed in Appendix 5.2. Reference parameters other than the initial system compliance are taken to be the same as for Subphase 2.1. The net initial cooling power applied to the subvolume occupied by single-phase fluid, $(\dot{Q}_{1\phi})_0$ (see Figure 5.1), is the absolute value of the difference between the combined cooling power of CMT and PRHR (computed in Appendix 5.2), minus the core heating power (specified decay heat, see Appendix 4.3). The reference volumetric flow rate, Φ_0 , is the initial break flow rate at the beginning of Phase 2, and the thermophysical properties β_T , ρ , c_p , v_{fn} , and h_{fg} are evaluated at initial conditions of Phase 2. The net initial heating power applied to the subvolume occupied by two-phase mixture, $(\dot{Q}_{2\phi})_0$, (see Figure 5.1) is the cooling power of condensation in the Steam Generator (see Appendix 5.2).

The *causative process related* Π -Groups in Table 6.32 show the significance of phenomena (system volumetric compliance) and processes (external heating and cooling) relative to the process of fluid discharge through the break. By the methods and criteria described in Sections 4.5 and 4.6, and summarized at the beginning of Section 6.2 on Page 6-22, Table 6.32 shows for Subphase 2.2 that (1) phase change in the Pressurizer, Core Make-up Tanks, and Steam Generator dominates the rate of primary system inventory draining; and (2) **there is one significant scale distortion in APEX** for inventory depletion in the primary system. The liquid volume retention is less in APEX due to the relatively low PRHR cooling power in APEX. The distortion in APEX is, therefore, conservative.

Table 6.32 Causative Process Related Π -Groups for Loss of Inventory in Primary System During Phase 2.2, After Accumulator Trip

Definition of Π -Group	Symbol of Π -Group	Π -Groups for				Comments
		AP600	APEX	ROSA	SPES	
Volumetric Compliance (Eq. (6-15))	Π_{VC}	5.06	4.18	6.03	5.09	
Phase Change (PRZ, CMT, and SG) (Eq. (6-16))	$\Pi_{V, \dot{Q}, 2\phi}$	1.69	1.09	1.55	1.75	
Thermal Exp. by Net Heating in Core/PRHR (Eq. (6-4))	$\Pi_{\dot{Q}, 1\phi}$	1.23	0.41	0.74	1.13	low PRHR power in APEX and ROSA.
Break Flow (reference)	Π_{bk}	1	1	1	1	
UHD Heating (Eq. (6-16))	$\Pi_{V, \dot{Q}_{UHD}, 2\phi}$	0.001	0.006	0.019	0.084	

Table 6.33 presents the numerical values of the *fractional* Π -Groups. They are obtained from the *vapor mass conservation equation*, Eq. (6-17), applied to the control volume of the two-phase mixture in primary system as defined in Table 3.1 for Subphase 2.2 (see Figure 3.1 and Section 3.3.1 for the definition of Subphase 2.2). The *fractional* Π -Groups in Table 6.33 show the fractional impact that processes (external heating and cooling) have on the time-rate of liquid inventory change in the primary system. Each *column* entry in Table 6.33 shows *how much* the tangent of the *vapor* inventory vs. time curve in Figure 4.3 is rotated from the horizontal by the phenomenon associated with the row of the entry and, consequently, *how important* that phenomenon is during Subphase 2.2. Differences between the entries in a *row* of Table 6.33 imply differences in the system response due to the phenomenon associated with that row and, consequently, the strength of *scale distortion* for that phenomenon on liquid draining. See Sections 4.5 and 4.6 for the interpretations of row and column elements in Table 6.33.

As the *causative process related* Π -Groups in Table 6.32, the *fractional* Π -Groups in Table 6.33 show also that (1) phase change in the Pressurizer, Core Make-up Tanks, and Steam Generator dominates the rate of primary system inventory draining, break flow, net heating of subcooled liquid in core and PRHR are equally important (of the same order of magnitude); and (2) **there is one conservative significant scale distortion in APEX** for inventory depletion in the primary system during Subphase 2.2 (for the definition of “significant distortion” see Section 4.6). The explanation for the distortion is given in the last column of Table 6.33.

By combining the results presented in Tables 6.29 and 6.33 for primary-system inventory depletion during Phase 2 one reaches the total distortion assessment of **one significant distortion each in APEX**, caused by relatively low PRHR cooling power in APEX (also in ROSA, but not enough to meet the distortion criterion in Section 4.6).

Table 6.33 Fractional Π -Groups for Loss of Inventory During Subphase 2.2, After Accumulator Trip

Definition of Π -Group	Symbol of Π -Group	Π -Groups for				Comments
		AP600	APEX	ROSA	SPES	
Phase Change (PRZ, CMT, and SG) (Eq. (6-19))	$\Pi_{\dot{\alpha}, \dot{Q}_{2\phi}}$	0.33	0.26	0.26	0.34	
Thermal Exp. by Net Heating in Core, PRHR; (Eq. (6-18))	$\Pi_{\dot{\alpha}, \dot{Q}_{1\phi}}$	0.24	0.10	0.12	0.22	Rel. to core power, PRHR power in APEX and ROSA are low; computed PRHR power is confirmed for ROSA and SPES, no data for APEX.
Break Flow (Eq. (6-21))	$\Pi_{\dot{\alpha}, bk}$	0.20	0.24	0.17	0.20	
UHD Heating (Eq. (6-19))	$\Pi_{\dot{\alpha}, \dot{Q}_{UHD, 2\phi}}$	1.9×10^{-4}	1.4×10^{-3}	3.2×10^{-3}	2.9×10^{-3}	

6. Scaling Groups

6.2.2.3 Temperature Changes During Phase 2, Passive Heat Removal

Primary System, Before Accumulator Trip

The temperature change of the liquid in the primary system is modeled in Section 5.4.1.4 on the basis of energy conservation applied to the control volume of the single-phase liquid in the primary system, and for Phase 2 (see Figure 3.1 and Section 3.3.1 for the definition of Phase 2). The scaled temperature equation for change dominated by PRHR cooling, Eqs. (6-32) through (6-37), is shown in Section 6.1.3.1. The reference temperature difference is the difference between the arithmetic mean of Hot-Leg and Cold-Leg temperatures and the initial CMT temperature (temperature of the containment atmosphere)

$$\Delta T_0 = (T_{mean,ps})_0 - (T_{CMT})_0 \quad (6-93)$$

Table 6.34 below presents the numerical values of the *causative process related* Π -Groups for liquid temperature response during Phase 2. The *causative process related* Π -Groups show the significance of phenomena (system thermal compliance) and processes (external heating and cooling, CMT circulation) relative to the process of heat transfer to the PRHR system. To read Tables 6.34, through 6.36, recall the table description for Table 6.1 on page 6-24: each Π -Group is interpreted in the text next to the equation that defines it, and the defining equation is indicated in the first column of each table. The second column in Table 6.34 shows the same Π -Group symbols as defined in Eqs. (6-32) through (6-37), the third through sixth columns list the numerical values of the Π -Groups for the AP600 and the three related facilities APEX, ROSA, and SPES, and the last column is provided for comments explaining distortions, where applicable.

Table 6.34 Causative Process Related Π -Groups for Change of System Liquid Temperature During Subphase 2.1

Definition of Π -Group	Symbol of Π -Group	Π -Groups for				Comments
		AP600	APEX	ROSA	SPES	
Thermal Compliance of Liquid (EQ. (6-32))	$\Pi_{TC,2}$	5.16	10.67	6.57	7.22	
Cooling by PRHR Circulation (reference)	$\Pi_{T,PRHR}$	1	1	1	1	
Cooling by CMT Circulation on PRZ side (Eq. (6-37))	$\Pi_{T,CMT;A}$	0.37	0.39	0.29	0.38	
Cooling by CMT Circulation on side of break (Eq. (6-37))	$\Pi_{T,CMT;B}$	0.33	0.38	0.28	0.35	
Heating/Cooling of Single-Phase Liquid (Eq. (6-33))	$\Pi_{T,\dot{Q}_{1\varphi},2}$	0.34	1.22	0.68	0.37	
Effect of Break Flow (Eq. (6-36))	$\Pi_{T,bk,2}$	0.05	0.06	0.06	0.04	
SG and UHD Net Heat Transfer (Eq. (6-35))	$\Pi_{T,\dot{Q}_{2\varphi},2}$	0.05	0.004	0.06	0.08	

All geometric parameters appearing in the Π -Group definitions, Eqs. (6-32) through (6-37) are found in Appendix 1, i.e., in the data basedocument delivered separately to the NRC. The initial conditions and initial thermophysical properties are found also there in Appendix 4.3. The initial thermal compliance of the liquid and computed reference parameters appearing in the Π -Group definitions were computed through EXCEL and are listed in Appendix 5.2.

By the methods and criteria described in Sections 4.5 and 4.6, and summarized at the beginning of Section 6.2 on Page 6-22, it is seen from Table 6.34 that (1) the temperature change is nearly quasi-steady and PRHR cooling is the most important process affecting the change of primary system temperature; and (2) there are **three significant scale distortions, two in APEX and one in ROSA**, affecting the change of subcooled liquid temperature during Phase 2. Π -Groups in Table 6.34 which reflect scale distortions beyond the $\{1/2, 2\}$ limits established in Section 4.6 are printed in **red**. The distortions are discussed in detail later, on the basis of the fractional scaling groups in Table 6.37.

Core Make-up Tank, Before Accumulator Trip

The temperature change of the liquid in the Core Make-up Tank is modeled in Section 5.4.1.4 on the basis of energy conservation, Eq. (6-38) applied to the control volume of the single-phase liquid in the CMT, and for Phase 2 (see Figure 3.1 and Section 3.3.1 for the definition of Phase 2). The scaled equation for CMT temperature change is Eq. (6-39). The scaling groups are defined by Eqs. (6-40) and (6-41), shown in Section 6.1.3.1. The reference temperature difference is the same as for the primary system, see Eq. (6-93).

Table 6.35 below presents the numerical values of the *causative process related* Π -Groups for liquid temperature response in the CMT during Phase 2. As pointed out above, the *causative process related* Π -Groups show the significance of phenomena (system thermal compliance) and processes (external heating and cooling) relative to the process of convective heat transfer to the CMTs due to CMT circulation. Table 6.35 is to be interpreted as the previous Π -tables. The second column shows the same Π -Group symbols as defined in Eqs. (6-40) and (6-41), the third through sixth columns list the numerical values of the Π -Groups for the AP600 and the three related facilities APEX, ROSA, and SPES, and the last column is provided for applicable comments on distortions.

Table 6.35 Causative Process Related Π -Groups for CMT Cooling During Subphase 2.1

Definition of Π -Group	Symbol of Π -Group	Π -Groups for				Comments
		AP600	APEX	ROSA	SPES	
Thermal Compliance of CMT Liquid (Eq. (6-40))	$\Pi_{TC, CMT}$	1.93	4.17	3.16	2.23	Factor of 1.6 due to lower CMT flow in APEX relative to break flow (high CMT-loop impedance); factor of 1.5 due to lower temperature diff. $T_{ps} - T_{CMT}$
CMT Circulation Flow (reference)	$\Pi_{TW, CMT}$	1	1	1	1	
CMT Wall Heat Transfer (Eq. (6-41))	$\Pi_{T, \dot{Q}_{CMT}}$	0.02	0.01	0.06	0.02	

6. Scaling Groups

It is seen from Table 6.35, by the methods and criteria described in Sections 4.6 and 4.7, that the causative process of CMT circulation is also the dominant process, and that **there is one significant scale distortion in APEX**. The thermal compliance affecting the rate of change of liquid temperature in the CMT of APEX during Phase 2 is too large; the distortion is nonconservative.

Passive Residual Heat Rejection System, Before Accumulator Trip

The temperature change of the liquid on the tube side of the Passive Residual Heat Rejection System (PRHR) is also modeled in Section 6.1.3.1. The scaling groups are defined by Eqs. (6-42) and (6-43), shown in Section 6.1.3.1. The reference temperature difference is the same as for the primary system, see Eq. (6-93).

Table 6.36 below presents the numerical values of the *causative process related* Π -Groups for liquid temperature response in the PRHR during Phase 2. As pointed out above, the *causative process related* Π -Groups show the significance of phenomena (system thermal compliance) and processes (external heating and cooling) relative to the process of convective heat transfer to the PRHR due to PRHR circulation. Table 6.36 is to be interpreted as Table 6.35. Geometric parameters appearing in the Π -Group definitions, Eqs. (6.42) and (6-43), are found in Appendix 1. The initial conditions and initial thermophysical properties are found in Appendix 4.3. The computed reference parameters appearing in the Π -Group definitions were computed through EXCEL and are listed in Appendix 5.2.

Table 6.36 shows, by the methods and criteria described in Sections 4.5 and 4.6, that the causative process of PRHR circulation is also the dominant process, and that **there is no significant scale distortion** for PRHR cooling during Subphase 2.1 in any of the test facilities.

Table 6.36 Causative Process Related Π -Groups for PRHR Cooling During Subphase 2.1

Definition of Π -Group	Symbol of Π -Group	Π -Groups for				Comments
		AP600	APEX	ROSA	SPES	
PRHR Wall Heat Transfer (Eq. (6-43))	$\Pi_{T, \dot{Q}_{PRHR}}$	1.19	1.07	1.22	1.17	
PRHR Circulation Flow (reference)	$\Pi_{TW, PRHR}$	1	1	1	1	
Thermal Compliance of PRHR Liquid (EQ. (6-42))	$\Pi_{TC, PRHR}$	0.11	0.15	0.14	0.06	

Fractional Scaling of Temperature Response During Subphase 2.1, Before Accumulator Trip

Having completed the causative process related scaling of temperature change during Subphase 2.1, we turn now to the fractional scaling of the same temperature changes.

Tables 6.37, 6.38, and 6.39 present the *fractional* Π -Groups of temperature response in the primary system, the CMTs, and the PRHR system, respectively, during the Passive Heat Rejection Phase prior to the Accumulator trip, that is, the fractional Π -Groups for Subphase 2.1. The advantage of fractional scaling was introduced in Section 4.4.5.2 as presenting reference time ratios which measure the *fraction* to which a specific process is completed during the reference time of the system. The fractional Π -Groups show the impact that processes (external heating and cooling) have on the *time-rate of temperature change*, or, in other words, *how much* the tangent of the temperature vs. time curve in Figure 4.3 is rotated from the horizontal by the phenomenon associated with the row of the entry in the table and, consequently, *how important* that phenomenon is during the respective phase.

Included in Table 6.37 is the scaling group for the *release of stored energy* from the core to the coolant

$$\Pi_{T, \dot{Q}_{str}} = \frac{(Mc)_{fuel} + (Mc)_{str}}{(M_l c_{p,l})_0}, \quad (6-94)$$

where (Mc) is the heat capacity, with subscripts *fuel*, *str*, and *l* denoting fuel, structures, and liquid, respectively. The fuel includes the nuclear uranium oxide or the ceramic of the electrical heaters. The structures include the metal parts and vessel walls of the lower part of the reactor vessel.

The scaling group is the ratio of the thermal response times

$$t_{th} = \frac{\sum Mc}{\bar{h}_c A_w}, \quad (6-95)$$

for fuel and structures over that of the fluid, or equivalently, the ratio of the rate of energy release from structures over the rate of energy release from the coolant. The rates of energy release are estimated on the basis that the time rates of temperature change in coolant and structures are the same. The symbols \bar{h}_c and A_w are the mean convective heat transfer coefficient and heat transferring wall area.

Tables 6.37, 6.38, and 6.39 and the methods and criteria presented in Sections 4.5 and 4.6 are the basis for assessing importance of processes and scale distortion for the passive heat rejection Subphase 2.1, prior to the Accumulator discharge trip. For the thermal response of the liquid in the primary side, in the CMTs, and in the PRHR system, there are **eight important processes** (i.e., processes of first-order magnitude, see Section 4.5), namely five for the primary system, one for the CMT, and two for the PRHR temperature changes. One of the five for the primary system, i.e., the stored energy release, is of first-order priority. Both wall heating and convection by circulation in the PRHR are of first-order priority.

Table 6.37 shows **one important processes scale-distorted each in APEX, ROSA, and SPES**. The scale distortions are related in the last columns of the tables to the high heat capacity of the vessel solid structures in ROSA and SPES, and to the low-pressure operation and the small PRHR volume in APEX. The high heat capacities in ROSA and SPES reduce subcooling of the primary system faster than in AP600; the associated scale distortions are, therefore, *conservative*. The lesser cooling in APEX is also *conservative*.

Table 6.38 for CMT temperature change indicates one scale distortion in APEX. The lower temperature change in the CMT implies higher primary-system temperature. The APEX distortion of CMT temperature change is, therefore, *conservative*.

6. Scaling Groups

Table 6.37 Fractional Π -Groups for System Liquid Temperature Change During Subphase 2.1 (see Eqs. (6-48) and (6-49))

Definition of Π -Group	Symbol of Π -Group	Π -Groups for				Comments
		AP600	APEX	ROSA	SPES	
Stored Energy Release (Eq. (6-94))	$\Pi_{T, \dot{Q}_{str}}$	0.26	0.26	0.93	1.69	Large heat capacity of vessel internals in ROSA and SPES
Cooling by PRHR Circulation (Eq. (6-54))	$\Pi_{T, PRHR}$	0.19	0.09	0.15	0.14	Low PRHR mass flow rate in APEX (30 %); low-pressure properties (70 %)
Cooling by CMT Circulation on PRZ side (Eq. (6-53))	$\Pi_{T, CMT;A}$	0.07	0.04	0.04	0.05	
Heating/Cooling of Single-Phase Liquid (Eq. (6-51))	$\Pi_{T, \dot{Q}_{1\phi}}$	0.07	0.11	0.10	0.05	
Cooling by CMT Circulation on side of break (Eq. (6-53))	$\Pi_{T, CMT;B}$	0.06	0.04	0.04	0.05	
Effect of Break Flow (Eq. (6-49))	$\Pi_{T, bk}$	0.01	0.01	0.01	0.01	
SG and UHD Net Heat Transfer (Eq. (6-52))	$\Pi_{T, \dot{Q}_{2\phi}}$	0.01	4e-4	0.01	0.01	

Table 6.38 Fractional Π -Groups for CMT Cooling During Subphase 2.1

Definition of Π -Group	Symbol of Π -Group	Π -Groups for				Comments
		AP600	APEX	ROSA	SPES	
CMT Circulation Flow (reciprocal of Eq. (6-40))	$\Pi_{TW, CMT}$	0.52	0.24	0.32	0.45	Low rate of enthalpy injection in APEX: factor of 1.6 due to lower CMT flow; factor of 1.5 due to lower temperature diff. $T_{ps} - T_{CMT}$
CMT Wall Heat Transfer (Eqs. (6-41) and (6-40), division of former by latter)	$\Pi_{T\dot{Q}, CMT}$	0.01	0.00	0.02	0.01	Low wall heating rate in APEX due to small tank diameter (same flow velocity but heat transfer proportional to $d^{0.8}$)

By the criteria adopted in Section 4.6, Table 6.39 shows no scale distortions in any test facility.

Table 6.39 Fractional Π -Groups for PRHR Cooling During Subphase 2.1

Definition of Π -Group	Symbol of Π -Group	Π -Groups for				Comments
		AP600	APEX	ROSA	SPES	
PRHR Wall Heat Transfer (Eq. (6-43) divided by Eq. (6-42))	$\Pi_{T, \dot{Q}_{PRHR}}$	11.02	7.16	8.49	19.32	
PRHR Circulation Flow (reciprocal of Eq. (6-42))	$\Pi_{TW, PRHR}$	9.24	6.68	6.98	16.47	

Primary System, After Accumulator Trip

The Accumulator trip initiates water injection into the primary system and heat transfer from the Accumulator tanks to the nitrogen gas as it expands and cools off. The scaled temperature equation for system change dominated by PRHR cooling after Accumulator trip is given by Eq (6-45). It has, relative to the scaled equation for Subphase 2.1, the additional scaling group for nitrogen gas heating defined by Eq. (6-47) and the minor modification to the thermal response function, Eq. (6-46), as shown in Section 6.1.3.1 under “Primary System Temperature Change, after Start of Accumulator Injection.” The reference temperature difference for Subphase 2.2 is the same as for Subphase 2.1.

Table 6.40 below presents the numerical values of the *causative process related* Π -Groups for liquid temperature response during Subphase 2.2, i.e., after the Accumulators started to inject liquid into the primary system. The *causative process related* Π -Groups are those appearing in Eq. (6-45) and show, by their magnitude shown in the third column of Table 6.40 for AP600, the significance of phenomena (system thermal compliance) and processes (external heating and cooling, CMT circulation) relative to the process of heat transfer to the PRHR system. Table 6.40 for Subphase 2.2 shows almost the same results for primary-system temperature change as Table 6.34 for Subphase 2.1.

Table 6.41 presents the *fractional* Π -Groups of temperature response in the primary system during the Passive Heat Rejection Phase *after* the Accumulator trip, that is, the fractional Π -Groups for Subphase 2.2, according to Eq. (6-48). The advantage of fractional scaling was introduced in Section 4.4.5.2 as presenting reference time ratios which measure the fraction to which a specific process is completed during the reference time of the system. The fractional Π -Groups show the impact that processes (external heating and cooling) have on the *time-rate of temperature change*, or, in other words, *how much* the tangent of the temperature vs. time curve in Figure 4.3 is rotated from the horizontal by the phenomenon associated with the row of the entry in the table and, consequently, *how important* that phenomenon is during the respective phase.

All geometric parameters appearing in the Π -Group definitions, Eqs. Eqs. (6-32) through (6-37) and (6-47) are found in Appendix 1. The initial conditions and initial thermophysical properties are found in Appendix 4.3. The initial thermal compliance of the liquid and computed reference parameters appearing in the Π -Group definitions were computed through EXCEL and are listed in Appendix 5.2.

The scaling groups of Subphase 2.1 remain essentially unaltered for Subphase 2.2, i.e., after start of accumulator injection. Table 6.41 for Subphase 2.2 shows almost the same results for primary-system temperature change as Table 6.37 for Subphase 2.1. Based on the $\{1/2, 2\}$ limits established for scale distortion in Section 4.6, there are two significant scale distortions, both in APEX, affecting the change of subcooled liquid temperature during Subphase 2.2.

6. Scaling Groups

The influence of the heat transfer between Accumulator tank walls and nitrogen on the primary-system liquid temperature is insignificant. Therefore, what was found before for Subphase 2.1 applies to the entire Phase 2. While being important for scaling the depressurization, the partitioning of Phase 2 turned out to be unimportant for the thermal response of the liquid.

Table 6.40 Causative Process Related Π -Groups for System Liquid Temperature Change During Subphase 2.2 (Eq. (6-45))

Definition of Π -Group	Symbol of Π -Group	Π -Groups for				Comments
		AP600	APEX	ROSA	SPES	
Thermal Compliance of Liquid (Eq. (6-32))	$\Pi_{TC,2}$	4.77	10.47	6.02	6.81	Low PRHR power due to low PRHR flow and low primary syst. temp.
Cooling by PRHR Circulation (reference)	$\Pi_{T,PRHR}$	1	1	1	1	
Cooling by CMT Circulation on PRZ side (Eq. (6-37))	$\Pi_{T,CMT:A}$	0.37	0.39	0.29	0.38	
Cooling by CMT Circulation on side of break (Eq. (6-37))	$\Pi_{T,CMT:B}$	0.33	0.38	0.28	0.35	
Heating/Cooling of Single-Phase Liquid (Eq. (6-33))	$\Pi_{T,\dot{Q}_{1\varphi},2}$	0.32	1.20	0.64	0.35	Same as above.
Effect of Break Flow (Eq. (6-36))	$\Pi_{T,bk,2}$	0.09	0.11	0.10	0.08	
SG and UHD Net Heat Transfer (Eq. (6-35))	$\Pi_{T,\dot{Q}_{2\varphi},2}$	0.22	0.22	0.25	0.25	
Heating of Nitrogen by Accumulator (Eq. (6-47))	$\Pi_{T,ACC}$	7.9e-03	1.1e-02	7.8e-04	1.1e-02	

6.2.2.4 Flow Rates, Inertia and Impedance for Phase 2

It was shown in Section 5.4.2 that the dynamic interaction between system components takes place in the connecting pipes and that is modeled with the system momentum balance. There were four loops for AP600, APEX, and SPES modeled and scaled for Phase 1, and two loops for ROSA. For Phase 2, there are seven loops for AP600, APEX, and SPES, as can be seen in Figure 5.7. There are five loops for ROSA since in ROSA each Steam Generator has only one Cold Leg. The system momentum balance is the vector equation, Eq. (5-49), in Section 5.4.2, i.e., the set of loop momentum balances which provide, via the loop momenta, M_j , the volumetric flow rates, Φ_m , according to the linear algebraic equations, Eqs. (5-36). The scaling of Eq. (5-49) leads to the scaled momentum balance for natural circulation in Phase 2, Eq. (6-68). The two Π -Groups of that equation are defined in Eqs. (6-69) through (6-71) and scale the *global system response*. The transient splits and distribution of flows among the components in the seven loops for AP600, APEX, and SPES, and in the five loops for ROSA are scaled by the three metrics, or *scaling arrays* S_i , S_G , and S_p in Eq. (6-56) characterizing, respectively, the *distribution* of inertia, gravity, and flow resistance (impedance). S_i , S_G , and S_p are defined in Eqs. (6-62), (6-63), and (6-64).

Table 6.41 Fractional Π -Groups for System Liquid Temperature During Subphase 2.2 (see Eq. (6-48))

Definition of Π -Group	Symbol of Π -Group	Π -Groups for				Comments
		AP600	APEX	ROSA	SPES	
Stored Energy Release (Eq. (6-94))	$\Pi_{T, \dot{Q}_{str}}$	0.26	0.26	0.93	1.69	Large heat capacity of vessel internals in ROSA and SPES
Cooling by PRHR Circulation (Eq. (6-54))	$\Pi_{T, PRHR}$	0.21	0.10	0.17	0.15	Low PRHR mass flow rate in APEX (30 %); low-pressure properties (70 %)
Cooling by CMT Circulation on PRZ side (Eq. (6-53))	$\Pi_{T, CMT;A}$	0.08	0.04	0.05	0.06	
Cooling by CMT Circulation on side of break (Eq. (6-53))	$\Pi_{T, CMT;B}$	0.07	0.04	0.05	0.05	
Heating/Cooling of Single-Phase Liquid (Eq. (6-51))	$\Pi_{T, \dot{Q}_{1\phi}}$	0.07	0.12	0.11	0.05	
Effect of Break Flow (Eq. (6-49))	$\Pi_{T, bk}$	0.02	0.01	0.02	0.01	
SG and UHD Net Heat Transfer (Eq. (6-52))	$\Pi_{T, \dot{Q}_{2\phi}}$	0.05	0.02	0.04	0.04	
Heating of Nitrogen by Accumulator (Eq. (6-55))	$\Pi_{T, ACC}$	2.0e-03	1.5e-03	1.5e-04	1.7e-03	

The reference flow rates needed to evaluate Eqs. (6-62) through (6-67) are computed in Appendix 5.2 from the steady-state momentum balance for the respective loop; symmetry is used to determine the reference flows in the two and four loops, respectively, of ROSA and of AP600 and SPES. The gravity forces of the PRHR loop are used as gravity reference.

Table 6.42 presents the numerical values of the Π -Groups of dynamic component interaction and shows that main-loop flow impedance is initially not balanced by the reference gravity forces; inertia forces are small, the system re-adjusts flows in a small fraction of the system reference time, and the system is not at steady state. Table 6.42 reveals that impedance and gravity forces are not balanced at the beginning of Phase 2 because the high flow rates at the start of Phase 2, i.e., after the trip of the reactor coolant pumps. The imbalance initiates a sharp transient to natural circulation. The inertia forces are disproportionally small in ROSA and cause the fastest dynamic response of all facilities, the **global dynamic response is distorted in ROSA** by an order of magnitude, but the scale distortion is not expected to affect inventory or liquid subcooling temperature.

Table 6.43. By dividing the Π -Groups in the first two rows of Table 6.42, i.e., the scaling groups for impedance and gravity effects, through the Π -Groups for inertia shown in the last row of Table 6.42, one finds the fractional Π -Groups shown in Table 6.43. As a result of the small inertia Π -Groups in Table 6.42, one obtains very large Π -Groups reflecting very large rates of flow change (accelerations), and Table 6.42 shows again that the system adjusts very quickly to any changes in impedance change, such as changes in valve settings. Flow adjustments are much faster than those of pressure, level elevations, and temperature.

6. Scaling Groups

Table 6.42 Causative Process Related Π -Groups of Dynamic Interaction Between Components During Phase 2

Definition of Π -Group	Symbol of Π -Group	Π -Groups for				Comments
		AP600	APEX	ROSA	SPES	
System Impedance (Eq. (6-71))	$\Pi_{RS, GR}$	9.09	3.66	0.32	6.91	PRHR gravity in ROSA matches AP600, but the main-loop impedance is too low in ROSA
System Gravity (PRHR gravity is reference)	Π_{GR}	1	1	1	1	
System Inertia (Eq. (6-69))	$\Pi_{IN, GR}$	0.012	0.012	0.001	0.006	Aspect ratio L/A is 13 times greater in ROSA than in AP600, but W_{cr}/t_{ref} is 1/200 times that of AP600

Table 6.43 Fractional Π -Groups of Dynamic Interaction Between Components During Phase 2

Definition of Π -Group	Symbol of Π -Group	Π -Groups for				Comments
		AP600	APEX	ROSA	SPES	
System Impedance (Eqs. (6-71) and (6-69))	$\Pi_{\dot{W}RS, P}$	731	318	308	1097	Low main-loop impedance in APEX, high inertia, and low core flow.
System Gravity (reciprocal of Eq. (6-69))	$\Pi_{\dot{W}G, P}$	80	87	954	159	Low inertia in ROSA (7%), gravity matched

The Inertia Metric, S_i , is defined in Eq. (6-62) and obtained by applying that definition to the entries of Table 5.7 for AP600 and of the tables in Appendix 7 for AP600, ROSA and SPES. As explained in section 6.1.4.1, the diagonal -elements show the relative magnitude of the *loop inertia* associated with the loop of the row. The off-diagonal S_i -elements are a measure of the cross-coupling between the loops by inertia.

Notice that the S_i -elements in the row of only the main loops add up to one, because of the scaling relative to the Symmetric main loops (see Eq. (6-62)). The Inertia Metric reveals how quickly the flow re-adjusts in a loop segment to changes in flow conditions: the larger the S_i -elements of a row are, the slower responds the fluid in the loop associated with that row, and relative to the responses in other loops.

Table 6.44 Inertia Metric S_1 for Seven-Loop Operation During Phase 2, Passive Heat Rejection: AP600
(All lines being filled with single-phase liquid)

Loop		Flow Rate leaving from							Flow Rate from	
on Side	through	CMT Branch of Loop _{B1} to RPV	CMT Branch of Loop _{B2} to CMT _A	SG Exit of Loop _{A1}	SG Exit of Loop _{A2}	CMT Branch of Loop _{B1} to CMT _B	CMT Branch of Loop _{B2} to RPV	PRHR Branch of Loop _A to PRHR	Surge Line to Hot Leg of Loop _A	Break in Loop _{B1}
B	Cold Leg ₁	0.568	0.006	0.042	0.042	0.007	0.337	0	0	-0.001
A	CMT _A	-0.006	0.289	-0.006	-0.006	0	-0.159	0	0	0.000
A	Cold Leg ₁	0.042	0.001	0.568	0.337	0.001	0.042	-0.012	-0.007	-0.001
A	Cold Leg ₂	0.042	0.001	0.337	0.568	0.001	0.042	-0.012	-0.007	-0.001
B	CMT _B	-0.159	0	-0.006	-0.006	0.322	-0.006	0	0	0.000
B	Cold Leg ₂	0.415	0.007	0.042	0.042	0.007	0.568	0	0	-0.001
A	PRHR	0.042	0.001	0.314	0.109	0.001	0.042	0.816	-0.001	-0.001

By comparing the Inertia Metrics in Tables 6.45, 6.46, and 6.47 for APEX, ROSA, SPES, respectively, with the Inertia Metric in Table 6.44 for AP600, one assesses the inertia distortion, that is, the distortion of the dynamic response of the flows in the parallel loops and of the inertia coupling between the flows of the loops. The criteria of scale distortion, based on Π -Groups, have been adopted in Section 4.6. The same criteria are applied here to scaling metrics of inertia, gravity, and impedance: elements of inertia metrics of APEX, ROSA, and SPES which differ by more than a factor of two from the corresponding inertia metric element of AP600 are printed in **red** in Tables 6.45, 6.46, and 6.47.

The comparison of Tables 6.45 and 6.44 reveals that APEX has three inertia distortions of minor consequence, none in the main loops, one nonconservative in the PRHR loop, and two nonconservatives in the PRZ surge line.

ROSA is difficult to compare with AP600 because it has only one Cold Leg each on Sides A (with Pressurizer) and B. One could compute the seven and five eigenvalues, respectively, for AP600 and ROSA. While it is not possible to compare the eigenvalues directly, one could determine whether ROSA is stable or unstable where AP600 is not. However, ROSA has nineteen inertia distortions, five in the main loops, six in the CMT loops, three in the PRHR loop, two in the PRZ surge line, and three affecting the break flow. This large number of inertia distortions renders the comparison of stability domains to be a task beyond the scope of this scaling analysis. None of the inertia metric distortions affect the RPV inventory, even though nine of the nineteen inertia distortion in ROSA are, in principle, nonconservative. The extent to which the nonconservative distortions are compensated by the ten conservative distortions must be determined by simulation.

6. Scaling Groups

SPES has eight inertia distortions, none in the main loops, four nonconservatives in the CMT loops, one nonconservative in the PRHR loop, and three nonconservatives in the PRZ surge line. None of the inertia metric distortions affect the RPV inventory.

It should be recalled, that inertia distortions are important only temporarily during dynamic flow transients, during flow oscillations, and when rapid condensation accelerates the flow.

Table 6.45 Inertia Metric S_1 for Seven-Loop Operation During Phase 2, Passive Heat Rejection: APEX
(All lines being filled with single-phase liquid)

Loop		Flow Rate leaving from							Flow Rate from	
on Side	through	CMT Branch of Loop _{B1} to RPV	CMT Branch of Loop _{B2} to CMT _A	SG Exit of Loop _{A1}	SG Exit of Loop _{A2}	CMT Branch of Loop _{B1} to CMT _B	CMT Branch of Loop _{B2} to RPV	PRHR Branch of Loop _A to PRHR	Surge Line to Hot Leg of Loop _A	Break in Loop _{B1}
B	Cold Leg 1	0.575	0.004	0.036	0.036	0.006	0.344	0	0	-9.7e-04
A	CMT _A	-0.005	0.291	-0.005	-0.005	0	-0.214	0	0	1.3e-04
A	Cold Leg 1	0.036	4e-04	0.575	0.344	0.001	0.036	-0.010	-2.9e-04	-8.5e-04
A	Cold Leg 2	0.036	4e-04	0.344	0.575	0.001	0.036	-0.010	-2.9e-04	-8.5e-04
B	CMT _B	-0.211	0	-0.005	-0.005	0.397	-0.005	0	0	1.3e-04
B	Cold Leg 2	0.365	0.004	0.036	0.036	0.006	0.575	0	0	-9.7e-04
A	PRHR	0.036	4e-04	0.267	0.036	0.001	0.036	0.758	0	-9.7e-04

The Gravity Metric, S_G , defined by Eq. (6-31) has, for Phase 2, the distinct elements for the main and CMT loops that are shown in **Table 6.48**. The PRHR loop inertia term is dominant and the reference for gravity in Table 6.48 and also in Tables 6.42 and 6.43. The elements of S_G should be repeated once for CMT and, respectively, once and thrice for ROSA and for AP600 and SPES to make up all the gravity elements, $(S_G G^*)_j$, in the vector momentum equation, Eq. (6-68).

The Impedance Metric, S_p , is defined in Eq. (6-64) and obtained for Phase 2 by applying that definition to the entries of Table 5.14 for AP600, and of Tables A.8.1 through A.8.3 in Appendix 8 for APEX, ROSA, and SPES. Tables 6.49 through 6.52 show the S_p elements of the impedance metrics for AP600, APEX, ROSA, and SPES. As explained in Section 6.1.4.1, the S_p -elements in a row determine the *distribution of flow impedances* in the loop associated with that row, and, therefore, the flow distribution particularly as the steady state is being approached. Repeated S_p -elements in a column indicate *cross-coupling by impedance between the loops* that are associated with the rows containing the repeated S_p -elements. Table 6.49 with the impedance metrics for AP600 is on Page 6-66.

Table 6.46 Inertia Metric S_1 for Five-Loop Operation During Phase 2, Passive Heat Rejection: ROSA
(All lines being filled with single-phase liquid)

Loop		Flow Rate leaving from					Flow Rate from	
on Side	through	CMT Branch of Loop _{B1} to RPV	CMT Branch of Loop _{B2} to CMT _A	SG Exit of Loop _{A1}	CMT Branch of Loop _{B1} to CMT _B	PRHR Branch of Loop _A to PRHR	Surge Line to Hot Leg of Loop _A	Break in Loop _{B1}
B	Primary Loop	0.867	0.033	0.072	0.033	0	0	-5.1e-03
A	CMT _A	-0.099	1.094	-0.002	0.411	0	0	1.2e-04
A	Primary Loop	0.072	0.003	0.867	0.003	0.058	-3.4e-06	-5.1e-03
B	CMT,B	-0.099	0.004	-0.002	0.990	0	0	1.2e-04
A	PRHR	0.072	0.003	0.324	0.003	3.487	-4.1e-06	-5.1e-03

Table 6.47 Inertia Metric S_1 for Seven-Loop Operation During Phase 2, Passive Heat Rejection: SPES
(All lines being filled with single-phase liquid)

Loop		Flow Rate leaving from							Flow Rate from	
on Side	through	CMT Branch of Loop _{B1} to RPV	CMT Branch of Loop _{B2} to CMT _A	SG Exit of Loop _{A1}	SG Exit of Loop _{A2}	CMT Branch of Loop _{B1} to CMT _B	CMT Branch of Loop _{B2} to RPV	PRHR Branch of Loop _A to PRHR	Surge Line to Hot Leg of Loop _A	Break in Loop _{B1}
B	Cold Leg ₁	0.466	0.007	0.070	0.070	0.008	0.401	0	0	-0.002
A	CMT _A	-0.006	0.070	-0.006	-0.006	0	-0.016	0	0	1.8e-04
A	Cold Leg ₁	0.070	0.001	0.466	0.401	0.001	0.070	-0.017	2.8e-05	-0.001
A	Cold Leg ₂	0.070	0.001	0.401	0.466	0.001	0.070	-0.017	2.8e-05	-0.001
B	CMT,B	-0.016	0	-0.006	-0.006	0.069	-0.006	0	0	1.8e-04
B	Cold Leg ₂	0.436	0.008	0.070	0.070	0.008	0.466	0	0	-0.002
A	PRHR	0.070	0.001	0.118	0.072	0.001	0.070	0.556	4.8e-05	-0.002

6. Scaling Groups

Table 6.48 Gravity Metric S_G for Seven-Loop Operation During Phase 2, Passive Heat Rejection

Definition of Π -Group	Symbol of S_G -Group	S_G -Groups for				Comments
		AP600	APEX	ROSA	SPES	
Gravity Metric for PRHR Loop	$S_{G, PRHR}$	1	1	1	1	
Gravity Metric for CMT Loops	$S_{G, CMT}$	1.00	1.02	0.97	1.00	
Gravity Metric for Main Loops	$S_{G, main}$	0.004	0.010	0.090	0.003	Greater buoyancy in ROSA because of greater temperature difference (confirmed by test data)

Notice that the S_p -elements in the rows of only the main loops add up to one, as a consequence of the scaling according to Eq. (6-64) and of the symmetry among the four loops.

Table 6.49 Impedance Metric S_p for Seven-Loop Operation of AP600 During Phases 2 Through 4 ,

(for definition of S_p -elements, see Eq. (6-64); for identification of unscaled R -elements, see Table 5.13 and Fig. 5.12)

Loop		S_p elements of Loop Sections between Branch Points:								
on Side	through	RPV to PRHR of Loop _A	PRHR to SRL of Loop _A	(Remainder of) Hot Leg and SG	SG to CMT Branch in Loop _B	(Remainder of) Cold Leg	Upper Down-comer	Vessel from DVI to Upper Plenum	CMT from Cold Leg to DVI	PRHR from Hot Leg to SG in Loop _A
B	Cold Leg ₁	0	0	0.561	0.004	0.023	-0.003	0.416	0	0
A	CMT _A	0	0	0	0	0.023	0.003	0	0.134	0
A	Cold Leg ₁	0.004	0.019	0.538	0	0.026	-0.003	0.416	0	0
A	Cold Leg ₂	0.004	0.019	0.538	0	0.026	-0.003	0.416	0	0
B	CMT _B	0	0	0	0	0.023	0.003	0	0.169	0
B	Cold Leg ₂	0	0	0.561	0.004	0.023	-0.003	0.416	0	0
A	PRHR	0.004	0	0	0	0.026	-0.003	0.416	0	0.140

Table 6.49 above presents the S_p -elements of the AP600 reference impedance metric. The following pages present Tables 6.50 through 6.52 with the corresponding S_p -elements for APEX, ROSA, and SPES.

By comparing the Impedance Metrics in Tables 6.50, 6.51, and 6.52 for APEX, ROSA, SPES, respectively, with the Impedance Metric in Table 6.49 for AP600, one assesses the impedance distortion, that is, the distortion of the dynamic response of the flows in the parallel loops and of the impedance coupling between the flows of the interconnected loops in the system. The impedance metric is equally important for the distribution of the steady-state flows in the system.

The same criteria of scale distortion, as adopted in Section 4.6 for Π -Groups, are applied here to the scaling metrics of impedance: elements of impedance metrics of APEX, ROSA, and SPES which differ by more than a the factor of two from the corresponding impedance metric element of AP600 are printed in **red** in Tables 6.50, 6.51, and 6.52.

Table 6.50 presents the impedance metric for APEX, which has, in the formulation used in this report, 33 non-zero elements, the same number as AP600. Most of the impedances are concentrated in the Steam Generators, Cold Legs, and Vessel. For **APEX, 19 smaller of the 33 impedance metric elements are distorted**, all 19 distortions are caused by four loop sections with distorted flow resistances (primarily form losses): in PRHR and CMT Loops, in Cold Legs, and in the Upper Downcomer. All distortions imply greater flow resistance outside the reactor vessel of APEX than of AP600. This causes the coolant to prefer accumulation in the vessel of APEX more than in the reactor vessel of AP600, and the distortions are, therefore, not conservative. The importance, however, of the increased ex-vessel resistances must be assessed by simulation.

Table 6.50 Impedance Metric S_p for Seven-Loop Operation of APEX During Phases 2 Through 4,
(for identification of R , see Fig. 5.12)

Loop		S_p elements of Loop Sections between Branch Points:								
on Side	through	RPV to PRHR of Loop _A	PRHR to SRL of Loop _A	(Remainder of) Hot Leg and SG	SG to CMT Branch in Loop _B	(Remainder of) Cold Leg	Upper Downcomer	Vessel from DVI to Upper Plenum	CMT from Cold Leg to DVI	PRHR from Hot Leg to SG in Loop _A
B	Cold Leg 1	0	0	0.567	0.019	0.153	-0.073	0.334	0	0
A	CMT _A	0	0	0	0	0.156	0.073	0	0.246	0
A	Cold Leg 1	0.014	0.031	0.521	0	0.172	-0.073	0.334	0	0
A	Cold Leg 2	0.014	0.031	0.521	0	0.172	-0.073	0.334	0	0
B	CMT _B	0	0	0	0	0.153	0.073	0	0.265	0
B	Cold Leg 2	0	0	0.567	0.016	0.156	-0.073	0.334	0	0
A	PRHR	0.014	0	0	0	0.172	-0.073	0.334	0	0.281

6. Scaling Groups

Table 6.51 Impedance Metric S_p for Five-Loop Operation of ROSA During Phases 2 Through 4,
(for identification of R , see Fig. 5.12)

Loop		S_p elements of Loop Sections between Branch Points:									
on Side	through	RPV to PRHR of Loop _A	PRHR to SRL of Loop _A	(Remainder of) Hot Leg and SG	SG to CMT Branch in Loop _B	(Remainder of) Cold Leg	Upper Down-comer	Vessel from DVI to Upper Plenum	CMT from Branch Point to DVI *	CMT from Cold Leg to DVI	PRHR from Hot Leg to SG in Loop _A
B	Primary-Side Loop	0	0	0.070	0.001	0.003	2.1e-04	0.926	0	0	0
A	CMT _A	0	0	0	0	0.003	2.1e-04	0	1.371	2.607	0
A	Primary-Side Loop	0.002	0.001	0.067	0	0.004	2.1e-04	0.926	0	0	0
B	CMT _B	0	0	0	0	0.003	2.1e-04	0	1.371	2.845	0
A	PRHR	0.002	0	0	0	0.004	2.1e-04	0.926	0	0	4.018

* unique branch in ROSA

Table 6.52 Impedance Metric S_p for Seven-Loop Operation of SPES During Phases 2 Through 4,
(for identification of R , see Fig. 5.12)

Loop		S_p elements of Loop Sections between Branch Points:								
on Side	through	RPV to PRHR of Loop _A	PRHR to SRL of Loop _A	(Remainder of) Hot Leg and SG	SG to CMT Branch in Loop _B	(Remainder of) Cold Leg	Upper Down-comer	Vessel from DVI to Upper Plenum	CMT from Cold Leg to DVI	PRHR from Hot Leg to SG in Loop _A
B	Cold Leg ₁	0	0	0.653	0.038	0.003	0.267	0.039	0	0
A	CMT _A	0	0	0	0	0.003	-0.267	0	0.158	0
A	Cold Leg ₁	0.003	0.102	0.640	0	0.040	0.267	0.039	0	0
A	Cold Leg ₂	0.003	0.102	0.640	0	0.040	0.267	0.039	0	0
B	CMT _B	0	0	0	0	0.003	0.267	0	0.184	0
B	Cold Leg ₂	0	0	0.653	0.038	0.003	-0.267	0.039	0	0
A	PRHR	0.003	0	0	0	0.040	0.267	0.039	0	0.184

Table 6.51 shows the impedance metric for ROSA. ROSA has only 24 non-zero elements and is, therefore, difficult to compare with AP600: it has only one Cold Leg on each side and an atypical branch point in the CMT loops. The loop elements that are common to ROSA and AP600 are compared in Table 6.51. According to this table, **ROSA has 20 of 24 impedance elements distorted**, the 20 distortions are caused by eight loop sections with distorted flow resistances (primarily form losses): Hot Leg, PRHR and CMT Loops, CMT branch segment, two cold-leg segments, *vessel interior*, and Upper Downcomer. Most importantly, ROSA has greater flow resistance in the reactor vessel than AP600, which retards the flow into the core and makes the leading scale distortions of flow impedance in ROSA conservative.

Table 6.52 presents the impedance metric for SPES, which has 33 non-zero elements, the same number as AP600. For **SPES, 18 of 33 impedance metric elements are distorted**. The most important distortions are in the Upper Downcomer and retard DVI flows escaping through the cold leg. The distortions in SPES are caused by four loop sections with distorted flow resistances (primarily form losses): two cold-leg segments, vessel interior, and Upper Downcomer. Notice that SPES has much lower (1/10) resistance in the reactor vessel than AP600, which enhances the flow into the core and makes the leading scale distortions of flow impedance in SPES nonconservative. It should be noted, that impedance distortion are important during dynamic flow transients, flow oscillations, and when rapid condensation accelerates the flow, *as well as during quasi steady-state conditions*.

6.2.3 Phase 3, ADS-123 Depressurization

This section presents the results of the numerical evaluation of the Π -Groups for the Phase 3, the ADS-123 depressurization phase. See Table 3.1 on Page 3-2 which shows that this phase begins at the instant that the collapsed liquid level in at least one of the CMTs reaches the designer-specified 67%-volume mark, thereby opening the first three valve banks of the Automatic Depressurization System (ADS). The phase ends when the collapsed liquid level in one of the CMTs reaches the designer-specified 20%-volume mark, thereby tripping the fourth bank of ADS valves to open. Figure 3.1 identifies Phase 3 in the system pressure versus time plot. Table 3.1 lists the major events of Phase 3, and a brief description of Phase 3 is given in Section 3.3.

Presented in this section are the scaling groups for depressurization, system inventory depletion, and system temperature change. Flow rate scaling for Phase 3 is taken to be the same as for Phase 2 because there are no changes of the loop configurations in AP600, APEX, ROSA, and SPES, and the fluid density changes during Phase 2 in these facilities are taken to be the same. Consequently, the geometry-dominated flow distribution should be scaled or distorted during Phases 3 (and 4) approximately the same as during Phase 2. The scaling groups are presented in the general and reduced forms the characteristics and advantages of which are explained in Section 4.4.5.

The ADS-1 trip-signal is taken to open simultaneously valve banks 1, 2, and 3 because the time span between the first and last valve opening of 210 seconds is small compared with the 10^4 second duration of Phase 3. The reference time for scaling Phase 3 is the time it takes to displace the reference system volume V_0 through the ADS-123 valves with the initial critical volumetric flow rate, $(\Phi_{123})_0$, i.e., $t_{ref} = V_0 / (\Phi_{123})_0$, where the reference volume is the combined volume of the Steam Generators, the Pressurizer, the Core Make-up Tanks, the Accumulators, the PRHR tube-side volume, and the Cold Legs, Hot Legs, and Surge Line. The critical flow through the ADS-123 valves is computed as if homogeneous equilibrium choking occurred at the valve flow cross-section, with the flow entering the valves as steam (void fraction $\alpha = 1$) from the empty Pressurizer.

There is no unique ADS-123 valve flow cross-sectional area for the AP600 design. Instead a range of areas is proposed for certification. The proposed range of ADS-123 valve flow cross-sectional area for AP600 vary by the factor of 2 (Bessette Fax Transmission of May 28, 1998, 3:24 pm, from NRC to BNL). The results presented here were obtained with documented specifications (RELAP5, proprietary data), i.e., an area near the median of the NRC- specified range of ADS-123 valve flow cross-sectional areas, as shown in Appendix 1.2 of the data documentation that has been sent separately to the NRC. Some of the reported ADS-123 valve flow cross-sectional areas for AP600 are outside the NRC-specified range.

6. Scaling Groups

The estimated mass flow rate through the ADS-123 valves, $(W_{123})_0$, was compared with test data and found to be *greater* by 30, 3 and 12 %, respectively, for APEX, ROSA, and SPES (see Table 5.15). The estimated depressurization rates for APEX and ROSA, however, are 52% and 39% *smaller*, respectively, than the experimentally determined depressurization rates. There is no accuracy of the mass flow measurements reported for APEX, ROSA, and SPES. The mass flow rate is directly proportional to the valve flow cross-sectional area. Reported ADS-123 valve flow cross-sectional areas for APEX, for example, vary by the factor of 2.4 (see [7, p. 5-66; 15, p. 8-5]; OSU-NE 9204, p. 167; and Bessette Fax Transmission of May 28, 1998, 3:24 pm, from NRC to BNL). Orifice plates are being exchanged between tests, and it appears impossible to identify the correct ADS-123 valve flow cross-sectional area. The results reported here for APEX were obtained with ADS-123 valve flow cross-sectional area taken from [6, p. 3-64, Table 3.16-1] because this reference was published shortly after the completion of Test No. SB05, the subject of this scaling analysis.

The computed reference time, based on volume displacement, is shorter (approximately $\frac{1}{3}$ for all facilities) than the depressurization time computed according to Eqs. (6-74) through (6-78) which agrees with test data within 5% (see Table 5.15). However, t_{ref} as defined above is more directly related to the plant-specific geometry and specifications, and its choice does not affect the phenomena ranking or the scale distortion. The computation is found in Appendix 5.3.

The reference pressure difference, Δp_0 , is the difference between Accumulator trip set point pressure and the initial containment pressure (see Appendix 5.3). The selected Δp_0 assures the scaled pressure p^* to be of the order of unity.

The initial vapor, mixture, and liquid volumes determine the initial system compliances and are identified in Table 3.1 and shown in Figure 5.3; their values are computed from the volumes listed in Appendix 1.1, and shown in Appendix 5.2. The combination of reference pressure difference, reference time, and initial system mechanical compliance is confirmed by the comparison of the predicted initial depressurization rate with the depressurization rate obtained from the experiments; the comparison is shown in Table 5.15.

The reference cooling powers for PRHR, CMTs, reactor core, and Upper Head cooling power are computed in Appendix 5.3, using the mass flow rate of natural circulation which are obtained from the steady-state momentum balance discussed in Section 5.5 and shown also in Appendix 5.3.

6.2.3.1 Depressurization

Table 6.53 presents the numerical values of the *causative process related* Π -Groups of depressurization for Phase 3. They are obtained from the scaled *depressurization equation*, Eq. (6.1), applied to the control volume shown in Figure 5.3 for Phase 3 (see Figure 3.1 and Section 3.3.1 for the definition of Phase 3). The *causative process related* Π -Groups show the significance of phenomena (system elasticity or system pressure response to volume changes) and processes (external heating and cooling) relative to the dominant process of fluid discharge through the ADS-123 depressurization valves.

Each Π -Group in Table 6.53 is interpreted in the text of Section 6.1, next to the equation that defines it, and the defining equation is again indicated in the first column of Table 6.53. The second column shows the Π -Group symbol as used in Eq. (6-1), the third through sixth columns list the numerical values of the Π -Groups, and the last column explains distortions, if any.

All geometric parameters appearing in the Π -Group definitions, Eqs. (6-2) through (6-5) and (6-10) through (6-13) for Tables 6.53 and 6.54 are found in Appendix 1. The initial conditions and initial thermophysical properties are found in Tables A.4.4.1 and A.4.4.2 of Appendix 4.3. The initial system compliance and computed reference parameters appearing in the Π -Group definitions were computed through EXCEL and are listed in Appendix 5.3.

By the methods and criteria presented in Sections 4.5 and 4.6 for assessing importance of processes and scale distortion, Table 6.53 shows for depressurization during Phase 3, that the causative process of ADS-123 discharge is also the dominant process and that **there is one significant scale distortion each for PRHR condensation in APEX**

and in ROSA. The lower condensation rate retards inventory discharge less, and reduces subcooling temperature less in APEX and ROSA than in AP600. The two scale distortions are, therefore, conservative.

Table 6.53 Causative Process Related Π -Groups for ADS-123 Depressurization During Phase 3

Definition of Π -Group	Symbol of Π -Group	Π -Groups for				Comments
		AP600	APEX	ROSA	SPES	
Mechanical Compliance (Eq. (6-2))	Π_{MC}	1.57	1.57	1.42	1.92	
ADS-123 Discharge (reference)	$\Pi_{\Phi_{ref}}$	1	1	1	1	
Condensation in PRHR (Eq. (6-5))	$\Pi_{\dot{Q}_{2\phi, PRHR}}$	0.36	0.05	0.08	0.37	Small driving temperature difference in APEX, relative low PRHR heat transfer in APEX and Rosa.
Thermal Exp. by Decay Heating (Eq. (6-4))	$\Pi_{\dot{Q}_{1\phi, l}}$	0.02	0.01	0.04	0.03	
Break Flow (see paragraph above (Eq. (6-3))	$\Pi_{\Phi_{bk}}$	0.01	0.01	0.01	0.02	
Heating in SG (Eq. (6-4))	$\Pi_{\dot{Q}_{1\phi, SG, v}}$	7.5e-3	7.4e-3	7.1e-3	4.7e-3	
UHD Heating of vapor (Eq. (6-4))	$\Pi_{\dot{Q}_{1\phi, UHD, v}}$	6.9e-4	1.2e-3	1.3e-2	7.2e-2	
Heating in Accumulators (Eq. (6-6))	$\Pi_{\dot{Q}_{N_2}}$	5.2e-4	1.8e-4	3.8e-5	8.6e-4	

Table 6.54 presents the numerical values of the *fractional* Π -Groups. They are obtained from the scaled fractional depressurization equation, Eq. (6.7), applied to the control volume shown in Figure 5.3 for Phase 3. The *fractional* Π -Groups in Table 6.54 show the impact that processes (external heating and cooling) have on the time-rate of pressure change. Each *column* entry in Table 6.54 shows an estimate of the fractional pressure change caused by, or *how much* the tangent of the pressure vs. time curve in Figure 4.3 is rotated from the horizontal, by the phenomenon associated with the row of the entry and, consequently, *how important* that phenomenon is during Phase 3. The larger the entry, the stronger is the effect on the slope of the depressurization curve. Differences between the entries in a *row* of Table 6.54 imply differences in the system response due to the phenomenon associated with that row and, consequently, the strength of *scale distortion* for that phenomenon.

Both Tables 6.53 and 6.54 show that during Phase 3, the *discharge from the ADS-123 valves dominates depressurization*, followed by the condensation heat transfer in the Passive Residual Heat Rejection system. All other phenomena are found to have insignificant effects on depressurization during Phase 3.

6. Scaling Groups

By applying the methods and criteria presented in Section 4.6 for assessing scale distortion, one finds from Tables 6.53 and 6.54 also that the dominant process is scaled in all facilities and that **APEX and ROSA have one significant scale distortion each for PRHR condensation** during Phase 3. Since the lower condensation rate retards inventory discharge less and reduces subcooling temperature less in APEX and ROSA than in AP600, the two scale distortions are conservative.

Table 6.54 Fractional Π -Groups for Depressurization During Phase 3

Definition of Π -Group	Symbol of Π -Group	Π -Groups for				Comments
		AP600	APEX	ROSA	SPES	
ADS-123 Discharge (Eq. (6-13))	$\Pi_{\dot{p}, \Phi_{ref}}$	0.64	0.64	0.71	0.52	
Condensation in PRHR (Eq. (6-11))	$\Pi_{\dot{p}, \dot{Q}_{2\phi, PRHR}}$	0.23	0.03	0.06	0.19	Small driving temperature difference in APEX, relative low PRHR heat transfer in APEX and Rosa.
Thermal Exp. by Decay Heating (Eq. (6-10))	$\Pi_{\dot{p}, \dot{Q}_{1\phi, l}}$	0.014	0.005	0.026	0.015	
Break Flow (see paragraph above Eq. (6-8))	$\Pi_{\dot{p}, \Phi_{bk}}$	0.009	0.005	0.007	0.008	
Heating in SG (Eq. (6-10))	$\Pi_{\dot{p}, \dot{Q}_{1\phi, SG, v}}$	4.8e-3	4.7e-3	5.0e-3	2.4e-3	
UHD Heating of vapor (Eq. (6-10))	$\Pi_{\dot{p}, \dot{Q}_{1\phi, UHD, v}}$	4.4e-4	7.5e-4	9.1e-3	3.7e-2	
Heating in Accumulators (Eq. (6-12))	$\Pi_{\dot{p}, \dot{Q}_{N_2}}$	3.3e-4	1.1e-4	2.7e-5	4.5e-4	

6.2.3.2 Inventory Change

The system inventory changes during Phase 3 take place in the refilling of the pressurizer (PRZ) and in the draining of the Core Make-up Tanks (CMT). These two components are separate and, therefore, modeled and scaled individually. The scaling groups associated with the PRZ and CMT are collected below in Tables 6.55 and 6.56. Liquid inventory change during Phase 3 is modeled, as for the previous phases, as the compliment of vapor volume change. The model for the rate of vapor volume change is presented in Section 5.4.1.3. The scaling of the general vapor volume equation, Eq. (6.14) is presented in Section 6.1.2.1 and applied to the pressurizer. The CMT modification of the general vapor volume equation, Eq. (6.79) is found in Section 6.2.2.2.

Pressurizer Inventory Change During Phase 3

The scaled inventory equation, Eq. (6.14), is shown in Section 6.1.2.1. Equation (6.14) is applied to the PRZ volume as the control volume and modified for the PRZ having inflow through the surge line and discharge from the top

through the ADS-123 valves. The modified equation is simplified on the basis of the results in Table 6.53: the terms from PRHR phase change, Accumulator heating, single-phase liquid expansion, and break flow, all affecting flashing due to depressurization, are neglected relative to the depressurization caused by ADS-123 discharge. The scaling groups are evaluated for the conditions at the beginning of Phase 3 when the PRZ is filled with vapor ($\alpha = 1$), and when single-phase liquid enters the PRZ through the surge line.

The *causative process related* Π -Group of *volumetric compliance* equals the ratio of system over PRZ response times, divided by the correction due to flashing

$$\Pi_{VC,PRZ} = \frac{\frac{V_0}{V_{PRZ}}}{1 - V_{PRZ} \left(\frac{\Psi_{\alpha,PRZ}}{V \chi_V} \right)_0}, \quad (6-97)$$

where the reference volume, V_0 , is the same as defined above for the scaling of depressurization. The *causative process related* Π -Group of *PRZ heating* equals the ratio of vapor volume generation rate by wall heating over vapor volume discharge rate by ADS, divided by the correction due to flashing

$$\Pi_{V,\dot{Q},2\phi,PRZ} = \frac{\left(\frac{\dot{Q}_{PRZ}}{\rho_g h_{fg}} \right)_0}{1 - V_{PRZ} \left(\frac{\Psi_{\alpha,PRZ}}{\chi_V} \right)_0}, \quad (6-98)$$

where the heating rate, \dot{Q}_{PRZ} , is estimated from the thick-walled heat conduction model, as used in Eq. (5-56). The equation scaled by the *causative process related* method for the change of vapor volume in the Pressurizer is

$$\begin{aligned} \Pi_{VC,PRZ} \frac{d\alpha_{PRZ}}{dt^*} &= - \left(\alpha - V_{PRZ} \frac{(\Psi_{\alpha})_{PRZ}}{\chi_V} \right)^* \Phi_{ADS123}^* \\ &+ \Pi_{V,\dot{Q},2\phi,PRZ} \frac{\dot{Q}_{PRZ}^*}{(\rho_g h_{fg})^*} \end{aligned} \quad (6-99)$$

Table 6.55 below presents the numerical values of the *causative process related* Π -Groups for PRZ inventory change during Phase 3. The *causative process related* Π -Groups in Table 6.55 show the significance of phenomena (system volumetric compliance) and processes (external heating and cooling) relative to the process of ADS-123 valve discharge.

Table 6.55 is to be read in the manner as the previous tables. An explanation for the table entries is found on Page 6-24 for Table 6.1. All geometric parameters appearing in the Π -Group definitions, Eqs. (6-97) and (6-98) are found in Appendix 1. The initial conditions and initial thermophysical properties are found in Appendix 4.4. The initial system compliance and computed reference parameters appearing in the Π -Group definitions were computed through EXCEL and are listed in Appendix 5.3 of the data base document (submitted to the USNRC separately).

6. Scaling Groups

Table 6.55 Causative Process Related Π -Groups for PRZ Inventory Change During Phase 3

Definition of Π -Group	Symbol of Π -Group	Π -Groups for				Comments
		AP600	APEX	ROSA	SPES	
ADS Discharge (reference)	$\Pi_{V, \Phi_{ref}}$	1	1	1	1	
Volumetric Compliance (Eq. (6-97))	Π_{VC}	0.10	0.11	0.10	0.10	
Wall Heating (Eq. (6-98))	$\Pi_{V, \dot{Q}, 2\phi}$	0.079	0.005	0.003	0.001	

Table 6.55 for PRZ inventory change shows the dominance of the causative process of ADS-123 discharge, a rapid transient due to the small volumetric compliance, and no significant distortion.

Table 6.56 presents the numerical values of the *fractional* Π -Groups for PRZ inventory change during Phase 3. The fractional form of the scaled vapor volume equation is obtained by dividing Eq. (6.99) by the Π -Group of PRZ volumetric compliance, $\Pi_{VC,PRZ}$. The numerical values of the *fractional* Π -Groups for PRZ inventory change during Phase 3., shown in Table 6.56, are, therefore, obtained by dividing the elements of the first and last two rows in Table 6.55 by the respective elements in the second row of Table 6.55.

The *fractional* Π -Groups show the impact that processes (wall heating and ADS-123 discharge) have on the time-rate of liquid inventory change. Each *column* entry in Table 6.56 shows *how much* the tangent of the PRZ vapor inventory vs. time curve in Figure 4.3 is rotated from the horizontal by the phenomenon associated with the row of the entry and, consequently, *how important* that phenomenon is during Phase 3. The larger the entry in a row, the stronger is the effect on the rate of change of the liquid inventory in the Pressurizer. Differences between the entries in a *row* of Table 6.56 would imply differences in the system response due to the phenomenon associated with that row and, consequently, they would show the strength of *scale distortion relative to AP600* for that phenomenon on liquid refilling of the PRZ.

Table 6.56 Fractional Π -Groups for PRZ Inventory Change During Phase 3

Definition of Π -Group	Symbol of Π -Group	Π -Groups for				Comments
		AP600	APEX	ROSA	SPES	
ADS Discharge (Eq. (6-97))	$\Pi_{\dot{v}, \Phi_{ref}}$	9.61	9.37	10.07	9.73	
Wall Heating (Eqs. (6-98) and (6-97))	$\Pi_{V, \dot{Q}, 2\phi}$	0.76	0.05	0.03	0.01	

Based on the methods and the criterion given in Section 4.5, one sees from Table 6.55 that the “significant” discharge through the ADS-123 valves dominates the change of PRZ inventory during Phase 3. By combining the results presented in Tables 6.55 and 6.56 for the PRZ inventory during Phase 3 one finds **no distortion of a significant phenomenon**. See Sections 4.5 and 4.6, respectively, for the definitions of “significant phenomena” and “significant scale distortions.”

Inventory Change in Core Make-up Tanks During Phase 3

For Phase 3, the scaled inventory equation for the CMT is, as for Phase 2, the vapor mass balance, Eq. (6-79), shown in Section 6.2.2.2, since liquid inventory change is modeled as the compliment of vapor volume change. Equation (6-79) applies to the CMT volume as the control volume and is simplified on the basis of the results in Table 6.53: only the ADS-123 discharge term is retained for the CMT fluid dilatation due to flashing. The draining rate is computed from the steady-state momentum balance, Eq. (5-55). Since the CMT circulation is disrupted during Phase 3, the difference between draining and entering volumetric flow rates is computed from the volumetric flux divergence equation, Eq. (5-5), where the time rate of depressurization is given by Eq. (5-8). The heat transfer rate, $\dot{Q}_{2\phi, CMT}$, is computed from Eq. (6-86). The scaled inventory equation (normalized by the causative process of CMT flow) for the CMT is, from Eq. (6-79) after simplification,

$$\begin{aligned} \Pi_{VC, CMT} \frac{d\alpha_{CMT}}{dt^*} = & \Phi_{CMT}^* + \Pi_{V, \dot{Q}_{CMT}} \left(\frac{v_f}{h_{fg}} \right)^* \dot{Q}_{2\phi, CMT}^* \\ & + \Pi_{V, CMT, ADS} \left(\frac{\Psi_{\alpha, CMT}}{\chi_V} \right)^* \Phi_{ADS}^*, \end{aligned} \quad (6-100)$$

where the *causative process related* Π -Group of *volumetric compliance*, $\Pi_{VC, CMT}$, is the ratio of CMT over system reference times and defined by Eq. (6-81), the *causative process related scaling group for phase change in the CMT*, $\Pi_{V, CMT, \dot{Q}_{2\phi}}$, or the ratio of the rate of volume change due to phase change in the CMT over the rate of volume displaced by draining is defined by Eq. (6-84), and the *causative process related scaling group for the effect on the CMT draining from flashing due to volume displacement through the break*, $\Pi_{V, CMT, ADS}$, or the ratio of the CMT reference time over the CMT liquid volume response time to ADS flow, is defined by Eq. (6-85) with ADS-123 flow replacing the break flow.

Table 6.57 lists the *causative process related* Π -Groups defined by Eqs. (6-81), (6-84), and (6-85), for CMT inventory change during Phase 3 (see Figure 3.1 and Section 3.3.1 for the definition of Phase 3). All geometric parameters appearing in the Π -Group definitions, Eqs. (6-81) through (6-84) are found in Appendix 1. The fluid properties for the CMT which occur in Eqs. (6-81), (6-84), and (6-85) are evaluated with the initial CMT void fraction $(\alpha_{CMT})_0 = 0.33$. Reference parameters for the primary system which occur in Eqs. (6-81), (6-84), and (6-85) are the same as for the scaling of the Phase 3 depressurization discussed in Section 6.2.3.1 and shown in Appendix 5.3.

The *causative process related* Π -Groups in Table 6.57 show, through the magnitudes of the elements on a *column*, the significance of phenomena (CMT volumetric compliance) and processes (external heat transfer) relative to the process of fluid drainage from the CMT.

To read Table 6.57, recall that each Π -Group is interpreted in the text above next to the equation that defines it, and the defining equation is indicated in the first column of Table 6.57. The second column shows the Π -Group symbol as in Eq. (6-100) with the subscript *CMT* omitted (since CMT is in the table heading), the third through sixth columns list the numerical values of the Π -Groups for the AP600 and the three related facilities APEX, ROSA, and SPES, and the last column is provided for comments explaining distortions.

By the methods and criteria presented in Sections 4.5 and 4.6 for assessing importance of processes and scale distortion, Table 6.57 shows for CMT inventory change during Phase 3, that the causative process of CMT draining is also the dominant process and that **there is one significant scale distortion each in APEX and ROSA**. The larger volumetric compliance in APEX slows down the CMT draining and leads to a lower pressure at the end Phase 3. That scale distortion in APEX is, therefore, not conservative. The scale distortion on in ROSA is also nonconservative because it increases subcooling temperature more in ROSA than in AP600.

6. Scaling Groups

Table 6.57 Causative Process Related Π -Groups for CMT Inventory Change During Phase 3

Definition of Π -Group	Symbol of Π -Group	Π -Groups for				Comments
		AP600	APEX	ROSA	SPES	
CMT Volumetric Compliance (Eq. (6-81))	Π_{VC}	4.77	12.39	7.62	3.94	Rel. low CMT drainage flow in APEX.
CMT Draining (reference)	$\Pi_{V,drn}$	1	1	1	1	
Effect of CMT Phase Change (Eq. (6-84))	$\Pi_{V,\dot{Q}_{2\phi}}$	0.20	0.26	0.09	0.36	Rel. low CMT wall heat transfer rate in ROSA and high CMT flow rate.
Effect of ADS Flow (Eq. (6-85))	$\Pi_{V,ADS}$	1.8e-02	8.4e-03	3.6e-02	1.2e-02	

Table 6.58 presents the numerical values of the *fractional* Π -Groups for CMT drainage during Phase 3 (see Figure 3.1 and Section 3.3.1 for the definition of Phase 3). The *fractional* Π -Groups are introduced in Section 4.4.5.2. For CMT drainage during Phase 3, they are obtained by dividing the causative process related Π -Groups given in the last three rows of Table 5.57 by the elements in the first row of Table 5.57.

Table 6.58 Fractional Π -Groups for CMT Inventory Change During Phase 3

Definition of Π -Group	Symbol of Π -Group	Π -Groups for				Comments
		AP600	APEX	ROSA	SPES	
CMT Draining (Eq. (6-88))	$\Pi_{\dot{a},\Phi_{CMT}}$	0.21	0.08	0.13	0.25	Rel. low CMT drainage flow in APEX.
Effect of CMT Phase Change (EQ. (6-89))	$\Pi_{\dot{a},\dot{Q}_{CMT}}$	0.04	0.02	0.01	0.09	Rel. low CMT wall heat transfer rate in ROSA and high CMT flow rate; the opposite in SPES.
Effect of ADS-123 Flow (EQ. (6-92))	$\Pi_{\dot{a},CMT,ADS}$	3.8e-03	6.8e-04	4.7e-03	3.0e-03	

As explained in Section 4.4.5.2, the *fractional* Π -Groups show the impact that processes (external heating and draining) have on the time-rate of CMT liquid inventory change.

By the methods and criteria presented in Sections 4.5 and 4.6 for assessing importance of processes and scale distortion, Table 6.58 shows for importance of processes to CMT inventory change during Phase 3 the same results as Table 6.57, namely that the causative process of CMT draining is also the dominant process. However, for scale distortion, results from the two tables differ. **APEX, ROSA, and SPES have one significant scale distortion each.** The scale distortion in APEX and ROSA are nonconservative, as explained for Table 6.57. The scale distortion on in SPES is conservative.

6.2.3.3 Temperatures

During Phases 1 and 2, fluid dilation was shown to be insignificant, except during Subphase 1.2 when the large liquid volume of the primary system experienced full-power cooling in the steam generators and only decay heating in the core. Thus, liquid temperature change was important only during Subphase 1.2.

During Phase 3, the change of global system temperature follows the change in saturation temperature and is dominated by the change of pressure rather than the rates of heat transfer between structures and fluid. The change of system pressure is scaled in Section 6.2.3.1. Most importantly, the thermal expansion or contraction of the single-phase liquid has insignificant impact on depressurization and on liquid inventory. This is seen from the scaling results presented in Tables 6.53 through 6.58 in Sections 6.2.3.1 and 6.2.3.2. Therefore, evaluation of the scaling groups presented in Section 6.1.3.1 for Eq. (6-22) of the rate of temperature change would not reveal any new scale distortions and is omitted.

6.2.3.4 Flow Rates, Inertia and Impedance

The number of loops and the loop configurations in AP600, APEX, ROSA, and SPES are the same during Phases 2, 3 and 4. The flow through the ADS valves is choked flow and, as the break flow, determined by system pressure through quasi-steady momentum and mass balances for equilibrium critical-flow, rather than by inertia and flow impedances. Since all facilities have the same level elevations in the CMTs and the PRHR system is filled with steam on the tube side, there are no significant differences in the fluid density distributions among the facilities. The scaling for the momentum balance is dominated by the geometry affecting inertia and form losses (inertia). Therefore, evaluation for Phases 3 and 4 of the scaling groups presented in Section 6.2.2.4 for the momentum balance, Eq. (6-68), for natural circulation would not reveal any new scale distortions beyond those presented in Section 6.2.2.4 for Phase 2. The evaluation for Phases 3 and 4 of the scaling groups presented in Section 6.2.2.4 for the momentum balance and is, therefore, omitted.

6.2.4 Phase 4, ADS-4 Depressurization

This section presents the results of the numerical evaluation of the Π -Groups for the Phase 4, the ADS-4 blowdown phase. See Table 3.1 on Page 3-2 which shows that this phase begins at the instant that the collapsed liquid level in at least one of the CMTs reaches the designer-specified 20%-volume mark, thereby opening the fourth and last valve banks of the Automatic Depressurization System (ADS) at the top of vertical pipe sections emanating from each Hot Leg (see Fig. 5.9). The phase ends when the system pressure is sufficiently low for gravity draining from the In-containment Refueling Water Storage Tank (IRWST). Figure 3.1 identifies Phase 4 in the system pressure versus time plot. Table 3.1 lists the major events of Phase 4, and a brief description of Phase 4 is given in Section 3.4.

Presented in this section are the scaling groups for depressurization, system inventory depletion, CMT inventory draining, Reactor Pressure Vessel (RPV) inventory change and RPV temperature change. Flow rate scaling for Phase 4 is taken to be the same as for Phase 2 because there are no changes of the loop configurations in AP600, APEX,

6. Scaling Groups

ROSA, and SPES, and the fluid density changes during Phase 2 in these facilities are taken to be the same. Consequently, the geometry-dominated flow distribution should be scaled or distorted during Phases 4 approximately the same as during Phase 2. The scaling groups are presented in the general and reduced forms the characteristics and advantages of which are explained in Section 4.4.5.

Both ADS-4 valves are modeled to open simultaneously. The reference time for scaling Phase 4 is the time it takes to depressurize the primary system from the Phase 4-starting pressure, p_0 , to the end pressure, p_e , at which gravity permits injection from the IRWST. The reference time is computed from Eq. (5-52); the computation is shown in the last continuation of Table A.5.4 in Appendix 5.4, using the ADS-4 volumetric flow rate as the reference flow rate. The estimated reference time is compared, in the section for Phase 4 of Table 5.15, with the experimentally determined blowdown time.

The reference pressure drop, $\Delta p_0 = p_0 - p_e$, is computed in Table A.5.3 of Appendix 5.3, by integrating the depressurization equation, Eq. (5-8) to estimate p_0 , using the Accumulator trip set point pressure as the starting pressure for the integration. The integral of Eq. (5-8) is given by Eq. (5-53) and Eqs. (5-54) through (56). The end pressure, p_e , is computed from the specified containment pressure and the gravity head of the stagnant fluid in the IRWST. The estimated starting pressure is also compared, in the section for Phase 4 of Table 5.15, with the experimentally determined starting pressure.

The reference volumetric flow rate is computed as critical homogeneous equilibrium flow, using the Phase 4-starting pressure and the core exit vapor mass fraction that was obtained with the drift flux model for churn-turbulent bubbly flow. The computation is found in Appendix 4.5, and the comparison with experimental flow rates in Table 5.15.

The initial vapor, mixture, and liquid volumes determine the initial system compliances and are identified in Table 3.1 and shown in Figure 5.4; their values are computed from the volumes listed in Appendix 1.1, and shown in Appendix 5.4. The combination of reference pressure difference and initial system mechanical compliance is confirmed by the comparison of the predicted blowdown time with the blowdown time obtained from the experiments (see Table 5.15).

The reference cooling powers for PRHR, CMTs, reactor core, and Upper Head cooling power are computed in Appendix 5.4, using the mass flow rate of natural circulation which are obtained from the steady-state momentum balance discussed in Section 5.5 and shown also in Appendix 5.4.

6.2.4.1 ADS-4 Depressurization

Table 6.59 presents the numerical values of the *causative process related and fractional* Π -Groups of primary-system depressurization during Phase 4. They are obtained from the scaled *depressurization equation*, Eq. (6.1), applied to the control volume shown in Figure 5.4 for Phases 4 (see Figure 3.1 and Section 3.3.1 for the definition of Phase 4). The *causative process related* Π -Groups show the significance of phenomena (system elasticity or system pressure response to volume changes) and processes (external heating and cooling) relative to the dominant process of fluid discharge through the ADS-4 depressurization valves. The *causative process related* Π -Groups are the same as the *fractional* Π -Groups because the reference time for Phase 4 is the characteristic time of depressurization.

Table 6.59 is read as all previous tables: each Π -Group is interpreted in the text of Section 6.1.1.1, next to the equation that defines it, and the defining equation is again indicated in the first column of Table 6.59. The second column shows the Π -Group symbol as used in Eq. (6-1), the third through sixth columns list the numerical values of the Π -Groups for AP600 and the related test facilities, and the last column explains distortions. All geometric parameters appearing in the Π -Group definitions, Eqs. (6-2) through (6-5) and (6-10) through (6-13) for Tables 6.59 and 6.60 are found in Appendix 1. The initial conditions and initial thermophysical properties are found in Tables A.4.5.1 and A.4.5.2 of Appendix 4.5. The initial system compliance and computed reference parameters appearing in the Π -Group definitions were computed through EXCEL and are listed in Appendix 5.4 of the data base document.

Table 6.59 Causative Process Related and Fractional Π -Groups for ADS-4 Blowdown During Phase 4

Definition of Π -Group	Symbol of Π -Group	Π -Groups for				Comments
		AP600	APEX	ROSA	SPES	
Mechanical Compliance (set equal to 1, to define reference time)	Π_{MC}	1	1	1	1	
ADS-4 Blowdown, (reference)	$\Pi_{\Phi_{ADS-4}}$	1	1	1	1	
Boiling Heat Transfer in Core (Eq. (6-5))	$\Pi_{\dot{Q}_{2\varphi}}$	0.98	6.40	3.48	1.02	Low pressure in APEX; low subcooling in APEX and ROSA.
ADS-123 Depressurization, (Eq. (6-3))	$\Pi_{\Phi_{ADS-123}}$	0.08	0.07	0.09	0.04	
Heating in Accumulators (Eq. (6-6))	$\Pi_{\dot{Q}_{N_2}}$	0.011	6.2e-4	4.3e-5	4.1e-4	
Thermal Exp. of Subcooled Liquid by Decay Heating (Eq. (6-4))	$\Pi_{\dot{Q}_{1\varphi,l}}$	1.8e-3	8.5e-4	9.4e-4	6.1e-4	
Break Flow (see paragraph above (Eq. (6-3))	$\Pi_{\Phi_{bk}}$	1.4e-3	3.3e-3	1.7e-3	5.9e-4	

The *fractional* Π -Groups of primary-system depressurization during Phase 4, which were introduced in Section 4.4.5.2, are identical to the *causative process related* Π -Groups listed in Table 6.59, because the choice of reference time renders the Π -Group of mechanical compliance to be equal to 1. Thus, the *causative process related* Π -Groups in Table 6.59 show also the impact that processes (external heating and cooling) have on the time-rate of pressure change: each *column* entry in Table 6.59 shows *how much* the tangent of the pressure vs. time curve in Figure 4.3 is rotated from the horizontal by the phenomenon associated with the row of the entry and, consequently, *how important* that phenomenon is during the respective phase. Differences between the entries in a *row* of Table 6.59 imply differences in the system response due to the phenomenon associated with that row and, consequently, the strength of *scale distortion* for that phenomenon.

Table 6.59 shows that during Phase 4, the *discharge from the ADS-4 valves and phase change in the core dominate depressurization*. All other phenomena are found to have insignificant effects on depressurization. For depressurization during Phase, **there are two significant scale distortions in the core vapor generation rate: one in APEX and one in ROSA**. The distortion is due to the relative lower core inlet subcooling and larger evaporation rate in APEX and ROSA, and to the low pressure in APEX. The phase change in APEX and ROSA are relatively greater than in AP600, causing greater expulsion of inventory from the primary system, and the scale distortions are, therefore, conservative

6.2.4.2 Inventory Changes During Phase 4

The system coolant inventory is depleted during Phase 4 by fluid discharge of initially critical homogeneous equilibrium flow through the ADS-4 valves, and by fluid discharge through the ADS-123 valves and spargers where the flow becomes

6. Scaling Groups

subcritical early in Phase 4. Scaled are for this phase the inventory changes in the whole primary system, the Reactor Pressure Vessel, the Pressurizer, and the Core Make-up Tanks.

The scaled system vapor inventory equation, Eq. (6.14), is shown in Section 6.1.2.1. Equation (6.14) is applied to the system control volume shown in Figure 5.4, with the components as described in Table 3.1.

System Inventory Change During Phase 4

Table 6.60 below presents the numerical values of the *causative process related* Π -Groups for system inventory change during Phase 4. The *causative process related* Π -Groups in Table 6.60 show the significance of phenomena (system volumetric compliance) and processes (external heating and cooling) relative to the process of ADS-4 valve discharge.

Table 6.60 is read as the previous tables, according to the explanation given on Page 6-24 for Table 6.1. While phase change effects appear unimportant for AP600, they are significant in APEX. The scale distortion is, however, conservative and has the same cause as the APEX scale distortion for depressurization.

Table 6.60 Causative Process Related Π -Groups for System Inventory Change During Phase 4

Definition of Π -Group	Symbol of Π -Group	Π -Groups for				Comments
		AP600	APEX	ROSA	SPES	
ADS-4 Discharge (reference)	$\Pi_{V, \Phi_{ADS-4}}$	1	1	1	1	
Volumetric Compliance (Eq. (6-15))	Π_{VC}	0.35	0.41	0.42	0.29	
ADS-123 Discharge ($\Phi_{ADS-123} / \Phi_{ADS-4}$)	$\Pi_{V, \Phi_{ADS-123}}$	0.08	0.07	0.09	0.04	
Phase Change Effects (Eq. (6-16))	$\Pi_{V, \dot{Q}, 2\phi}$	3.8e-2	3.7e-1	9.5e-2	6.9e-2	High evaporation rate at low pressure in APEX
Thermal Exp. of Single-Phase Liquid (Eq. (6-4))	$\Pi_{V, \dot{Q}, 1\phi}$	1.8e-3	8.5e-4	9.4e-4	6.7e-4	
Break Flow (Φ_{bk} / Φ_{ADS-4})	$\Pi_{V, bk}$	1.4e-3	3.3e-3	1.7e-3	5.9e-4	
Accumulator Heating (Eq. (6-12))	$\Pi_{V, \dot{Q}_{N_2}}$	1.7e-4	4.2e-8	1.0e-7	2.0e-9	

Table 6.61 presents the numerical values of the *fractional* Π -Groups for system inventory change during Phase 4. The fractional form of the scaled vapor volume equation is Eq. (6.17). The numerical values of the *fractional* Π -Groups for system inventory change during Phase 4 are obtained by dividing the elements of the first and the last five rows in Table 6.60 by the respective elements in the second row of Table 6.60. The *fractional* Π -Groups show the impact that processes (wall heating and ADS-123 discharge, etc.) have on the time-rate of system liquid inventory change.

See Sections 4.5 and 4.6 for the method and criteria for evaluating Table 6.61. Tables 6.60 and 6.61 show that system inventory changes during Phase 4 are dominated in AP600 by ADS-4 flow rate, and that there are no significant scale

distortions in ROSA and SPES. **APEX has one phenomenon distorted which is not important for AP600:** boiling in the core is more pronounced in APEX than in AP600 because of lower subcooling in the core and because the vessel pressure is relatively low in APEX. The scale distortion is, however, conservative and has the same cause as the APEX scale distortion for depressurization.

Table 6.61 Fractional Π -Groups for System Inventory Change During Phase 4

Definition of Π -Group	Symbol of Π -Group	Π -Groups for				Comments
		AP600	APEX	ROSA	SPES	
ADS-4 Discharge (reference)	$\Pi_{\dot{\alpha}, \Phi_{ADS-4}}$	2.91	2.41	2.39	3.49	
ADS-123 Discharge ($\Phi_{ADS-123} / \Phi_{ADS-4}$)	$\Pi_{\dot{\alpha}, \Phi_{ADS-123}}$	0.23	0.18	0.22	0.13	
Phase Change Effects (Eq. (6-16))	$\Pi_{\dot{\alpha}, \dot{Q}, 2\phi}$	0.11	0.88	0.23	0.24	High evaporation rate at low pressure
Thermal Exp. of Single-Phase Liquid (Eq. (6-4))	$\Pi_{\dot{\alpha}, \dot{Q}, 1\phi}$	5.2e-3	2.0e-3	2.3e-3	2.3e-3	
Break Flow (Φ_{bk} / Φ_{ADS-4})	$\Pi_{\dot{\alpha}, bk}$	4.2e-3	8.0e-3	4.2e-3	2.0e-3	
Accumulator Heating (Eq. (6-12))	$\Pi_{\dot{\alpha}, \dot{Q}_{N_2}}$	4.9e-4	1.0e-7	2.4e-7	6.9e-9	

Inventory Change in Reactor Pressure Vessel

The liquid inventory change in the Reactor Vessel (RPV) is modeled for Phase 4 as the equation for the time rate of liquid volume change and normalized to obtain this scaled equation in terms of the liquid mass flows entering the RPV, the subcooling enthalpy flow at the core entrance, and the time rate of pressure change (which is scaled in Section 6.2.4.1). The liquid inventory equation, scaled by the causative process related scaling method, is:

$$\begin{aligned}
 \Pi_{VC, RPV} \frac{d\alpha_{l, RPV}}{dt^*} = & \sum_{ADS, CMT, PRZ, bk} \Pi_{V, W_l} W_l^* - \Pi_{V, \dot{Q}_{2\phi}} \frac{\dot{Q}_{2\phi}^*}{h_{fg}^*} \\
 & + \Pi_{V, sub} W_{CR}^* \left(\frac{\Delta h_{sub}}{h_{fg}} \right)^* \\
 & - \Pi_{V, \dot{p}} \left(\frac{1 - \sum_{f, g} \alpha_k \rho_k h_k'}{h_{fg}} + \alpha_f \rho_f' \right)^* \dot{p}^*, \quad (6-101)
 \end{aligned}$$

6. Scaling Groups

where the ADS-4 flow is the term of the causative process, i.e., $\Pi_{V, W_{ADS-4}} = 1$, and the scaling group of the *volumetric compliance*, or the ratio of RPV over system (depressurization) response times is given by

$$\Pi_{VC, RPV} = \frac{V_{RPV}(\rho_l)_o (\Phi_{ADS-4})_o}{\Delta p_o (\chi_V)_o (W_{ADS-4})_o}, \quad (6-102)$$

and the scaling groups of vessel *liquid in and out flows* for in flows from the CMTs and the PRZ, and the out flows to the break are given by the ratios

$$\Pi_{V, W_l} = \frac{(W_l)_o}{(W_{ADS-4})_o}, \quad (6-103)$$

the scaling group of *core heating* or the ratio of the decay heat power over the ADS-4 enthalpy discharge rate is given by

$$\Pi_{V, \dot{Q}_{2\phi}} = \frac{(\dot{Q}_{CR})_o}{(h_{fg} W_{ADS-4})_o}, \quad (6-104)$$

the scaling group of *subcooling in the core*, or the ratio subcooling enthalpy over ADS-4 discharge enthalpy flow rates is given by

$$\Pi_{V, sub} = \frac{(\Delta h_{sub} W_{CR})_o}{(h_{fg} W_{ADS-4})_o}, \quad (6-105)$$

and the scaling group of *depressurization effects on RPV liquid inventory*, or the ratio of mass displacement rate due to flashing over mass displacement rate due to ADS-4 discharge is given by

$$\Pi_{V, \dot{p}} = \frac{V_{2\phi} (\Phi_{ADS-4})_o}{(\chi_V W_{ADS-4})_o} \left| \frac{1 - \rho_f h_f'}{h_{fg}} + \rho_f' \right|_o. \quad (6-106)$$

All the symbols in Eqs. (6-102) through (6-106) have the same definitions as given in the previous Π -Group definitions for Phase 4. Geometric parameters appearing in Eqs. (6-102) through (6-106) are found in Appendix 1, the initial and operating conditions in Appendix 4.5, and the evaluation of the Π -Groups in Eqs. (6-102) through (6-106) is presented in Appendix 5.4 of the proprietary data base document (submitted separately to the USNRC).

Table 6.62 lists the numerical values of the *causative process related* Π -Groups for PRV inventory change during Phase 4, defined by Eqs. (6-102) through (6-106). The *causative process related* Π -Groups listed in the third through sixth columns of Table 6.62 show, through their relative magnitude, the significance of phenomena (system volumetric compliance) and processes (external heating and cooling) relative to the process of ADS-4 valve discharge.

Table 6.62 is read as the previous tables, according to the explanation given on Page 6-24 for Table 6.1. By the methods and criteria described in Sections 4.5 and 4.6, and summarized at the beginning of Section 6.2 on Page 6-22, one finds from Table 6.62 that (1) the flow from PRZ is the dominant process (at least initially); and (2) **there are one scale distortion each in APEX and ROSA, and two in SPES**. ROSA and SPES have backfilling of the PRZ (see the negative signs in Table 6.62), a conservative scale distortion. The scale distortion in APEX is nonconservative. PRZ injection is not scaled by any test facility and affects the inventory in the reactor vessel at the beginning of Phase 5, when the minimum inventory is expected in the vessel.

Table 6.62 Causative Process Related Π -Groups for RPV Inventory During Phase 4

Definition of Π -Group	Symbol of Π -Group	Π -Groups for				Comments
		AP600	APEX	ROSA	SPES	
Effect of PRZ Injection (Eq. (6-103))	$\Pi_{V, W_{PRZ}}$	2.11	8.09	-2.10	-0.94	Low ADS-4 flow in APEX; inflow in PRZ of ROSA and SPES
ADS-4 Flow (reference)	$\Pi_{V, W_{ADS-4}}$	1	1	1	1	
RPV Volumetric Compliance (Eq. (6-102))	$\Pi_{VC, RPV}$	0.65	1.11	0.54	0.52	
Effect of CMT Injection (Eq. (6-103))	$\Pi_{V, W_{CMT}}$	0.37	0.31	0.26	0.13	Rel. high ADS-4 flow in SPES
Effect of ADS-123 Discharge (Eq. (6-103))	$\Pi_{V, W_{ADS-123}}$	0.10	0.09	0.11	0.05	
Effect of Phase Change in Core (Eq. (6-104))	$\Pi_{V, \dot{Q}_{2\phi}}$	0.07	0.07	0.06	0.03	
Effect of Subcooling in Core (Eq. (6-105))	$\Pi_{V, sub}$	0.06	0.04	0.04	0.02	
Effect of RPV Flashing (Eq. (6-106))	$\Pi_{V, \dot{p}}$	1e-3	1e-3	5e-4	2e-3	
Effect of Break Flow (Eq. (6-103))	$\Pi_{V, bk}$	7e-3	2e-2	6e-3	3e-3	

6. Scaling Groups

Table 6.63 presents the numerical values of the *fractional* Π -Groups for RPV inventory change during Phase 4. The scaled liquid volume equation, based on the fractional scaling method, is obtained by dividing Eq. (6-101) by the Π -Group of RPV volumetric compliance, $\Pi_{VC,RPV}$. Consequently, the numerical values of the *fractional* Π -Groups for RPV inventory change during Phase 4., shown in Table 6.63, are obtained by dividing the elements of the first and last seven rows in Table 6.62 by the respective elements in the second row of Table 6.62. The *fractional* Π -Groups show the impact that processes (wall heating and injection flow rates) have on the time-rate of liquid inventory change.

Table 6.63 is arranged consistently with the previously presented tables, each entry showing the fractional change of RPV inventory, i.e., *how much* the tangent of the RPV liquid inventory vs. time curve in Figure 4.3 is rotated from the horizontal by the phenomenon associated with the row of the entry. Consequently, the entries of a *column* show *how important* that phenomenon is for the facility of the column during Phase 4. Differences between the entries in a *row* of Table 6.63 imply differences in the system response (relative to AP600) due to the phenomenon associated with that row and, consequently, they show the strength of *scale distortion* for that phenomenon on liquid inventory of the RPV.

Table 6.63 Fractional Π -Groups for RPV Inventory During Phase 4

Definition of Π -Group	Symbol of Π -Group	Π -Groups for				Comments
		AP600	APEX	ROSA	SPES	
Effect of PRZ Injection (Eqs. (6-103) and (102))	$\Pi_{\dot{u}_p, W_{PRZ}}$	3.30	7.32	-3.88	-1.81	Low ADS-4 flow in APEX; <i>inflow</i> in PRZ of ROSA and SPES
ADS-4 Flow (reciprocal of Eq. (6-102))	$\Pi_{\dot{u}_p, W_{ADS-4}}$	1.57	0.90	1.84	1.93	
Effect of CMT Injection (Eqs. (6-103) and (102))	$\Pi_{\dot{u}_p, W_{CMT}}$	0.58	0.28	0.48	0.24	Rel. high ADS-4 flow in SPES
Effect of ADS-123 Discharge (Eqs. (6-103) and (102))	$\Pi_{\dot{u}_p, W_{ADS-123}}$	0.16	0.08	0.21	0.09	
Effect of Phase Change in Core (Eqs. (6-104) and (102))	$\Pi_{\dot{u}_p, \dot{Q}_{2\phi}}$	0.11	0.06	0.12	0.05	
Effect of Subcooling in Core (Eqs. (6-105) and (102))	$\Pi_{\dot{u}_p, sub}$	0.09	0.03	0.07	0.03	
Effect of RPV Flashing (Eqs. (6-106) and (102))	$\Pi_{\dot{u}_p, \dot{p}}$	1.1e-2	1.5e-2	1.2e-2	4.9e-3	
Effect of Break Flow (Eqs. (6-103) and (102))	$\Pi_{\dot{u}_p, bk}$	1.5e-3	8.9e-4	9.0e-4	3.1e-3	

Based on the definitions, criteria, and methods discussed in Sections 4.5 and 4.6 for importance of processes and relevant distortions, respectively, one sees from Tables 6.62 and 6.63 that PRZ, CMT, and ADS-4 flows dominate the change of RPV inventory in AP600 during Phase 4, and that for the RPV inventory change during Phase 4 there are **one scale distortion each in APEX and ROSA, and two in SPES**. While AP600 and APEX have *draining* from the Pressurizer into the reactor vessel (according to the estimated liquid level elevation and the flow resistances in the surge line and Hot Leg), ROSA and SPES have *refilling* (see also the above negative $\Pi_{\dot{u}_p, W_{PRZ}}$ -values in Table 6.63)

of the Pressurizer at the beginning of Phase 4. The scale distortions of PRZ injection in ROSA and SPES are conservative, the one in APEX is nonconservative. Both scale distortions in SPES are conservative.

PRZ injection is not scaled by any test facility and affects the inventory in the reactor vessel during Phase 4 and therefore at the beginning of Phase 5, when the minimum inventory is expected in the vessel. However, the quantitative assessment of the effect from PRZ injection is to be determined by simulation, since the PRZ injection cannot be expected to last the whole of Phase 4. The ADS-4 flow in APEX is low on account of the relatively low APEX pressure. This gives rise to the large $\Pi_{V,W_{PRZ}}$ -value in Table 6.62, and its associated value in Table 6.63.

Inventory Change in Core Make-up Tank During Phase 4

For Phase 4, the scaled inventory equation for the Core Make-up Tanks (CMT) is, as for Phases 2 and 3, the vapor mass balance, Eq. (6-79), shown in Section 6.2.2.2, since liquid inventory change is modeled as the compliment of vapor volume change. Equation (6-79) applies to the CMT volume as the control volume and is simplified here on the basis of the results in Table 6.59: the ADS-4 discharge and the last four unimportant phenomena in Table 6.59 which all cause flashing are combined and normalized directly with the reference depressurization rate according to Eq. (5-52):

$$\frac{\Delta p_0}{\Delta t_{\Delta p}} = \frac{\chi_{V,0} V}{(\Phi_{ADS-4})_0}, \quad (6-107)$$

where $\Delta t_{\Delta p}$ is the reference time of Phase 4, as explained in the third paragraph of Section 6.2.4. This combination eliminates the repetition of scaling groups that have already been ranked and assessed in Section 6.2.4.1. The reference volumetric flow rate is the initial vapor volumetric flow rate through the Pressure Balance Lines (PBL) which is estimated from the volumetric flow rate of liquid draining and the volumetric condensation rate.

$$(\Phi_{PBL})_0 = (\Phi_{CMT})_0 - \left(\frac{v_{fg}}{h_{fg}} \dot{Q}_{CMT, 2\phi} \right)_0, \quad (6-108)$$

where the volumetric flow rate of CMT drainage, $(\Phi_{CMT})_0$, is computed from the steady-state momentum balance, Eq. (5-55). The reference heat transfer rate, $\dot{Q}_{2\phi, CMT}$, is computed from Eq. (6-86). The Phase 4 inventory equation for the CMT is, from Eq. (6-79) (the equation derived by the causative process related scaling method), after the above simplification,

$$\begin{aligned} \Pi_{VC, CMT} \frac{d\alpha_{CMT}}{dt^*} = & \Phi_{g, CMT}^* + \Pi_{V, \dot{Q}_{CMT}} \left(\frac{v_g}{h_{fg}} \right)^* \dot{Q}_{2\phi, CMT}^* \\ & - \Pi_{V, CMT, \dot{p}} \Psi_{\alpha, CMT}^* \dot{p}^*, \end{aligned} \quad (6-109)$$

where the Π -Group of *volumetric compliance*, $\Pi_{VC, CMT}$, is the ratio of CMT over system reference times and, corresponding to Eq. (6-81),

$$\Pi_{VC, CMT} = \frac{\alpha_0 V_{CMT}}{t_{ref} (\Phi_{PBL})_0} = \frac{\alpha_0 V_{CMT} (\Phi_{ADS-4})_0}{\Delta p_0 (V \chi_V)_0 (\Phi_{PBL})_0}, \quad (6-110)$$

the scaling group for *phase change in the CMT*, $\Pi_{V, CMT, \dot{Q}_{2\phi}}$, or the ratio of the rate of volume change due to phase change in the CMT over the rate of volume displaced by draining, is defined by

6. Scaling Groups

$$\Pi_{V, CMT, \dot{Q}_{2\phi}} = \frac{(\dot{Q}_{2\phi})_0}{(\Phi_{PBL})_0} \left(\frac{v_g}{h_{fg}} \right)_0, \quad (6-111)$$

and the scaling group for the *effect on the CMT draining from flashing due to depressurization*, $\Pi_{V, CMT, \dot{p}}$, or the ratio of the CMT depressurization reference time over the system reference time, where the CMT depressurization reference time is the time it takes to displace the CMT volume by depressurization, and where the system reference time is defined in the third paragraph of Section 6.2.4.

$$\Pi_{V, CMT, \dot{p}} = \frac{(\Phi_{ADS-4})_0}{(\Phi_{CMT})_0} \left(\frac{\Psi_{\alpha, CMT}}{V \chi_V} \right)_0 V_{CMT}, \quad (6-112)$$

with $\Psi_{\alpha, CMT}$ defined by Eq. (6-80) and χ_V by Eq. (5-9).

Table 6.64 lists the *causative process related* Π -Groups defined by Eqs. (6-110), (6-111), and (6-112), for CMT inventory change during Phase 4 (see Figure 3.1 and Section 3.3.1 for the definition of Phase 4). All geometric parameters appearing in the Π -Group definitions, Eqs. (6-110), (6-111), and (6-112), are found in Appendix 1. The fluid properties for the CMT which occur in Eqs. (6-110), (6-111), and (6-112), are evaluated with the initial CMT void fraction of $(\alpha_{CMT})_0 = 0.80$. Reference parameters for the primary system which occur in Eqs. (6-110), (6-111), and (6-112) are the same as for the scaling of the Phase 4 depressurization which is discussed in Section 6.2.4.1. The computation of the reference parameters is shown in Appendix 5.4. Table 6.64 is read as the previous tables, according to the explanation given on Page 6-24 for Table 6.1.

Table 6.64 Causative Process Related Π -Groups for CMT Inventory Change During Phase 4

Definition of Π -Group	Symbol of Π -Group	Π -Groups for				Comments
		AP600	APEX	ROSA	SPES	
PBL Flow (vapor, reference)	$\Pi_{V, PBL}$	1	1	1	1	
Effect of CMT Phase Change (Eq. (6-111))	$\Pi_{V, \dot{Q}_{2\phi}}$	0.99	1.00	0.98	1.00	
Effect of Depressurization, ADS Flows (Eq. (6-112))	$\Pi_{V, \dot{p}}$	0.13	0.08	0.19	0.16	
CMT Volumetric Compliance (Eq. (6-110))	Π_{VC}	0.047	0.032	0.11	0.055	

Recalling the definitions, criteria, and methods discussed in Sections 4.5 and 4.6 for importance of processes and relevant distortions, respectively, one sees from the *causative process related* Π -Groups in Table 6.64, through the magnitudes of the elements in a *column*, the significance of phenomena (CMT volumetric compliance) and processes (external heat transfer) relative to the process of fluid drainage from the CMT. The small CMT volumetric compliance of AP600 indicates an early completion of the CMT draining. The phase change in the CMT due to CMT wall heat

transfer is as important as the vapor supply through the Pressure Balance Line. There appear to be no significant scale distortions of CMT inventory drainage during Phase 4, even though the CMT volumetric compliance in ROSA is relatively large.

Table 6.65 presents the numerical values of the *fractional* Π -Groups for CMT inventory change during Phase 4. The numerical values of the *fractional* Π -Groups for system inventory change during Phase 4 are obtained by dividing the elements of the first three rows in Table 6.64 by the respective elements in the last row of Table 6.64. The *fractional* Π -Groups show the impact that processes (wall heating and ADS-4 discharge, etc.) have on the time-rate of CMT liquid inventory change.

Table 6.65 Fractional Π -Groups for CMT Inventory Change During Phase 4

Definition of Π -Group	Symbol of Π -Group	Π -Groups for				Comments
		AP600	APEX	ROSA	SPES	
PBL Flow (vapor, reference)	$\Pi_{\dot{a}, PBL}$	21.2	30.9	8.7	18.2	Rel. large volumetric compliance in ROSA because of disproportionately low PBL flow
Effect of CMT Phase Change (Eq. (6-109))	$\Pi_{\dot{a}, \dot{Q}_{2\phi}}$	21.0	30.8	8.5	18.1	
Effect of ADS Flow (Eq. (6-110))	$\Pi_{\dot{a}, \dot{p}}$	2.8	2.5	1.6	2.9	

Each *column* entry in Table 6.65 (pertaining to the facility of the column) shows the multiple change of CMT inventory at the beginning of Phase 4, or *how much* the tangent of the CMT vapor inventory vs. time curve in Figure 4.3 is rotated from the horizontal by the phenomenon associated with the row of the entry, i.e., *how important* that phenomenon is during Phase 4 to the change in CMT liquid inventory. Differences between the entries in a *row* of Table 6.65 imply differences in the system response due to the phenomenon associated with that row and, consequently, they show the strength of *scale distortion* for that phenomenon on CMT inventory depletion during Phase 4.

Tables 6.64 and 6.65 show that CMT inventory changes during Phase 4 are dominated in AP600 by CMT phase change and ADS-4 discharge flow. Table 6.65 shows that, on account of the single phenomenon of low PBL flow in ROSA, **ROSA has two significant scale distortions** in the effects of PBL flow and Phase Change. The scale distortions are conservative because the slower CMT inventory drainage in ROSA relative to AP600 leads to a lower vessel inventory at the end of Phase 4. The difference between the distortions shown in Tables 6.64 and 6.65 is explained in Section 6.3. **APEX and SPES have no distortions.**

Inventory Change in Pressurizer During Phase 4

Vapor is being discharged through the ADS-123 valves from the Pressurizer (PRZ) at the start of the blowdown phase, Phase 4, while low-void two-phase mixture passes through the Surge Line (SRL). The scaled inventory equation, Eq. (6.14), is shown in Section 6.1.2.1. Equation (6.14) is applied to the PRZ volume as the control volume, modified for the PRZ having inflow through the surge line and discharge from the top through the ADS-123 valves at the threshold of critical flow. The modified equation is simplified on the basis of the results in Table 6.59: the terms affecting flashing due to depressurization, are combined and the time rate of pressure change is normalized according to Eq. (6-107). The resulting equation for the change of inventory is, as obtained from the causative process related scaling method,

6. Scaling Groups

$$\begin{aligned} \Pi_{VC,PRZ} \rho_g^* \frac{d\alpha_{PRZ}}{dt^*} &= \Pi_{V,SRL,PRZ} W_{g,SRL}^* - W_{g,ADS-123}^* \\ &\quad - \Pi_{V,\dot{p},PRZ} \rho_g^* \Psi_{\alpha,PRZ}^* \dot{p}^*. \end{aligned} \quad (6-113)$$

Here, the Π -Group of *volumetric compliance* equals the ratio of the time needed to sweep out the Pressurizer volume over the system response time which is the time required for depressurization through the reference pressure drop

$$\Pi_{VC,PRZ} = \frac{V_{PRZ} (\Phi_{ADS-4})_0}{\Delta P_0 (\chi_V)_0 (\Phi_{ADS-123})_0}, \quad (6-114)$$

the Π -Group of *Surge Line flow* equals the ratio of SRL over ADS-123 mass flow rates

$$\Pi_{V,SRL,PRZ} = \frac{(W_{SRL})_0}{(W_{ADS-123})_0}, \quad (6-115)$$

and the Π -Group of *depressurization effects* (flashing) equals the ratio of volumetric phase change rate over volumetric expansion rates

$$\Pi_{V,\dot{p},PRZ} = \frac{(\Phi_{ADS-4})_0 (\Psi_{\alpha,PRZ})_0}{(\Phi_{ADS-123})_0 (\chi_V)_0}, \quad (6-116)$$

where Ψ_{α} is given by Eq. (5-12) and χ_V is given Eq. (5-9) and evaluated in Appendix 5.4.

Table 6.66 below presents the numerical values of the *causative process related* Π -Groups for PRZ inventory change during Phase 4. The *causative process related* Π -Groups in Table 6.66 show the significance of phenomena (system volumetric compliance) and processes (external heating and cooling) relative to PRZ discharge through the ADS-123 valves.

Table 6.66 is arranged in the familiar way of the previous tables (see Page 6-24 for Table 6.1). All geometric parameters appearing in the Π -Group definitions, Eqs. (6-113), (6-114), and (6-115) are found in Appendix 1. The initial conditions and initial thermophysical properties are found in Appendix 4.5. The initial system compliance and computed reference parameters appearing in the Π -Group definitions were computed through EXCEL and are listed in Appendix 5.4.

The significance of the phenomena affecting the change of PRZ inventory during Phase 4 is seen by comparing in Table 6.66 the magnitudes of the entries in each *column* having a facility heading, most importantly in the AP600 column. The comparison reveals that phase change is the leading phenomenon, and that Surge Line, and ADS-123 flows are all of the same order of importance. The comparison of the fourth through sixth entries in a *row* with the AP600 entry (third entry of the same row) reveals the scale distortion. **There is one distortion in ROSA**, as a consequence of low SRL flow (large flow restriction). The (conservative) effect of that distortion has been addressed already in connection with Tables 6.62 and 6.63.

Table 6.66 Causative Process Related Π -Groups for PRZ Inventory Change During Phase 4

Definition of Π -Group	Symbol of Π -Group	Π -Groups for				Comments
		AP600	APEX	ROSA	SPES	
PRZ Phase Change (Eq. (6-116))	$\Pi_{V,\dot{p}}$	6.24	5.16	3.32	9.52	
Surge Line Flow (Eq. (6-115))	$\Pi_{V,SRL}$	1.70	1.24	0.44	1.06	ROSA SRL volumetric flow rate is too low;
ADS-123 Discharge Flow (reference)	$\Pi_{V,ADS-123}$	1	1	1	1	
Volumetric Compliance (Eq. (6-114))	Π_{VC}	0.64	0.98	0.73	1.26	

Table 6.67 presents the numerical values of the *fractional* Π -Groups for PRZ inventory change during Phase 4. The fractional form of the scaled vapor volume equation is obtained by dividing Eq. (6.113) by the Π -Group of PRZ volumetric compliance, $\Pi_{VC,PRZ}$, which is defined by Eq. (6-114). The numerical values of the *fractional* Π -Groups for PRZ inventory change during Phase 4., shown in Table 6.67, are, therefore, obtained by dividing the elements of the first three rows in Table 6.66 by the respective elements in the last row of Table 6.66. The *fractional* Π -Groups show then the impact that processes have on the time-rate of liquid inventory change (refer to Section 4.4.5.2). Each *column* entry in Table 6.67 shows *how much* the tangent of the PRZ vapor inventory vs. time curve in Figure 4.3 is rotated from the horizontal by the phenomenon associated with the row of the entry and, consequently, *how important* that phenomenon is during Phase 4. Differences between the entries in a *row* of Table 6.67 imply differences in the system response due to the phenomenon associated with that row and, consequently, they show the strength of *scale distortion relative to AP600* for that phenomenon on liquid refilling of the PRZ.

Table 6.67 Fractional Π -Groups for PRZ Inventory Change During Phase 4

Definition of Π -Group	Symbol of Π -Group	Π -Groups for				Comments
		AP600	APEX	ROSA	SPES	
PRZ Phase Change (Eqs. (6-116) divided by (6-114))	$\Pi_{\dot{\alpha},\dot{p}}$	9.75	5.29	4.57	7.54	
Surge Line Flow (Eq. (6-115) divided by (6-114))	$\Pi_{\dot{\alpha},SRL}$	2.66	1.27	0.60	0.84	ROSA: SRL volumetric flow rate is too low; SPES: high ADS-4 and low SRL flows (compared to design flow ratios).
ADS-123 Discharge Flow (inverse of Eq. (6-114))	$\Pi_{\dot{\alpha},ADS-123}$	1.56	1.02	1.38	0.79	

6. Scaling Groups

Based on the definition for “significant phenomena” given in Section 4.5, one sees from Table 6.67 that phase change by flashing dominates the change of PRZ inventory during Phase 4. Table 6.67 reveals **two distortions of a significant phenomenon**, based on the definitions of “significant scale distortions” adopted in Section 4.6. The distortions are the result of low SRL flows in ROSA and SPES and high ADS-4 flow in SPES and have already been addressed in connection with the scaling of RPV inventory change (see Tables 6.62 and 6.63).

6.2.4.3 Temperature Changes During Phase 4

The important temperature of the primary system is, during Phase 4, the subcooling temperature in the reactor vessel. The coolant elsewhere is either a saturated mixture or stagnant superheated vapor (Upper Head, Steam Generators) and does not affect the primary system pressure or inventory.

The change of subcooling temperature is modeled with the energy balance applied to the control volume containing the liquid in the downcomer and the Lower Plenum. The liquid mass is taken to be constant in the control volume, and the effect of depressurization on liquid enthalpy is ignored. Liquid enters the control volume from the Core Make-up Tanks (CMT) through the Direct Vessel Injection (DVI) lines and leaves the control volume through the core entrance: $W_{CR} = W_{DVI} = W_{CMT}$. With the normalized enthalpy of the liquid in the control volume defined in terms of the initial saturation enthalpy, $(h_f)_0$, and the initial liquid enthalpy in the CMT, $(h_{l,CMT})_0$, by

$$h_l^* = \frac{(h_f)_0 - h_l}{(h_f)_0 - (h_{l,CMT})_0}, \quad (6-117)$$

and with the normalized enthalpy of the liquid in the CMT defined by

$$h_{l,CMT}^* = \frac{(h_f)_0 - h_{l,CMT}}{(h_f)_0 - (h_{l,CMT})_0}, \quad (6-118)$$

one gets the scaled equation for the enthalpy change of the subcooled liquid in the reactor vessel during Phase 4

$$\frac{dh_l^*}{dt^*} = \Pi_{sub,RPV} (h_{CMT}^* - h_l^*) \omega_{mix}^*, \quad (6-119)$$

where the Π -Group of *RPV subcooling* is the product of Phase 4 reference time and mixing frequency. It is given by

$$\Pi_{sub,RPV} = t_{ref} (\omega_{mix})_0 = \frac{\Delta p_0 (\chi_S)_0}{(\Phi_{ADS-4})_0} \frac{(\Phi_{CMT})_0}{V_{DC} + V_{LPL}}, \quad (6-120)$$

where the reference time t_{ref} has been introduced already in the third paragraph of Section 6.2.4. In Eq. (6-119), the normalized mixing frequency is $\omega_{mix}^* = \Phi_{CMT} / (\Phi_{CMT})_0$.

Table 6.68 lists the four numerical values of the *fractional* Π -Group, $\Pi_{sub,RPV}$, for AP600, APEX, ROSA, and SPES, respectively. The volumes V_{DC} and V_{LPL} are listed in Appendix 1. The other reference parameters in Eq. (6-120) are computed through EXCEL as shown in Appendix 5.4.

Table 6.68 Π -Groups for Reactor Pressure Vessel Liquid Subcooling During Phase 4

Definition of Π -Group	Symbol of Π -Group	Π -Groups for				Comments
		AP600	APEX	ROSA	SPES	
RPV Subcooling (Eq. (6-120))	$\Pi_{sub,RPV}$	0.83	0.28	0.50	0.36	APEX: charact. time of depressuriz., t_{ref} is less than $\frac{1}{2}$ of that of AP600 and CMT flow is low; low charact. time of depressuriz., t_{ref} in SPES.

Differences between the entries in Table 6.68 imply differences in the RPV subcooling temperature response to CMT flow and, consequently, they show the strength of *scale distortion relative to AP600* for CMT flow during Phase 4 on RPV subcooling temperature change.

Based on the adopted definition for “distorted” given in Section 4.6, Table 6.67 reveals **two distortions of RPV temperature response**, one in APEX and one in SPES. The scale distortions are the result of low CMT flows in APEX and distorted reference times characteristic of depressurization in APEX and ROSA. The scale distortions produce less subcooling in APEX and SPES and are, therefore, conservative.

6.2.4.4 Flow Rates, Inertia and Impedance for Phase 4

As explained in Section 6.2.3.4, the number of loops and the loop configurations in AP600, APEX, ROSA, and SPES are the same during Phases 2, 3 and 4. The flow through the ADS-123 and ADS-4 valves is, as the break flow, determined by system pressure through quasi-steady momentum and mass balances for equilibrium critical, transonic or subsonic flows, rather than by inertia and flow impedances. Since all facilities have the same level elevations in the PRZ, CMTs, and the PRHR system is filled with steam on the tube side, there are no significant differences in the fluid density distributions among the facilities. The scaling for the momentum balance is dominated by the geometry affecting inertia and form losses (inertia). Therefore, evaluation for Phase 4 of the scaling groups presented in Section 6.2.2.4 for the momentum balance, Eq. (6-68), for natural circulation would not reveal any new scale distortions beyond those presented in Section 6.2.2.4 for Phase 2. The evaluation for Phases 3 and 4 of the scaling groups presented in Section 6.2.2.4 for the momentum balance and is, therefore, omitted.

6.2.5 Phase 5, IRWST and SUMP Injections

This section presents the results of the numerical evaluation of the Π -Groups for the Phase 5, the phase of RPV injection from the In-containment Refueling Water Storage Tank (IRWST) and the sump. See Table 3.1 on Page 3-2 which shows that this phase begins when the system pressure is sufficiently low for gravity draining from the IRWST and continues for the AP600 indefinitely, but ends for APEX, ROSA, and SPES with the termination of the respective experiment. Injection from the Sump is initiated by check valve action when the IRWST and Sump level elevations are equal. Figure 3.1 identifies Phase 5 in the system pressure versus time plot, which shows that the system pressure is near containment pressure. Table 3.1 lists the major events of Phase 5, and a brief description of Phase 5 is given in Section 3.5. The distribution of subcooled liquid, two-phase mixture, single-phase vapor, and nitrogen at the beginning of Phase 5 is shown also in Table 3.1.

There are no scaling groups of depressurization computed for Phase 5 because the system depressurization is completed during Phase 4.

6. Scaling Groups

Presented in this section are the scaling groups for Reactor Pressure Vessel (RPV) inventory depletion, PRZ inventory draining, IRWST inventory draining, RPV energy change, RPV subcooling temperature change, and system momentum for the flow rates from IRWST, PRZ, and CMTs. The scaling groups are presented in the causative process related and fractional forms the characteristics and advantages of which are explained in Section 4.4.5.

ADS-123 and 4 valves and the break are modeled to continue discharging, but under the influence of gravity rather than excess pressure above containment pressure. The reference time for scaling Phase 5 is the time it takes to empty the specified liquid volume in the IRWST with the initial draining volumetric flow rate

$$t_{ref} = \frac{(V_{l,IRWST})_0}{2(\Phi_{IRWST})_0} = \frac{\rho_l(V_{l,IRWST})_0}{2(W_{IRWST})_0}, \quad (6-121)$$

where W_{IRWST} is the mass flow rate in one Direct Vessel Injection (DVI) line and computed by solving Eqs. (5-67) through (5-73) and (5-75), using MATHCAD. The MATHCAD results are tabulated in Appendix 5.5. The estimated reference mass flow rates for IRWST, ADS-4, and the break are compared with experimental data in the section for Phase 5 of Table 5.15 in Chapter 5.

Geometric parameters, including form loss coefficients and flow resistances (see Eq. (5-41)), which are needed for scaling of Phase 5 equations are listed in Appendix 1. Initial conditions used for normalizing the modeling equations of Phase 5 are given in Appendix 4.6. The reference elevations are computed in Appendix 5.5.

6.2.5.1 Depressurization

Depressurization is not scaled for Phase 5, because the system depressurization is completed during Phase 4.

6.2.5.2 Inventory Changes During Phase 5

For Phase 5, the change of inventory is scaled for the Reactor Pressure Vessel (RPV), the Pressurizer (PRZ), and the In-containment Refueling Water Storage Tank (IRWST).

Inventory Change of Reactor Pressure Vessel During Phase 5

The Reactor Pressure Vessel (RPV) is modeled to receive, at the beginning of Phase 5, coolant from the In-containment Refueling Water Storage Tank (IRWST), ($2 \cdot W_{IRWST}$), which enters through the Direct Vessel Injection (DVI) lines, and to lose coolant through the Hot Legs ($W_{1A} + W_{1B}$) and through the Cold Legs ($W_{CL,A} + W_{CL,B} + W_{bk}$) where $W_{CL,B}$ is the flow downstream of the break. Figure 5.10 on Page 5-15 displays the flow directions that are implied in the sign convention for the mass flow rates of the RPV mass balance, Eq. (6-122) below. The Hot and Cold Leg flows, W_{1A} , W_{1B} , $W_{CL,A}$, and $W_{CL,B}$, are replaced by the components flows, W_{SRL} , W_{ADS-4} , and W_{SG} , respectively, through the Surge Line, ADS-4 valves, and into the Steam Generators. This yields the RPV mass balance in term of the state variable mass flow rates defined by Eqs. (5-67) through (5-73) and (5-75):

$$\frac{dM_{RPV}}{dt} = 2W_{IRWST} + W_{SRL} - W_{bk} - \sum_{A,B} W_{ADS-4} - \sum_{A,B} W_{SG}, \quad (6-122)$$

where W_{SG} is the net mass storage in the Steam Generator (lower plena). After expressing the RPV inventory in terms of the level elevation in the RPV Upper Plenum, and after scaling, one obtains the causative process related (cf. Section 4.4.5.1) of the scaled RPV inventory equation

$$\begin{aligned} \Pi_{VC,RPV} \frac{dL_{RPV}^*}{dt^*} = & 2 W_{IRWST}^* + \Pi_{V,W_{SRL},RPV} W_{SRL} - \Pi_{V,W_{bk},RPV} W_{bk} \\ & - \sum_{A,B} \Pi_{V,W_{ADS-4},RPV} W_{ADS-4} - \sum_{A,B} \Pi_{V,W_{SG},RPV} W_{SG}. \end{aligned} \quad (6-123)$$

The Π -Group of *RPV volumetric compliance* in Eq. (6-123) is the ratio of the RPV response over the system reference time, where the RPV response time equals the time it would take to fill the reactor core with the IRWST flow

$$\Pi_{VC,RPV} = \frac{(\bar{\rho}_{CR})_0 A_{CR} L_0}{2 \rho_l (W_{IRWST})_0}. \quad (6-124)$$

The Π -Group of *RPV inventory change due to PRZ draining* in Eq. (6-123) is the ratio of SRL over IRWST mass flow rates

$$\Pi_{V,W_{SRL},RPV} = \frac{(W_{SRL})_0}{2 (W_{IRWST})_0}. \quad (6-125)$$

The Π -Group of *RPV inventory change due to break flow* in Eq. (6-123) is the ratio of break over IRWST mass flow rates

$$\Pi_{V,W_{bk},RPV} = \frac{(W_{bk})_0}{2 (W_{IRWST})_0}. \quad (6-126)$$

The Π -Group of *RPV inventory change due to break flow* in Eq. (6-123) is the ratio of ADS-4 over IRWST mass flow rates

$$\Pi_{V,W_{ADS-4},RPV} = \frac{(W_{ADS-4})_0}{2 (W_{IRWST})_0}. \quad (6-127)$$

The Π -Group of *RPV inventory change due to break flow* in Eq. (6-123) is the ratio of net SG mass in-flow over IRWST mass flow rates

$$\Pi_{V,W_{SG},RPV} = \frac{(W_{SG})_0}{2 (W_{IRWST})_0}. \quad (6-128)$$

6. Scaling Groups

The net mass in-flow of the Steam Generators turned out to be zero because there was no condensation on account of the hotter secondary side; the net out-flow due to vapor expansion at nearly constant pressure was neglected. All the mass flow rates appearing in Eqs. (6-124) through (6-128) are computed from the momentum balances, Eqs. (5-67) through (5-73) and (5-75).

Table 6.69 below presents the numerical values of the *causative process related* Π -Groups for RPV inventory change during Phase 5. The *causative process related* Π -Groups in Table 6.69 show the significance of phenomena (RPV volumetric compliance) and processes (external mass flow) relative to the process of IRWST injection.

Read Table 6.69 according to explanations given on Page 6-24 for Table 6.1. Geometric parameters, including form loss coefficients and flow resistances (see Eq. (5-41)), which are needed for scaling of Phase 5 equations are listed in Appendix 1. Initial conditions used for normalizing the modeling equations of Phase 5 are given in Appendix 4.6. The reference elevations are computed in Appendix 5.5.

Table 6.69 Causative Process Related Π -Groups for RPV Inventory Change During Phase 5

Definition of Π -Group	Symbol of Π -Group	Π -Groups for				Comments
		AP600	APEX	ROSA	SPES	
SRL Drainage (Eq. (6-125))	$\Pi_{V, W_{SRL}}$	3.5	0.2	3.5	5.8	APEX: SRL flow to low by factor 33, relative to design flow rate ratio
ADS-4 Discharge in Loop A (Eq. (6-127))	$\Pi_{V, W_{ADS-4,A}}$	2.7	0.9	3.4	3.4	APEX: IRWST flow is 50% smaller than required for design flow ratio, but ADS-4 flow is 4 times and 14 times lower in A and B, respectively
ADS-4 Discharge in Loop B (Eq. (6-127))	$\Pi_{V, W_{ADS-4,B}}$	1.7	0.2	1.0	3.3	
IRWST Injection (reference)	$\Pi_{V, W_{IRWST}}$	1	1	1	1	
Break Flow (Eq. (6-126))	$\Pi_{V, W_{bk}}$	0.1	0.1	0.1	0.1	
Volumetric Compliance (Eq. (6-126))	$\Pi_{VC, RPV}$	0.01	0.01	0.01	0.01	
SG Storage (Eq. (6-128))	$\Pi_{V, W_{SG}}$	0.0	0.0	0.0	0.0	flow is near zero but into SGs

Table 6.69 shows PRZ drainage to be most important for RPV inventory, at least at the beginning of Phase 5, for AP600, ROSA, and SPES. The very small volumetric compliance shows a very fast thermal response of RPV to the convective flow from IRWST. **APEX has two conservative scale distortions** due to low flows in the Surge Line, DVI Line from IRWST, and **one conservative scale distortion** due to lower ADS-4 flows.

Table 6.70 presents the numerical values of the *fractional* Π -Groups for RPV inventory change during Phase 5. The fractional form of the scaled vapor volume equation is obtained by dividing Eq. (6.123) by the RPV volumetric compliance scaling group defined by Eq. (6-124). The numerical values of the *fractional* Π -Groups in Table 6.70 for RPV inventory change during Phase 5 are obtained by dividing the elements of the first five and the last rows with numerical data in Table 6.69 by the respective elements in the sixth row of Table 6.69. The *fractional* Π -Groups show the impact that PRZ, ADS, and break flows have on the time-rate of system liquid inventory change.

Table 6.70 has the same layout as Table 6.69. Each *column* entry in Table 6.70 shows *how much* the tangent of the RPV liquid level elevation vs. time curve in Figure 4.3 is rotated from the horizontal by the phenomenon associated with the row of the entry and, consequently, *how important* that phenomenon is during Phase 5. Differences between the entries in a *row* of Tables 6.69 and 6.70 imply differences in the RPV level response due to the phenomenon associated with that row and, consequently, they show the strength of *scale distortion* for that phenomenon on RPV inventory depletion during Phase 5.

Tables 6.69 and 6.70 show that the RPV liquid change is dominated in AP600, at least at the beginning of Phase 5, by drainage from the Pressurizer through the Surge Line (dominant process), by ADS-4 discharge flows, and by IRWST injection (both flows are processes of first-order importance; see the **green entries** in the third columns of Tables 6.69 and 6.70). As described before for Table 6.69, Table 6.70 shows also (**red entries** in APEX column) that there are **three significant scale distortions in APEX** due to distorted SRL and ADS-4 flows which are caused by large flow resistances in APEX surge and ADS-4 lines, and by a lower liquid level elevation in the Pressurizer in APEX. One scale distortion is due to low flow in the Surge and DVI Lines and conservative. The other two scale distortions are due to lower ADS-4 flows and also conservative, because the low ADS-4 flow causes the RPV mixture level to be depressed more in APEX than in AP600.

Table 6.70 Fractional Π -Groups for RPV Inventory Change During Phase 5

Definition of Π -Group	Symbol of Π -Group	Π -Groups for				Comments
		AP600	APEX	ROSA	SPES	
SRL Drainage (Eq. (6-125) and Eq. (124))	$\Pi_{L, W_{SRL}}$	438	31	542	719	APEX: SRL flow too low by factor 33, relative to design flow rate ratio
ADS-4 Discharge in Loop A (Eq. (6-127) and Eq. (124))	$\Pi_{L, W_{ADS-4,A}}$	345	165	526	420	APEX: IRWST flow is 50% smaller than required for design flow ratio, but ADS-4 flow is 4 times and 14 times lower in A and B, respectively
ADS-4 Discharge in Loop B (Eq. (6-127) and Eq. (124))	$\Pi_{L, W_{ADS-4,B}}$	211	34	150	418	
IRWST Injection (reciprocal of Eq. (124))	$\Pi_{L, W_{IRWST}}$	126	191	154	125	
Break Flow (Eq. (6-126) and Eq. (124))	$\Pi_{L, W_{bk}}$	7.4	22.6	19.9	7.1	
SG Storage (Eq. (6-128) and Eq. (124))	$\Pi_{L, W_{SG}}$	0.0	0.0	0.0	0.0	

6. Scaling Groups

Inventory Change of Pressurizer During Phase 5

The scaling of RPV inventory showed that the draining of fluid through the Surge Line (SRL) from the Pressurizer (PRZ) is important for the vessel inventory change at least at the beginning of Phase 5. While liquid is being drained through the Surge Line, back flow into the PRZ through the ADS-123 lines from the submerged spargers in the IRWST is being prevented by vacuum breaker valves which maintain containment pressure in the gas space above the liquid level in the Pressurizer. The scaled inventory equation applies to the PRZ volume as the control volume, and reads

$$\Pi_{VC, PRZ} \frac{dL_{PRZ}^*}{dt^*} = -W_{SRL}^*, \quad (6-129)$$

where the Π -Group of *PRZ volumetric compliance* equals the ratio PRZ over IRWST drain times

$$\Pi_{VC, PRZ} = \frac{\rho_f A_{PRZ} (L_{PRZ})_0 (W_{IRWST})_0}{\rho_l (V_{IRWST})_0 (W_{SRL})_0}. \quad (6-130)$$

The cross-sectional area of the Pressurizer, A_{PRZ} , is taken from Appendix 1. The densities ρ_f and ρ_l are listed in Appendix 4.6. The mass flow rates appearing in Eq. (6-130) are computed from the momentum balances, Eqs. (5-67) through (5-73) and (5-75); the results are listed in Appendix 5.5. Table 6.71 below presents the numerical values of the *causative process related* Π -Groups for PRZ inventory change during Phase 5. The single *causative process related* Π -Groups in Table 6.71 show s only how important the PRZ volumetric compliance is relative to PRZ draining and possible scale distortions in APEX, ROSA, and SPES.

Table 6.71 lists the causative process related Π -Groups for inventory change in the Pressurizer during Phase 5. The Π -Group is interpreted in the text above, next to the defining equation, Eq. (6-130), as indicated in the first column of Table 6.71. The second column shows the symbol of the Π -Group appearing in the scaled equation, Eq. (6.129), the third through sixth columns list the numerical values of the Π -Group for the AP600 and the three related facilities APEX, ROSA, and SPES, and the last column is for comments explaining distortions. Equation (6-129) has only one causative process related (or driving) term. The volumetric compliance is extremely small for all facilities, which indicates that PRZ draining is completed in a small fraction of the IRWST draining time(see Eq. (6-121) for the expression of IRWST draining time).

Table 6.71 Causative process related Π -Groups for PRZ Inventory Change During Phase 5

Definition of Π -Group	Symbol of Π -Group	Π -Groups for				Comments
		AP600	APEX	ROSA	SPES	
PRZ Drainage (reference)	$\Pi_{V, W_{SRL}}$	1	1	1	1	
PRZ Volumetric Compliance (Eq. (6-130))	$\Pi_{VC, PRZ}$	1.8e-03	3.0e-02	2.0e-03	9.4e-04	

Table **6.72** presents the numerical values of the *fractional* Π -Group for PRZ inventory change during Phase 5. The fractional form of the scaled equation for liquid level elevation is obtained by dividing Eq. (6.129) by the Π -Group of PRZ volumetric compliance, $\Pi_{VC, PRZ}$, which is defined by Eq. (6-130). The numerical values of the *fractional* Π -Group for PRZ level motion during Phase 5., shown in Table 6.72, are, therefore, the reciprocal of the respective elements in the last row of Table 6.71.

Table 6.72 Fractional Π -Group for PRZ Inventory Change During Phase 5

Definition of Π -Group	Symbol of Π -Group	Π -Groups for				Comments
		AP600	APEX	ROSA	SPES	
PRZ Drainage (reciprocal of Eq. (6-130))	$\Pi_{V, W_{SRL}}$	559	33	503	1069	APEX: SRL flow too low relative to design flow rate ratio

The *fractional* Π -Group in Table 6.72 shows the impact that the SRL drainage has on the time-rate of liquid inventory change in the PRZ during Phase 5 (refer to Section 4.4.5.2). Each entry in Table 6.72 shows *how much* the tangent of the PRZ level elevation vs. time curve in Figure 4.3 is rotated from the horizontal by the PRZ draining. Differences between the entries in the *row* of Table 6.72 imply differences in the PRZ level response to gravity draining and, consequently, they show the strength of *scale distortion relative to AP600*.

Table 6.71 shows that IRWST draining provides a quasi-steady environment for rapid PRZ draining is. Table 6.72 shows that PRZ draining is completed in APEX in the small fraction of 1/559 of the Phase 5 reference time, but that it takes 1/33 of the IRWST draining time in APEX. The rate of PRZ draining is important at the beginning of Phase 5 when the minimum RPV inventory is expected to occur. The discharge *rate* is not important for the RPV inventory afterward, since the entire PRZ content is discharged into the vessel. Therefore, the scale distortion of PRZ draining in APEX during IRWST injection is conservative.

Inventory Change of In-containment Refueling Water Storage Tank During Phase 5

The scaling of RPV inventory showed that the injection of fluid through the Direct Vessel Injection (DVI) line from the In-containment Refueling Water Storage Tank (IRWST) is also important for the vessel inventory change during Phase 5. The IRWST drains through the DVI lines, but receives liquid condensate and liquid from the ADS-123 system discharge. The condensate stems from the vapor portions of ADS-123 and ADS-4 discharges. The scaled inventory equation applies to the volume of the IRWST as the control volume, and reads

$$\Pi_{V, IRWST} \frac{dL_{IRWST}^*}{dt^*} = - (W_{IRWST})_{tot}^* - \Pi_{V, ADS-4, IRWST} \sum_{123,4} (W_{ADS})_v^*, \quad (6-131)$$

where the Π -Group of *IRWST volumetric compliance* equals 1 because the IRWST draining time is the system reference time, where the Π -Group of *IRWST draining*, $\Pi_{V, dm, IRWST}$, also equals 1 because the IRWST drainage mass flow rate is taken as reference mass flow rate, and where the Π -Group of IRWST condensate return flow is the ratio of total condensate over IRWST drainage mass flow rates

$$\Pi_{V, ADS} = \frac{(x_e W_{ADS-4})_0}{(W_{IRWST})_0}. \quad (6-132)$$

The core exit quality, $(x_e)_0$, at the beginning of Phase 5 is computed from Eq. (5-66), with the drift-flux parameters evaluated for bubbly flow. The mass flow rates appearing in Eq. (6-132) are computed from the momentum balances, Eqs. (5-67) through (5-73) and (5-75); the results are listed in Appendix 5.5. Table 6.73 below presents the numerical values of the *causative process related* Π -Groups for IRWST inventory change during Phase 5 (see Section 4.4.5.1

6. Scaling Groups

for the significance of *causative process related* Π -Groups). The single *causative process related* Π -Groups in Table 6.71, which differs from unity, show only how important the condensate return flow is relative to IRWST draining through the DVI lines, and possible scale distortions in APEX, ROSA, and SPES.

Table 6.73 Causative Process Related and Fractional Π -Groups for IRWST Inventory Change During Phase 5

Definition of Π -Group	Symbol of Π -Group	Π -Groups for				Comments
		AP600	APEX	ROSA	SPES	
IRWST Volumetric Compliance (by definition)	$\Pi_{VC, IRWST}$	1	1	1	1	
IRWST Drainage (reference)	$\Pi_{V, dm}$	1	1	1	1	
IRWST Condensate Return Flow (Eq. (132))	$\Pi_{V, ADS}$	2.1e-02	2.9e-03	2.3e-02	3.1e-02	

Table 6.73 presents the causative process related Π -Groups for IRWST inventory change during Phase 5. There is no numerical difference between the *causative process related* Π -Groups introduced in Section 4.4.5.1 and the *fractional* Π -Groups that were introduced in Section 4.4.5.2, since the IRWST volumetric compliance is unity on account of the equality between IRWST and system response times. The numerical values of the Fractional Π -Groups are shown in the last two rows of Table 6.73. Table 6.73 is arranged in the same way as the previous tables in Section 6.2; see Page 6-24 for the explanation of Table 6.1.

Table 6.73 shows that condensate return flow is the least important process for the IRWST inventory change during Phase 5, and that **IRWST drainage during Phase 5 is scaled by all test facilities without distortion.**

6.2.5.3 Temperatures During Phase 5

The important temperature change of the primary system during Phase 5 is the subcooling temperature in the reactor vessel, because the subcooling temperature determines, for given decay heating power and given flow rates, the amount of vapor formation in the reactor vessel. The rate of vapor generation in the Reactor Pressure Vessel (RPV) is modeled in terms of the RPV total internal energy, U_{RPV} , the subcooling enthalpy, h_s , and the nonboiling length, z_i .

RPV Internal Energy

The change of internal energy is modeled with The energy balance applied to The control volume containing The coolant in The RPV. The mass balance for The same control volume is modeled in Section 6.2.5.2 (see Page 6-90). Enthalpy flows are entering through The Direct Vessel Injection (DVI) lines. Enthalpy flows are leaving through The Hot Legs and Cold Legs. The energy balance is

$$\frac{dU_{RPV}}{dt} = h_{IRWST} \sum W_{IRWST} - (h_l)_{DC} (\sum W_{CL} + W_{bk}) - (h_m)_{CRE} \sum W_{HL}, \quad (6-133)$$

where the enthalpy of the IRWST fluid is taken to equal the initial enthalpy, $h_{IRWST} = (h_{IRWST})_0$, the enthalpy of the subcooled liquid is governed by the energy balance, Eq. (6.135) below, for the fluid contained in the Downcomer (DC), Lower Plenum (LPL, subscript LP), and core entrance section (CE), and the core exit enthalpy is given by

$$(h_m)_{CRE} = (h_l)_{CRI} + \frac{\dot{Q}_{CR}}{W_{CR}}. \quad (6-134)$$

Here, the liquid enthalpy at the core inlet, $(h_l)_{CRI}$, is approximated by the volume-average liquid enthalpy in DC, LPL, and CE, $(h_l)_{CRI} = (h_l)_{DC}$, the core heating power, \dot{Q}_{CR} , is the specified decay heat, and all mass flow rates in Eqs. (6-133) and (6-135), (6-137) through (6-139), and (6-141) through (6-142) below are computed from the momentum balances given by Eqs. (5-67) through (5-73) and (5-75); the results of the computation are listed in Appendix 5.5.

The enthalpy of the subcooled liquid is governed by the energy balance for the fluid contained in the Downcomer (DC), Lower Plenum (LPL, subscript LP), i.e., in $V_l = V_{DC} + V_{LP} + V_{CE}$

$$\rho_l V_l \frac{dh_l}{dt} = (h_{IRWST} - h_l) \sum W_{IRWST} - (h_f - h_l) (W_{CR} - \rho_l A_{CR} \dot{z}_\lambda), \quad (6-135)$$

where A_{CR} is the core cross-sectional area \dot{z}_λ is the nonboiling length of the core. Since $W_{CR} \gg \rho_l A_{CR} \dot{z}_\lambda$, the scaled form of Eq. (6-133) is

$$\begin{aligned} \Pi_{TC, RPV} \frac{dU_{RPV}^*}{dt^*} - \Pi_{T, \Delta h, RPV} \frac{dL_{RPV}^*}{dt^*} &= [h_{IRWST} - (h_l)_{DC}]^* \sum W_{IRWST}^* \\ &- \Pi_{T, \dot{Q}, RPV} [h_{CRE} - (h_l)_{DC}]^* \sum W_{HL}^*, \end{aligned} \quad (6-136)$$

where the level speed, dL_{RPV}^*/dt^* , is given by Eq. (6-123), and where the Π -Group of *RPV thermal compliance* is the ratio of RPV thermal response over system reference times which equals the ratio of initial stored excess internal energy above saturation in the RPV over initial stored excess enthalpy above saturation enthalpy in the IRWST and is given by

$$\Pi_{TC, RPV} = \frac{(\Delta U_{RPV})_0}{\rho_l V_{IRWST} (\Delta h_{RPV})_0}. \quad (6-137)$$

In Eq. (6-136), the Π -Group of *RPV versus IRWST temperature difference* or the ratio of the RPV response over the system reference time, times the ratio of initial liquid over IRWST enthalpies, i.e.,

$$\Pi_{T, \Delta h, RPV} = \Pi_{VC, RPV} \frac{(h_l)_0}{(\Delta h_{IRWST})_0}, \quad (6-138)$$

where the Π -Group of RPV of volumetric compliance, $\Pi_{VC, RPV}$, is defined by Eq. (6-124).

6. Scaling Groups

The Π -Group of *RPV heating* in Eq. (6-136) is the ratio decay heating power over core cooling power, times the ratio of Hot Leg over IRWST mass flow rates

$$\Pi_{T, \dot{Q}, RPV} = \frac{(\dot{Q}_{RPV})_0}{(W_{CR})_0 (\Delta h_{IRWST})_0} \frac{\sum (W_{HL})_0}{\sum (W_{IRWST})_0}. \quad (6-139)$$

Table 6.74 below presents the numerical values of the *causative process related* Π -Groups for RPV internal energy change during Phase 5. The *causative process related* Π -Groups in Table 6.74 show the significance of phenomena (RPV thermal compliance) and processes (external enthalpy convection into the RPV) relative to the process of IRWST coolant injection. See Section 4.4.51 for the significance of the *causative process related* Π -Groups. The volumes appearing in the above Π -Group definitions are listed in Appendix 1. The other reference mass flow rates are computed through EXCEL as shown in Appendix 5.5.

To read Table 6.74, recall that each Π -Group is interpreted in the text above, next to the equation that defines it, and the defining equation is indicated in the first column of Table 6.74. The second column shows the Π -Group symbol appearing in Eq. (6.136), the third through sixth columns list the numerical values of the Π -Groups for the AP600 and the three related facilities APEX, ROSA, and SPES, and the last column is provided for comments explaining distortions, if any.

Table 6.74 Causative Process Related Π -Groups for RPV Internal Energy Change During Phase 5

Definition of Π -Group	Symbol of Π -Group	Π -Groups for				Comments
		AP600	APEX	ROSA	SPES	
RPV versus IRWST Temperature Difference (Eq. (6-139))	$\Pi_{T, \Delta h}$	1.38	1.26	1.18	1.38	
IRWST Injection (reference)	$\Pi_{T, W_{IRWST}}$	1	1	1	1	
RPV Heating (Eq. (6-139))	$\Pi_{T, \dot{Q}}$	0.79	1.43	1.39	0.84	
RPV Thermal Compliance (Eq. (6-137))	$\Pi_{TC, RPV}$	0.15	0.09	0.12	0.13	

Table 6.75 presents the numerical values of the *fractional* Π -Groups for RPV internal energy change during Phase 5. See Section 4.4.52 for the significance of the fractional Π -Groups. The fractional form of the scaled energy conservation equation is obtained by dividing Eq. (6.136) by the RPV thermal compliance scaling group defined by Eq. (6-138). The numerical values of the *fractional* Π -Groups in Table 6.75 for RPV internal energy change during Phase 5 are obtained by dividing the elements of the first and the last two rows in Table 6.74 by the respective elements in the second row of Table 6.74. The *fractional* Π -Groups show the impact that injection flows have on the time-rate of RPV internal energy change, i.e., how much they each rotate the initial tangent of the internal energy versus time curve from the horizontal, as shown in Figure 4.3, or what fraction they contribute to the total change.

Table 6.75 Fractional Π -Groups for RPV Internal Energy Change During Phase 5

Definition of Π -Group	Symbol of Π -Group	Π -Groups for				Comments
		AP600	APEX	ROSA	SPES	
RPV versus IRWST Temperature Difference (Eq. (6-138) and Eq. (6-137))	$\Pi_{T, \Delta h}$	9.30	14.11	9.91	10.28	
IRWST Injection (reciprocal of Eq. (6-137))	$\Pi_{T, W_{IRWST}}$	6.75	11.18	8.38	7.47	
RPV Heating (Eq. (6-139) and Eq. (6-137))	$\Pi_{T, \dot{Q}}$	5.36	15.98	11.66	6.30	High RPV heat transfer in APEX, ROSA.

Tables 6.74 and 6.75 show that RPV internal energy is governed during Phase 5 by level motion, by the difference between single-phase liquid temperatures in RPV and IRWST, and by the IRWST injection rate. Tables 6.74 and 6.75 show also that there is **one conservative scale distortion each in APEX and ROSA** regarding the simulation of RPV internal energy change during Phase 5, based on the distortion criterion adopted in Section 4.6.

Liquid Subcooling Temperature

Scaling of Eq. (6-135) yields for the time rate of change of subcooling enthalpy in the RPV during Phase 5

$$\begin{aligned} \Pi_{TC, l, RPV} \frac{d\Delta h_{l, RPV}^*}{dt^*} &= - (h_f - h_{IRWST})^* \sum W_{IRWST}^* \\ &\quad - \Pi_{T, l, DCLP, RPV} (\Delta h_l)^* W_{CR}^*, \end{aligned} \quad (6-140)$$

In Eq. (6-140) for the time rate of change of subcooling enthalpy in the RPV, the Π -Group of *RPV subcooled liquid thermal compliance* is the ratio of RPV subcooled liquid thermal response over system reference times which equals the ratio of initial subcooled liquid mass in the RPV over initial IRWST mass and is given by

$$\Pi_{TC, l, RPV} = \frac{\rho_f (V_l)_0}{\rho_l (V_{IRWST})_0}. \quad (6-141)$$

In Eq. (6-140) for the time rate of change of subcooling enthalpy in the RPV, the Π -Group of *RPV subcooled liquid discharge from the downcomer* equals the ratio of RPV core over IRWST mass flow rate and is given by

$$\Pi_{T, l, DCLP, RPV} = \frac{(W_{CR})_0}{\sum (W_{IRWST})_0}. \quad (6-142)$$

6. Scaling Groups

Table 6.76 below presents the numerical values of the *causative process related* Π -Groups for RPV subcooling enthalpy (temperature) change during Phase 5. The *causative process related* Π -Groups (see Section 4.4.5.1) in Table 6.76 show the significance of phenomena (thermal compliance of single-phase subcooled liquid in the RPV) and processes (external enthalpy convection into the RPV) relative to the process of IRWST coolant injection. The volumes appearing in the above Π -Group definitions are listed in Appendix 1. The other reference mass flow rates are computed through EXCEL as shown in Appendix 5.5. To read Table 6.76, see the explanation of table entries on Page 6-24 for Table.

As expected, Table 6.76 reveals that the liquid temperature in the downcomer responds very quickly during the long time of IRWST draining, and that supply of coolant liquid from the IRWST and the discharge from the downcomer are equally important for the downcomer liquid subcooling. Table 6.76 shows also that there are **no significant scale distortion** for liquid subcooling during Phase 5 in any test facility.

Table 6.76 Causative process related Π -Groups for RPV Subcooling Enthalpy (Temperature) Change During Phase 5

Definition of Π -Group	Symbol of Π -Group	Π -Groups for				Comments
		AP600	APEX	ROSA	SPES	
IRWST Injection (reference)	$\Pi_{T,l,W_{IRWST}}$	1	1	1	1	
Discharge from DC to Core (Eq. (6-142))	$\Pi_{T,l,DCLP}$	0.88	0.83	0.97	0.92	
RPV Thermal Compliance (Eq. (6-137))	$\Pi_{TC,l,RPV}$	0.02	0.03	0.02	0.01	

Table 6.77 Fractional Π -Groups for RPV Subcooling Enthalpy (Temperature) Change During Phase 5

Definition of Π -Group	Symbol of Π -Group	Π -Groups for				Comments
		AP600	APEX	ROSA	SPES	
IRWST Injection (reciprocal of (Eq. (6-137)))	$\Pi_{T,l,W_{IRWST}}$	64.7	38.7	43.6	77.2	
Discharge from DC to Core (Eq. (6-142) and (Eq. (6-137)))	$\Pi_{T,l,DCLP}$	57.3	32.1	42.5	70.8	

Table 6.77 presents the numerical values of the *fractional* Π -Groups for RPV subcooling enthalpy change during Phase 5. See Section 4.4.5.2 for the significance of the fractional Π -Groups and Page 6-24 for the explanation of table entries in Table.6.77. The fractional form of the scaled energy conservation equation for the subcooled liquid, i.e., the temperature at the core entrance, is obtained by dividing Eq. (6.140) by the thermal compliance scaling group defined by Eq. (6-141). The numerical values of the *fractional* Π -Groups in Table 6.77 for core entrance temperature change during Phase 5 are obtained by dividing the elements of the first two rows in Table 6.76 by the respective elements in the last row of Table 6.76. The *fractional* Π -Groups show the impact that injection and discharge flows of downcomer and Lower Plenum have on the time-rate of core entrance temperature change, i.e., how much these flows each rotate

the initial temperature versus time curve from the horizontal, as shown in Figure 4.3, or what fraction they contribute to the total temperature change.

Tables 6.76 and 6.77 indicate both that the RPV liquid subcooling temperature is governed during Phase 5 by IRWST and core flows. Tables 6.77 and 6.78 show also that there is **no scale distortion in any of the three test facilities** on simulating RPV subcooling during Phase 5, based on the distortion criterion adopted in Section 4.6.

Nonboiling Length in Core

The effect of the time rate of change of nonboiling length in Eq. (6-135) was neglected in the derivation of Eq. (6-136), but the position of the net vapor generation point, z_λ , is needed for computing the initial RPV internal energy, $(U_{RPV})_0$, in Eq. (6-137). The position of the net vapor generation point, z_λ , is estimated from

$$z_\lambda = \frac{W_{CR} \Delta h_{sub}}{\dot{Q}_{CR}} L_{CR}. \quad (6-143)$$

Equation (6-143) shows that the dynamics of the motion of the net vapor generation point, z_λ , is already scaled by Eqs. (6-123) and (6-140).

6.2.5.4 Flow Rates, Inertia and Impedance

It was shown in Section 5.4.2 that the dynamic interaction between IRWST, CMT, PRZ, and RPV, with ADS and break discharges, takes place in the connecting pipes and that is modeled with the system momentum balance. For Phase 5, there are six loops with seven junctions modeled for AP600, APEX, ROSA, and SPES, as can be seen in Figure 5.10, since the two Cold Legs are combined. Check valves prevent CMT Accumulator back flows. The PRZ vacuum breakers are open and impose containment pressure on the space above the liquid in the PRZ. For natural circulation, the flows are driven entirely by gravity and retarded by friction and form losses. Inertia terms are neglected because of the hour-long duration of Phase 5.

The system of six quasi-steady momentum balances is given by Eqs. (5-67) through (5-73) in Section 5.5.4. The system of momentum balances is combined with the three mass balances given by Eqs. (5-75).

The six loops are: (1) Loop A, (2) Loop B, (3) the loop from Containment through PRZ and ADS-4(A) and back to Containment, (4) the loop from Containment through PRZ and ADS-4(B) and back to Containment, (5) the loop from Containment through IRWST and ADS-4(A) and back to Containment, and (6) the loop from Containment through IRWST and out through the break back to Containment. The three mass balances given by Eqs. (5-75) apply to the RPV, and the Cold Legs of Loop A and of Loop B.

The scaled momentum equation, Eq. (6-68), with the inertia term set equal to zero, yields a single Π -Group, $\Pi_{RS, GR}$, of *global flow impedance* which equals the ratio of loop impedance over driving gravity forces, as defined in Eq. (6-71). The main loop and reference loop is the loop from Containment through IRWST and ADS-4(A) and back to Containment.

Table 6.78 lists the numerical values of $\Pi_{RS, GR}$ for global flow impedance during Phase 5. The table shows, as expected, that gravity and resistance forces balance and that there is **no significant global scale distortion in the forces of any one of the test facilities**.

6. Scaling Groups

Table 6.78 Π -Groups for Global Flow Impedance During Phase 5

Definition of Π -Group	Symbol of Π -Group	Π -Groups for				Comments
		AP600	APEX	ROSA	SPES	
Flow Impedance (Eq. (6-71))	$\Pi_{RS, GR}$	1.16	0.70	0.74	1.73	
Gravity (reference)	$\Pi_{GS, GR}$	1	1	1	1	

As shown in Eq. (6-68), one needs to consider in Eq. (6-68) the scaling arrays S_G , and S_p of *gravity and impedance distribution*. The evaluation of the gravity metric, S_G , is based here on density, instead of the temperature difference indicated in Eq. (6-63). The impedance metric is defined by Eq. (6-64).

The reference component elevations are taken from Appendix 1; the initial reference level elevations needed for evaluating Eqs. (6-63) are computed in Appendix 5.5. The reference flow rates needed to evaluate Eqs. (6-64) are computed in Appendix 5.5 from the coupled steady-state momentum balances, Eqs. (5-67) through (5-73).

Table 6.79 presents the numerical values of the gravity metric (vector, S_G) for the AP600 and the test facilities APEX, ROSA, and SPES and shows that the gravity forces of Loops A and B are insignificant, the gravity forces of PRZ and IRWST elevations are equally important, and that there is **no significant scale distortion of gravity force distribution**.

Table 6.79 Gravity Metric for Six-Loop IRWST Injection During Phase 5

Loop	Symbol of Scaling Metric	Scaling Metric for				Comments
		AP600	APEX	ROSA	SPES	
Loop A		1.3e-04	2.1-05	4.9e-4	1.8e-03	
Loop B		1.3e-04	2.1-05	1.1e-04	2.0e-03	
PRZ to ADS-4(A)		0.86	0.83	0.89	0.73	
PRZ to ADS-4(B)		0.86	0.83	0.89	0.76	
IRWST to ADS-4(A)		1	1	1	1	
IRWST to Break		0.87	0.79	0.91	0.99	

Tables 6.80, 6.81, 6.82, and 6.83 present the numerical values of the impedance metric (matrix, S_p) for, respectively, the AP600 and the test facilities APEX, ROSA, and SPES. The S_p elements are computed from the resistance coefficients and pump impedances in Table A.1.7.1 of Appendix 1 and from the reference flow rates which satisfy Eqs. (5-67) through (5-73) and are shown in Table A.5.5 of Appendix 5.5. S_p elements of APEX, ROSA, and SPES which differ from the corresponding AP600 S_p elements by more than the factor 2 are considered to reflect distortion and are shown in red (see Section 4.6 for the definition of scale distortion).

Table 6.80 Impedance Metric for AP600 Six-Loop IRWST Injection During Phase 5

Loop		Elements of Impedance Metric S_p of Loop Sections between Branch Points:												
on Side	fom - to or through	RPV to ADS4/SRL of Loop _A	ADS4/SRL to SGI	SGI to SGE of Loop _A	SGE of Loop _A to bk/RPV	bk to RPV	Upper Down-corer	Vessel from DVI to Upper Plenum	Surge Line to HL/ADS4	ADS-4/A	ADS-4/B	ADS4 of Loop _B to RPV	IRWST	Break (bk)
A	PRZ to ADS4/A	0	0	0	0	0	0	0	0.102	0.150	0	0	0	0
A	both CL	2e-06	1e-06	2e-08	4e-05	0	2e-08	9e-05	0	0	0	0	0	0
B	both CL	0	1e-06	5e-08	3e-05	4e-07	2e-08	9e-05	0	0	0	9e-06	0	0
A/B	PRZ to ADS4/B	2e-06	0	0	0	0	0	0	0.102	0	0.150	9e-06	0	0
A/B	IRWST to ADS4/A	2e-06	0	0	0	0	0	9e-05	0	0.150	0	0	0.850	0
A/B	IRWST to bk	0	0	0	0	4e-07	2e-08	0	0	0	0	0	0.850	0.484

Table 6.81 Impedance Metric for APEX Six-Loop IRWST Injection During Phase 5

Loop		Elements of Impedance Metric S_p of Loop Sections between Branch Points:												
on Side	fom - to or through	RPV to ADS4/SRL of Loop _A	ADS4/SRL to SGI	SGI to SGE of Loop _A	SGE of Loop _A to bk/RPV	bk to RPV	Upper Down-corer	Vessel from DVI to Upper Plenum	Surge Line to HL/ADS4	ADS-4/A	ADS-4/B	ADS4 of Loop _B to RPV	IRWST	Break (bk)
A	PRZ to ADS4/A	0	0	0	0	0	0	0	8e-05	0.197	0	0	0	0
A	both CL	1e-06	7e-09	2e-10	2e-06	0	2e-08	2e-05	0	0	0	0	0	0
B	both CL	0	2e-07	2e-09	4e-12	7e-13	2e-08	2e-05	0	0	0	4e-07	0	0
A/B	PRZ to ADS4/B	1e-06	0	0	0	0	0	0	8e-05	0	0.197	4e-07	0	0
A/B	IRWST to ADS4/A	1e-06	0	0	0	0	0	2e-05	0	0.197	0	0	0.803	0
A/B	IRWST to bk	0	0	0	0	7e-13	2e-08	0	0	0	0	0	0.803	0.869

6. Scaling Groups

Table 6.82 Impedance Metric for ROSA Six-Loop IRWST Injection During Phase 5

Loop		Elements of Impedance Metric S_p of Loop Sections between Branch Points:												
on Side	fom - to or through	RPV to ADS4/SRL of Loop _A	ADS4/SRL to SGI	SGI to SGE of Loop _A	SGE of Loop _A to bk/RPV	bk to RPV	Upper Down-comer	Vessel from DVI to Upper Plenum	Surge Line to HL/ADS4	ADS-4/A	ADS-4/B	ADS4 of Loop _B to RPV	IRWST	Break (bk)
A	PRZ to ADS4/A	0	0	0	0	0	0	0	0.034	0.333	0	0	0	0
A	both CL	6e-07	1e-06	4e-08	8e-04	0	3e-11	2e-04	0	0	0	0	0	0
B	both CL	0	1e-06	3e-08	2e-04	1e-07	3e-11	2e-04	0	0	0	2e-07	0	0
A/B	PRZ to ADS4/B	6e-07	0	0	0	0	0	0	0.034	0	0.333	2e-07	0	0
A/B	IRWST to ADS4/A	6e-07	0	0	0	0	0	2e-04	0	0.333	0	0	0.667	0
A/B	IRWST to bk	0	0	0	0	1e-07	3e-11	0	0	0	0	0	0.667	0.988

Table 6.83 Impedance Metric for SPES Six-Loop IRWST Injection During Phase 5

Loop		Elements of Impedance Metric S_p of Loop Sections between Branch Points:												
on Side	fom - to or through	RPV to ADS4/SRL of Loop _A	ADS4/SRL to SGI	SGI to SGE of Loop _A	SGE of Loop _A to bk/RPV	bk to RPV	Upper Down-comer	Vessel from DVI to Upper Plenum	Surge Line to HL/ADS4	ADS-4/A	ADS-4/B	ADS4 of Loop _B to RPV	IRWST	Break (bk)
A	PRZ to ADS4/A	0	0	0	0	0	0	0	0.068	0.145	0	0	0	0
A	both CL	6e-07	3e-04	1e-05	0.025	0	4e-07	6e-06	0	0	0	0	0	0
B	both CL	0	5e-04	1e-05	4e-03	2e-04	4e-07	6e-06	0	0	0	1e-06	0	0
A/B	PRZ to ADS4/B	6e-07	0	0	0	0	0	0	0.068	0	0.154	1e-06	0	0
A/B	IRWST to ADS4/A	6e-07	0	0	0	0	0	6e-06	0	0.145	0	0	0.855	0
A/B	IRWST to bk	0	0	0	0	2e-04	4e-07	0	0	0	0	0	0.855	0.319

By comparing the numerical values of Tables 6.81 through 6.83 for APEX, ROSA, and SPES, respectively, with the corresponding values of Table 6.80 for AP600, one finds that 14, 20, and 19 of 27 elements are distorted by more than the factor of two, respectively, for APEX, ROSA, and SPES. While the global balance between gravity and friction forces is scaled in all facilities, the ***distribution of impedances is distorted in all test facilities***, particularly relative to the impedance of the IRWST loop to the ADS-4 valves. The distribution of impedances, or flow resistances, governs during nearly steady-state flow conditions the distribution of flows: the flow from the IRWST prefers the path of least resistance. When the flow of a test facility has a greater tendency to accumulate in the Reactor Pressure Vessel (RPV) than it has in AP600 then the flow is called nonconservatively scale distorted (see Section 4.6).

In APEX, the flow prefers, relative to the flow in AP600, to accumulate in the Steam Generators, to leave through the break, and it finds more resistance in the vessel. Consequently, the flow will not accumulate as readily in the vessel of APEX as in the vessel of AP600. However, the steam will vent more readily through the ADS-4 valves. This produces less backpressure in the vessel upper plenum and a higher mixture level in the upper plenum. The RPV-to-ADS-4 flow resistance in APEX is nonconservatively scale distorted.

In ROSA, the flow is retarded through the break and the ADS-4 valves and finds it easier to get into the vessel due to five nonconservative scale distortions. ROSA loses PRZ inventory more readily through ADS-4. The associated scale distortions are conservative.

In SPES, impedances are nonconservatively scale distorted, because the flows in SPES prefer to escape through ADS-4, to get into the vessel, and have difficulties escaping from the break. The flows prefer to accumulate in the Steam Generators, and are difficult to drain from the PRZ. The impedances in these flow paths are conservatively distorted.

6.3 Summary of Scale Distortions and their Interpretation

Scope of Scaling Analysis

Section 6.2 above presents the numerical evaluation of 124 *causative process related* and 127 *fractional scaling* groups for global phenomena and processes in the primary coolant system of AP600, APEX, ROSA, and SPES. The advantages of causative process related and fractional scaling methods are given in Sections 4.4.5.1. and 4.4.5.2, respectively. The *causative process related* scaling or Π -Groups scale, compare, and rank phenomena relative to the respective causative process, which initiates a phase. The *causative process related* scaling method affords the determination of the relative speed of the transient with a single Π -Group, the capacitance scaling group. The *fractional scaling* method, on the other hand, exhibits directly the fractional impact of a transport process on the total time rate of change of a system-defining state variable (pressure, mass inventory, temperature, and flow rate). The assessment of phenomenon ranking and scale distortion can be achieved with either method. The fractional scaling method alone is used for the assessment in this section.

The number of scaling groups is dictated by the number of governing equations (which equals the number of state variables: pressure, liquid volume fraction, temperature, and flow rates, see Section 4.4) that is needed to describe the transient blowdown in

- the entire Primary System,
- the Reactor Pressure Vessel (RPV),
- the Core Make-up Tanks (CMT),
- the Pressurizer (PRZ), and
- the In-containment Refueling Water Storage Tank (IRWST)

during five time segments or phases, with five subphases, as shown in Figure 3.1.

6. Scaling Groups

Important Phenomena

The definition of importance is introduced in Section 4.5. A phenomenon or process is considered *important* for a facility if the associated Π -Group is greater than 1/10 of the largest Π -Group in the equation and evaluated for that facility. This choice is based on the common engineering standard of keeping under consideration first-order terms and ignoring second-order terms. For assessing very important scale distortions, phenomena and processes are said in this report to have top-priority importance if their associated AP600 scaling groups differ by less than 20% from the largest Π -Group in the same equation.

The same important phenomenon may affect the depressurization, inventory change, and/or temperature change. Such an important phenomenon appears through more than one important scaling group.

Phase 1 has two subphases, covers the initial depressurization and is identified in Figure 3.1. Of the twenty-seven fractional Π -Groups scaling Phase 1, twelve represent processes of first-order importance, but only four arise from top-priority phenomena: namely the break flow, the thermal contraction and liquid temperature change due to net cooling of single-phase fluid, and the self-scaling balance of flow resistance by the reactor coolant pumps. The phenomena of first-order importance for AP600 are identified by green numbers in the AP600 columns of the Π -Group matrices (tables) in Section 6.2, Π -Groups of top-priority phenomena are printed in bold green.

Phase 2 has four subphases as shown in Figure 3.1 and covers the passive heat removal. Forty-four fractional Π -Groups scale Phase 2. Thirty of these fractional scaling groups are of first-order importance. Of top-priority importance is phase change in Steam Generators, Pressurizer, and Core Makeup Tanks (CMT), thermal expansion due to net heating of liquid, stored energy in liquid, CMT circulation flow, and heat transfer in the Passive Residual Heat Rejection System.

Phase 3 covers the first three stages of depressurization by the Automatic Depressurization System (ADS). See Figure 3.1. Of the 12 fractional Π -Groups of Phase 3, five represent processes of first-order importance, but only three top-priority phenomena are caused by two flows, the ADS-123 valve flow and the CMT drainage flow. The ADS-123 flow is governed by the important ADS-123 orifice dimensions.

Phase 4 covers the fourth and last depressurization stage by ADS-4. See Figure 3.1. Twenty-eight fractional Π -Groups scale Phase 4. Fifteen of these fractional scaling groups are of first-order importance. Eight top-priority Π -Groups identify (1) ADS-4 valve flow, (2) phase change in reactor core, CMTs and PRZ, (3) the PRZ discharge into the primary system, and (4) the CMT flow as the most important phenomena for system depressurization, and for RPV, CMT, and PRZ inventory changes during Phase 4.

Phase 5 is the phase of coolant injection from the In-containment Refueling Water Storage Tank (IRWST). Sixteen fractional Π -Groups scale Phase 5. Thirteen of these fractional scaling groups are of first-order importance. Eight top-priority Π -Groups indicate great importance of PRZ discharge to RPV and PRZ inventory, IRWST drainage flow to IRWST inventory and RPV subcooling temperature, IRWST temperature to RPV subcooling temperature, and the match between flow impedances and gravitational forces in the IRWST flow loop.

The number of evaluated global scaling criteria or Π -Groups that are of first-order importance for any time period or subphase varies between five (for Subphase 1.2, or initial depressurization after scram) and 18 (for Subphase 2.1, or passive heat removal before Accumulator activation). Except for the high-pressure limitation in APEX for Phase 1, it appears possible to meet, by proper design and test operation, in principle, all important scaling criteria in the test facilities for any phase because the modest number of scaling groups (≤ 19) contain a much larger number of adjustable geometric and operating parameters. However, it appears impossible to meet all the 75 important scaling criteria for all the phases of the transient simultaneously.

Scale Distortions

Section 4.6 defines scale distortion and conservative scale distortion for this report. A phenomenon or process is taken to be scale-distorted in a test facility, relative to the same phenomenon or process in the AP600 if the ratio of test facility over AP600 Π -Groups is less than $\frac{1}{2}$ or greater than 2. This implies a difference of the order of 100%. Since the adoption of this convention affects the number of important scale distortions, we have repeated the count of important scale distortions with the criterion of “less than $\frac{1}{3}$ or greater than 3,” to indicate the sensitivity of the assessment to the thresholds of $\frac{1}{2}$ and 2. It turns out that for each test facility approximately half the fractional Π -Groups outside the $\{\frac{1}{2}, 2\}$ bracket fall also outside the $\{\frac{1}{3}, 3\}$ bracket. A scale distortion is called conservative if the associated process tends to reduce RPV inventory and subcooling temperature in the test facility more than in the AP600.

Based upon the $\{\frac{1}{2}, 2\}$ criterion adopted in Section 4.6, **all important global phenomena are scaled without distortion in at least one test facility, except for these two phenomena:**

- (1) Flow inertia, or the ratio of inertia over pump forces during Phase 1, the Initial Depressurization Phase. See Table 6.8. APEX does not scale this phase at all; ROSA and SPES have disproportionately low inertia during normal loop operation. *This distortion has no impact on minimum reactor vessel inventory.*
- (2) The effect of Reactor Pressure Vessel (RPV) Injection from the Pressurizer (PRZ), during Phase 4, the ADS-4 Blow-down Phase. See the Scaling Group $\Pi_{\alpha, W_{PRZ}}$ in Table 6.63. This scaling group equals the product of the characteristic time (of depressurization) for Phase 4 times the characteristic frequency for PRZ injection, i.e. the mass flow rate in the surge line divided by the liquid inventory in the RPV. Table 6.63 reveals that at the start of Phase 4 the rate of injection from the PRZ into the RPV would *fill* the AP600 RPV in one third of the Phase 4 depressurization time, while it would take only one seventh of the Phase 4 depressurization time in APEX. ROSA and SPES have inflows into the PRZ at the initial rates which would *empty* the RPV, respectively in one fourth and one half of the Phase 4 depressurization time.

The distortion is caused in APEX by disproportionately low ADS-4 flow, and in ROSA and SPES there is inflow into the PRZ, instead of outflow due to low liquid level elevation in the PRZ. *The scale distortion of PRZ Surge Line flow in all test facilities could affect the inventory at the beginning of Phase 5 when the minimum RPV inventory is expected to occur.* Based on the greater RPV injection rate in APEX and the PRZ inflow (and the corresponding RPV inventory loss) in ROSA and SPES, one concludes that the Phase 4 simulation of AP600 is *non-conservative in APEX* and *conservative in ROSA and SPES*. However, APEX appears to discharge more liquid than AP600 through the ADS-4 valve on the PRZ side, and as a result may simulate AP600 *conservatively* also. The effects from a combination of opposing scale distortions needs to be determined by simulation.

The *fractional* Π -Groups or global scaling criteria of first-order importance that are presented in Section 6.2 show that 23 (or 33%) are scale-distorted for APEX, 21 (or 28%) for ROSA, and 12 (or 19%) for SPES. Sections 6.3.1 through 6.3.3 below summarize the causes for scale distortions and their grouping in conservative and nonconservative scale distortions.

The assessment of scale distortion below applies to *transients* only. While the conservation equations of Chapter 5 may be applied also to steady-state conditions, the capacitance terms appearing in Sections 6.1 and 6.2 would not enter the scaling analysis for steady-state conditions. The distortions arising from capacitance terms would not come into the assessment of scale distortion for steady-state conditions.

6.3.1 Global Scale Distortions in APEX

APEX was designed, built, and operated after the completion of a scaling analysis [7]. APEX has the largest number of, namely twenty-three, scale distortions, but *seventeen are conservative* and *nine are explained by only five causes:*

6. Scaling Groups

- (1) Low-pressure thermophysical properties have not been properly scaled. The ratio v_{fg} / h_{fg} of specific volume over enthalpy changes increases strongly with decreasing pressure because v_{fg} grows much more strongly than h_{fg} as the pressure decreases. The ratio affects the mechanical compliance, χ_v , that is defined by Eq. (5-9). The mechanical compliance affects the depressurization rate, the characteristic time of depressurization, and the internal flow rates caused by internal dilation of two-phase regions. The ratio v_{fg} / h_{fg} also affects separately the volume generation or annihilation rate due to phase change. The ten scale distortions caused by low-pressure thermophysical property effects are given in Tables 6.24, 6.25 (secondary system depressurization), 6.27, 6.31 (2), 6.37, 6.41, 6.59, 6.61, and 6.68. It is shown in Section 6.2 that *only three of these ten scale distortions are nonconservative* (see Tables 6.25, 6.61, and 6.68), the remaining *seven are conservative*.
- (2) Low PRHR heat transfer rates, relative to the nominal decay heating power, is responsible for the five scale distortions given in Tables 6.24, 6.27, 6.29, 6.33, and 6.54. *All five scale distortions are conservative*.
- (3) Low PRHR flow rates due to high flow impedance is responsible for the two scale distortions of thermal expansion by decay heating, and of PRHR cooling during Phase 2, as presented in Tables 6.27 and 6.41. The PRHR cooling distortion shown in Table 6.37, and the stored-energy distortion shown in Table 6.41 are caused by low-pressure effects on thermophysical properties *and* by low PRHR flow rates. *The three scale distortions are conservative*.
- (4) Low ADS-4 flow rate, relative to the design flow ratio, is responsible for the two scale distortions of PRZ injection and of ADS-4 discharges from both loops, as presented, respectively, in Tables 6.63 and 6.70. Both scale distortions affect RPV inventory, *the first and nonconservative scale distortion* applies to Phase 4, *the second and conservative scale distortion* to Phase 5.
- (5) Low SRL flow due to high SRL resistance and low liquid level in PRZ during Phase 5 is the cause of one scale distortion in two components, namely of RPV and of PRZ inventory changes due to SRL drainage during Phase 4 (see Tables 6.70 and 6.72). The scale distortion is *nonconservative*.

The causes for the remaining 4 scale distortions are:

- (6) low CMT flow in Phase 2.1, causing a *conservative* scale distortions in CMT circulation flow (see Table 6.38);
- (7) low main loop impedance in Phases 2 through 4 (see Table 6.43), which causes the natural-circulation flow in APEX to bypass the RPV, a *nonconservative scale distortion*;
- (8) low ADS-4 flow in Phase 5 causes poor RPV venting and lowering of the RPV mixture level, a *conservative* scale distortion (see Table 6.70);
- (9) low RPV thermal heat capacity and large core heating during Phase 5 cause the core heating to be *conservatively* distorted, as shown in Table 6.75.

This shows that **nine** phenomena are scale-distorted in APEX, five of these conservatively. These nine phenomena are the cause for the twenty-three first-order global scaling criteria not being met.

6.3.2 Global Scale Distortions in ROSA

There is no previously published scaling analysis available in support of simulating AP600 with ROSA. According to the fractional II-Group evaluations presented here, ROSA has the total of twenty-one scale distortions. Only three are *nonconservative*. Five causes are responsible for the distortions of the fifteen first-order scaling criteria:

6. Scaling Groups

- (1) Low initial core power, i.e., only 16% of the scaled-down full power, is used at the start of the test and is responsible for the five scale distortions during Phase 1, as presented in Tables 6.6, 6.18, 6.20, and 6.22. The low core power results in low Steam Generator cooling power and a smaller thermal contraction rate, which causes a slower depressurization. The two scale distortion of primary system subcooling temperature shown in Table 6.6 are *nonconservative*, the ones in Tables 6.18 and 20 cancel each other, and the scale distortions in Tables 6.18 and 22 are the same and *conservative*. While the scale distortion is significant for code assessment of Phase 1, it is not important for simulating minimum inventory occurring during Phase 5.
- (2) Relatively low heat transfer in the PRHR causes three *conservative* scale distortions of thermal expansion and phase change effects during Phase 2, and condensation in the PRHR during Phase 3, as presented in Tables 6.24, 6.27, and 6.54. The reference heat transfer rates, which were used for evaluating the Π -Groups associated with the distortions, were confirmed with experimental data. The low PRHR cooling power affects the subcooling temperature later in Phase 4 and the core heat transfer at the beginning of Phase 5.
- (3) Low inertia in the ROSA main cooling loops gives rise to three scale distortions during Phases 1 and 2, as presented in Tables 6.8 and 6.43. See also Item (1) at the beginning of Section 6.3, concerning phenomena that are not simulated by any test facility. While this scale distortion affects code assessment of Phases 1 and 2, it is not important for simulating minimum inventory occurring during Phase 5. The scale-distorted inertia affects the flow response to break and valve openings, intermittent pipe clearing by falling and rising liquid levels, and to condensation surges, but not the slow natural circulation flows which follow these transition events. Test facilities with low flow inertia may exhibit flow fluctuations that will not occur in AP600. Test facilities with low inertia miss the inertia coupling of loops that is needed for code assessment.
- (4) Large heat capacities of the Reactor Pressure Vessel and its internal structures cause the two *conservative* scale distortions of stored energy, as presented in Tables 6.37 and 6.41. While these two scale distortions are listed only in tables of Phase 2, they prevail also in Phases 3 through 5 and cause disproportionately high RPV heat transfer during these phases.
- (5) Low flow rates through the Pressure Balance Line during Phase 4 causes the two *conservative* scale distortions of PBL flow and phase change in the CMTs, as presented in Table 6.65. This scale distortion affects RPV inventory at the beginning of Phase 5, during which that inventory reaches its minimum.

The causes for the remaining six scale distortions are:

- (6) Low loop flow impedance causes the second scale distortion of ROSA during Phases 2 through 4, as shown in Table 6.43. The impedance determines flow distributions between components of the primary system during Phases 3 and 4, and the inventory in the Pressurizer, Steam Generators, and CMTs at the beginning of Phase 5. The low loop flow impedance diverts the coolant from the reactor vessel and causes low core flow. This scale distortion of ROSA is, therefore, *conservative*.
- (7) Low CMT flow rate and low CMT heat transfer cause the *nonconservative* scale distortion of CMT condensation during Phase 3, as shown in Table 6.58. This distortion affects also code assessment of CMT phase change.
- (8) Low RPV subcooling causes the scale distortion of heat transfer and vapor generation in the core during Phase 4, as shown in Table 6.59. This *conservative* scale distortion affects the inventory at the beginning of Phase 5.
- (9) The effect of Reactor Pressure Vessel (RPV) Injection from the Pressurizer (PRZ) is scale-distorted during Phase 4, as seen in Table 6.63. The *conservative* scale distortion is causes up-flow into the PRZ in ROSA, instead of outflow. The reverse SRL flow is due to low liquid level elevation in the PRZ. According to

6. Scaling Groups

Table 6.63 the coolant injection from the PRZ into the RPV lasts one third of the Phase-4 time and does affect the inventory during Phase 5.

- (10) Low SRL flow rate causes the *conservative* scale distortion of Surge Line flow and PRZ inventory during Phase 4, as shown in Table 6.67. This distortion affects PRZ level elevation and PRZ flow rate at the start of Phase 5.
- (11) The high heat transfer rate in the RPV causes the *conservative* scale distortion of vapor generation and inventory in the RPV during Phase 5, that is shown in Table 6.75.

This shows that **eleven** reasons in ROSA cause 21 important global scaling criteria to differ from the corresponding scaling groups of AP600 by more than the factor of 2.

6.3.3 Global Scale Distortions in SPES

There is no previously published scaling analysis available to support the experimental simulation of AP600 in the SPES facility. According to the evaluations of the fractional Π -Groups presented here, SPES has the total of eleven scale distortions. All but one are conservative. Seven of the eleven first-order scale distortions have only three causes:

- (1) Large ADS-4 flow in SPES is responsible for the three scale distortions of CMT injection, Surge Line flow, and RPV cooling presented in Tables 6.63, 6.67, and 6.68. All three scale distortions are *conservative*.
- (2) The large heat capacity of the RPV structure and its solid internals distort strongly the vessel heat transfer and thereby the RPV inventory during all phases. See the two scale distortions presented in Tables 6.37 and 6.41. Both are *conservative*.
- (3) Low flow inertia in SPES causes the two scale distortions of RCP pumping, system impedance, and system gravity forces during Phase 1, as shown in Table 6.8. See also Item (1) at the beginning of Section 6.3, concerning phenomena that are not simulated by any test facility. While this scale distortion affects code assessment of Phases 1 and 2, it is not important for simulating minimum inventory occurring during Phase 5. The scale-distorted inertia affects the flow response to break and valve openings, intermittent pipe clearing by falling and rising liquid levels, and to condensation surges, but not the slow natural circulation flows which follow these transition events. Test facilities with low flow inertia may exhibit flow fluctuations that will not occur in AP600. Test facilities with low inertia miss the inertia coupling of loops that is needed for code assessment.

The causes for the remaining three scale distortions are:

- (4) low thermal response function (thermophysical property), affecting liquid subcooling temperature and introducing a *nonconservative* scale distortion during Phase 1, as shown in Table 6.6;
- (5) high heat capacity of the Upper Head structure introducing a relevant conservative distortion of a depressurization scaling criterion, which is not important for AP600 depressurization;
- (6) low CMT heat transfer rate and high CMT flow cause the *conservative* scale distortion of CMT phase change during Phase 3 that is presented in Table 6.58, and
- (7) reverse flow in the Surge Line is caused by low PRZ inventory at the beginning of Phase 4 and gives rise to the *conservative* scale distortion of RPV coolant injection in SPES presented in Table 6.63.

This shows that **six** reasons in SPES cause ten important global scaling criteria to differ from the corresponding scaling groups of AP600 by more than the factor of 2. SPES was found to have the smallest number of scale distortions but the largest scale distortion arising from excessive heat capacities in the Reactor Pressure Vessel.

6.3.4 Scale Distortions of Local Inertia, Gravity, and Impedance Distributions

Section 4.4.6 presents the *concepts* of modeling and scaling the dynamic interaction of components in a multi-loop hydraulic system. Section 5.4.2 presents the general vector momentum balance for predicting the dynamics of hydraulic interactions between components in the multi-loop systems of AP600, APEX, ROSA and SPES. The model introduces the vector momentum balance with its vectors of pumping and gravity forces and the matrices of flow inertia and flow impedance. Section 6.1.4 presents the derivations of the scaled matrices or *metrics* of gravity, flow inertia, and flow impedance *distributions* for forced and natural circulation.

Tables 6.9 through 6.16, 6.44 through 6.52 and 6.79 through 6.83 present the numerical evaluations of the metric elements, giving the measures of gravity, flow inertia, and flow impedance *distributions*. Each metric is evaluated for AP600, APEX, ROSA, and SPES. AP600, APEX, and SPES have metrics of the same dimensions. As explained in Section 6.2, differences between the metrics of APEX, ROSA, and SPES and the metrics of AP600 are used to determine whether the coolant flows tend to enter the reactor core more readily in APEX, ROSA, and SPES than in AP600. Where this is observed, the corresponding distortion of *distribution* scaling is called *nonconservative*.

Phase 1 is the initial depressurization phase and has normal operating flows through *four* loops in AP600, APEX (which is not used for Phase 1), and SPES, but only through *two* loops in ROSA. The comparison of the inertia metrics in Tables 6.9 through 6.12 shows that SPES has 20% stronger cross coupling by inertia between the loops of the same plant side than AP600. ROSA and SPES have twice the inertia cross-coupling between loops of the opposite side. The inertia distribution of APEX matches the distribution of AP600. The facilities' systems response is so fast, however, that the S_i distortions during Phase 1 will not affect minimum core coolant inventory and subcooling temperature. According to Tables 6.13 through 6.15, there is *local* impedance distortion in ROSA because there is twice as much impedance in the reactor vessel of ROSA as in AP600, which encourages the coolant in ROSA to bypass the vessel. The Phase 1 distortion of impedance in ROSA, while unimportant for Phase 5 and minimum RPV inventory, is *conservative* because it has the ability to retard the replacement of RPV coolant and reduce the subcooling temperature in later phases. There is *local* impedance distortion also in APEX because there is more impedance in the Cold Legs, but less impedance in the reactor vessel of APEX than in AP600. This encourages in APEX more than in AP600 the coolant to enter the vessel. However, APEX does not simulate Phase 1, and the nonconservative distortion of impedance distribution in APEX prior to Phase 2 has no impact on Phase 5 and minimum RPV inventory.

Phases 2 to 4. While the passive systems, i.e., Core Make-up Tanks (CMT) and Accumulators, are active, the gravity metrics are not scale-distorted. The comparison of Tables 6.44 and 6.49 for AP600 with tables 6.45 to 6.47 and 6.50 to 6.52, respectively, shows that inertia and impedance metrics of all three facilities are distorted: three inertia and 19 impedance elements in APEX, 19 inertia and 20 impedance elements in ROSA, and eight inertia and 18 impedance elements in SPES. This means that the transient and quasi-steady *flow distributions* between Reactor Pressure Vessel, Steam Generators, Pressurizer (PRZ), Core Make-up Tanks (CMT), and Accumulators, and the resulting liquid level motions, are not simulated in any test facility during Phases 2 through 4. We consider first the less important inertia and then the impedance distortions.

Specifically, the comparison of Tables 6.45 and 6.44 reveals that APEX has three *inertia* distortions of *minor consequence*, none in the main loops, one nonconservative one in the PRHR loop, and two nonconservative ones in the PRZ surge line.

ROSA is difficult to compare with AP600 because it has only one Cold Leg each on Sides *A* (with Pressurizer) and *B*. One could compute the seven and five eigenvalues, respectively, for AP600 and ROSA. While it is not possible to compare the eigenvalues directly, one could determine whether ROSA is stable or unstable where AP600 is not. However, ROSA has nineteen inertia distortions, five in the main loops, six in the CMT loops, three in the PRHR loop, two in the PRZ surge line, and three affecting the break flow. This large number of inertia distortions renders the comparison of stability domains to be a task beyond the scope of this scaling analysis. None of the inertia metric distortions affect the RPV inventory, even though *nine of the nineteen inertia* distortions in ROSA are, in principle, *nonconservative*. The extent to which the nonconservative distortions are compensated by the ten conservative distortions must be determined by simulation.

6. Scaling Groups

SPES has eight inertia distortions, none in the main loops, four nonconservative ones in the CMT loops, one nonconservative in the PRHR loop, and three nonconservative ones in the PRZ surge line. None of the inertia metric distortions affect the RPV inventory, because the flows respond in a very small fraction of the characteristic times of depressurization, inventory change, or thermal response.

It should be recalled, that inertia distortions are important only temporarily during dynamic flow transients, during flow oscillations, and when rapid condensation accelerates the flow.

The impedance metric for APEX, which is given in Table 6.50, has the same number of non-zero elements as that for AP600, given in Table 6.49. Most of the impedances are concentrated in the Steam Generators, Cold Legs, and Vessel. Nineteen smaller of the thirty-three impedance metric elements are distorted, all distortions are caused by four loop sections with distorted flow resistances (primarily form losses), namely in PRHR and CMT Loops, in Cold Legs, and in the Upper Downcomer. All distortions imply greater flow resistance outside the reactor vessel of APEX than of AP600. This causes the coolant to prefer accumulation in the vessel of APEX more than in the reactor vessel of AP600, and the distortions are, therefore, *not conservative*. The importance, however, of the increased ex-vessel resistances must be assessed by simulation.

The impedance metric for ROSA is given in Table 6.51 and has only 24 non-zero elements and is, therefore, difficult to compare with AP600: it has only one Cold Leg on each side and an atypical branch point in the CMT loops. The loop elements that are common to ROSA and AP600 are compared and show that ROSA has 20 of 24 impedance elements distorted. The 20 distortions are caused by eight loop sections with distorted flow resistances (primarily form losses): Hot Leg, PRHR and CMT Loops, CMT branch segment, two cold-leg segments, *vessel interior*, and Upper Downcomer. Most importantly, ROSA has greater flow resistance in the reactor vessel than AP600, which retards the flow into the core and makes the *leading scale distortions* of flow impedance in ROSA *conservative*.

The impedance metric for SPES (see Table 6.52) has the same number of non-zero elements as AP600. For SPES, eighteen of thirty-three impedance metric elements are distorted. The most important distortions are in the Upper Downcomer and retard DVI flows escaping through the cold leg. The distortions in SPES are caused by four loop sections with distorted flow resistances (primarily form losses): two cold-leg segments, vessel interior, and Upper Downcomer. SPES has much lower (1/10) resistance in the reactor vessel than AP600, which enhances the flow into the core and makes the leading scale distortions of flow impedance in SPES *nonconservative*. It should be noted, that impedance distortion are important during dynamic flow transients, flow oscillations, and when rapid condensation accelerates the flow, *as well as during quasi steady-flow conditions*.

Phase 5. Inertia metrics were not evaluated for Phase 5 because of the long duration of Phase 5 and the resulting insignificance of inertia during the long and quasi-steady Phase 5 of injection from the In-Containment Refueling Water Storage Tank (IRWST). Of the four important gravity, and twenty-seven impedance, metric elements, no gravity elements are distorted in any test facility; fourteen impedance elements are distorted in APEX, twenty impedance elements in ROSA, and 19 impedance elements in SPES. This means that the quasi-steady *flow distributions* between RPV, SGs, PRZ, CMT, and IRWST, and the resulting liquid level motions, are not simulated in any test facility during Phase 5.

In APEX, the flow prefers to accumulate in the Steam Generators, to leave through the break, and it finds more resistance in the vessel. Consequently, the flow will not accumulate as readily in the vessel of APEX as in the vessel of AP600. This distortion is, therefore, *conservative*. However, the steam will vent more readily through the ADS-4 valves. This produces less back pressure in the vessel upper plenum and a higher mixture level in the upper plenum. The RPV-to-ADS-4 flow resistance in APEX is *nonconservatively* scale distorted.

In ROSA, the flow is retarded through the break and the ADS-4 valves and finds it easier to get into the vessel due to five *nonconservative* scale distortions. ROSA loses PRZ inventory more readily through ADS-4. The associated scale distortions are *conservative*.

6. Scaling Groups

In SPES, impedances are *nonconservatively* scale distorted, because the flows in SPES prefer to escape through ADS-4, to get into the vessel, and have difficulties escaping from the break. The flows prefer to accumulate in the Steam Generators, and have difficulties to drain from the PRZ. The impedances in these flow paths are *conservatively* distorted.

6. Scaling Groups

7. PRESENT VERSUS PREVIOUS SCALING ANALYSIS RESULTS

The US NRC had contracted Idaho National Engineering Laboratory (INEL) to carry out a global system scaling analysis for AP600 and the related test facilities APEX, ROSA, and SPES. The analysis concentrated mainly on the last two phases of the transient, namely on the automatic depressurization by the fourth stage of the Automatic Depressurization System (ADS-4), and on the long-term cooling by gravity injection from the In-containment Refueling Water Storage Tank (IRWST) and from the containment sump.

Westinghouse performed its own AP600 scaling analysis [16] and evaluated the scaling groups for AP600, APEX of OSU, and for SPES.

The USNRC requested a comparison of the scaling analyses carried out by (INEL), Westinghouse, and Brookhaven National Laboratory, for the purpose of coordinating the results. This chapter presents the comparison of the two scaling analyses by INEL and Westinghouse with the scaling work reported here to identify the similarities and differences in the methodology and the results of the three analyses.

All three scaling analyses employ the partitioning of the transient into time periods or phases, although there are minor differences in the phase definitions. Westinghouse has six phases but omits the one of initial depressurization. The lumping of the ADS-123 blowdown phase with the natural circulation phase in the INEL analysis, however, is a disregard for the important, strong change of the dominant discharge flow, from the break to the much stronger ADS-123 discharge flow. This change is attended by a change in characteristic depressurization times.

The results of the INEL and Westinghouse scaling analyses cannot be expected to be equal to the results presented in Chapter 6 of this report, primarily because the first scaling principle stated in Section 4.3 of this report, which requires that

“the governing equations are normalized such that the normalized variables, y^ , and their derivatives with respect to normalized time and space coordinates are of order unity and the magnitude of each term of the normalized conservation equation is measured by its normalizing, constant coefficient”*

is frequently not satisfied in the INEL and Westinghouse scaling analyses, even though the intent to meet this requirement is clearly stated in [15] and [16]. See, for example, Eqs. (6-17), (6-21), (6-22), (6-44), (A-6), and (C-13) in the INEL scaling analysis [15], and Eqs. (3-14), (3-57), (3-86), and (3-91) in the Westinghouse scaling analysis [16] where a large number of *different mass flow rates* were normalized with a *common reference mass flow rate* in each conservation equation, and *different heating rates* were normalized in Eqs. (3-19) and (3-44) of [16] with the *same reference heating rate* in each equation. The use of common reference parameters leads to a drastic reduction in the number of scaling groups and to a diminished ability of identifying scale distortions.

The following sections present respective comparisons of the INEL and Westinghouse analyses with the scaling analysis presented in this report. The comparison is limited to the modeling, the scope of the scaling analysis, the scaling method, the scaling principles, and the scaling results.

7.1 The INEL Scaling Analysis

The INEL scaling analysis concentrates primarily on the ADS-4 blowdown and IRWST injection phases. It includes integrations of some of the *scaled* governing conservation equations [15]. The integrations are facilitated by additional simplifying assumptions. The purpose of the integrations was to confirm the simplified conservation equations and the scaling method used in the INEL scaling analysis. It was pointed out, however, in Section 5.2 that the operations of multiplication and division involved in scaling does not alter the conservation equations. Therefore, adherence to the scaling principles cannot be confirmed by comparing the integration results with test data. Plotted test data will “collapse” if normalization errors are applied consistently to all test facilities. It is better to use the

7. Present vs. Previous Scaling Analysis Results

complete conservation equations without omissions, and it is more important to confirm estimates of reference parameters, since the estimates may imply modeling assumptions. INEL did not confirm the reference data used for the scaling analysis (see, for example, the arbitrary selection of initial pressures in Tables 6.4 and 6.7 of [15]: INEL used 70 bar for the initial pressure of “Intermediate Subphase II” which is said to end with the initiation of the S-Signal; the S-Signal trips at 128 bar).

The INEL analysis implies many simplifications, based on subjective (unquantified) assumptions regarding the importance of phenomena. It should have been the objective of the scaling analysis to *demonstrate quantitatively* what is unimportant.

The a priori simplifications and the normalization with disregard of the scaling principle explained at the beginning of this chapter are the reason for the small number of scaling criteria produced by the INEL analysis.

Reference [17] by Wulff is cited but there are important differences in the scaling of the depressurization (see Section 6.6.1 in this report) and the dynamic interaction between components (momentum balance, see Section 6.1.4 in this report). The differences are pointed out below.

7.1.1 Modeling in the INEL Scaling Analysis

The mass and energy conservation equations are combined to derive the equation for the time rate of pressure change, as in Section 5.4.1.2 of this report. However, for the system containing single-phase liquid in some parts and two-phase mixtures in other parts the ad hoc derivation of the depressurization equation, Eq. (A-48) of [15], is incorrect: the system elasticity does not apply to the combination of the single-phase liquid and two-phase mixture shown in Figure 6.1 of [15]. Equation. (A-48) of [15] does not account for the contributions of volume dilatations from the single-phase liquid and two-phase mixture. See Eq. (5-8) in this report to recognize the different effect that heat transfer has, depending on whether it takes place in the region of single-phase liquid or in the region of two-phase mixture. The INEL model in Eq. (A-48) fails to account for the important difference between thermal contraction of single-phase liquid in the Steam Generators and volume expansion by phase change due to Pressurizer Heating, for example, in a two-phase mixture. Similarly, Eq. (6-15) in [15] makes no distinction between two different heat transfer rates to different types of fluid, neither by differences in reference parameters, nor by differences in volume change. The derivation of Eq. (C-17) does account for the important difference between thermal contraction of single-phase liquid and phase change in a two-phase mixture. However, Eq. (C-17) does account for the elasticity of the nitrogen gas.

The mass conservation equation is used in [15] to derive the equations for inventory change and level motion.

The energy conservation equation is used in [15] to derive the equations for the time rate of subcooling temperature change in the Reactor Pressure Vessel. Eq. (C-6) has the expansion term missing which may be important for adiabatic expansion. All the property derivative terms are far more complicated than is necessary.

The momentum balance is used by INEL only in its steady-state form, and all flow paths are decoupled [15]. INEL does not model, analyze, and scale the component interaction through multiple loop systems. The modeling of the surge line flow in [15] implies a rising cap bubble. This is strange for the 14-inch diameter surge line in AP600. The resulting mass flow rate according to the expression in [15] is 50 times larger in AP600 than the flow according to Bernoulli.

7.1.2 Scope of the INEL Scaling Analysis

The INEL scaling analysis [15] concentrates on the last two phases of the transient: the IRWST “injection” Phase, and the IRWST Draining and Sump Injection Phase. These two phases were treated in this report as one phase. INEL treated the three preceding phases under the proposition that the system pressure at the beginning of the ADS-4 injection

7. Present vs. Previous Scaling Analysis Results

phase is almost independent of the prior history. While the CMT inventory at the beginning of the ADS-4 injection phase is fixed by design, the pressure at the beginning of the ADS-4 injection phase depends on how much heat is being transferred to the primary system prior to the beginning of the ADS-4 injection phase. The range of possible pressures at this time is determined by the difference between adiabatic and isothermal expansions, starting from the initial pressure of 155 bar and ending when the inventory loss in the CMT trips the ADS-4 valves.

The INEL scaling analysis includes integrations of some of the *scaled* governing conservation equations [15], which was discussed above at the beginning of Section 7.1, but it lacks the scaling of the system momentum balances. Momentum scaling criteria are limited to CMT and IRWST line segments.

7.1.3 INEL Scaling Method and Scaling Principles

The INEL scaling analysis is also based on the normalization of the governing conservation equations [15]. The driving processes used for the normalization are not identified. The INEL scaling method corresponds to the *fractional* scaling analysis presented in Section 6.2 of this report (see Section 4.4.5.1 for the description of the *causative process related* scaling analysis). Notice the finding on normalization methods regarding the scaling analyses by Westinghouse and INEL at the beginning of this chapter. The disregard of the scaling principle explained there are a reason for the small number of scaling criteria produced by the INEL analysis.

It is pointed out in Section 4.4.3 that the normalization of the conservation equations must be performed with plant-specific parameters of geometry, of specified initial operating conditions, and of specified trip set points. INEL, however, used frequently postulated reference parameters that were not confirmed by experiment, instead of parameters estimated from plant-specific design data. For example, INEL used 70 bar for the initial pressure of “Intermediate Subphase II” which is said to end with the initiation of the S-Signal; the S-Signal trips at 128 bar. The origin of reference parameters should be identified by INEL (see Appendix F [15]!).

7.1.4 INEL Scaling Results

Section 6.3 summarizes the results of the scaling analysis presented in this report, by collecting 127 scaling groups of which 75 (59%) were found to represent global scaling criteria of first-order importance (expressed as *fractional* Π -Groups, see Section 4.4.5.2). Of the 75 important processes, 24 (or 32%) show scale distortion for APEX, 21 (or 28%) for ROSA, and 11 (or 15%) for SPES. This assessment is based upon the $\{1/2, 2\}$ or factor 2 criterion adopted in Section 4.6. Most of the scale distortions are found to be conservative, by producing in the test facilities lower minimum RPV inventory and less subcooling than in AP600 (see Section 6.3.1).

The “Summary of Important Nondimensional Groups by Transient Phase” on Page iv of [15] shows the evaluation results of 15 “important” groups for six phases or subphases. There is no definition offered for “important.” The count of 15 includes the unit scaling groups, some of which are unity by arbitrary definition of reference parameters. This definition is correct for reference times, but only for those conservation equations in which the characteristic response time equals the system reference time; it cannot be correct for two conservation equations governing the same phase.

INEL is in agreement with the results of this report in stating that ADS flows (ADS-123 and ADS-4 flows) and line resistances in IRWST, CMT, and PRZ Surge lines are important. However, the statement does not agree with the Summary [15], which shows fifteen important phenomena.

INEL states that the ratios of ADS-4 over CMT mass flow rates are distorted in APEX (OSU), ROSA, and SPES during the ADS-4 blowdown phase and the ADS-4 flow during the IRWST injection phase, and that otherwise there is no distortion during the IRWST injection and long-term cooling phases. However, the “Summary of Important Nondimensional Groups by Transient Phase” on Page iv of [15] shows significant differences in scaling groups: four

7. Present vs. Previous Scaling Analysis Results

for APEX, one for ROSA, and three for SPES. INEL did not distinguish between conservative and nonconservative scale distortions.

7.2 The Westinghouse Scaling Analysis

The Westinghouse scaling analysis distinguishes itself by the inclusion of the scaling of the *transient* momentum balance. Reference [17] by Wulff is cited as a basis for the scaling analysis but there are important differences in the scaling of the depressurization (see Section 6.6.1 in this report) and the dynamic interaction between components (momentum balance, see Section 6.1.4 in this report). The differences are pointed out below.

7.2.1 Modeling in the Westinghouse Scaling Analysis

The mass and energy conservation equations are combined to derive the equation for the time rate of pressure change, as in Section 5.4.1.2 of this report. However, for the system containing single-phase liquid in some parts and two-phase mixtures in other parts the ad hoc derivation of the depressurization equation, Eq. (3-55) of [16], is incorrect: while the system elasticity, Eq. (3-53), is the volume-weighted sum of the single-phase liquid and two-phase mixture elasticities, as in Eq. (5-9) of this report, Eq. (3-56) of [16] does not account for the contributions of volume dilatations from the single-phase liquid and two-phase mixture. See Eq. (5-8) in this report to recognize the different effect that heat transfer has, depending on whether it takes place in the region of single-phase liquid or in the region of two-phase mixture. The Westinghouse model fails to account for the potentially important difference between thermal contraction of single-phase liquid and volume annihilation by condensation in a two-phase mixture, both being caused by the cooling power. The effects are seen to arise naturally in the systematic derivation of Eq. (5-8) in this report. Also, Westinghouse omitted the elasticity of nitrogen gas (which is important) and the heating of the nitrogen in the Accumulators (which turned out to be unimportant).

The energy conservation equation is used in [16] to derive the equations for the time rate of temperature change, Eqs. (3-19), (3-27), and (3-42). Equation (3-18) for the change in stored internal energy is used for the derivation, but it is wrong. The rate of internal energy is, in the nomenclature of [16]

$$V_{ML} \frac{d(\rho e)}{dt} = V_{ML} \left[\left(\frac{\partial \rho e}{\partial T} \right)_v \frac{dT}{dt} + \left(\frac{\partial \rho e}{\partial v} \right)_v \frac{dv}{dt} \right], \quad (7-1)$$

which differs from Eq. (3-18) of [16]: Eq. (3-18) has several terms missing and the $c_v = (\partial e / \partial T)_v$ obviously must not be differentiated with respect to time.

The loop momentum balance is used to model the dynamic exchange of mass between the system components. However, the four, seven and six loop systems that are active during CMT, PRHR, ACC and primary-system flows, are represented by Westinghouse by a single loop momentum balance. It is therefore impossible to account for asymmetries in the system and to differentiate the primary-system loop from the passive loop system characteristics.

Finally, Westinghouse's model has more time derivatives and, therefore, primary state variables than conservation equations (see Eqs. (3-12), (3-14), (3-21), (3-22), (3-30), (3-31), (3-44), (3-67), and (3-68), all of which have two time derivatives). The system of modeling equations could not be integrated.

7.2.2 Scope of the Westinghouse Scaling Analysis

The Westinghouse scaling analysis concentrates, as do the other two analyses by INEL and BNL, on minimum inventory. Westinghouse, however, omits to scale the initial depressurization phase on the ground that the depressurization in AP600 is the same as in current power reactors. The questions as to whether APEX (OSU) and SPES depressurize as AP600, and whether differences are of any consequence, remain unanswered.

Westinghouse *assumes* isobaric expansion of the primary-system fluid during the natural circulation phase. This is not justified by Eq. (5-8) of this report or by experiments. Isobaric expansion would require that the numerator of Eq. (5-8) be zero. There is no compelling reason for the net heat transfer to compensate for the break flow. Considering the experiments: the natural circulation phase begins at 128 bar and ends near the Accumulator trip set point of 49 bar. How can these endpoint pressure be connected by an isobaric expansion?

7.2.3 Westinghouse Scaling Method and Scaling Principles

The Westinghouse scaling analysis is also based on the normalization of the governing conservation equations. The driving process is used for the normalization. The *driving process related* scaling method coincides for most equations with the *causative process related* scaling analysis presented in Section 6.2 of this report (see Section 4.4.5.1 for the description of the *causative process related* scaling analysis). Notice the finding on normalization methods regarding the scaling analyses by Westinghouse and INEL at the beginning of this chapter. The normalization without adherence to the scaling principle of normalizing individual processes individually is the major reason for the small number of scaling criteria produced by the Westinghouse scaling analysis.

It is pointed out in Section 4.4.3 that the normalization of the conservation equations must be performed with plant-specific parameters of geometry, of specified initial operating conditions, and of specified trip set points. Westinghouse, however, used frequently experimental or code-computed data. Experimental data from a test facility that may have scale distortions are also scale-distorted. Scaling groups evaluated with scale-distorted parameters may mask scale distortions of the test facility. The use of test data is, therefore, misleading. Moreover, the use of test data (e.g., mass flow rates) replaces plant-specific geometric and operating parameters (flow cross-sectional area, excess pressure, etc.) from the scaling groups, parameters which would occur in the scaling group if the reference parameter were defined in terms of plant-specific design and operating parameters. Test data may serve to confirm the modeling for the computation of reference parameters, but they are unacceptable as reference parameters. Reference parameters, that are calculated by a computer code (that is still to be assessed) are not reliable because their computations are difficult to scrutinize; their relation to plant-specific parameters may be corrupted by compensating errors in the computer code.

The reference data that Westinghouse used for the calculation of the scaling groups have not been confirmed by test data. The large difference between scaling groups listed with the designation “hand-calculated,” “data,” and “WCOBRA/TRAC” indicates large differences between estimated and measured reference data, and great uncertainties in the Π -Group calculations (see, for example Π_2 in Tables 3.5-2 and 3.5-3 in [16]). The assumptions in Section 3.3.1 of [16] are questionable. The report does not indicate where the AP600 data came from for the Π -Group calculations reported in [16].

7.2.4 Westinghouse Scaling Results

Section 6.3 summarizes the results of the scaling analysis presented in this report, by collecting 127 scaling groups of which 75 (59%) were found to represent global scaling criteria of first-order importance (expressed as *fractional* Π -Groups, see Section 4.4.5.2). Of the 75 important processes, 24 (or 32%) show scale distortion for APEX, 21 (or 28%) for ROSA, and 11 (or 15%) for SPES, based on the $\{1/2, 2\}$ criterion adopted in Section 4.6. Most of the scale

7. Present vs. Previous Scaling Analysis Results

distortions are found to be conservative, by producing in the test facilities lower minimum RPV inventory and less subcooling than in AP600.

Westinghouse evaluated the total of 45 scaling groups. Westinghouse did not offer a criterion for “importance.” Of the 45 scaling groups evaluated, 31 (or 69%) appear to be important for AP600 by the criterion used in this report. Westinghouse agrees with the results of this report in stating that inertia is small and unimportant, that gravity and flow impedance are important, and that decay heating and steam generator heat transfer are important.

Westinghouse did not offer a criterion for the determination of scale distortion. By applying the criterion used in this report, one finds that 15 and 12 scaling criteria differ in SPES and APEX (OSU), respectively, by more than a factor of 2 from the corresponding AP600 scaling criteria. The scale distortions arise primarily from mismatch of gravity and impedance forces in the momentum balance. As can be seen from Table 3.4-7 in [16], Westinghouse offers no scaling of gravity, inertia, and impedance *distributions* (see Sections 6.2.1.1.4, 6.2.4.4, and 6.2.5.4 of this report). Westinghouse did not distinguish between conservative and nonconservative scale distortions.

8. CONCLUSIONS

The scaling analysis presented in this report and the review of previously published scaling analyses for the AP600 and the related test facilities APEX, ROSA, and SPES lead to the following conclusions:

1. The number of global (fractional) scaling criteria or Π -Groups that are of first-order significance for any one of the eight time periods or subphases analyzed varies between 5 and 18. The number of top priority scaling groups varies between 3 and 10 for any subphase. The total of first-order significant scaling groups for the entire transient is 75, that of top priority scaling groups is 39. First-order and top priority importance is defined in Section 4.5 on the basis of scaling groups: a scaling criterion and its associated phenomenon are of first-order or top priority importance, respectively, if the corresponding scaling group is greater than 1/10 or 8/10 of the largest scaling group in its normalized conservation equation for AP600.
2. None of the test facilities APEX, ROSA, and SPES represents AP600 without scale distortions for all the phases of the transient. Scale distortion is defined in Section 4.6 on the basis of scaling groups: an important phenomenon is considered to be scale-distorted in a test facility if the associated scaling group differs from the corresponding scaling group of AP600 by more than the factor of 2.
3. Together, the three test facilities APEX, ROSA, and SPES simulate without scale distortion every important phenomenon for every phase of the transient at least once, except for two phenomena: (a) Flow inertia, or the ratio of inertia over pump forces during the Initial Depressurization Phase. This distortion is important for code assessment regarding the simulation of flow response to valve actions during the Initial Depressurization Phase, but it has no impact on minimum reactor vessel inventory. (b) The effect of Reactor Pressure Vessel (RPV) injection from the Pressurizer during the ADS-4 Blow-down Phase. See Table 6.63. The distortion is caused in APEX by disproportionately low ADS-4 flow, and in ROSA and SPES there is inflow into the PRZ, instead of outflow due to low liquid level elevation in the PRZ.

This distortion does affect the RPV inventory at the beginning of Phase 5 during which the RPV inventory is expected to reach its minimum. It is explained on Page 6-109 that the distortion may lead to nonconservative simulation of AP600 minimum inventory by APEX, depending on whether the effect of lower-quality discharge through the ADS-4 valve on the PRZ side fails to cancel the beneficial effect from the greater RPV injection rate from the PRZ. It is also explained on Page 6-109 that ROSA and SPES simulate the impact on RPV minimum inventory from PRZ injection into the RPV conservatively.

4. Of the total of 75 first-order important *global* scaling criteria evaluated as *reduced-form* Π -Groups (see Section 4.4.5.2) for each test facility, twenty-three (or 31%) show scale distortion for APEX Test SB05. Seventeen scale distortions are conservative and six nonconservative. Nine scale distortions are the consequence of five causes, primarily incorrect low-pressure scaling. See Section 6.3.1.

Twenty-one (or 28%) of the first-order important *global* scaling criteria, evaluated for ROSA, are found to show distortion, only three are nonconservative distortions. Fifteen scale distortions lead to only five causes, primarily low initial core power and low heat transfer rates in the PRHR, due to low PRHR flow rates. This and the other causes for scale distortions in ROSA are detailed in Section 6.3.2.

Eleven (or 15%) of the first-order important *global* scaling criteria, evaluated for SPES, show scale distortions, one of which is nonconservative, and seven of which have only three causes. The strongest *global* scale distortions in SPES are caused by the disproportionately large structural heat capacities in the Reactor Pressure Vessel. This and the other causes for scale distortions in ROSA are detailed in Section 6.3.3. SPES was found to have the smallest total number of global scale distortions.

8. Conclusions

The assessment of scale distortion is based upon the factor 2 criterion adopted in Section 4.6. If a lesser { $\frac{1}{3}$, 3} or factor 3 criterion had been adopted then only half as many scaling groups would have shown scale distortion. The difference between these two evaluation exhibits the sensitivity of the assessment to the criterion of scale distortion, and it shows also the strength of the distortions.

5. The dynamic and quasi-static flow *distributions* in the system, or the *component interactions*, are scaled by the metrics of gravity, flow inertia and flow impedance, respectively. AP600, APEX, and SPES have four interconnected flow loops prior to the activation of CMT and PRHR systems, seven loops prior to IRWST activation, and six loops after IRWST activation. Tables 6.9 through 6.16, 6.44 through 6.52 and 6.79 through 6.83 present the numerical evaluations of the metric elements for gravity, flow inertia, and flow impedance *distributions* for natural circulation. None of the three test facilities simulates flow distribution without scale distortion, except for normal operation (Phase 1), prior to the break opening, where ROSA shows no scale distorted distributions of inertia and impedance, but has only two, instead of four, coolant loops.

While the passive systems, i.e., Core Make-up Tanks (CMT) and Accumulators, are active during Phases 2 to 4, only the gravity metrics are not scale-distorted. The inertia and important impedance metrics of all three facilities are distorted.

APEX has three *inertia* distortions of *minor consequence*, none in the main loops, one nonconservative one in the PRHR loop, and two nonconservative ones in the PRZ surge line. All *impedance* distortions imply greater flow resistance outside the reactor vessel of APEX than of AP600. This causes the coolant to prefer accumulation in the vessel of APEX more than in the reactor vessel of AP600, and the distortions are, therefore, *not conservative*.

ROSA is difficult to compare with AP600 because it has only one Cold Leg each on side. ROSA has nineteen inertia distortions, five in the main loops, six in the CMT loops, three in the PRHR loop, two in the PRZ surge line, and three affecting the break flow. None of the inertia metric distortions affect the RPV inventory, even though *nine of the nineteen inertia* distortions in ROSA are, in principle, *nonconservative*. ROSA has greater flow resistance in the reactor vessel than AP600, which retards the flow into the core and makes the *leading scale distortions* of flow impedance in ROSA *conservative*.

SPES has eight *inertia* distortions, none in the main loops, four *nonconservative* ones in the CMT loops, one *nonconservative* in the PRHR loop, and three *nonconservative* ones in the PRZ surge line. None of the inertia metric distortions affect the RPV inventory, because the flows respond in a very small fraction of the characteristic times of depressurization, inventory change, or thermal response. SPES has much lower resistance in the reactor vessel than AP600, which enhances the flow into the core and makes the leading scale distortions of flow *impedance* in SPES *nonconservative*.

During IRWST and Sump injection, i.e., during Phases 5, only impedance distributions are important.

During Phase 5, the flow in APEX prefers, relative to AP600, to accumulate in the Steam Generators, to leave through the break, and it finds more resistance in the vessel. The ex-vessel impedance distortion is, therefore, *conservative*. However, the steam will vent more readily through the ADS-4 valves, reducing the Upper Plenum pressure and raising the mixture level in the Upper Plenum. The RPV-to-ADS-4 flow resistance in APEX is *non-conservatively* scale distorted.

During Phase 5, the flow in ROSA is retarded through the break and the ADS-4 valves and finds it easier to get into the vessel due to five *nonconservative* scale distortions. ROSA loses PRZ inventory more readily through ADS-4. The associated scale distortions are *conservative*.

For SPES during Phase 5, impedances are *nonconservatively* scale distorted, because the flows in SPES prefer to escape through ADS-4, to get into the vessel, and have difficulties escaping from the break. The flows prefer to accumulate in the Steam Generators, and have difficulties to drain from the PRZ. The impedances in these flow paths are *conservatively* distorted.

6. Inertia distortions are important only temporarily during dynamic flow transients, during flow oscillations, and when rapid condensation accelerates the flow. During monotonic depressurization, inertia scale distortions do not affect RPV minimum inventory, because inertia is so small that the flows in all loops respond to control functions and level changes in a very small fraction of the system response time. Impedance scale distortions, however, are important during dynamic flow transients, flow oscillations, and when rapid condensation accelerates the flow, *as well as during quasi steady-flow conditions*, because the flows seek the path of least resistance (impedance).
7. The review of the INEL [15] and Westinghouse [16] scaling analyses and their comparison with the analysis presented here shows that all three scaling analyses employ the partitioning of the transient into time periods or phases although there are minor differences in the phase definitions. The lumping of the ADS-123 blowdown phase with the natural circulation phase in the INEL analysis disregards the strong change of the dominant discharge flow, from the break to the much stronger ADS-123 discharge flow. All three scaling analyses are based on the normalization of the governing conservation equations and the evaluation and comparison of the resulting scaling groups. INEL and BNL (this report) employed the fractional scaling method, Westinghouse the dominant process related method, and BNL used also the causative process related method, which is nearly the same as the dominant process related method see Section 4.4.5.

The results of the INEL [15] and Westinghouse [16] scaling analyses cannot be expected to be equal or equal to the results presented in Chapter 6 of this report, primarily because the first scaling principle stated in Section 4.3 of this report has not been satisfied in INEL's and Westinghouse's scaling analyses. Consequently, (a) many scaling groups in [15] and [16] are not actually representative of their associated phenomena, and (b) the total number of scaling groups is too small as several phenomena are represented by a single scaling group; possible scale distortions remain undetected.

8. Instead of demonstrating *quantitatively* what is unimportant, the INEL analysis implies many simplifications, based on *subjective* (unquantified) *assumptions* regarding the importance of phenomena. This is the second reason for the small number of scaling criteria obtained by INEL.

INEL and Westinghouse missed the differences in coolant volume changes by heating of single- and two-phase fluids; INEL missed the thermal contraction by imbalanced cooling in the Steam Generators during the early phases; Westinghouse missed the distinction in all phases.

The Westinghouse model has more time derivatives and, therefore, primary state variables than conservation equations, the system of modeling equations is not closed (incomplete). INEL used frequently *postulated* reference parameters. This removed plant-specific design parameters from the scaling analysis. Westinghouse used frequently experimental or code-computed data as reference parameters. The use of test data also deletes plant-specific parameters from the scaling analysis. The large difference between scaling groups that were obtained in [16] with reference parameters of different origin indicates large uncertainties in the Π -Group calculations of Westinghouse (the Westinghouse report does not cite references for the "experimental AP600 data" used for the Π -Group calculations in [16]). The reference data used for the calculation of the scaling groups in [16] have not been confirmed by test data.

9. The "Summary of Important Nondimensional Groups by Transient Phase" on Page iv of the INEL report [15] shows the evaluation results of only 15 "important" groups for six phases or subphases, including the unit scaling groups. There is no definition offered for "important." INEL is in agreement with the results of this report, in stating that ADS-123 and ADS-4 flows and line resistances in IRWST, CMT, and PRZ Surge lines are important.

8. Conclusions

This number of five important phenomena is in conflict with the list of 15 in the above Summary [15]. INEL states that the ratios of ADS-4 over CMT mass flow rates are distorted in APEX (OSU), ROSA, and SPES during the ADS-4 blowdown phase and the ADS-4 flow during the IRWST injection phase, and that otherwise there is no distortion during the IRWST injection and long-term cooling phases. However, the “Summary of Important Nondimensional Groups by Transient Phase” on Page iv of [15] shows significant differences in many more scaling groups: 4 for APEX, 1 for ROSA, and 3 for SPES. It is not clear which distortions are conservative and which are nonconservative. Details of the INEL analysis are found in Section 7.1.4.

Westinghouse evaluated the total of 45 scaling groups. Westinghouse did not offer a criterion for “importance.” Of the 45 scaling groups evaluated, 31 (or 69%) appear to be important for AP600 by the criterion used in this report. Westinghouse agrees with the results of this report in stating that inertia is small and unimportant, that gravity and flow impedance are important, and that decay heating and steam generator heat transfer are important. Westinghouse did not offer a criterion for the determination of scale distortion. By applying the criterion used in this report, one finds that 15 and 12 scaling criteria differ in SPES and APEX (OSU), respectively, by more than a factor of 2 from the corresponding AP600 scaling criteria. Westinghouse offered no distinction between conservative and nonconservative scale distortions. Details of the Westinghouse analysis are found in Section 7.2.4.

Neither INEL nor Westinghouse offered any scaling of *flow distributions* in interconnected loops, as described above in Item 6.

10. It is claimed by INEL on Page 32 of [15] that the break flow does not affect the inventory and system pressure at the time of ADS-4 initiation, and that Phases 1 through 3 of the transient are, therefore, unimportant for the assessment of the minimum RPV inventory which occurs during Phase 5. The claim is derived from the assertion that the system pressure at the time of ADS-123 initiation does not depend on the processes occurring during Phases 1 through 3. The claim is wrong.

The system inventory at ADS initiations is weakly dependent of what happens during Phases 1 through 3 (and of SBLOCA break size) because the ADS-123 and ADS-4 trips are tightly connected to CMT *inventory*. Minimum RPV inventory, however, depends on the excess primary system pressure above the containment pressure at the time of ADS-123 initiation. The pressure at the time of ADS-123 initiation may vary between the terminal pressures of adiabatic and isothermal volume discharges from the primary system, depending on the time of discharge and, consequently, the amount of heat transfer between the coolant and the solid structures. The time of discharge depends on break size and mechanical compliance. Figure 6.4 in [15], when redrawn in nondimensional form and for *several* break sizes, would demonstrate the dependence of ADS-123 initiation pressure on break size and on heat transfer rates (and phase change rates) prior to ADS-123 initiation.

Secondly, unless all terms related to phase change, Accumulator injection, and heat transfer in the mass conservation and depressurization equations, Eqs. (5-8) and (5-11) can be ignored, the break size cannot be canceled from the quotient $(d\alpha_i / dp)$, which is formed from Eqs. (5-8) and (5-11), by dividing $(d\alpha_i / dt) / (dp_1 / dt)$. If the endpoint (α_e, p_e) were independent of break size, one would have to be able to cancel the break size from the quotient $(d\alpha_i / dp)$. Since the cancellation is impossible, the end pressure p_e cannot be independent of break size, and the above claim is wrong.

11. The assessment of relative importance and of scale distortion is needed to ascertain that transport phenomena take place in the same heat transfer and flow regimes in the test facilities as in the full-size plant. This assessment is not possible with any computer code, unless the computer code is programmed to evaluate scaling criteria. Without the assessment, one cannot use test data to determine whether or not the closure relations in a computer code are applicable to the full-size plant. All three test facilities are required for assessing the capability of a code to predict AP600 transients, as each facility is limited to phases and phenomena identified in the matrices of Π -Groups in Section 6.2.

9. REFERENCES

1. Westinghouse Electric Company, "AP600 Standard Safety Analysis Report," Simplified Passive Advanced Light Water Reactor Plant Program (Proprietary Report) (June 1992) and revisions.
2. M. Rigamonti, "SPES-2 Facility Description;" Westinghouse Proprietary Class 2 Report WCAP 14073, Piacenza, Italy, (May 1994).
3. M. Tarantini and O. Vescovi, "SPES-2 Pre-Operational Test Results," Quick Look Report, Westinghouse Proprietary Class 2 Report, SIET No. 00238-RP93 (April 1994).
4. M. Bacchiani, "SPES-2 Hot Pre-Operational Test Results," Westinghouse Proprietary Class 2 Report, SIET No. 00311-RP94, (June 1993).
5. Cunningham, J.P., et al. "AP600 SPES-2 Test Analysis Report," Vols. I and II, WCAP-14254 (1995).
6. L.E. Hochreiter, J.N. Reyes, L.K. Lau, "Low Pressure Integral System Test Facility Description Report," Westinghouse Proprietary Class 2, WCAP 14124, Vols. 1 and 2, (July 1994).
7. J.N. Reyes, L.E. Hochreiter, L.K. Lau, and A.Y. Lafi, "Low Pressure Integral System Test Facility Scaling Report," Westinghouse Proprietary Class 2, WCAP 14270, (January 1995).
8. "AP600 Low-Pressure Integral Systems Test at Oregon State University," Final Data Report, Westinghouse Proprietary Class 2 Report, WCAP-14252, Vols. I, II, III (May 1995).
9. "AP600 Low-Pressure Integral Systems Test at Oregon State University," Test Analysis Report WCAP-14292, Rev. 1 (Sept. 1995).
10. R.A. Shaw et al. "Summary of the LSTF Characterization Tests Performed in Conjunction with the ROSA/AP600 Experiments," Japan Atomic Energy Research Institute, JAERI Memo 07-037 (February 1995).
11. The ROSA-V Group, "Large Scale Test Facility; System Description for the ROSA/AP600 Configurations (for the installed core)," Japan Atomic Energy Research Institute, JAERI Memo 08-070 (March 1996).
12. Shaw, R.A., Yonomoto, T., and Kukita, Y, "Quick Look Report for ROSA/AP600 Experiment AP-CL-03," Thermohydraulic Safety Engineering Laboratory, Dept. of Reactor Safety Research, Tokai Research Establishment, JAERI Memo 06-249 (1994).
13. D. Bessette, M. DiMarzo and P. Griffith, "Phenomenology Observed in the AP600 Integral Systems Test Programs Conducted in the ROSA-AP600, APEX, and SPES-2 Facilities," Nuclear Regulatory Commission Draft Report (December 1996).
14. K.E. Carlson et al., "RELAP5/MOD3 Code Manual," Idaho National Engineering Laboratory, NUREG/CR-5535, Vols. 1 - 7, (August 1995).
15. S. Banerjee, M.G. Ortiz, T.K. Larson, and J.M. Gozzuol, "Top-Down Scaling Analysis Methodology for AP600 Integral Tests," Draft Report prepared for USNRC by INEL, Advanced Nuclear Energy Products, Lockheed Martin Idaho Technologies Company, under Contract DE-AC07-94IID 13223, contains proprietary information, INEL-96/0040 (December 1996).
16. L.E. Hochreiter, M.J. Loftus, and W.L. Brown, "AP600 Scaling and PIRT Closure Report, Westinghouse Proprietary Class 2 Report WCAP-14727, Revision 0, (August 1996).

9. References

17. W. WULFF, "Scaling of Thermohydraulic Systems," *Nuclear Engineering and Design*, 163 (1996) 359-395.
18. C.D. Fletcher, G.E. Wilson, C.B. Davis, and T.J. Boucher, "Interim Phenomena Identification and Ranking Tables for Westinghouse AP600 Small-Break Loss of Coolant Accident, Main Steam line Break, and Steam Generator Tube Rupture Scenarios," Idaho National Laboratory Report No. INEL-04/0061, Lockheed Idaho Technologies Company, Idaho Falls, ID (Nov. 1994).
19. C.D. Fletcher, G.E. Wilson, C.B. Davis, and T.J. Boucher, "Interim Phenomena Identification and Ranking Tables for Westinghouse AP600 Small-Break Loss of Coolant Accident, Main Steam line Break, and Steam Generator Tube Rupture Scenarios," Idaho National Laboratory Report No. INEL-04/0061, Appendix H (proprietary), Lockheed Idaho Technologies Company, Idaho Falls, ID (Nov. 1994).
20. N. Zuber, "A hierarchical, Two-tiered Scaling Analysis," Appendix D of *An Integrated Structure and Scaling Methodology for Severe Accident Technical Issue Resolution*, US Nuclear Regulatory Commission, NUREG/CR-5809, Nov. 1991.
21. W. Wulff, "Integral Methods for Two-Phase Flow in Hydraulic Systems," *Advances in Heat Transfer*, J.P. Hartnett, T.F. Irvine, Jr., Y.I. Cho, and G.A. Greene, editors, Vol. 31 (1997).
22. D. Bestion, "Document de Synthesis CATHARE," CENG/SETh/LEMh-EM Report 88-129 (1988).
23. I.E. Idelchick, *Handbook of Hydraulic Resistance*, Second Edition, revised and augmented, Hemisphere Publishing Corporation, Washington, New York, London (1986).
24. L. Haar, J.S. Gallagher, and G.S. Kell, *NBS/NRC Steam Tables, Thermodynamic and Transport Properties and Computer Programs for Vapor and Liquid States of Water*, Hemisphere Press, New York (1984).
25. Westinghouse, "Westinghouse AP600 Long Term Cooling Test at Oregon State University, Facility Drawings, Piping and Instrumentation Diagrams," Westinghouse Proprietary Class 2, September 17, 1993.
26. J.N. Reyes, Jr., Data transmission by Facsimile from Oregon State University, Nuclear Engineering, to Dr. Rohatgi, Brookhaven National Laboratory, at 4:11 pm on November 26, 1996.
27. CRANE Engineering Division, "Flow of Fluids Through Valves, Fittings, and Pipe," Technical Paper No. 410, Eleventh Printing, CRANE Company, 300 Park Avenue, New York, NY 10022 (1970).